Advantages and Challenges of Perforated Monopiles in Deep Water Sites

G.A.Santamaria Gonzalez

Delft University of Technology

Advantages and Challenges of Perforated Monopiles in Deep Water Sites

by

Gabriel Andres Santamaria Gonzalez 5028256

A comparative study of stress concentrations and fatigue loads on monopile foundations in deep water sites

Delft University of Technology
Offshore and Dredging Engineering
October 20, 2023

Supervisor(s): Dr. ir. Oriol Colomes
PhD Candidate Marco Vergassola

TU Delft

This page has intentionally been left blank

Table of Contents

List of Figures

List of Tables

Preface

When asked about how I ended up studying Offshore engineering, I always tell a story of when I was a toddler and my parents took me to the beach. To their surprise, even though I could not talk or even walk, I would find my way into the water as if it was calling my name. Little did I know that later on I would understand waves and the offshore environment in a completely different way.

Ten years ago, I decided to go down the road of offshore engineering. Back then, I already had an ultimate goal of coming to TU Delft to study but life had different plans for me and had me to Korea first, and then to Mexico, giving me the opportunity to meet friends, mentors and role models that I will keep in my heart forever.

The past two years have been crucial in defining the direction of my focus. A year ago this meant a research project supervised by Oriol Colomés and Marco Vergassola, my supervisors, who I've grown to admire and inspired me to delve into the unknown realm of fatigue analysis of structures through structural modelling.

Thanks to them, the unconditional support of my loved ones at home and the rainy weather forcing me to stay in and work for weeks at a time, I can say I've become a TU delft alumni with this Thesis.

Lastly, words cannot describe how grateful I am to have the kind of support my family gives me. Thanks to them, I can proudly assure that I am and will forever be unconditionally loved.

Gabriel Santamaria October 20, 2023

"*Sometimes we climb mountains just to remind ourselves how small our problems really are...*

...sometimes we'll do it just for the view."

Abstract

The potential for developing more efficient offshore wind support structures becomes increasingly critical as the offshore wind sector is faced with challenges such as rising commodity prices and shrinking profit margins. These challenges not only impact the industry's capacity to meet growing global demand but also hinder efforts to address the imperative challenge of decarbonization. As the offshore wind industry expands, the roles of cost-effectiveness and ongoing research will be pivotal in driving the advancement of offshore wind energy on a global scale.

The support structure is responsible for supporting the turbine, transferring loads to the ground, and allowing access for inspection and maintenance purposes. The environmental loads acting on an offshore wind support structure (OWSS) result from a combination of waves, wind speed, turbulence intensity acting on the shape of the turbine components. These loads can be grouped in a scatter diagrams that depict the probability of occurrence of a given wind wave combined condition which is also known as a "sea state". Different sea states lead to significant vibrations and stresses on the foundation, which can cause fatigue and failure over time.

The perforated monopile consists of a monopile with holes around the splash zone to reduce frontal area, which reduces hydrodynamic loads on the foundation. Assesing the potential of perforated monopiles in deep waters was based on a comparative study of the loads acting on the monopile by developing a model that considers the structural response of the system to different sea states. FEM studies are essential in identifying potential stress concentrations and their effects on the overall integrity and safety of the structure. Thus, analysis focused on assessing the performance of both a reference monopile and a perforated monopile structural models under both parked and power production conditions, including sea states with 50-year and 1-year return periods. The simulations encompassed 35 distinct sea states and computed maximum stresses at critical locations, including the mudline, perforations, and the splash zone.

The study found that the perforated monopile displayed an average reduction of 17% in the maximum stresses found at the mudline compared to the reference monopile. This reduction was attributed to improved flow dynamics facilitated by the perforations. However, the splash zone of the perforated monopile experienced increased stresses around the splash zone of up to a factor of four, attributed to higher overturning moments around the perforated area. Next, the analysis continued with a fatigue life assessment, highlighting sea states that could potentially challenge the structural integrity and longevity of the monopiles over their intended operational lifespan.

The study explored alternative solutions, such as varying thickness parameters at high-stress areas and using different materials at the splash zone. Additionally, the possibility of different perforation geometries was considered, although it could impact natural frequencies and cause resonance with loading frequencies.

To conclude, the research underscores the importance of a comprehensive assessment of monopile designs in offshore renewable energy structures with a discussion and recommendations for further research on the subject. It emphasizes the need for careful consideration of design choices based on specific environmental conditions at the installation site. The findings contribute valuable insights into optimizing monopile designs for long-term performance and structural reliability in varying sea state conditions during power production scenarios.

Introduction

In the past decade, offshore wind has become a mainstream source of renewable energy around the world because of how the technology can help to reduce greenhouse gas emissions and mitigate climate change. With its energy cost being reduced owing to more mature technology, market forces, and government incentives. These same drivers have also led to the development of bigger wind turbines that perform exponentially better than the conventional models that have been used in the past. However, bigger offshore wind turbines require higher wind speeds and an increased distance between each other to make up for the increased wake effect for an efficient energy production rate. Hence, research of the viability of alternatives for the deployment of offshore wind turbines in deeper waters to benefit from the increased surface area and quality of the offshore wind resource is increasingly relevant.

The perforated monopile has been introduced as a promising offshore wind support structure alternative to reduce hydrodynamic loads on traditional monopiles for deeper waters. However, it important to recognize the potential risks of adding perforations to a monopile and the possible changes in stress concentrations and the cumulative damage throughout the design life of the offshore wind turbine (OWT). This thesis study is intended to dive into the potential of perforated monopiles as an alternative to be used in offshore wind turbines in deep waters. A common approach to do so is by starting with a comparative study of offshore wind turbine technologies. The report describes the process that lead to answering the research question:

Is the structural reliability of a perforated monopile improved in deep water conditions when considering a dynamic fluid-structure interaction model?

To create an overview of the problem, the first chapter focuses over the current outlook of the offshore wind sector, its growth over the past years, and its potential for meeting renewable energy goals for the upcoming decades. Then, the outlook and the relevance of current research to reach the potential of monopiles in deep water is introduced and the current research gaps are identified. The first chapter ends with the statement of a research methodology with the objective to close the research gaps that current research projects have left.

The next phase encompasses the gathering of information relevant for the modelling of both a reference monopile and the perforated monopile. This includes the environmental conditions, structural constraints and initial dimentions of the monopile. These, in combination with the research question will give purpose to the modelling of the monopile on ANSYS, a FEM analysis software, with the aim of understanding in more detail the response of the structure to environmental loads. For this, a modal analysis is carried on and a set of simmulations with the aim of comparing the maximum stresses occuring at different parts of both the reference and the perforated monopile.

Finally, the report ends with a fatigue analysis at the areas where the highest stress concentrations were found for both monopiles. Using Miner's rule to calculate the equivalent fatigue damage on both monopiles, the resulting damages are found and analyzed from which conclusions and discussion points were drawn and alternative solutions are proposed.

1 Background

1.1. Literature study

1.1.1. Current offshore wind industry status and future outlook

With the emergence of renewable energy being recognised as a critical concern of the current times, both national and international ambitious initiatives have been announced. These include the Netherlands aim for a transition to a carbon neutral economy which targets to reduce green house gas emissions by 49% by 2030 and 95% by 2050 (IEA, 2019).

Meeting the Climate Agreement emissions reduction targets will require the share of renewables in electricity generation to reach around 70% by 2030. The emissions reduction attributed to the electricity sector in the Climate Agreement translates to 94 TWh of renewable electricity generation by 2030. Of this, 49 TWh is expected to come from offshore wind, with the Netherlands' offshore wind energy road map aiming to deliver 11.5 GW of total offshore wind capacity by 2030 MEACP, 2019.

The Netherlands has since raised its target to 21 GW by 2030 (GWEC, 2022b).These goals coupled with renewed policy urgency for achieving energy independence from Russian oil and gas, and volatility in fossil fuel markets in general, the global offshore wind market outlook in the medium and long-term looks extremely promising (GWEC, 2022a). Netherlands was one of four North Sea countries, alongside Germany, Belgium and Denmark, to commit to accelerating the build-out of offshore wind to achieve 65 GW of installed capacity by 2030 and 150 GW by 2050 (European Comission, 2022). The pledge was prompted in part by the energy security crisis arising from the military conflict in Ukraine.

With Europe as the main developer of wind turbines, the North Sea is most likely the area that will be continued to be used for the development of the future goals on renewable energy generation. Currently, OWT are placed in water depths of up to 30 meters. However, given the future electricity generation requirements, and constant development of bigger wind turbines gives rise to the need to expand the deployment of OWT into deeper waters to benefit of the increased surface area and quality of the offshore wind resource in deep waters (Fig. 1.1).

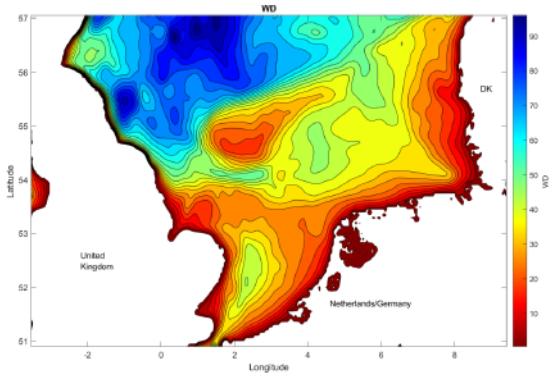

Figure 1.1: North sea water depth gradient (Star, 2022)

Wind power generation more than doubled from around 5 TWh in 2012 to 10.6 TWh in 2018, when it represented around 9% of total electricity generation (NEA, 2023). The rapid increase in wind generation was aided by offshore wind projects coming on line in 2015 and 2016. In 2018, offshore wind accounted for almost a third of total wind generation. Currently, in addition to the new capacity from Asia, Europe is the only region which reported new offshore wind installations. The UK had a record year in 2021 with more than 2.3 GW reaching grid connection; however, it lost its title as the world's largest offshore wind market in total installations to China. Coming in second for new installations in Europe is Denmark with 605MW commissioned last year, followed by Netherlands 392 MW and Norway 3.6MW (GWEC, 2022a).

In total installations, Europe remains the largest offshore wind regional market as of the end of 2021. The region was responsible for 50.4% of total cumulative global offshore wind installations, followed by Asia with 49.5% market share. Outside Europe and Asia, North America has 42 MW offshore wind in operation as of the end of last year, contributing only 0.1% of total offshore wind installations (GWEC, 2022b).

1.1.2. Offshore wind support structures potential in deep water regimes

Offshore wind installations are also moving further from shore and into deeper water where better quality wind resources are available. As shown in fig. 1.4, most projects commissioned to date have been within 50 km off shore. However, several large projects in the pipeline are 100 km or more from shore (IEA, 2019). This is becoming more common as developers look to install turbines in deeper water with improved construction techniques that reflect learning from earlier projects and from the offshore oil and gas industry.

The support structure can be seen in figure 1.2 and is defined as: The structure that supports the turbine and holds it in place and transfers the loads from the turbine to the ground (Fischer et al. 2010). The presence of the structure itself attracts hydrodynamic and aerodynamic loads which should also be transferred to the soil (Fischer et al. 2010). Secondary functions are to allow for means of exporting the power produced by the turbine and to allow access to the turbine for inspection and maintenance purposes (Fischer et al. 2010).

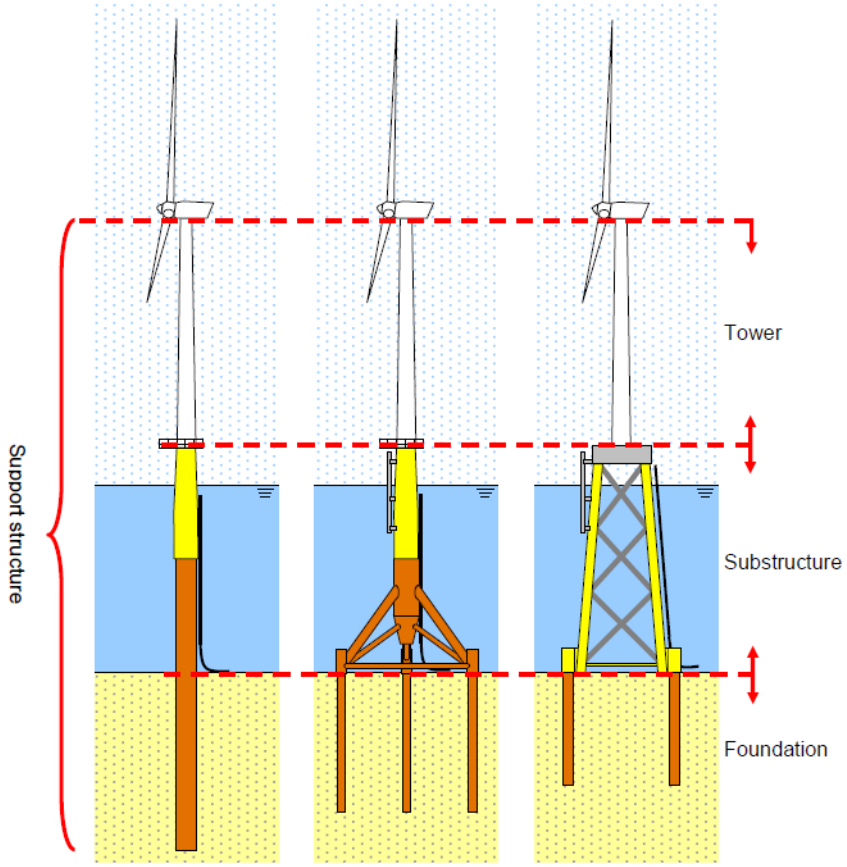

Figure 1.2: Wind turbine substructure (Fischer et al. 2010)

Because of the offshore wind park site conditions, a wide range of support structures have been developed including fixed-bottom foundations and floating foundations. Research on these OWSS concepts continue to be studied for their use in offshore wind farms as the potential for OWTs expands to deeper waters. Each type of structure has its unique advantages and limitations, and selecting the appropriate type of support structure is crucial to the success of an offshore wind farm.

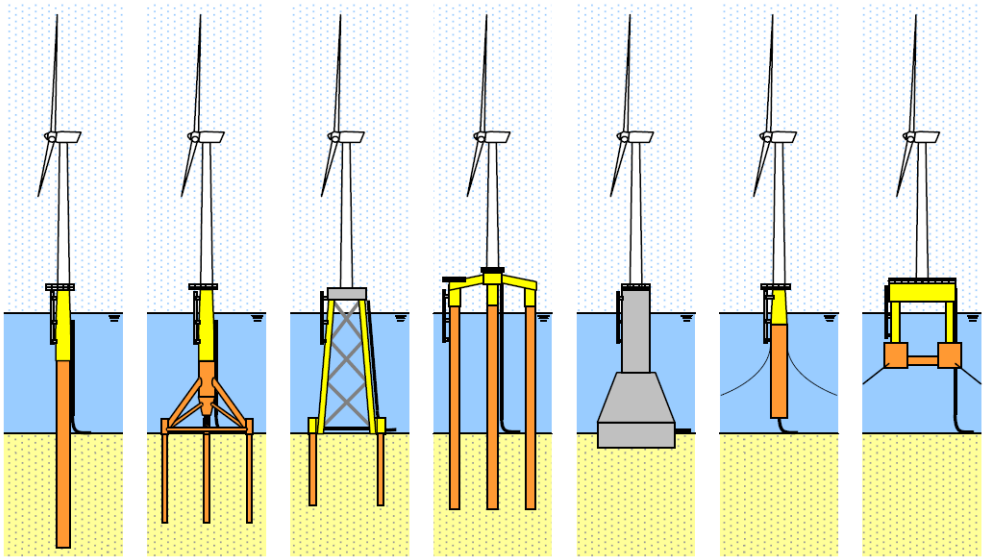

Figure 1.3: Support structure concepts (Fischer et al. 2010)

Monopile foundations have been the preferred choice for the majority of offshore wind projects

installed in water depths of less than 50 meters due to their relative low cost, ease of installation, and proven track record in the industry. Projects located in slightly deeper depths are also seeking to find ways to use monopile foundations rather than to have to adopt higher cost jacket and floating foundations. Hence, a focus for monopile structures on structural optimisation and pushing the boundaries of the range of application by integrated design is currently a very relevant research topic for the offshore sector (Fischer et al. 2010).

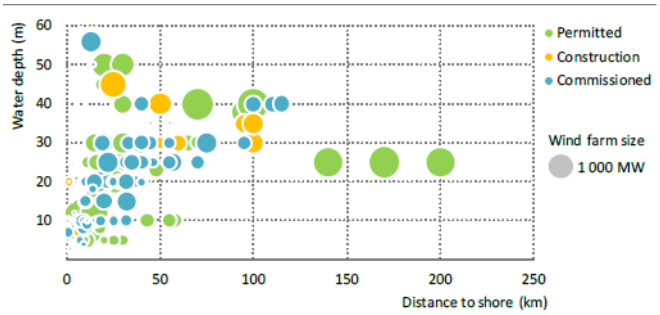

Figure 1.4: Water depth vs distance to shore of Offshore wind projects (IEA, 2019).

The monopile foundation (fig. 1.3, a) can be seen as an extension of the onshore turbine tower below the sea surface and into the seabed. The vertical loads are transferred to the soil through wall friction and tip resistance. Lateral loads dominate over vertical loads and are carrried to the foundation through bending. The loads are subsequently transferred laterally to the soil. To provide enough stiffness the diameter of the monopile foundation has to be large enough. This attracts relatively high hydrodynamic loads. On the other hand, the monopile foundation is easy to fabricate and install since there is no need for seabed preparation. Difficulties due to limited sizes of pile driving equipment may also be expected.

For offshore wind platforms with fixed bottoms, as can be seen in figure 1.5, the most expensive component is the turbine itself, contributing about 34.7% to the overall expense, while the assembly and installation is 10.4%, followed by the construction of foundation and substructure at 12.6% (GWEC, 2022a). On the other hand, for the FOWTs, the wind turbine and installation and assembly take up about 22.1% and 11.1% of the total cost, respectively, with the foundation and substructure being the most expensive components at 36.2% (IEA, 2019).

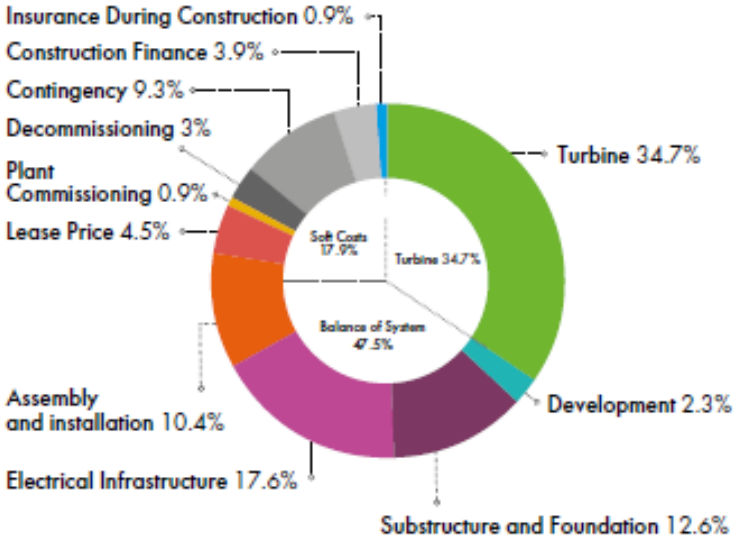

Figure 1.5: Bottom founded offshore wind turbine CAPEX. (GWEC, 2022a).

As the offshore wind industry continues to grow, optimizing the cost-effectiveness of support

structures for both fixed-bottom and floating platforms remains a key area of focus. By understanding the cost distribution among different components, developers and stakeholders can identify opportunities to streamline processes, reduce expenses, and further advance the deployment of offshore wind energy on a global scale (European Comission, 2022). Additionally, ongoing research and technological advancements are expected to play a vital role in driving down costs and making offshore wind energy even more competitive with conventional power generation sources.

Foundations account for a significant part of total project costs and even though there are many proposals for alternative support structures, monopile structures are currently the preferred technology, more than 60% of deployment (NEA, 2023). It is becoming possible to use this type of foundation in increasingly deep water (up to 55-60 m in some cases) thus reducing the need for more expensive jacket foundations, which are suited to deeper water and are the second most used technology globally (IEA, 2019). This gives potential and relevance to further research and development on monopile foundations as OWSS in deep waters. However, because of high stresses at the mudline due to the stuctural characteristics of this type of foundation hybrid concepts of monopiles (fig. 1.6a, fig. 1.6b) show promising results (Andersen et al. 2020, Van Der Ploeg, 2021) and are being studied for their effectiveness in deep water sites.

1.2. Perforated monopiles

Since the design of monopiles in deep water regimes will be ultimately dominated by the fatigue wave loads and constrained by manufacturability constraints (Liu, 2021). Novel concepts are being developed that take into consideration the limitations of the traditional monopile structure in the form of hybrid concepts (i.e. fig. 1.6b) to mitigate the loads acting on the structure for them to be feasible.

One of the promising concepts is the perforated monopile (fig. 1.6a), which consists of a monopile with holes around the splash zone for a reduced frontal area while maintaining the simplicity of fabrication and installation of the monopile. The holes made on the monopiles effectively reduce the frontal area and thus, reduce the hydrodynamic loads on the foundation (Van Der Ploeg, 2021). By allowing water to flow through the perforations, the pile experiences increased drag and better stability (Andersen et al. 2020). Despite being bearing the closest similarity to a monopile, the perforated monopile shares some technical similarities to a jacket substructure. These similarities lead to the potential of reducing hydrodynamic loads, especially fatigue wave loads on the monopile, in addition to the advantages previously mentioned.

(a) Perforated monopile (Andersen et al. 2020).

(b) Hybrid monopile design (Van Der Ploeg, 2021).

Furthermore, as the perforation allows for a discharge through the monopile, it is expected that the perforation will decrease the downflow and associated horseshoe vortices, ultimately reducing the local scour (Andersen et al. 2020). Proper design and maintenance is required to ensure the long-term stability and effectiveness of perforated monopiles as support structures for offshore wind turbines.

1.2.1. Recent developments

However, the use of perforated monopiles may also present some challenges, including the potential for seabed erosion and increased marine growth in the perforations. Perforation changes the flow pattern completely, thus the consequences with respect to loads are difficult to assess. To gain insight into the flow behavior through perforated monopiles, 3D CFD models of 3 different perforation geometries (fig. 1.7) by Van Der Ploeg, 2021 were made.

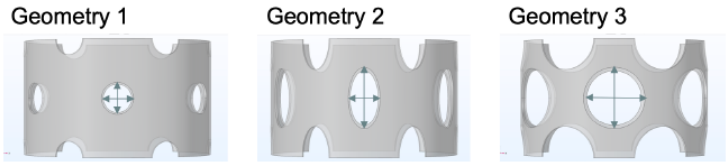

Figure 1.7: The three perforation geometries used in research (Van Der Ploeg, 2021).

In the research of Van Der Ploeg, 2021, it was shown that the preferred option would be the second geometry since it showed both increased flow (fig. 1.8) through the monopile and reduced drag and lift forces (fig. 1.9) in comparisson with the reference MP while maintaining the structural integrity of the monopile by staying below the maximum stress theshold for the applied load cases. The CFD model does not account for the deflection of the monopile under loading. The deflections could influence the flow through the pile and could change the computed drag and lift forces and the dynamic response of the system (Van Der Ploeg, 2021).

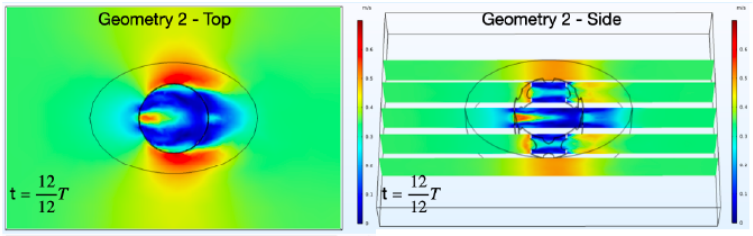

Figure 1.8: Flow velocities of geometry 2, top view on the left and side view on the right. (Van Der Ploeg, 2021).

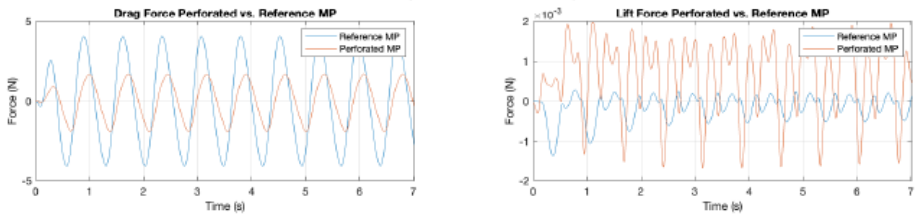

Figure 1.9: Geometry 2 and reference pile drag (left) and lift (right) spectra for most occurring conditions. (Van Der Ploeg, 2021).

The use of perforated monopiles is a relatively new technology and research is ongoing to determine their effectiveness in various seabed conditions and environmental factors. Some studies have found that perforated monopiles can improve the fatigue life of the foundation and reduce the amount of steel required, resulting in a more cost-effective and sustainable design (Van Der Ploeg, 2021). However, a remark was made for additional research on the development of a model that considers the dynamics of the system.

1.2.2. Accounting for dynamics, deflection and fatigue wave loads

Since the design of these monopiles will be dominated by the fatigue wave loads. It is important to focus on the study of design of a model that takes into account the deflection and dynamics of the system in order to verify the structural stability of a perforated monopile.

Here, deflection refers to the deformation or bending of a structure under a load, which can affect the distribution of stresses within the structure. If a structure is designed to withstand a particular load but it deflects excessively, the stresses may be redistributed and concentrated in certain areas, potentially leading to fatigue cracking or failure. On the other hand, the dynamic response refers to the behavior of a structure under dynamic or time-varying loads. Dynamic loads can cause the structure to vibrate or resonate, which can result in high-frequency cyclic loading that can accelerate fatigue damage.

Previous research has focused on how different sea states reduce the peak loads on a perforated monopile structure (Andersen et al. 2020) which lead to the relation in Fig. 1.10. These results were fitted into a curve and thus, equation 1.1 was obtained where the coefficients $a = 0.84$ and $b = 0.94$.

$$\Gamma(KC) = btanh(aKC) \tag{1.1}$$

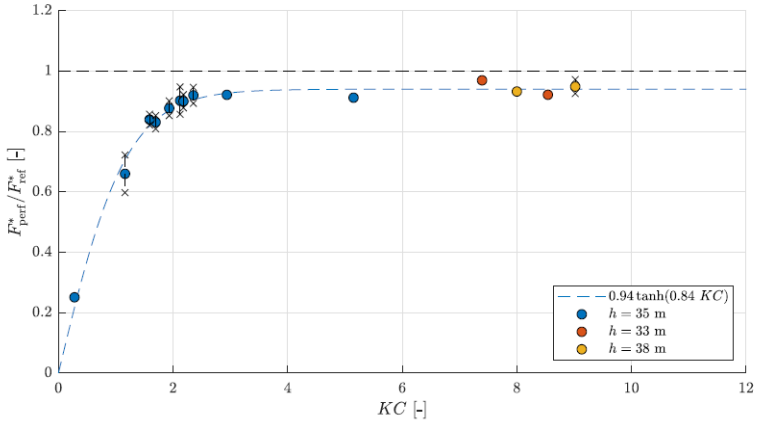

Figure 1.10: Experimental fit relation based on wave flume experiments (Andersen et al. 2020).

This relation was used for three different monopile models for a wide range of water depths for two sea states from the inertia and drag regime, six sea states from the inertia dominated region and one from the diffraction sector (Van Der Ploeg, 2021). Positive results were obtained and can be seen in Figure 1.11 for the 15MW turbine. However, a fully coupled fluid-structure interaction model that accounts for the monopile deflection and dynamics was recommended for further studies to have a more realistic idea of the response and the fatigue life of a perforated monopile.

Turbine	Manufact.	ULS - Power	ULS - Parked	FLS - B1	FLS - C1	FLS - D
Conventional	Yes	Passed	Up to d = 118 m	Passed	Passed	Not passed
Perforated	Yes	Passed	Passed	Passed	Passed	Up to d = 87 m

Figure 1.11: Result overview for the 15 MW reference turbine in combination with a non perforated reference pile and a geometry 2 perforated pile (Van Der Ploeg, 2021).

1.2.3. Potential risk of perforations

Abrupt changes originated from irregularities in the distribution of stresses are known as stress concentrators; these are presented for all types of stress, axial, bending or shear in the presence of fillets, holes, grooves, keyways, splines, tool marks or accidental scrapes (Santos, 2013). If the bar is cut in the cross section of the hole, the tensile stress will be as shown in Figure 1.12 (b), the stress distribution along the cut surface is substantially uniform until reaching the vicinity of the hole, where efforts suddenly increase (Santos, 2013).
Since the perforated monopile is composed of an array of perforations around the splash zone, an assesment of the stress concentrations to evaluate potential failure is crucial. For this, it has been

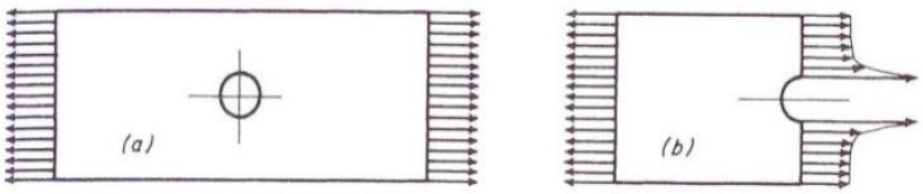

Figure 1.12: Stress distribution for a plate on tensile load (a) away from the hole; (b) in the section of central hole (Santos, 2013).

proven that the structural analysis software ANSYS can give accurate results that line up with the theoretical data found in literature (Santos, 2013).

As OWT grow and expand to deeper waters, the required material for maintaining the structural integrity increases because of the increased moments on the foundation. Thus, the need for new alternatives to the conventional monopile arises in the transitional range of 60-120 meter water depths. With one of the main drivers for offshore renewable energy being the need to reduce the levelized cost of energy(LCOE) and the support structure representing over 20% of the LCOE of the OWT projects (Oh et al. 2018), it becomes important to focus on solutions that improve the cost efficiency while maintaining the reliability of Offshore Wind Support Structures(OWSS).

1.3. Research gaps and objectives

Previously carried out research paved the way for this report. The potential of large diameter monopiles in deep water has been investigated extensively with the help of finite element modelling and simmulations that continue to improve the accuracy and reliability of monopiles in deep water. However, several research gaps still need to be addressed to fully understand the technical feasibility and commercial potential of this concept.

The potential of perforated monopiles as an alternative for deep water projects has been glanced upon with promising results for future development. The table below summarizes the most relevant findings and the missing aspects of the research done on monopiles in deep water regimes so far:

Table 1.1: Summary relevant Reports/Papers

Report/Paper	Conclusion	Missing
Van Der Ploeg, 2021	Fatigue life and stresses are limiting the use of perforated monopiles in deep water. Structural parameters of potential deep water perforated monopile foundation.	Fully coupled fluid structure interaction model. An optimization study of the geometry, number, and spacing of holes is recommended with respect to both stress concentrations and load reductions.
Liu, 2021	ULS and FLS analysis of a numerical Dynamic model for conventional monopiles in deep water regimes. Accumulated fatigue damage showed to be independent of the water depth as the increase of required structural steel neutralizes the increase of overturning moment. No fundamental technical limitations for a monopile supported 15 MW wind turbine in water depths of up to 120 meters, provided that the stiffness of the structure is sufficiently high.	Optimized geometry for conventional monopiles. Assesment of the potential of perforated monopiles as a support structure alternative. A full computational model including components such as the variability in magnitude, shear and turbulence of wind forcing, complete damping components and the rotor controller.
Andersen et al. 2020	Reduction in peak loads following relation: Gamma(KC)=b tanh(a KC) with a=0.84, b=0.94. 0<KC<4 showed higher wave load and moment reduction. For KC>2 load reduction stagnates at 6%.	Sea states with KC > 10 have not been investigated. Recommendation to perform numerical experiments in prototype scale in order to estimate scale effects. Contribution from KC < 1.5 wave loads to the total fatigue lifetime should be estimated.
Vergassola et al. 2020	The hydrodynamic load analysis highlighted that the monopile is subject to the highest hydrodynamic force.	Study should be extended to consider ULS and FLS analysis.
Arany et al. 2017	Recommended steps for MP design, recommended site characteristics, turbine data, load cases ground profile for substructure analysis.	Considerations of future monopile foundation technical feasibility and trends.

Although the current research done on perforated monopiles has shown good results in reducing wave loads and steel usage while increasing potential for its use in deeper waters. However, the design of a model that takes into account the dynamic response of the structure has not been studied extensively by means of numerical simulations.

Based on section 1.2, particular importance is given to look further into the fatigue loads caused by regular sea states as a limiting factor by analyzing the response of a coupled fluid-structure interaction model.

1.4. Research question

The novelty of this research lies in the comparisson in terms of stress concentrations between a dynamic model of a conventional model in comparisson with a model with the same dimentions with added perforations following the recommendations of Andersen et al. 2020 and Van Der Ploeg, 2021. The stress profile resulting from a range of sea state simmulations will be evaluated and compared between models at the points where the stress is found to be the highest.

The evaluation of a fully coupled fluid-structure interaction model that accounts for the monopile deflection and dynamics and asses the perforated monopile for the required design load cases DLC's to ensure technical viability. Hence, focusing on FLS as the most limiting factor leads to the question:

Does the structural integrity of a perforated monopile uphold in deepwater conditions when considering a dynamic fluid-structure interaction model?

To aid answering this question, the following research questions are made:

1. What are the limitations of conventional monopiles in deep water regimes?
2. What loads operational characteristics are to be considered when performing a dynamic analysis on a monopile support structure?
3. What a coupled fluid structure interaction model is and the information that is obtainable through the dynamic analysis of it.
4. What assumptions can be made to simplify the finite element modeling of a monopile support structure?
5. What steps need to be taken in the design of a structure before the FLS analysis is made, and do the fatigue wave loads induce structural failure at the mudline?
6. Is the dynamic response of the structure around the first natural frequency reduced compared to the reference monopile?
7. Given the answers to questions 4 and 5, what would an alternative solution to the perforations at the splash zone look like while maintaining the wave load reduction benefits of the perforated monopile?

By answering the research questions, a thesis outline can be structured which consists of three parts as follows:

Part 1: Technical Feasibility of Monopile Foundations in Deep Water

1. Introduction

Introduction to the current industry status and outlook. The motivation of pushing wind turbines to deeper waters is discussed, and current boundaries of deep water foundation techniques are stated. Also, an overview is provided on the current knowledge on offshore support structure engineering, monopile design, and anticipated limitations to the perforated monopile (RQ 1).

2. The Establishment of the Design Basis

The used environmental data of the reference location is explained, the design load cases are defined for power production and parked condition together with the corresponding sea states. Then, the basis to transferring the environmental data to forcing components is explained. (RQ 2)

3. Analysis Model Testing for Ultimate Limit States (ULS) and Monopile Geometry Optimization

The one-way coupled fluid-structure interaction (FSI) model is introduced and the modelling assumptions are discussed. The details of the models and the validation and verification through Finite Element Analysis (FEA) software are discussed, final geometries for the reference monopile and perforated monopile are established (RQ 3, 4).

Part 2: Model comparison between reference monopile and perforated monopile

1. Fatigue Limit States (FLS)

The results of the monopile geometry optimization process are discussed, and conclusions are drawn. These conclusions serve as the base of the proposed alternative strategies as will be discussed in Chapter 5. (RQ 5)

2. Assessment of Critical Parameters

The critical parameters for extending the use of monopile-based foundations are assessed, and solutions are proposed. Previous attempts found in literature on mitigating these limitations and their results are presented (RQ 6).

Part 3: Alternative Solutions on Increasing the Feasibility of Usage

1. Introduction of Novel Concept

Given the foreseeable limitations and considering the limiting factors, alternative solutions to reduce the impact of fatigue loads on the monopile structure are introduced. The solutions are aimed to options that reduce the resulting maximum stresses induced by critical sea states at the perforations (RQ 7).

2. Additional Model Runs

Based on the findings of Chapter 5 and the critical parameters, additional model runs are performed to assess the effect of damping, increasing the thickness at the perforations and different perforation geometries. The results are used as a basis for the discussion and to establish in what direction future research could continue.

2

Methodology

With the knowledge gaps identified and the research objectives stated, a plan of action to fill the research gap has to be made. In the following chapter the key aspects for the design of a monopile will be introduced and developed.

Since monopile foundations have not been deployed in deep waters so far, the calculations are based on the evaluation of results of previous research done through scaled experiments (Andersen et al. 2020) and numerical simulations (Van Der Ploeg, 2021). The design constraints and modelling requirements that must be addressed in the later stages of the thesis will be defined together with the required general assumptions.

2.1. General assumptions

The design considerations for monopile foundations start with taking into account the capacity of future offshore wind turbines which include 15+MW rated wind turbines with rotor diameters of up to 240 meters and hub heights of 150 meters above the platform (IEA, 2019). These aspects by themselves present engineers with the challenge of a larger swept area and turbine components which are exposed to harsh environmental loads of an open sea that will ultimately cause a significant increase of forcing. Examining the challenges posed by deep-water applications and exploring potential solutions to optimize their performance and robustly support the expanding offshore wind energy sector becomes a crucial starting point from an engineering point of view.

When venturing beyond the boundaries of proven technologies and familiar offshore conditions, the preliminary design of a monopile is often useful. It can provide insights into the sizing required to ensure financial viability for a given foundation type at a specified location. A simplified foundation design can be carried out based on site characteristics, turbine characteristics and ground profile (Arany et al. 2017).

In the context of deep water OWTs, several studies have been made for the design of novel support structure alternatives which required the selection of a representative future OWT with given site characteristics in order to analyze the loads. In the following sections the specific aspects of the required data for the preliminary design of an offshore wind turbine will be listed and explained, namely site conditions, turbine characteristics and design load considerations.

By considering and analyzing these crucial aspects, together with the underlying assumptions during the preliminary design phase, engineers can develop robust and optimized offshore wind turbine support structures that meet the demands of deep water installations while ensuring the long-term sustainability and success of offshore wind energy projects.

2.1.1. Manufacturability

When designing a monopile foundation, establishing a comprehensive framework outlining the material properties and dimensional constraints of the selected support structure is essential. This framework serves as a critical foundation for the systematic evaluation and comparative analysis of structural integrity and load-bearing performance across various design iterations. Within this framework, key parameters such as the outer diameter, wall thickness, D/t ratio, and cone angle play pivotal roles and warrant thorough examination.

The outer diameter of the monopile significantly influences its load-bearing capacity and overall stability. Selecting an appropriate diameter requires a meticulous balance between maximizing load distribution efficiency and ensuring ease of fabrication and transportation. Following the recommendations of Van Der Ploeg, 2021, is set at a max of 14.5m. A judicious choice of outer diameter can lead to optimal material utilization, cost-effectiveness, and manufacturability.

Similarly, the wall thickness of the monopile contributes to both its structural resilience and manufacturability. A robust wall thickness will not affect the response of the structure to dynamic loading as much as the outer diameter. However it is vital to withstand the applied loads and environmental conditions in terms of stress concentrations. Hence, it must be carefully tuned to prevent unnecessary material excess that might hinder fabrication processes. According to Van Der Ploeg, 2021, the maximum plate thickness is set to 150mm.

The D/t ratio, defined as the ratio of the monopile's outer diameter to its wall thickness, serves as a critical indicator of design efficiency. Maintaining an appropriate D/t ratio ensures structural soundness while preventing excessive material use. High slenderness ratio's can result in problems with local buckling or high stresses during installation (Van Der Ploeg, 2021). Additionally, the transportation and storage of very slender piles can become problematic (Van Der Ploeg, 2021). Hence, the maximum D/t-ratio is set to 160.

Furthermore, the cone angle, representing the tapering angle of the monopile's lower portion, impacts the foundation's penetration resistance and load distribution characteristics. A well-considered cone angle design facilitates easier installation into the seabed and enhances overall stability. However, a tapered section might start acting as a damper for these vertical forces if the angle is too large and must be optimized to avoid complicating manufacturing processes and to streamline construction efforts. In accordance to Van Der Ploeg, 2021, the maximum cone angle is set to 4.5°.

In summary, the meticulous consideration of material properties and dimensional constraints within the monopile foundation design framework is essential for evaluating its manufacturability. Balancing factors such as outer diameter, wall thickness, D/t ratio, and cone angle ensures that the foundation not only possesses the requisite structural integrity and load-bearing capabilities while optimizing the fabrication processes, cost reduction, and enhances the understanding the overall project viability.

2.1.2. Turbine characteristics

OWT are dynamically sensitive structures as their natural frequency is close to the forcing frequencies imposed by wind, wave, and mechanical and aerodynamic loads at the frequency of rotation (1P) and blade passing frequency (2P/3P) (DNV-GL, 2007). The preliminary design process requires detailed information about the wind turbine's specifications, including its rated capacity, rotor diameter, hub height, and power curve (Arany et al. 2017). This data is essential for assessing the turbine's dynamic behavior, loads, and response to various environmental conditions.

Particularly relevant for the design of the support structure is the rotational speed of the rotor. For a variable speed turbine this is given as a rotor speed range, from a minimum rotor speed to the nominal rotor speed. Other parameters of relevance are the rotor speed limits for turbine stops due to control of the safety system shut-downs. Together with the number of blades, the blade passing frequency range can be determined, by which the allowable range for the structure natural frequency is known (Fischer et al. 2010). Based on the 15MW reference turbine from (Van Der Ploeg, 2021) the wind turbine specifications selected for further research potential are as follows:

Table 2.1: Wind turbine specifications. (Van Der Ploeg, 2021)

Feature	Quantity	unit
Cut-in windspeed	3.00	m/s
Rated windspeed	10.6	m/s
Cut-in windspeed	25.0	m/s
Minimum rotor speed	5.00	rpm
Maximum rotor speed	7.56	rpm
Hub height	150	m
Rotor diameter	240	m
Rotor nacelle assembly mass	1017	ton
Tower mass	1135	ton
Tower bottom diameter	10.0	m
Tower top diameter	6.50	m
Tower wall thickness bottom	90.0	mm
Tower wall thickness top	30.6	mm
MP diameter (Splash zone)	10	m
Cone angle	3.3	degrees
MP diameter (Mudline)	13.1	m

2.1.3. Site conditions

When designing for a structure in an offshore location, the natural phenomena that occur at the given location is important to be accounted for because of the potential structural damage, operation disturbances and eventual failure of the structure due to these loads.

Site characteristics such as water depth, wave climate, and seabed conditions play a significant role in determining the appropriate design of a monopile. For this research, a deeper water depth may require a longer pile length to ensure sufficient support, while the wave climate may require a larger diameter to withstand the forces exerted on the structure. Furthermore, the seabed conditions, including soil type and strength, can affect the required embedded length of the monopile.

The statistical nature of the environmental loads was based on the measurements retrieved from the meteorological database BMT-AGROSS. These variations can be categorized and organized in a probability scatter diagram that include both extreme conditions and long- and short-term variations (DNV-GL, 2007). Depending on the type of analysis and the design standards that are used to carry out the structural design, the scatter diagrams can be used to recreate a combination of meteorological conditions, also known as a sea state (more extensively elaborated in section 2.3). Several reliable databases exist for offshore locations and can be retrieved and then transformed into a probability density spectrum.

Based on Van Der Ploeg, 2021, for the selected monopile, the site conditions chosen for a representative deep water site are off the coast of Norway with coordinates; N59 E2.5, as seen in fig. (2.1)). The BMT-AGROSS wave climate model was used as the source of meteorological data at this location. The BMT-AGROSS model provides a time series data set for the reining wind and wave conditions over all three hour period within the measurement period (1992-2019). The most important parameters are summarised in table 2.2 Van Der Ploeg, 2021. The significant wave height and period can be then extrapolated using empirical equations based on the maximum wave height (Holthuijsen, 2010). On table the table below the most relevant parameters can be visualized.

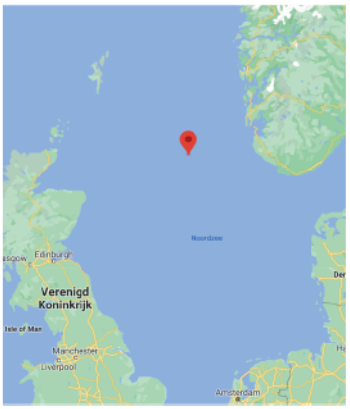

Figure 2.1: Chosen reference location for meteorological conditions (N59 E2.5) (Van Der Ploeg, 2021).

Table 2.2: Site condition summary. (Van Der Ploeg, 2021)

Characteristic	Most occuring	50-year return	unit
Significant wave height	2.25	11.9	m
Maximum wave height	4.26	22.6	m
Peak period(waves)	6.50	13.8	s
Zero crossing period(waves)	6.50	13.8	s
Current speed	1.35	2.10	m/s
Mean wind speed at 10m	8.24	29.7	m/s

2.2. Structural loads

Once the environmental conditions are known, the type of loading the OWT will experience can be known. The total loading that has to be withstood by the monopile consists of a variety of components. The loads can be divided in two main forcing groups: static and dynamic loads. As can be seen in fig.2.2 which depicts wind loads and hydrodynamic loads on a OWT structure. The wind and waveloads on a wind turbine foundation are calculated using Det Norske Veritas and Germanischer Lloyd (DNV-GL) standards. These standards provide guidelines for calculating the wind loads based on the wind speed, turbulence intensity, and other meteorological factors (DNV-GL, 2016, DNV-GL, 2010). The following subsections include the force determination of the two forcing groups.

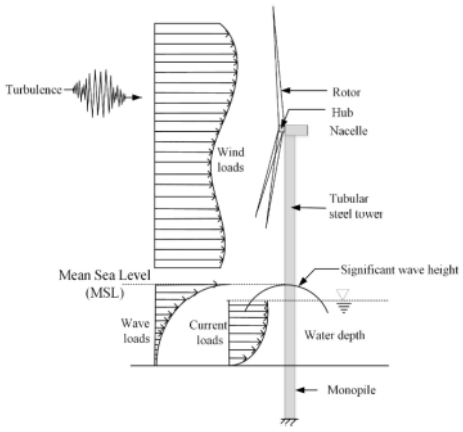

Figure 2.2: Loading cases on a wind turbine and substructure (Star, 2022).

2.2.1. Wind data

With the tower mounted on top of the monopile foundation, the wind loads acting on the tower are transferred to the foundation through the monopile. These forces can cause significant vibrations and

stresses on the foundation, which can lead to fatigue and failure over time.

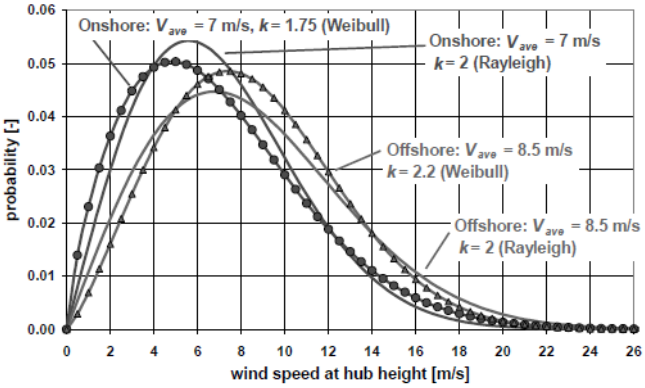

Figure 2.3: Wind speed distributions for typical sites onshore (U_{ave} = 7 m/s) and offshore (U_{ave} = 8.5 m/s) (solid: Rayleigh distribution, solid with markers: Weibull distribution) (Kuehn, 2001).

Wind speed data is usually derived from a value given at 10 meters above the sea level. The wind shear profile (fig. 2.4) is required to translate the wind speed up to the hub height (Fischer et al. 2010). Therefore, the power law (Equation 2.1 is used for scaling as it is independent of surface roughness).

$$U(h) = U(h_{ref})(\frac{h}{h_{ref}})^{\alpha} \tag{2.1}$$

Where h is the height to which the wind speed is scaled, in this case hub height, h_{ref} is the reference height and α is 0.12 for offshore locations (DNV-GL, 2010).

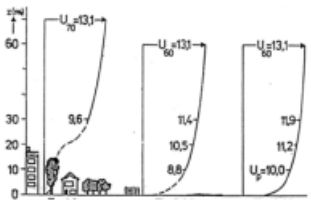

Figure 2.4: Schematic depiction of the wind shear effect and influence of surface roughness Van Der Ploeg, 2021.

The total force generated by the wind consists of four main thrust or drag components, namely, rotor thrust or drag, tower and dry monopile drag, nacelle drag, platform drag (Liu, 2021). In this study the drag force on the platform is considered negligible with respect to the other forcing components and is therefore not included in the design process (except for specific conditions mentioned in 2.3). Hence, total wind forcing can be found with Equation 2.2 .

$$F_{thrust} = \frac{1}{2}\rho_{air} C_t A_{swept} u_{wind}^2 \tag{2.2}$$

Here, A_{swept} is the swept rotor area during power production, u_{wind} is the occurring wind speed, given by the vertical wind profiles in fig. 2.4.

In addition to the mean wind speed, the turbulence component of the wind speed is included based on the Kaimal spectrum. The Kaimal spectrum is a frequency domain representation of the turbulence intensity. Using an inverse fourier transform, the turbulent wind speed component can be found and added to the wind force calculation (Arany et al. 2017). This makes it so that eq. 2.2 becomes eq. 2.3.

$$F_{thrust} = \frac{1}{2}\rho_{air} C_t A_{swept} (u_{wind} + u_{turb})^2 \tag{2.3}$$

Where u_{turb}, is the turbulent wind speed component at a given u_{wind}. The normal turbulence model for extreme loads was set to the characteristic ambient turbulence intensity at the site (DNV-GL, 2016).

According to DNV-GL, the characteristic values of the loads shall be determined by a statistical analysis of the extreme loading that occurs for normal design situations and shall correspond to the value corresponding to a 50-year return period, based on load extrapolation methods, considering the applied wind speed distribution and the corresponding turbulence model as either normal turbulence model (NTM) or the extreme turbulence model (ETM).

2.2.2. Wave data

In addition to wind loads, the wave loads on a wind turbine monopile foundation are primarily caused by the water particle velocities and pressures induced by the waves (Kuehn, 2001). Based on the site characteristics, the nature of the wave loads can be predicted using the significant wave height and wave period.

The force acting on a body (e.g., a vertical circular cylinder), defined by depth parameter D/L, wave steepness H/L, and the diffraction parameter D/L, may be written as $\frac{F}{(\rho g H D^2)} = f(\frac{d}{L}, \frac{H}{L}, \frac{D}{L})$, which for a given structure located at a given depth ($\frac{d}{L}$), subjected to infinite number of waves of relatively small steepness ($\frac{H}{L}$), as in waves described by the linear wave theory Figure 2.5, the normalized force may be approximated by $\frac{F}{(\rho g H D^2)} = f(\frac{D}{L})$ (Sarpkaya, 2010).

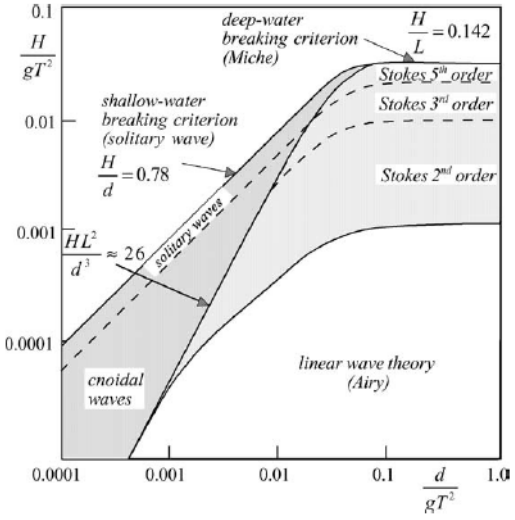

Figure 2.5: Ranges of applicability of different wave theories (Holthuijsen, 2010)

The decomposition of this force by using this criteria to select an appropriate wave theory is done by the use of the linearized Morison equation (2.4). Assuming the structure to remain stationary, considering the wave propagated in space and the time-dependent hydrodynamic force on all elements. The calculated forces are to be incorporated into the equation of motion of the structure, together with the appropriate mass, stiffness, and damping characteristics, to predict the time-dependent response(Sarpkaya, 2010).

$$F(t) = \frac{\pi}{4}\rho_w C_M D^2 \dot{u}(t) + \frac{1}{2}\rho_w C_D D u(t)|u(t)| \tag{2.4}$$

Hydrodynamic forcing is a combination of drag and inertia forces and can be calculated using equations 2.5 and 2.6:

$$F_D = \frac{\pi}{4}\rho_w C_M D_P^2 \dot{u}(t) \tag{2.5}$$

$$F_I = \frac{1}{2}\rho_w C_D D_P u(t)|u(t)| \tag{2.6}$$

Where C_M is the inertia coefficient C_D Hydrodynamic drag coefficient, ρ_w the sea water density and D_P the monopile diameter. $u(t)$ and $\dot{u}(t)$ are the water particle velocity and acceleration respectively which are obtained using airy wave theory (Sarpkaya, 2010),(Holthuijsen, 2010).

The drag coefficient consists of a roughness related part, C_{DS}, factored by a Keulegan-Carpenter number related wake amplification factor, $\psi(KC)$, which results in a drag coefficient given in eq. 2.7.

$$C_D = C_{DS}(\Delta)\psi(KC) \tag{2.7}$$

For high Reynolds numbers ($Re \geq 10^6$), which are the applicable conditions here, the roughness dependent part is given by eq. 2.8:

$$C_{DS}(\Delta) = \begin{cases} 0.65; \Delta \leq 10^{-4} & \text{(smooth)} \\ \frac{29}{4}\Delta \log_{10}(\Delta)/20; 10^{-4} \leq \Delta \leq 10^{-2} \\ 1.05; \Delta \geq 10^{-2} & \text{(rough)} \end{cases} \tag{2.8}$$

Since painted steel is considered to be smooth(DNV-GL, 2007), a surface roughness of $C_{DS} = 0.65$ is used. With D as the monopile diameter. The wake amplification factor can be estimated from Figure 2.6, where the Keulegan-Carpenter number is given by eq. 2.9.

$$KC = \frac{u_{max} T}{D_P} \tag{2.9}$$

u_{max}: maximum particle velocity at the mean water level (MWL)
D_P: monopile diameter
T: wave period

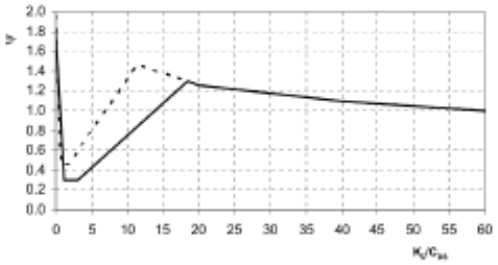

Figure 2.6: Wake amplification factor ψ as function of KC-number for smooth (C_{DS} 0.65 - solid line) and rough (C_{DS} = dotted line) (DNV-GL, 2010).

For $KC < 3$, according to potential theory, $C_m = 2.0$. For $KC > 3$, the inertia coefficient is given by eq. 2.10.

$$C_m = \max(2.0 - 0.044(KC - 3), 1.6 - (C_{DS} - 0.65)) \tag{2.10}$$

To create a clear estimate of the wave induced vibrations on a structure, the time series data from the location of interest to the frequency domain by constructing the JONSWAP spectrum according to

DNV-GL guidelines (K. Hasselmann et al. 1975), (DNV-GL, 2016). The significant wave height and the peak wave period are required as an input to create the JONSWAP spectrum (DNV-GL, 2010), which will be discussed in detail in section 3.4.

The surface profile in the vicinity of the structure is composed from wave trains and the kinematics of the water particles is determined entirely from the motion of the water surface vertically above as can be seen in Figure 2.7. The wave velocity is depth dependent and decays as the water depth increases according to eq. 2.11 for deep waters.

$$u_{wave} = \zeta \omega e^{kz} \tag{2.11}$$

ζ: Wave crest height

ω: Wave frequency (found with eq. 2.12)

k: Wave number (found with eq. 2.13)

z: depth from free surface

$$\omega = \frac{2\pi}{T} \tag{2.12}$$

$$k = \frac{4\pi^2}{gT^2} \tag{2.13}$$

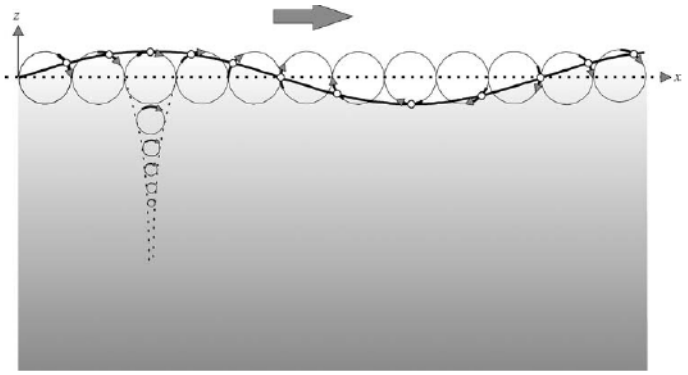

Figure 2.7: Orbital motion of water particles under a harmonic wave in deep water (Holthuijsen, 2010).

The wave crest height of a given frequency can be found performing an inverse Fourier transform of the JONSWAP spectrum. For this research, this was done for a random surface elevation time series at all time steps, which is then used to calculate the time dependent wave load profile(developed in detail in section 3.4). An additional aspect to be considered in the water particle velocity is the wave current velocity. However, because of the focus on dynamic loads for the study, the current was considered negligible.

2.3. Load cases

Understanding how the wind turbine's forces impact a monopile foundation is essential in its design process. The aforementioned environmental phenomena are usually described by physical values of variable nature (DNV-GL, 2010). Different combinations of environmental conditions will occur during the lifetime of an OWT. Hence, a good assesment of the environmental conditions they are likely to encounter during their operational lifetime is necessary.

The dynamics of the wind turbine differ for power production and parked conditions. Hence, both cases should be assessed in order to find the critical load combination. The requirements of several design load cases (DLCs) are listed in DNVGL-ST-0437DNV-GL, 2016. The following subsections will elaborate on which DLCs are assessed for the power production and parked conditions and discusses assumptions.

A design load case refers to a specific scenario or condition under which the turbine's structural components and supporting systems are analyzed to ensure that they can withstand the forces and

environmental conditions they are likely to encounter during their operational lifetime. In order to assess whether the stresses in the structure are within allowable limits, a series of Design Load Cases (DLCs) is specified in DNVGLST0437 (DNV-GL, 2016). These DLCs, which are often associated with the highest stresses in the structure, are selected. It should be noted that the load cases will only be introduced in this Section, i.e. all forces acting on the structure will be identified, but not yet calculated.

2.3.1. Power production

Since the forces and power output of the turbine vary at different wind speeds, it's important to determine the point where the forces on the rotor or structure are greatest in order to guide the design process. This operational regime can be divided into three segments based on the incoming wind velocity (U_w) as follows:

- $$U_{in} \leq U_w \leq U_{rated} \tag{2.14}$$
- $$U_{rated} \leq U_w \leq U_{out} \tag{2.15}$$
- $$U_{out} < U_w \tag{2.16}$$

Where U_{in} is the minimum wind speed required for the blades to start power production, U_{rated}, the rated power production wind speed for which the WT is designed for and U_{out} refers to the upper theshold for the wind velocity where the blades will pitch and feather reducing the aerodynamic efficiency. In figure 2.8 the relation between operational sectors, power, thrust(also referred to as lift force) and torque can be seen.

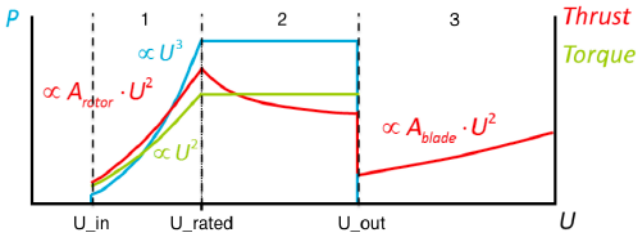

Figure 2.8: Operational regimes of WT and their relation to thrust, torque and power curves. (Zaaijer, 2006).

The force on the blades can be divided in thrust force and drag force as seen in figure 2.9. Where the forcing is proportional to the wind velocity squared times the rotor swept area (eq. 2.17). The performance characteristics of the wind turbine are given by its power (C_P) and thrust (C_T) coefficients. The power coefficient represents the power output resulting from the energy taken from the wind and the thrust coefficient accounts for the developed thrust force on the rotor blades (DNV-GL, 2010).

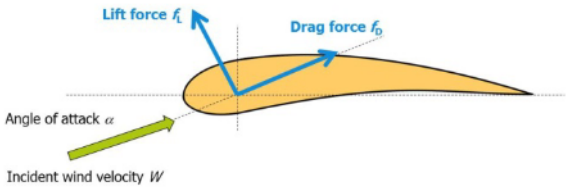

Figure 2.9: Drag and lift forces on wind turbine blades.

$$F_{thrust} = \frac{1}{2}\rho_{air} C_t A_{swept} u_{wind}^2 \tag{2.17}$$

The aerodynamic power coefficients vary depending on the wind speed and the blade angle which tilts during power production to stay constant. During power production load cases, the value thrust coefficient stays constant at a value of $C_T = 0.804$(2.10). Since the lift force is significantly higher than the drag force during power production, drag can be neglected when considering wind loading in these operational modes. Figure 2.11 shows how different shapes of airfoils relate in terms of drag and lift coefficients. From this relation it's shown that for a lift coefficient of zero, the drag coefficient corresponds to approximately $C_D = 0.018$ (fig. 2.11). The drag force is considered when then the wind exceeds the cut-out wind speed, the blades pitch to feather and the only force present is the drag force. Thus, it should be considered in the environmental load forcing.

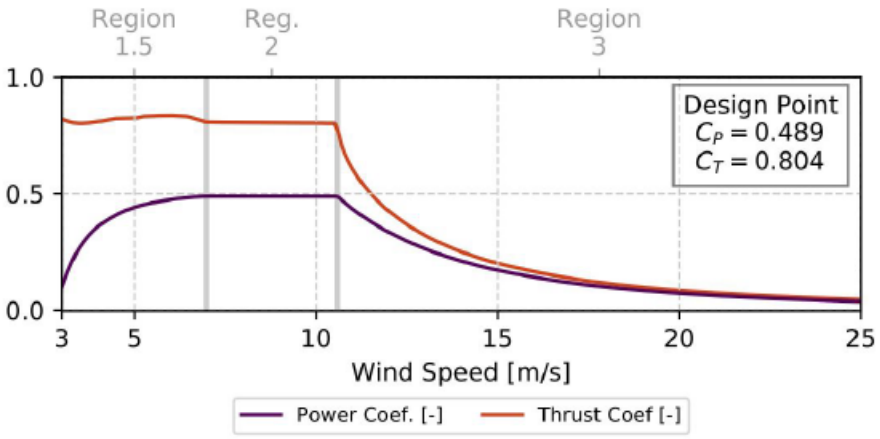

Figure 2.10: Aerodynamic performance coefficients. (Liu, 2021).

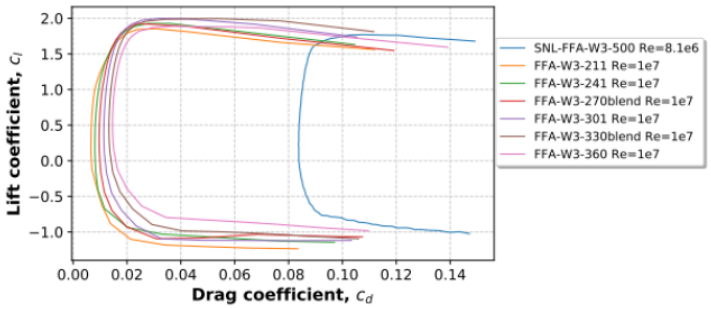

Figure 2.11: Airfoil family drag coefficients. (Van Der Ploeg, 2021).

The loading due to the rotation of the blades is frequency based and depends on the rotor and the blade passing frequency and are called 1P and 3P frequency respectively and are straight forward to calculate (eq. 2.18 and eq. 2.19) once the maximum and minimum rated rpm are known.

$$0.90\frac{\Omega_{min}}{60} \leq f_{1P} \leq 1.10\frac{\Omega_{max}}{60} \tag{2.18}$$

$$0.90\frac{3\Omega_{min}}{60} \leq f_{3P} \leq 1.10\frac{3\Omega_{max}}{60} \tag{2.19}$$

The dynamics of the wind turbine differ for power production and parked condition (Liu, 2021). The controller of the wind turbine pitches the blades for varying wind speeds to achieve optimal efficiency. Until the wind speed reaches its rated value. The turbine will be in 'power production mode' between the cut-in and cut-out wind speed and will deliver its full power potential between the rated and cut-out wind speed shown by the light blue line in Figure 2.8.

The aerodynamic damping of a wind turbine depends on whether there is wind or not, whether the turbine is in power production or at stand-still, and whether the wind is aligned or misaligned with other loads such as wave loads. Unless correct assumptions can be made about the aerodynamic damping of the wind turbine in accordance with the actual status of the wind loading regime, separate determination of the load effect due to wave load alone to be used with the partial safety factor format may not be feasible. In a structural time domain analysis of the turbine subjected concurrently to both wind and wave loading, the aerodynamic damping of the turbine will come out right since the wind loading is included, and the resulting combined load effect, usually obtained by simulations in the time domain, form the basis for interpretation of the characteristic combined load effect.

2.3.2. Parked conditions

When wind speeds at the hub height exceed the cut-out wind speed of the wind turbine, the power production stops and the system pitches the blades to feather to minimize their forcing. This situation is called 'the parked condition'. When the wind speeds at the hub height surpass the wind turbine's cut-out speed, the power generation ceases, and the system adjusts the blades' angle such that the blade lift coefficient converges to 0 and the rotor stops rotating (Van Der Ploeg, 2021), a state referred to as 'parked condition'. For this loading condition, a study DLC 6.2(DNV-GL, 2016r) is conducted. This load case states that the parked turbine should be loaded by a 50-year return period wind and wave conditions.

In order to asses the structural reliability of the monopile structure for this study, a focus is made on the design loads that involve fatigue damage assesment. Hence, the load cases in table 2.3 were chosen for an extensive analysis of the dynamics of the structure by time domain simmulations with the given site specific wind and wave conditions.

Table 2.3: Design load cases chosen for the study.

Design situation	DLC	Wind condition	Waves	Type of analysis
Power production	1.1	NTM ($V_{in} < V_{hub} < Vout$)	NSS	U
Power production	1.2	NTM ($V_{in} < V_{hub} < Vout$)	NSS	F/U
Parked condition	6.4	NTM ($V_{hub} < V_{in}$ and $Vout < V_{hub} < 0.7V_{ref}$)	NSS	F/U
Parked condition	7.2	NTM ($V_{hub} < Vout$)	NSS	F/U

2.3.3. Probability scatter diagrams

Once the DLCs of interest have been defined, a correlation with the probability scatter diagrams can be made in order to relate the load cases with the probability of occurrance of a given load case. Joint probabilities for extreme gust and extreme design waves can be derived assuming Gaussian wind turbulence and Rayleigh distributed waves. On this rationale Germanischer Lloyd recommends extreme load cases associated with either the most probable extreme wave or wind gust for a given sea state (DNV-GL, 2016). However, according to Kuehn, 2001, it is known that only two thirds of the maxima are higher than the most probable extreme value and only a probabilistic description is accurate.

A good start for this is to analyze probability scatter diagrams at a given location. Using the AGROSS data base, the probability of occurance of a combination of wind (speed) and waves (wave height and period) can be found and expressed in a 3D scatter diagram. Each combination of these three parameters is called a Sea State. In the present example a three-dimensional scatter diagram (fig. D.1) is constructed for classes of ΔHs = 1 m, ΔTz = 1 s and ΔV = 2 m/s by evaluation of the long-term AGROSS database (Appendix A). From the theoretically possible 260 combinations of the 7 wave height, 22 wave period and 21 wind speed classes only 67 sea states have a probability of 0.5% and higher (fig. D.1). Because of the nature of the environmental loading, the sea states should be interpreted in both

in the form of frequencies ranges and later as stresses and moments, which will be developed in detail in section 3.4.

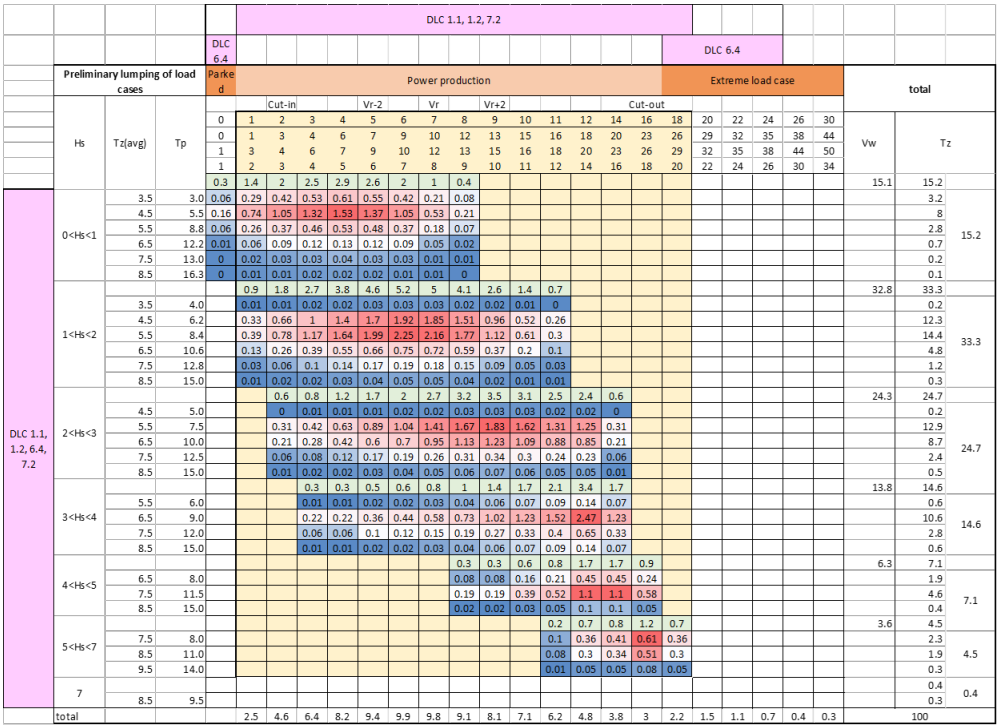

Figure 2.12: 3D scatter diagram with corresponding load cases following DNV-GL, 2016.

2.4. Soil conditions

As mentioned in section 2.2, the loads acting on the tower are transferred to the foundation through the monopile. The design basis of the foundation takes into account the predicted environmental loads and the geotechnical properties of the seabed. The foundation must be designed to withstand the dynamic loads caused by the wind and the waves, as well as any static loads from the weight of the tower and blades. The ground profile, including the soil type and strength, can also play a significant role in the design of a monopile. The geotechnical data of the seabed can be used to determine the appropriate type and length of pile required to withstand the forces exerted on the structure.

Depending on the purpose of the study, different ways of modelling the soil can be applied. When not focusing on the soil pile interaction, the soil can be modelled as a set of springs (rotational and lateral) at the seabed with the combined characteristics of the soil resistance (Zaaijer, 2006, Arany et al. 2017). Since the study is focused on the comparison between a conventional monopile against one with perforations, the soil modelling will be simplified to lateral springs at the seabed. The soil characteristics of the site can be found on table 3.1 and were retrieved from Van Der Ploeg, 2021, were a linear in-homogeneous dense sand soil is assumed.

Table 2.4: Design soil parameters. (Van Der Ploeg, 2021)

Feature	Quantity	unit
Internal friction angle	$\phi_{soil} = 35$	∘
Soil-Pile friction angle	$\delta = 30$	∘
Limit skin friction	$f = 95.7$	kPa
Bearing factor	$N_q = 40$	-
Limiting end bearing	$q = 9.6$	MPa
Submerged unit weight	$\gamma' = 10$	kN/m^3

Following Van Der Ploeg, 2021, an estimation of the soil stiffness as lateral springs of stiffness E_{py} can be

made following ISO guidelines(**ISO**). Where an estimate of the embedded length is made at four times the bottom diameter. The soil foundation plays an important role in determining the natural frequency of the system and can be determined following eq. 2.20.

$$p = A \cdot p_r \cdot \tanh\left(K \cdot \frac{X}{A \cdot p_r} \cdot y\right) \tag{2.20}$$

$$p_r = \min\{p_{us}, p_{ud}\} \tag{2.21}$$

$$p_{us} = (C1 \cdot X + C2 \cdot D) \cdot \gamma' \cdot X \tag{2.22}$$

$$p_{ud} = C3 \cdot D \cdot \gamma' \cdot X \tag{2.23}$$

$$E_{py} = \frac{p}{y} \tag{2.24}$$

Where:
p_r = respective lateral capacity
γ'= soil submerged unit weight
X = depth below the mudline
C1, C2, C3 = dimensionless coefficients as specified in the ISO and API guidelines
D = pile diameter
A = static or dynamic correction factor
k = rate of increase of the modulus of subgrade reaction
y = lateral pile displacement at depth X

2.5. Natural frequency

Natural frequencies of the support structure are very important as they determine the dynamic behaviour of the offshore wind turbine. If the frequency of excitation is near a natural frequency, resonance occurs and the resulting response will be larger than in the quasi-static case. This leads to higher stresses in the support structure and, more importantly to higher stress ranges, an unfavourable situation with respect to the fatigue life of the offshore wind turbine. Therefore it is important to ensure that the excitation frequencies with high energy levels do not coincide with a natural frequency of the support structure (Fischer et al. 2010).

Once they are known, a mapping of the frequencies of load excitation can be done. In Figure 2.13, regions of structural integrity of the reference 15MW turbine used in (Van Der Ploeg, 2021) can be seen, namely the soft-soft region below the 1P frequency block, soft-stiff region between the 1P and 3P frequency block and stiff-stiff regions above the 3P frequency block. It is common practice to set the target frequency between the 1P and 3P zones (soft-stiff regime) (Arany et al. 2017). Thus, by assessing the frequency diagrams of the 15MW reference turbine and taking into account the manufacturability constraints, a system target frequency of 0.18 Hz is selected.

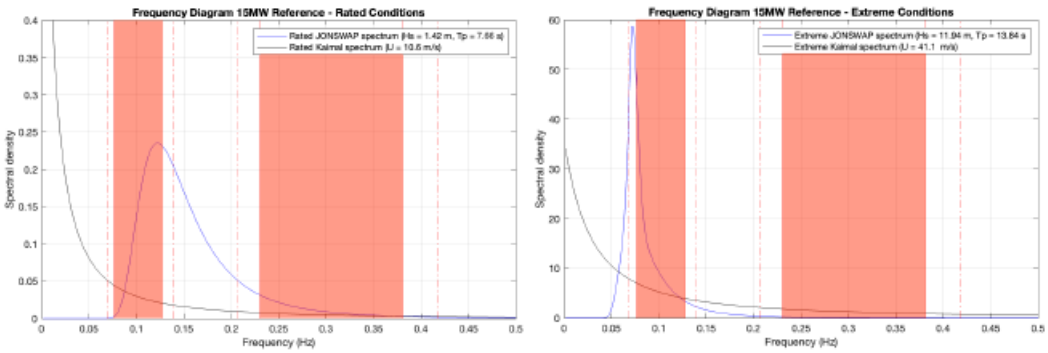

Figure 2.13: 15MW reference turbine frequency diagram for rated (left) and extreme (right) conditions. (Van Der Ploeg, 2021).

2.6. Fluid-structure interaction models

A coupled wave structure interaction model is a type of mathematical model that is used to simulate the interaction between a wave and an offshore structure. It is a system of equations that takes into account the hydrodynamic forces exerted by the waves on the structure, the structural response of the structure, and the interaction between the two (Kuehn, 2001). The model is used to predict the dynamic behavior of the structure in a given environment.

When analyzing the fatigue life of a structure, it is important to consider the deflection and dynamic response of the structure because they can have a significant contribution to the accumulation of fatigue damage.

Previous research on the feasibility of perforated monopiles in deep water regimes stated used a rigid model for the ULS and FLS load assessment (Van Der Ploeg, 2021). Hence, this thesis aims to add depth in the understanding of the response of the structure to the most occurring sea states at the chosen offshore location by assessing and modelling a dynamic (one-way coupled) fluid structure interaction model. Therefor, the differences between a rigid model and a one-way coupled fluid-structure interaction (FSI) model should be understood.

In a rigid model, the solid object (structure) is treated as completely rigid and immovable. It does not deform or interact with the fluid in any way. The fluid flow is computed independently of the solid object, without considering any feedback from the structure. This simplifies the simulation significantly and is often used in cases where the deformation of the structure is negligible or can be ignored.

In a one-way coupled FSI model, there is interaction between the fluid and the structure, but it is considered a one-way interaction. The fluid exerts forces and pressures on the structure, causing it to deform or move. However, the deformation or motion of the structure does not significantly affect the fluid flow (fig. 2.14).

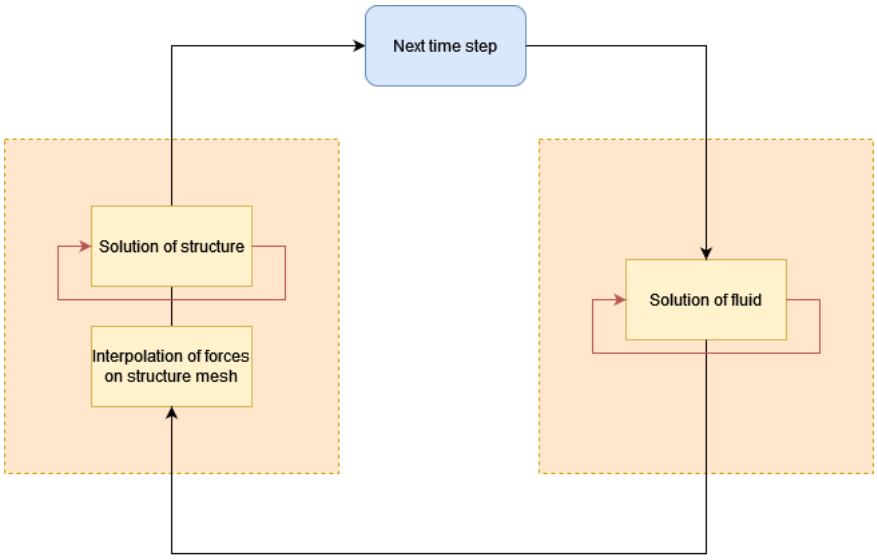

Figure 2.14: One-way coupled FSI model work-flow.

In situations where the interaction between the fluid and structure is significant and both influence each other, a two-way coupled FSI model would be used. In a two-way coupled FSI model, the deformation of the structure and the fluid flow are solved simultaneously, taking into account their mutual influence. This approach is more computationally intensive but provides a more accurate representation of real-world FSI problems.

For the purpose of this study The submerged part of such structures is relatively stiff in comparison to the dry section and structural velocities of the wet members are low (Kuehn, 2001). So the

hydrodynamic lift and drag forces, which depend quadratically on the velocities (Holthuijsen, 2010), are also low and any viscous hydrodynamic damping is negligible.

Consequently, the hydrodynamic drag forces are calculated based upon the Morison equation written in absolute water particle velocities. It is worth noting, however, the results of Van Der Ploeg, 2021, which indicated a phase shift from the resulting inertia forces to drag forces as can be seen in fig. **??**. This was considered out of the scope of the research and will be addressed in the discussion.

2.7. Modelling assumptions

In the context of a dynamic fluid structure interaction system, where a comparative Finite Element Analysis of two monopile foundation structures is made, the primary objective of this study is to understand and analyze the response of a perforated monopile foundation in comparison to a reference monopile, with a specific emphasis on fatigue loads.

After gathering the necessary input data, the recommended sequence of calculation steps, as outlined in Arany et al. 2017, are presented in Figure 2.15, which illustrates the procedural flow for conducting a structural analysis. Each of these steps will be elaborated upon in detail in Chapter 3.

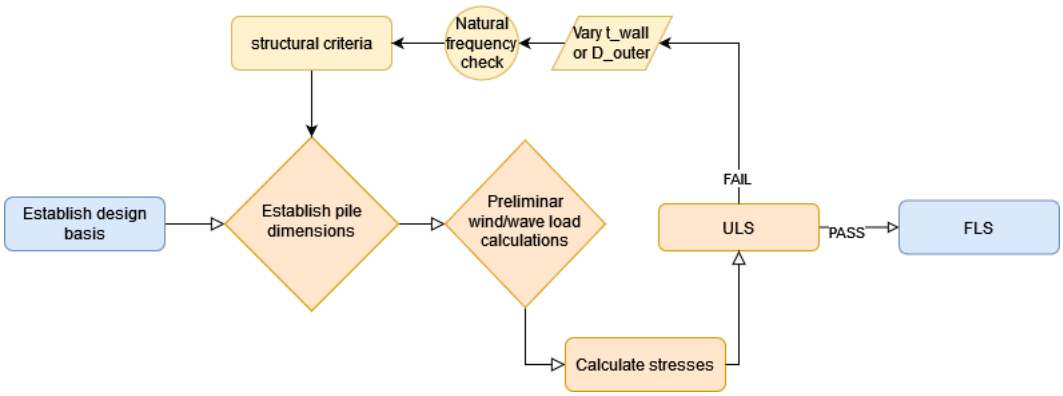

Figure 2.15: Standard design procedure for MP foundation design.

In the context of a dynamic fluid-structure interaction (FSI) system, several modelling assumptions have been made to streamline the analysis and focus on specific aspects of interest. These assumptions are necessary to simplify the problem but should be critically evaluated for their relevance and potential impact on the study's outcomes.

Super structure mass:

Treating the RNA as a point mass simplifies calculations but neglects the potential dynamic interactions between the RNA, tower and the foundation caused by gust slicing, wind shear, mass imbalance, yaw misalignment, tower shadow and blade pitch errors DNV-GL, 2010. Additionally, the torsional moments that are applied by the blades on the top mass and aerodynamic damping as a function of the first order static moment of inertia of the chord along the blade (Liu, 2021).

Furthermore, the wind wave misalignment leads to different results in terms of aerodynamic damping. In reality, the aerodynamic damping is a highly variable parameter which depends on a large set of internal and external parameters such as the wind climate, the pitch controller and rotational velocity. Also, due to the relatively low inherent damping of cross-wind tower vibrations, the cross-wind vibrations caused by wave loading misaligned by wind can decrease the fatigue life of the structure.

Geometry and feasibility of design:

The assumption that geometry and masses are derived from structures designed for similar conditions is practical but may not capture unique design features or site-specific requirements.

In practice, adding perforations to the splash zone of a monopile support stucture means that this area is susceptible to high stresses that could be caused by impact loads. These include the support system of the monopile on the vessel and the forces exherted on the structure while driving it into the soil.

While it's essential to consider fabrication, transportation, and installation constraints, this assumption may limit the exploration of innovative design solutions. Hence, for this study, it is assumed that the necessary equipment for the fabrication, transportation and installation of the monopile is suitable and readily available for this model.

Damping ratio:
The choice of a 3% damping ratio is a simplification and should be discussed in terms of its potential effect on the dynamic response of the structures. For dynamic systems, several assumptions in terms of damping should be made since including all the aspects that contribute to the total damping of the system can become a cumbersome task Kuehn, 2001.

Uniform soil conditions:
Uniform soil conditions simplify the analysis but may not represent real-world variations in soil properties. While for this model a uniform soil condition was assumed, soil types and the penetration depth are both factors that affect the modelling of the soil as distributed springs along the penetration depth of the monopile foundation (Arany et al. 2017).

The procedure explained in section 3.1 was carried out and compared to the values used by (Van Der Ploeg, 2021) for homogeneous sand. This resulted in a constant spring stiffness below the mudline. However, the effects of soil damping are not accounted for fully which could have an effect on the frequencies excited by fatigue loading. (Kuehn, 2001).

Wave loading:
For this study the forces were applied as a point load on cans (cylinders) with a 5 meter interval for all load cases. Additionaly, since the effect of braking waves above MSL is highly non-linear (Holthuijsen, 2010), the loads above mean sea level were applied assuming a submerged structure. Thus, the circular motion of particles as stated in section 2.2 was assumed for both the submerged area and the area with perforations above mean sea level.

The one way coupled FSI model approach is used when the structure's impact on the fluid is minimal, or when the computational cost of solving a fully coupled FSI model is too high. As a result, the incoming loads are not modified by the response of the structure. However, previous research showed potential shift in inertial loads towards the drag forces due to perforations imply that the hydrodynamic drag component could improve the performance of the perforated monopiles Van Der Ploeg, 2021.

Negligible influence from subsystems:
Marine growth, electric cables, ladders and other piping installations that the monopile could have below MSL are neglected for this study. The representative diameters of the subsystems are considerably smaller than the rest of the structure, instead a 10% added mass is considered for the submerged segment of the monopile.

Site-specific parameters:
It is important to consider site-specific parameters, met-ocean conditions, and other external factors when applying the research findings to practical wind farm projects. The study used a representative 80 meter water depth offshore location which is not necessarily representative of all offshore deep water locations. Hence, this study's results may limit the transferability of to different wind farm locations.

Turbine availability:
The simulations and fatigue load analysis should consider the turbine wind resource availability. The study considers an availability of 100% based on the probability scatter diagram (fig. D.1) which in reality does not happen (Kuehn, 2001). Since no data is available for wind turbine parks in deep water regimes, this parameter is left out of the consideration for the fatigue load assessment.

In conclusion, while modelling assumptions are necessary to focus the results on the area of interest, namely, the stress concentrations around the splash zone. It is important to recognize that these assumptions should be addressed in further research to get a more precise idea of the viability of monopile foundations in deep water regimes.

2.8. Tool selection

Throughout the research, several tools are used from different softwares. The reason for the selection of these are a combination of availability of resources, applicability and the student's previous knowledge gained during course work. A short reasoning behind the selection of the tools is given below accompanied by what parts of the research they will be used for.

2.8.1. Excel

Microsoft's Excel is used throughout the project to organize data and establish the main monopile design framework. This software was selected as the amount of input parameters is very large and one can quickly lose overview. Excel excels as a tool for data organization and visualization; however, for intricate data processing and complex calculations, the project leverages other specialized software. Excel's role primarily revolves around storing and presenting outputs, contributing to the comprehensibility of research outcomes.

2.8.2. Python

Python is a versatile and open-source coding environment essential for executing repetitive numerical calculations based on DNV-GL standardsDNV-GL, 2010. With the use of python scripting, the wind and wave spectra corresponding to each sea state is calculated. This computation generates a time series of randomized wave amplitudes, forming the bedrock for subsequent wave load calculations grounded in airy wave theory. Additionally, the information calculated can be plotted in intermediate steps. This not only enriches comprehension but also bolsters credibility by validating outputs against the theoretical background and estimates gathered from manual calculations.

2.8.3. Ansys(Space Claim/Mechanical)

The Ansys suite, particularly the Space Claim and Mechanical modules, play a pivotal role in the research by providing powerful finite element analysis capabilities. Space Claim is employed for efficient 3D solid modeling and geometry manipulation, allowing for the creation of an accurate monopile models. Meanwhile, the Mechanical module enables structural simulations to be conducted on said models. This tool was chosen due to its readily available licnese and advanced simulation features, enabling the exploration of various loading conditions, material properties, and structural responses. The interaction between soil-pile interaction and complex wave loading can be analyzed through these simulations, offering a comprehensive understanding of the monopile's behavior under real-world conditions.

2.8.4. Matlab (Vibrationdata toolbox)

Matlab, coupled with the Vibrationdata toolbox, aids in addressing the post-processing of the dynamic aspects of the monopile's stress time history data for each sea state at the places where the stresses are the highest. The toolbox aids in the analysis and processing of vibration data, enabling the investigation of structural responses to dynamic loads like wind-induced vibrations and wave-induced oscillations. By utilizing Matlab, the time-domain characteristics of the monopile's dynamic behavior can be studied, offering insights into potential resonance issues and structural integrity concerns. The toolbox provides specialized functions for such as rainflow counting which alignins with the research's need to evaluate the monopile's vibration response under varying conditions.

3

FEM Modelling and Simmulation results

Comparing stresses obtained from Finite Element Analysis (FEM) between two structures involves a systematic approach to analyze and interpret the results. This chapter contains the steps taken for the creation of FEM models using Ansys.

Starting from the monopile dimentions stated in Chapter 2, the dimensions of the monopile above the mudline are shown in fig. 3.1. The following analysis was based on these dimensions and were adjusted to work for the monopile as can be seen below:

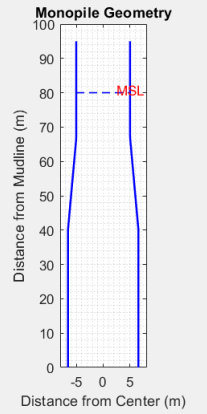

Figure 3.1: Reference MP geometry.

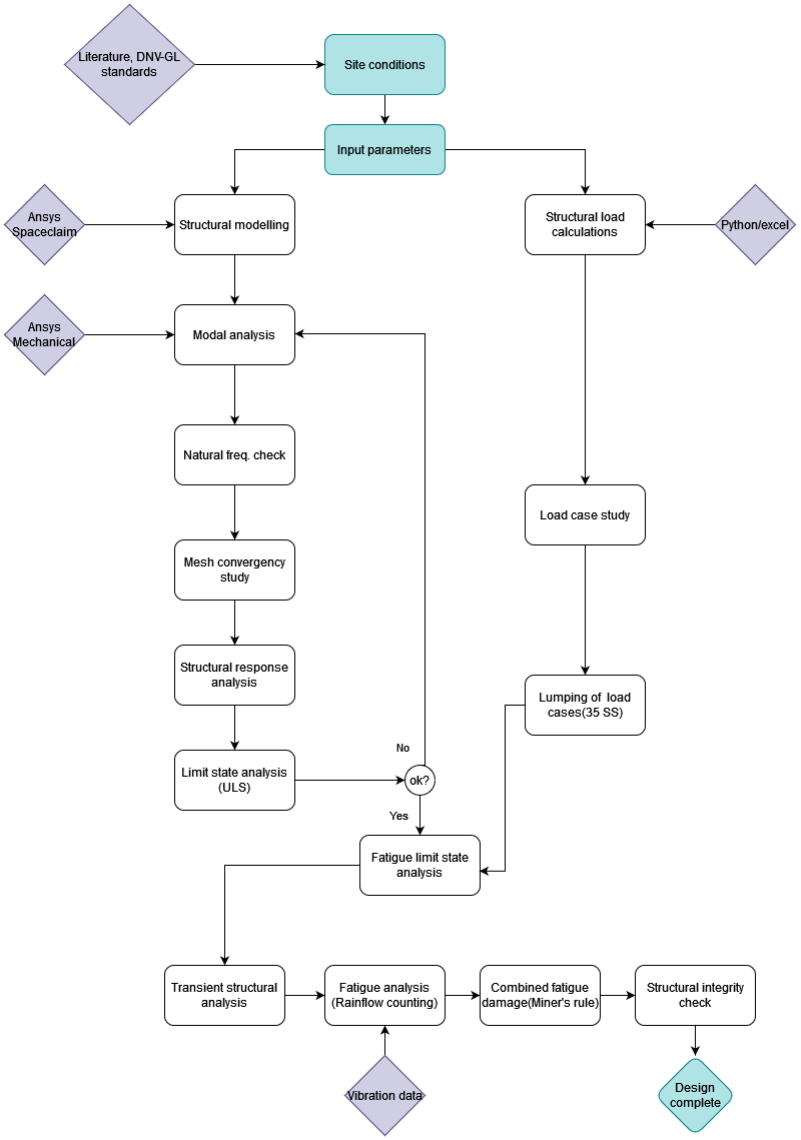

Figure 3.2: Underlying methodology to assess the potential of monopiles in deep water.

3.1. Geometry definition

After gathering the dimensions for the monopile as stated in the previous chapter, a structural model can be made. In the process of creating Finite Element Analysis (FEA) models for monopile structures in ANSYS starts with a sketch of the dimensions of the monopile (fig. 3.3) with which a crucial decision arises: whether to model the monopile as a shell or as a solid. This choice significantly influences the accuracy, computational efficiency, and applicability of the analysis.

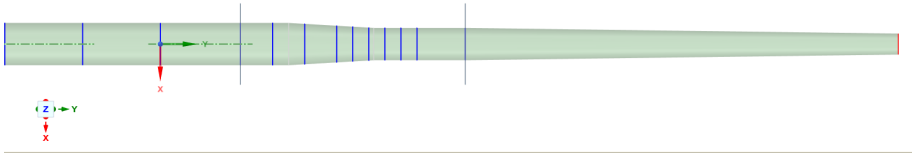

Figure 3.3: Ref. MP: Ansys Space Claim model.

For this research, the structure will be exposed to a vast amount of sea states and the objective is to get a better idea on where the resulting stresses (resulting from each sea state) are located for both the

reference monopile and the perforated monopile. Hence, the modelling of the monopile as a shell was made considering:

- The monopile is characterized by large dimensions in one direction and relatively small thickness, shell elements are particularly suitable for capturing bending behavior without unnecessary computational burden.
- Shell elements require fewer nodes and degrees of freedom compared to solid elements, which often results in faster computations.

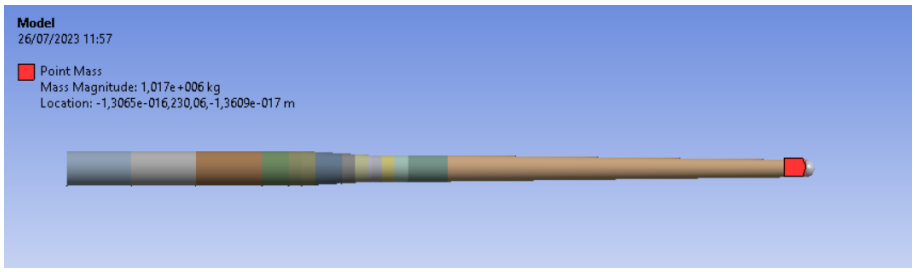

Figure 3.4: Ref. MP: Ansys Mechanical set-up.

Then, the structure is divided in segments every 5 meters below MSL to consider the lump loads acting on it. Below the mudline of the monopile a segmentation was made to take into account the boundary conditions (fig.3.4). Additionally, the shell surface element orientations are established in order ensure the thickness parameters of the monopile extrude correctly and the material properties are set as structural steel (S355ML graded steel) with the following characteristics:

Table 3.1: Structural parameters. (Van Der Ploeg, 2021)

Feature	Quantity	unit
Density	7850	kg/m^3
Young's Modulus	210	GPa
Poisson's ratio	0.3	-
Tensile yield strength	250	MPa
Compressive yield strength	250	MPa

3.2. Natural frequency validation

At this phase, the soil stiffness is added as an elastic support according to 2.2. The RNA is modelled as a point mass at the top of the tower. Then, a preliminary meshing is done and a modal analysis was carried out to verify the natural frequency matched the target natural frequency. The natural frequency of a dynamically loaded system is important calculate accurately since it will determine the loading frequencies that can result in significant damage to the structure.

Figure 2.13 shows the forcing components in the shape of a frequency diagram where the power spectral densities of the wind and wave frequencies were assesed based on the Kaimal and JONSWAP spectrums, respectively. As can be seen in fig. 2.13, the target natural frequency should be slightly below the 3P frequency band considering a 10% margin DNV-GL, 2007. In Van Der Ploeg, 2021, the resulting monopile model created for a 80m. water depth has a natural frequency of 0.18Hz which falls within the tolerance considered satisfactory for the present study.
An approximation for the first natural frequency can be made following the Rayleigh stepped tower model (Liu, 2021). The simplified methodology builds on the simple cantilever beam formula to estimate the natural frequency of the by factoring the approximation with suitable design coefficients given in eq. 3.1 (Arany et al. 2017):

$$f_n = C_L C_R C_S f_{FB} \tag{3.1}$$

where:

C_S: Substructure flexibility coefficient C_L: Lateral foundation flexibility coefficient

C_R: Rotational foundation flexibility coefficient f_{FB}: Fixed base first natural frequency

The fixed based natural period in equation 3.1 can be approximated using the Rayleigh stepped tower model (fig. 3.5). This model divides the monopile into segments with representative diameters and wall thickness corresponding to the dimensions of the monopile. By calculating and summing up the mass (eq. 3.2) and the 2nd mass moment of inertia (eq. 3.3) for each segments, an equivalent value for the beam as a whole is obtained.

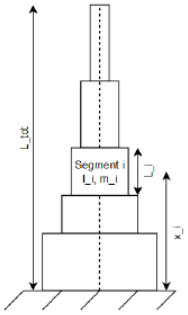

Figure 3.5: Rayleigh stepped tower model. Arany et al. 2017

$$I_{eq} = \frac{\sum_{j=1}^{n} I_j l_j \cos^2(\frac{\pi x_j}{2L})}{L} \tag{3.2}$$

$$m_{eq} = \frac{\sum_{j=1}^{n} m_j l_j (1-\cos^2(\frac{\pi x_j}{2L}))^2}{L} \tag{3.3}$$

where:

I_j: Moment of inertia of segment j [m^4] m_j: Distributed mass of segment j [$\frac{kg}{m}$]

l_j: Segment height [m] x_j: Distance to mudline of segment j [m]

The substructure flexibility coefficient is expressed in terms of two dimentionless parameters, the bending stiffness ratio $\chi = \frac{EI_T}{EI_P}$ (where EI_T is the tower stiffness), and the length ratio $\psi = \frac{L_S}{L}$ Arany et al. 2017. The substructure flexibility coefficient is calculated following eq.3.4:

$$C_S = \sqrt{\frac{1}{1+(1+\psi)^3\chi - \chi}} \tag{3.4}$$

On the other hand, the rotational and lateral coefficients coefficient were found based on the soil properties of the site and account for the foundation stiffness. The foundation flexibility coefficients can be calculated following eq.3.5 and 3.6 Arany et al. 2017:

$$C_R(\eta_L, \eta_R, \eta_{LR}) = 1 - \sqrt{\frac{1}{1+0.5\left(\eta_R - \frac{\eta_{LR}^2}{\eta_L}\right)}} \tag{3.5}$$

$$C_L(\eta_L, \eta_R, \eta_{LR}) = 1 - \sqrt{\frac{1}{1+0.6\left(\eta_L - \frac{\eta_{LR}^2}{\eta_R}\right)}} \tag{3.6}$$

Where η_R, η_{LR} and η_L are non-dimensional stiffnesses which can be calculated following equations 3.7, 3.8 and 3.9 respectively **Poulos and Davis**:

$$\eta_R = \frac{K_R L}{EI_{eq}} \tag{3.7}$$

$$\eta_{LR} = \frac{K_{LR} L}{EI_{eq}} \tag{3.8}$$

$$\eta_L = \frac{K_L L}{EI_{eq}} \tag{3.9}$$

To solve the equations, the soil dependent foundation stiffness K_R,K_{LR} and K_L are required, which, for slender piles in linear in homogenous soils can be calculated following equations 3.10, 3.11 and 3.12 **Poulos and Davis**.

$$K_R = 1.48 n_h^{\frac{1}{5}} (E_P I_P)^{\frac{4}{5}} \tag{3.10}$$

$$K_{LR} = -0.99 n_h^{\frac{2}{5}} (E_P I_P)^{\frac{3}{5}} \tag{3.11}$$

$$K_L = 1.074 n_h^{\frac{3}{5}} (E_P I_P)^{\frac{2}{5}} \tag{3.12}$$

An additional extra step of validation was made by modelling the equivalent beam model as a solid on Ansys Spaceclaim with the same constraints and performing a modal analysis to obtain the first natural frequency (fig.3.6). This showed a difference of 1% from the target natural frequency which was considered sufficient for the present study.

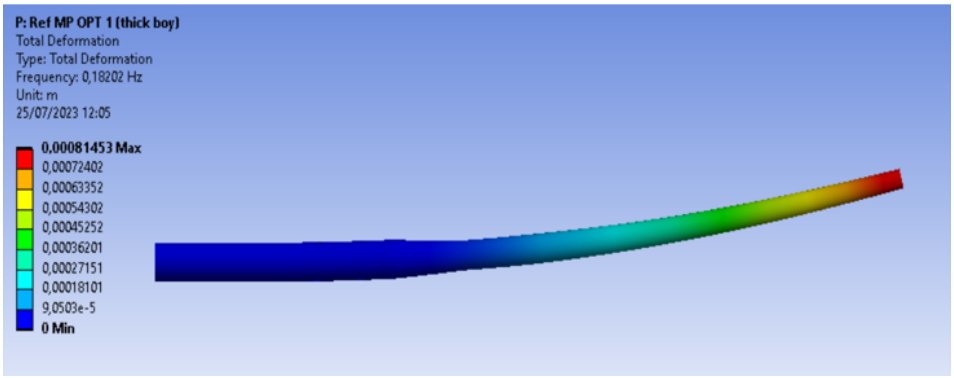

Figure 3.6: Ansys Mechanical, First bending mode result.

3.3. Mesh convergence

Once the natural frequency of the monopile was established, verified and close enough to the design standards. To ensure accurate representation of real-world behavior, a mesh convergence analysis is done with a simple load case by testing different mesh densities to ensure the results are not significantly impacted by mesh refinement. The mesh convergency study consists increasing the resolution of the mesh while maintaining the load constant and until finding a mesh size that converges with respect resulting deformation and stresses. This was done by reducing the mesh size in increments of 1/10 and carrying out the analysis of interest. For the reference monopile this resulted in the following output:

Table 3.2: Mesh convergency study results.

Mesh element size(m)	Number of elements	Deformation (m)
3,04218	2744	1,613E-02
2,70416	3024	1,615E-02
2,36614	3630	1,618E-02
2,02812	4640	1,619E-02
1,6901	5712	1,619E-02
1,35208	8904	1,618E-02
1,01406	16298	1,618E-02
0,84505	26338	1,618E-02

Which showed convergence plotting the maximum deformation on a y-axis against an increasing number of elements (3.7). As a result, a mesh size of 1.35m. was chosen since lower mesh element only led to higher computation time.

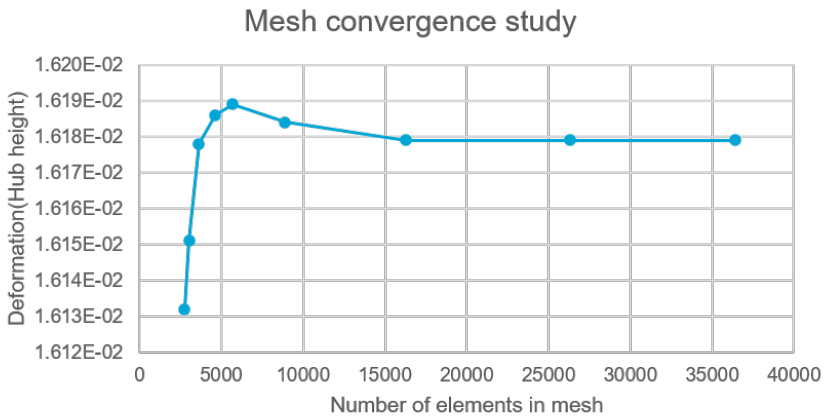

Figure 3.7: Displacement to mesh element size convergence study.

3.4. Structural load simulations

The process of FEM stress response analysis for monopile structures involves creating probability scatter diagrams to represent load variability, conducting preliminary lumping to simplify load distributions, selecting relevant load cases, and simulating transient load signals to comprehensively evaluate the structure's stress behavior under varying conditions.

3.4.1. Load case calculation

Parallel to the set-up of the structural model, the structural loads were generated using python script. Since the environmental loading consist of stochastic values, a code was used to obtain random samples from a probability density function for wave elevations and for turbulence at a given mean wind speed for each sea state during a 10 minute period. The irregular time signals were used as input for the calculation of the wave loads following the equations in 2.3.

For load cases with turbulent wind fields, the total period of load data shall be long enough to ensure statistical reliability of the estimate of the characteristic loads. At least six 10 min stochastic realizations with different turbulent seeds are required for each mean hub-height wind speed used in the simulations (DNV-GL, 2010).

For the generation of the load signals, first a preliminary lumping of load cases based on fig. D.1 in section 2.3 was done for sea stater with a probability of occurrence above 0.05. This resulted in 35 sea states which are shown in detail in Appendix B.

3.4.2. Sample sea state calculation

These load cases represent the most occurring sea states throughout a year and will should be assesed individually in order to carry out the FLS of the structure. Before this, representative sea states for extreme conditions were used to understand the locations of the maximum stresses on the structure. The procedure for the generation of load signals is specific for wind and wave loads because of how their relation to the Pierson Moskovitch (PM) spectrum and the Kaimal spectrum, respectively. Hence, the wave loads were calculated by generating a PM spectrum (fig. 3.9a) from which random frequency samples were taken and Fourier Transformed to obtain corresponding random wave elevations throughout a 10 minute time signal. The number of frequency samples was adjusted for each sea state in order to assure an irregular time series of wave elevations.

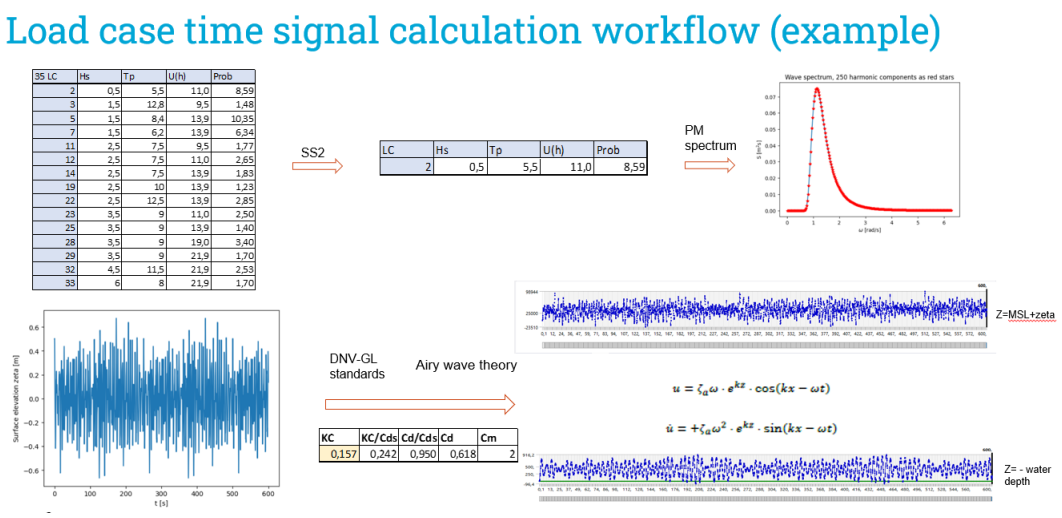

35 LC	Hs	Tp	U(h)	Prob
2	0,5	5,5	11,0	8,59
3	1,5	12,8	9,5	1,48
5	1,5	8,4	13,9	10,35
7	1,5	6,2	13,9	6,34
11	2,5	7,5	9,5	1,77
12	2,5	7,5	11,0	2,65
14	2,5	7,5	13,9	1,83
19	2,5	10	13,9	1,23
22	2,5	12,5	13,9	2,85
23	3,5	9	11,0	2,50
25	3,5	9	13,9	1,40
28	3,5	9	19,0	3,40
29	3,5	9	21,9	1,70
32	4,5	11,5	21,9	2,53
33	6	8	21,9	1,70

LC	Hs	Tp	U(h)	Prob
2	0,5	5,5	11,0	8,59

KC	KC/Cds	Cd/Cds	Cd	Cm
0,157	0,242	0,950	0,618	2

$$u = \zeta_a \omega \cdot e^{kz} \cdot \cos(kx - \omega t)$$

$$\dot{u} = +\zeta_a \omega^2 \cdot e^{kz} \cdot \sin(kx - \omega t)$$

Figure 3.8: Procedure for sea state time signal calculation.

The time signal minimum time step is defined based on the natural frequency of the structure by a minimum of $\Delta t = \frac{1}{20 \cdot f_n}$. Thus, a time signal with a time step of 0.1s was chosen to ensure all the frequencies present are present in the time signal. Which is then used to calculate the wave forcing at different water depths by applying wheeler stretchingHolthuijsen, 2010 to account for the loads above MSL and airy wave theory.

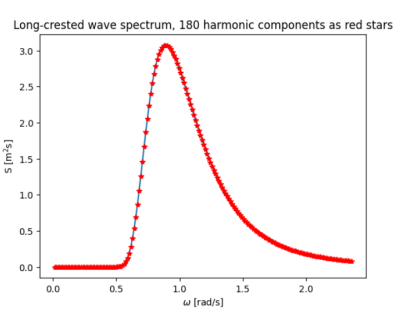

(a) Pierson Moskovitch Spectrum, SS30(Hs:4.5, T_0:11.5).

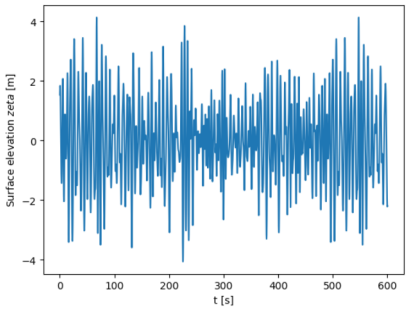

(b) SS30: 600 second random surface elevations.

Figure 3.9: Wave irregular time series modelling.

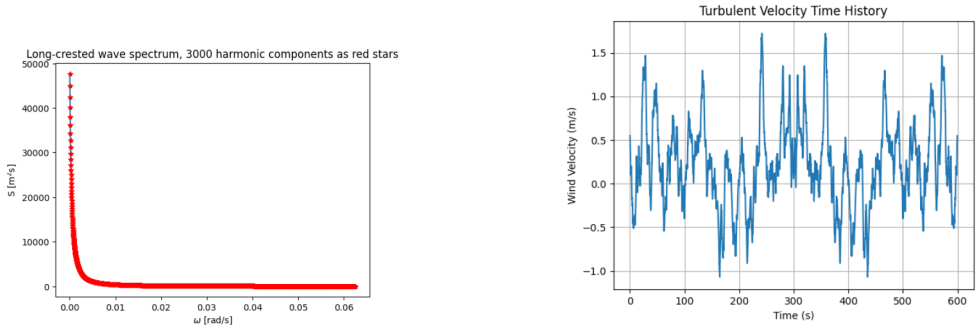

(a) Kaimal Spectrum, SS30(U_w:16.8).

(b) SS30: 600 second turbulence simulation.

Figure 3.10: Wind irregular time series modelling.

This results in a force time signal with a duration of 10 minutes. According to DNV-GL standardsDNV-GL, 2016, for site specific stochastic simulations, a minimum of 6 time series should be generated and the most extreme condition between these is the one chosen and verified based on theoretical wave load calculations using deterministic values the for the model following Airy wave theory wave load calculations from Holthuijsen, 2010 and Arany et al. 2017.

Next, the wind speed turbulence component should be modelled according to the reference wind speed by using a kaimal spectrum (fig. 3.10a). The same procedure for validation was used by comparing the turbulent wind speeds with theoretical approximations specified in DNV-GL, 2011.

The resulting load signals (figs. 3.11, 3.12) were found to be in the same order of magnitude as theoretical calculations following airy wave theory. It is worth mentioning that the KC number used to determine the drag coefficient was based on the significant wave period and wave height following equations 2.9 and **??**, in an irregular wave spectrum, many frequencies are present. Thus, the KC number will show some variations in time which is left as a recommendation for further research.

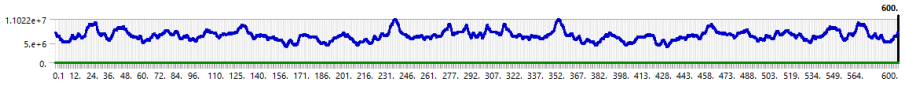

Figure 3.11: SS30: Wind load signal.

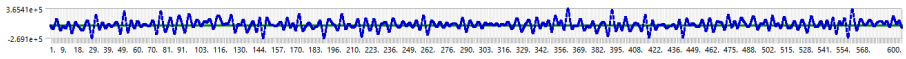

Figure 3.12: SS30: Wave load signal.

This procedure was repeated for each sea state in order to obtain the load signals which were then exported to an excel worksheet for bookkeeping purposes.

3.5. Ultimate Limit State Check

Von Mises stress is an equivalent value that is used to determine if a given material will begin to yield. A material will not yield as long as the maximum von Mises stress value does not exceed the yield strength of the material.

The comparative nature of tensile results and von Mises equivalent stress enables us to quickly calculate functional values (such as a factor of safety) by dividing the maximum allowable stress by the equivalent stress. When using the yield strength as the maximum allowable stress, the factor of safety must be over one for the design to not experience permanent deformation. This factor of safety provides the minimum performance target for the design and was set as 1.1 following industry standards (DNV-GL, 2016). Here, the von Mises stresses are calculated along the structure and compared to the yield strength of the material to ensure the yield limit is not exceeded. The von Mises

stresses are calculated according to equation 3.13 (DNV-GL, 2016).

$$\sigma_{\text{vm}} = \sqrt{\sigma_x^2 + \sigma_x\sigma_y + \sigma_y^2 + 3\tau_{xy}^2} \tag{3.13}$$

Since the stresses in the current study are a combination of pure axial and shear stresses, eq. 3.13 can be simplified to eq. 3.14.

$$\sigma_{\text{vm}} = \sqrt{\sigma_x^2 + 3\tau_{xy}^2} \tag{3.14}$$

Here, σ_x is the normal stress component consisting of a component caused by bending due to the overturning moment and a component from the axial force resulting from the top mass and own weight of the tower and monopile. τ_{xy} is the shear stress component.

An additional unity check of 0.90 is implemented in the comparison of the calculated von Mises stresses to the material yield stress. The von Mises unity check, as seen in eq. 3.15, is implemented to account for any error margins in the determination of the von Mises stresses.

$$\frac{\sigma_{\text{vm}}}{\frac{\sigma_y ield}{\gamma_m}} \leq 0.90 \tag{3.15}$$

In this Equation, σ_y is the yield strength of S355ML graded steel, which is the steel used by Sif for monopile production. The yield strength of S355ML varies depending on the plate thickness as can be seen in table 3.3. Additionally, a material safety factor, γ_m, is implemented to account for any material imperfections.

Table 3.3: Yield stress for different wall thicknesses(S355ML).

Wall thickness(mm)	Yield Stress(MPa)
3-16	355
16-40	345
40-63	335
63-100	325
100-150	295

In order to perform a global buckling check, DNV-GL standards specify that the transient analysis can be done by 6 simulations of 10 minutes with the loading conditions of the 1yr return period and the 50-year return period. For site-specific conditions, the resulting stresses should be assessed based on the maximum stress occurring in these simulations. In the case of this study, the parameters used to build the irregular time signal are the ones in 2.2. By selecting the worst conditions out of 6 different simulation seeds, the ultimate state limit check was done considering resulting equivalent Von Mises stress.

The current structure is checked on yield stress capacity for both load cases as explained in section 2.3. If the check is not passed over the entire structure, the wall thickness of the monopile is increased. After every step, it is checked whether the natural frequency is still within the allowed margins. If the yield check is passed, a global buckling check is conducted for the optimized geometry of the monopile. When the geometry passes both ultimate limit state checks, the geometry will be tested on fatigue resistance. The fatigue analysis is explained in Chapter 4.

3.6. The Perforated monopile

Once the structure's dimensions were fixed, an identical structure with a set of perforations at the splash zone was created. The perforations were made following Andersen et al. 2020 and considering the hole geometry recommendation in Van Der Ploeg, 2021 resulting in the dimensions shown in fig.

3.13b. Thus, the model as can be seen in fig. 3.13a was created.

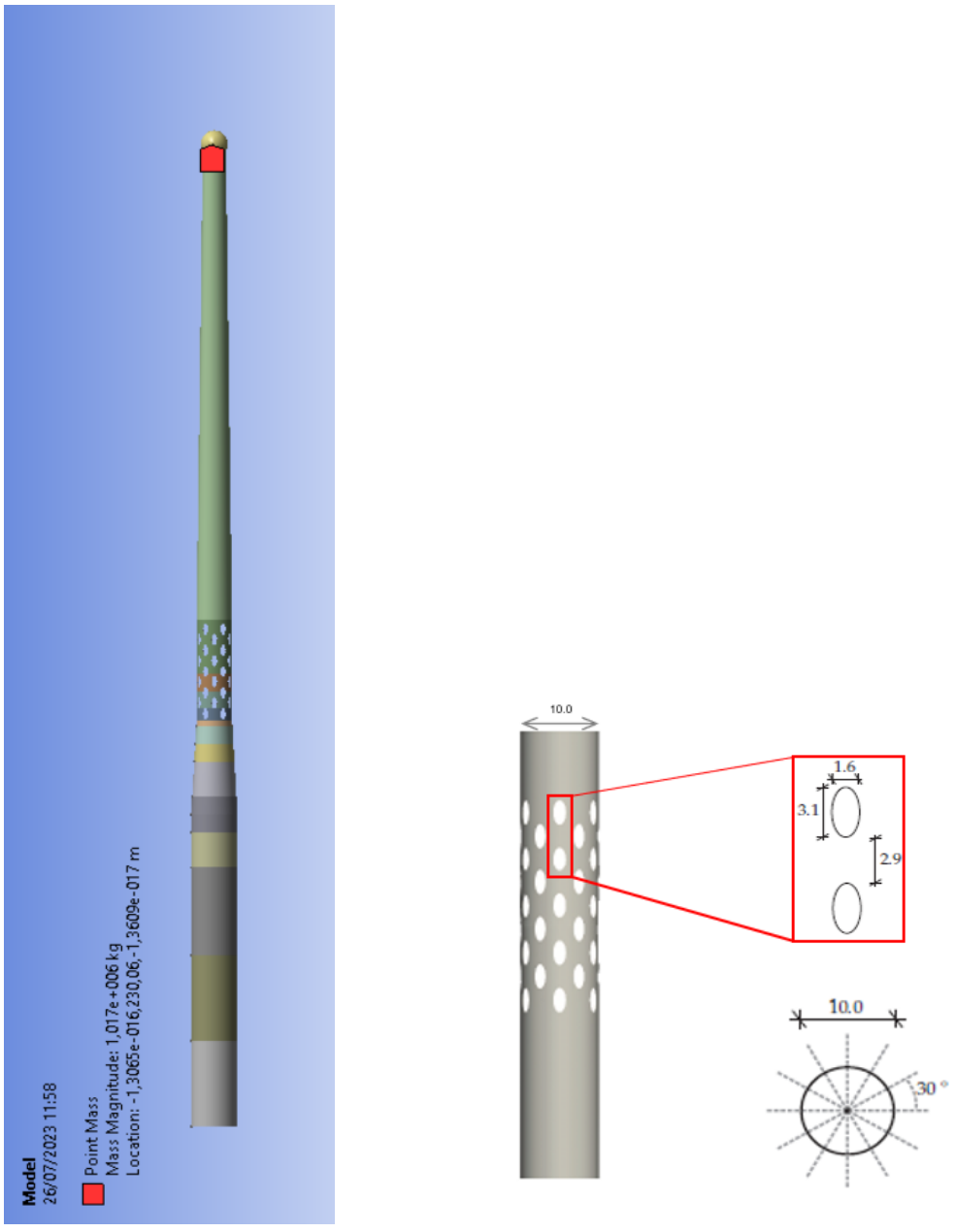

(a) Perforated MP, Ansys Mechanical model.

(b) Perforation geometry, offset and dimensions.

Figure 3.13: Perforated monopile model design.

By using the same pile diameter and perforation geometries, it is assumed that the structure will experience the same wave reduction as the relation obtained from Andersen et al. 2020 as can be seen in fig. 1.10 which led to the relation found in eq. 1.1 at the splash zone.

Using the same dimensions and constraints as the reference monopile, a model comparison can be made to understand the influence of the perforations on the structural response. However, given the dimensions and amount of holes, adding perforations resulted in a mass reduction of 5% leading to a difference in the natural frequency of the system of 6.5%. This could be adjusted by adding thickness or increasing the diameter at the perforated area and running a sensitivity analysis. However, due to the non-linear behaviour of these variations, this was considered out of the scope of the research and left as a discussion point.

4

FLS and model comparisson

4.1. Fatigue analysis of a structure

The FLS analysis is the study of a given structure under cyclic loading for a period of time representative to the life time of the structure. According to Det Norske Veritas (DNV-GL, 2010), fatigue analysis should be based on S-N data. The S-N curves are graphical presentations of the dependence of fatigue life (N) on fatigue strength (S) which vary depending on the type of weld and can be used as an empirical reference for fatigue life with the linear cumulative damage hypothesis (Palmgren-Miner rule) (Kauzlarich, 1989).

The S-N curves used in this research were based on the DNV-GL standards where the curves for seawater with cathodic protection were used (fig. 4.1). There are several labeled curves from which The assessed curves are the B1 curve for the bulk material, the C1 curve for grinded butt welds and the D curve for non grinded butt welds.

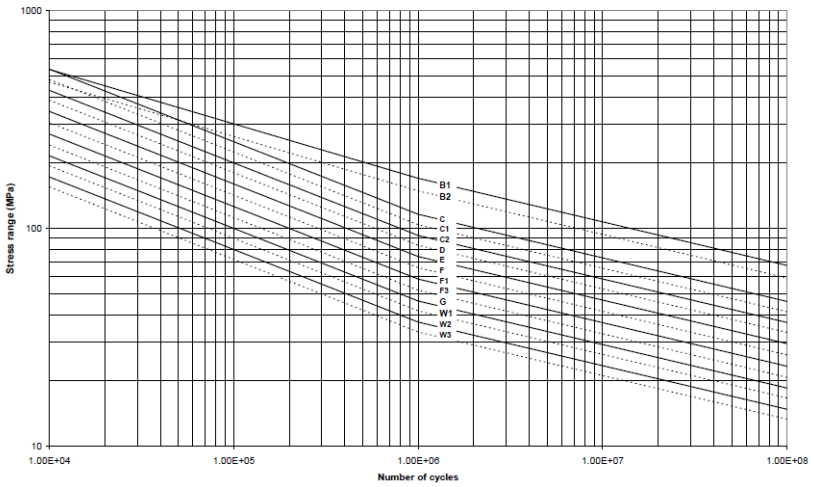

Figure 4.1: S-N curves in seawater with cathodic protection (DNV-GL, 2010).

These curves are described by eq.4.1

$$\log N = \log \overline{a} - m \log \Delta\sigma \tag{4.1}$$

Where,

N: predicted number of cycles to failure for stress range
m: negative inverse slope of S-N curve
$\Delta\sigma$: stress range
$\log \overline{a}$: intercept of log N-axis by S-N curve

The values for $\log \overline{a}$, slope m and thickness component k are given in table 4.1 where subscripts 1 and 2 correspond to high and low cycle amplitude loading respectively. Here, the B1 curve is used for bulk material and the C1 curve to account for non grinded butt welds.

Table 4.1: S-N parameters for B1 and C1.

S-N curve	m_1	$\log \overline{a_1}$	m_2	$\log \overline{a_2}$	k
B1	4.0	14.917	5.0	17.146	0
C1	3.0	12.049	5.0	16.081	0.15

Fatigue analysis is comprised of four steps (fig. 4.2), namely, stochastic environmental modelling, structural response calculation, establishment of stress range distribution and damage accumulation (Kuehn, 2001). Since the objective of this research is to see how the structure is affected by fatigue loads, these steps will be developed in detail below:

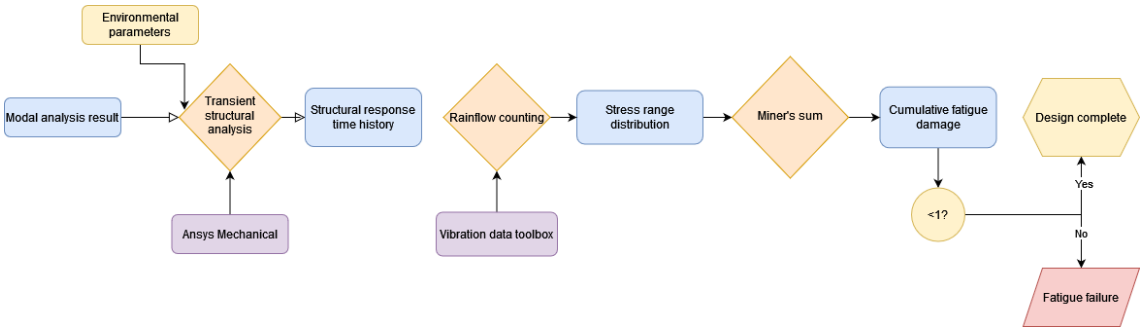

Figure 4.2: FLS analysis procedure and failure criteria (DNV-GL, 2010).

4.1.1. Stochastic environmental modeling

When analyzing the non-linear behavior of a coupled system subjected to wind and wave loads, the time domain approach was chosen to carry out the FLS of the structure. The time domain approach, involves generating random time series from wind and wave spectra and using time step integration techniques to simulate the system as shown in 3.4. Additionally, stress ranges are obtained by utilizing Rainflow counting.

For a simplified analysis it is generally sufficient to consider collinear andomnidirectional wind and waves. Consequently the environmental conditions can be described by a three-dimensional scatter diagram with classes for the significant wave height Hs, zerocrossing period Tz and mean wind speed at hub height Uw. The scatter diagram (Appendix A, D) visually presents the probabilistic distribution of these parameters, giving insight into the range of loading conditions the monopile might experience during its operational lifetime. By incorporating statistical data and probabilistic models, the scatter diagram aids in developing a more comprehensive understanding of the potential stress scenarios the monopile could be subjected to.

It's worth mentioning that the consideration of the operational modes of the OWTs is important since they determine whether or not aerodynamic damping has to be accounted for in the calculation of the hydrodynamic response associated with winds between the cut-in and the cut-out wind speed. In principle, two scatter diagrams are required for the production wind speed range: one with the load cases probabilities during actual production and another for failure and repair stateKuehn, 2001. Establishment of such load case probabilities is quite a cumbersome task and outside of the scope of this research.

4.1.2. Preliminary lumping

The load case lumping is chosen to be done in a conservative way by grouping the probability of occurance of lower sea states on to a dominating sea state so that the joind probability of occurance is

above 1% for all sea states.

Preliminary lumping is a step in the FEM stress response analysis process where the complex and continuous load signals are discretized into manageable segments or discrete loads. In the case of a monopile structure, this involves breaking down the dynamic and time-varying loads, such as those induced by waves and wind, into simplified and concentrated loads that can be applied at specific locations on the structure. This simplification is crucial to reduce the computational complexity of the analysis while still capturing the essential characteristics of the loads. Preliminary lumping allows engineers to strike a balance between accuracy and computational efficiency in the stress analysis of monopile structures subjected to various transient loads.

4.1.3. Load case selection and transient load signal simulation

Load case selection was done considering the DNV-GL(DNV-GL, 2016 DLC's of interest stated in 2.3. Together with the scatter diagrams the identification of the most relevant and extreme loading scenarios that the monopile structure may encounter during its operational lifespan is carried out. Once the load cases are defined, transient load signals are simulated following the procedure described in section 3.4.1 to represent the time-varying nature of the loads.

A modal analysis establishes the model. In this way, geometric data, the eigenmodes and eigenfrequencies are obtained (Kuehn, 2001). The simulation of transient load signals ensures that the FEM analysis captures the dynamic behavior of the monopile structure, providing insights into how it will withstand and adapt to changing environmental forces.

4.1.4. Structural Response Calculation

Once the stochastic environmental models are established, the next step is to calculate the structural response of the system to these varying environmental conditions. Transient simulations with Ansys Mechanical were used to simulate how the structure responds to different loading scenarios resulting in stress-time signals for each time step within the 600s. simulations. This step helps determine the stresses and strains experienced by the structure under various conditions. The FLS structural response calculations were performed for 35 load cases to capture the full range of environmental variability.

Time histories of displacements, loads and member forces are computed for the whole structure and exported as the result at the end of each simulation. Once the structural response is known, the nodes which present the highest stress concentrations throughout the simmulation were sampled and exported in order to perform Rainflow counting on the signal (Appendix C).

4.1.5. Establishment of Stress Range Distribution

After calculating the structural response for various environmental conditions, the next step is to establish the stress range distribution. Stress range is a critical factor in fatigue analysis because it represents the fluctuating stress levels that the structure experiences during its lifetime. This step involves extracting the stress range values from the structural response data. The matlab toolbox Vibration Data was used to analyze the stress range data by performing the rainflow counting on the stress time history data resulting from each simulation and characterize the distribution of stress ranges. This method involves a cyclic stress-strain curve being broken down into individual stress cycles, with each cycle representing a complete stress reversal from maximum to minimum values (DNV-GL, 2011). The method then counts the number of cycles in each stress range bin to obtain a histogram, which is then used to perform fatigue analysis.

When the long-term stress range distribution is expressed by a stress histogram, consisting of a convenient number of constant stress range blocks $\Delta\sigma_i$ each with a number of stress repetitions n_i the fatigue criterion reads:

$$D = \sum_{i=1}^{k} \frac{n_i}{N_i} = \frac{1}{\bar{a}} \sum_{i=1}^{k} n_i * (\Delta\sigma_i)^m \leq \eta \tag{4.2}$$

D= accumulated fatigue damage
$\bar{a}$= intercept of the design S-N curve with the log N axis
m = negative inverse slope of the S-N curve
k = number of stress blocks
n_i = number of stress cycles in stress block i
N_i = number of cycles to failure at constant stress range $\Delta\sigma_i$
η = usage factor

All significant stress ranges, which contribute to fatigue damage should be considered (DNV-GL, 2007). Dynamic effects should be duly accounted for when establishing the stress history.

4.1.6. Damage Accumulation

The final step in fatigue analysis is to estimate damage accumulation over time. This involves using fatigue damage models, such as Miner's Rule or Palmgren-Miner's Rule, to predict how accumulated damage affects the structure's fatigue life. Damage accumulation takes into account the number of stress cycles at different stress levels and their contribution to the overall fatigue life.
After the fatigue analysis with Rainflow-Counting method is used to identify and count the number of stress cycles that a component undergoes during its service life.
The Palmgren-Miner rule 4.3 is a linear damage accumulation model that is used to predict the fatigue life of a component based on the cumulative damage caused by cyclic loading (Kauzlarich, 1989). The rule assumes that the damage caused by each stress cycle is proportional to its magnitude and duration, and that the cumulative damage can be calculated as a linear sum of the damage caused by individual cycles.

$$\sum_{i=1}^{n} \frac{n_i}{N_i} = 1 \tag{4.3}$$

Where:

n : Total number of different stress levels
n_i : Actual number of cycles at each stress level i
N_i : Fatigue endurance limit (or cycles to failure) at each stress level i

4.2. Example case: FLS and comparison of SS10 for Reference and perforated monopile

The fatigue limit state analysis was carried on following the steps in section 4.1 for each sea state given that the environmental conditions were already calculated as stated in section 3.4.1. Figure 4.3 shows a summary of the procedure followed for the set-up of the simmulations together with the tools used for each step. Thereafter, the procedure is carried out for Sea state 10

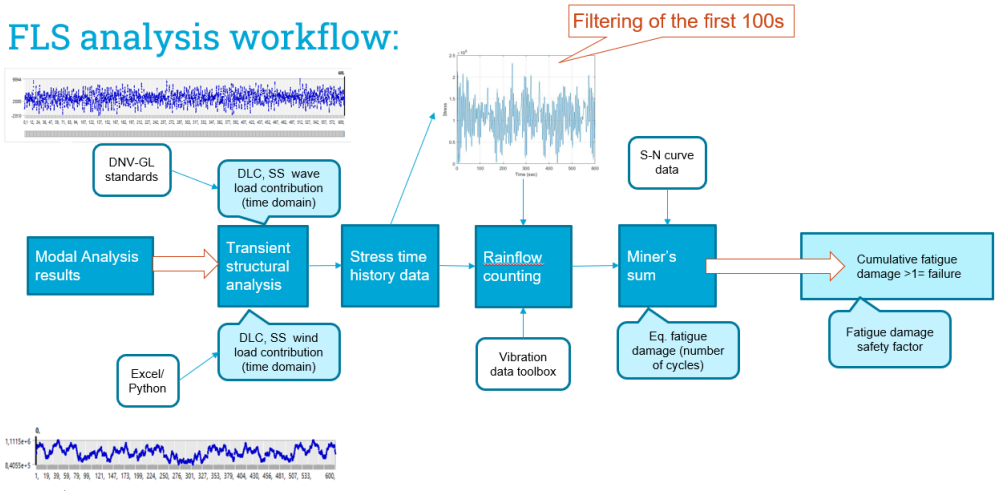

Figure 4.3: FLS analysis example workflow.

4.2.1. Sea state 10: H_s:2.5m, T_0:7.5s, U_w :8.0m/s.

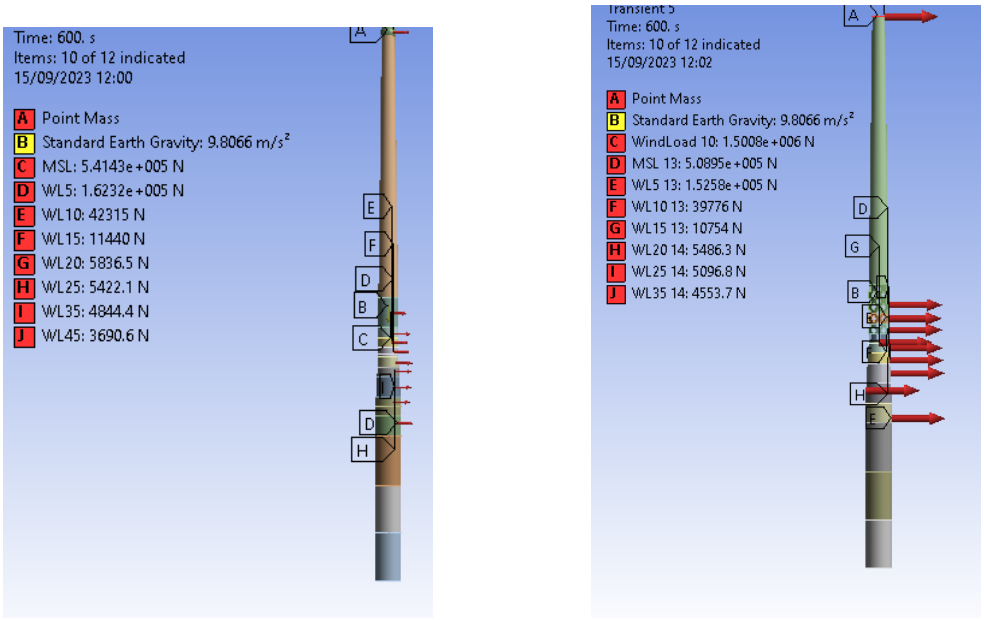

(a) Reference MP

(b) Perforated MP

Figure 4.4: Ansys Mechanical transient analysis model setup.

The same load cases were applied to both structures (fig. 4.4a, 4.4b). Here, the wind loads remain the same and the loads acting on the perforated segment were modified by a wave load reduction factor given in 1.1. The transient analysis was run using the same mesh refinement and solution settings for both analyses to maintain consistency for both structures to obtain stress distributions throughout the models. The initial results were used to establish the areas with maximum stresses which resulted to be the mudline and the end of the conical section for the reference monopile(fig. 4.5a) and the splash zone(lower perforations) for the perforated monopile(fig. 4.5b).

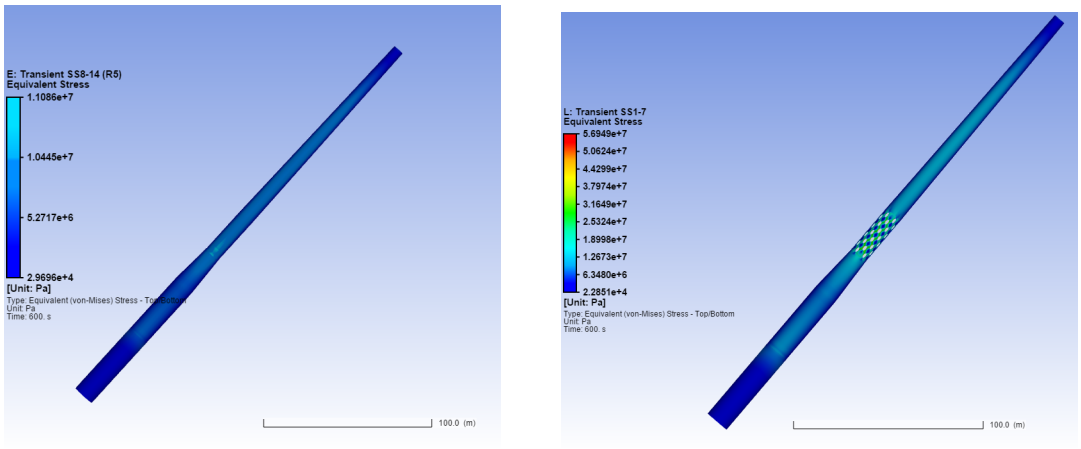

(a) Reference MP, (b) Perforated MP

Figure 4.5: Ansys Mechanical transient analysis stress concentration results.

The areas which presented the highest stress concentrations were analyzed and compared in more detail by taking a selection of nodes at the area of interest, namely, the mudline and the splash zone below MSL (fig. 4.7, 4.8). Which in the case of sea state 10 showed a 29% reduction at the mudline stresses but an increase by a factor of 4 at the perforation with respect to the maximum stress at the cone of the reference monopile. The stress history results were then obtained by exporting the nodal results.

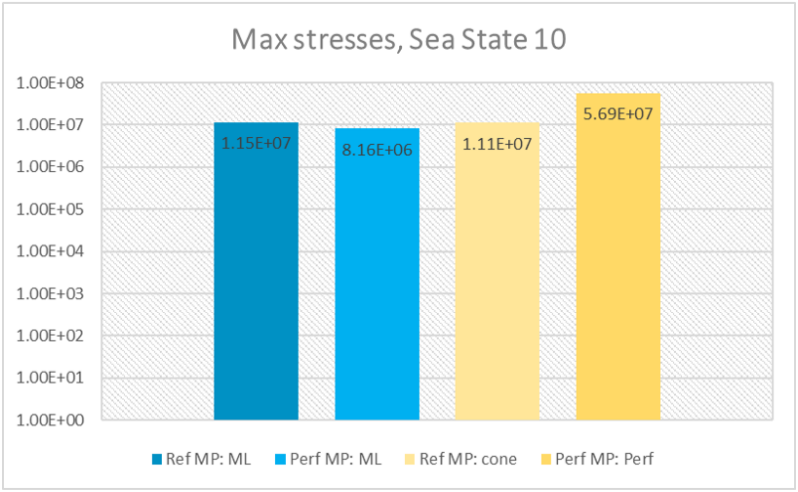

Figure 4.6: Reference monopile, max stress comparisson.

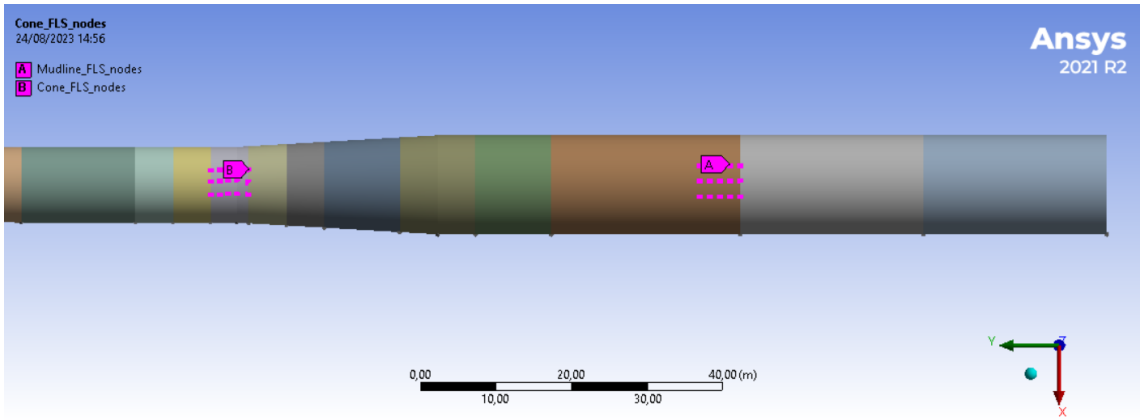

Figure 4.7: Reference monopile, nodal analysis.

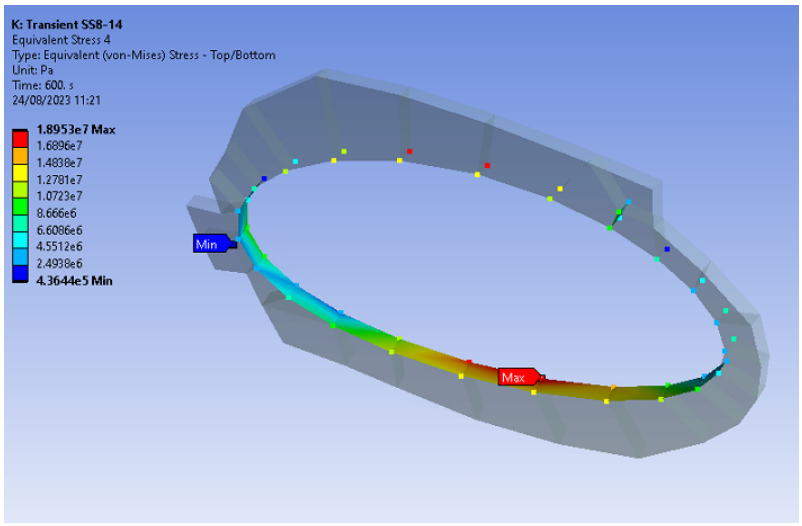

Figure 4.8: Reference monopile, nodal analysis.

The stress data was exported, filtered to account for ramp-up effects and then run through the vibration for rainflow cycle counting(fig. 4.9, 4.10). Thus, separating the data in bins of stress amplitude that were then used to calculate the equivalent fatigue damage corresponding to S-N the S-N curves in section 4.1, and then calculating the equivalent fatigue damage using miner's sum(fig. 4.11, 4.12).

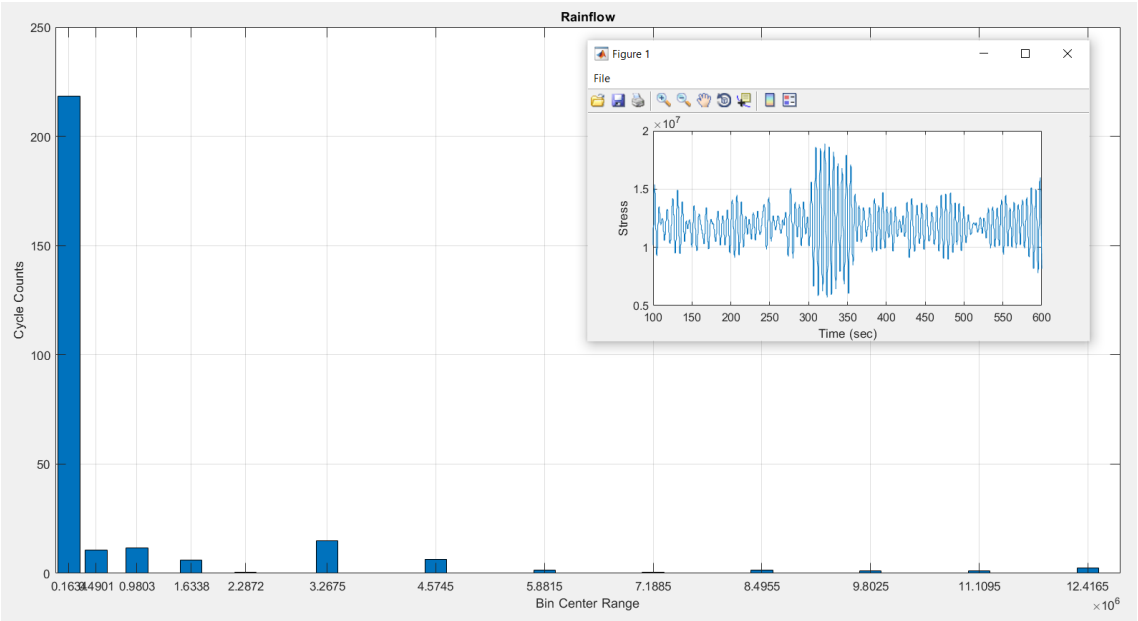

Figure 4.9: Reference MP, SS10, Rainflow counting results.

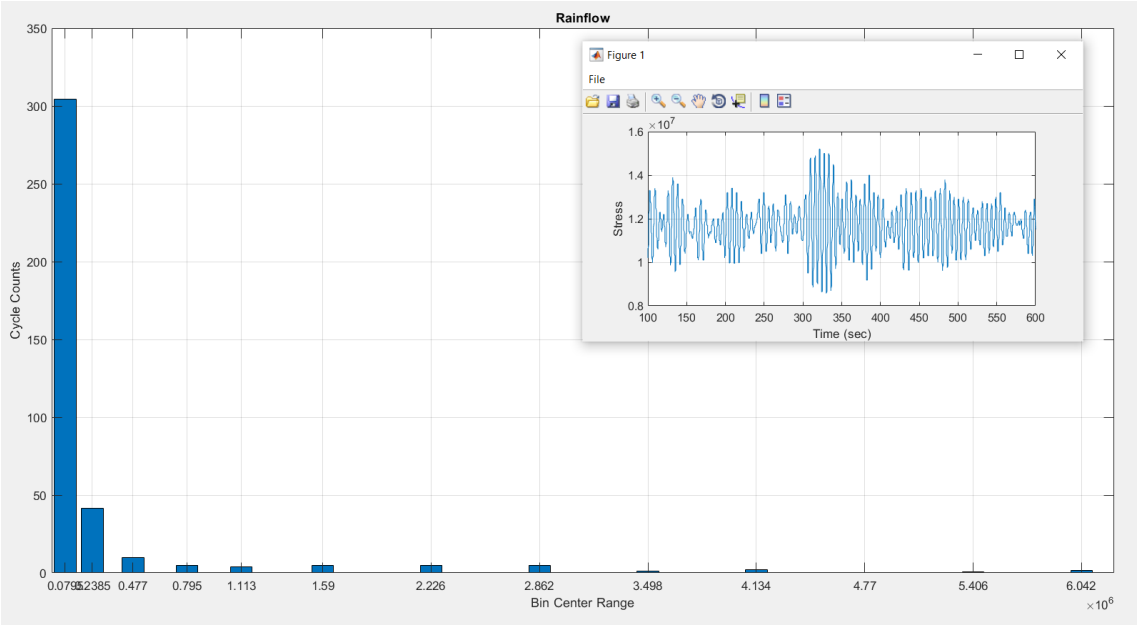

Figure 4.10: Perforated MP, SS10, Rainflow counting results.

SS	min amp	max amp	cycle	avg amp	total cycles/ y	Total cycles(D	Log N	N	Eq. Fatigue damage
10	1.29E+07	1.43E+07	3	7.00E+05	2839	70975	1.15E+01	3.44E+11	2.06E-07
	1.15E+07	1.29E+07	1.5	7.00E+05	1420	35488	1.15E+01	3.44E+11	1.03E-07
	1.00E+07	1.15E+07	1	7.50E+05	946	23658	1.14E+01	2.61E+11	9.06E-08
	8.60E+06	1.00E+07	0.5	7.00E+05	473	11829	1.15E+01	3.44E+11	3.44E-08
	7.17E+06	8.60E+06	1.5	7.15E+05	1420	35488	1.15E+01	3.16E+11	1.12E-07
	5.74E+06	7.17E+06	0.5	7.15E+05	473	11829	1.15E+01	3.16E+11	3.74E-08
	4.30E+06	5.74E+06	6	7.20E+05	5678	141950	1.15E+01	3.07E+11	4.62E-07
	2.87E+06	4.30E+06	13.5	7.15E+05	12776	319388	1.15E+01	3.16E+11	1.01E-06
	2.15E+06	2.87E+06	5	3.60E+05	4732	118292	1.27E+01	4.92E+12	2.41E-08
	1.43E+06	2.15E+06	7	3.60E+05	6624	165609	1.27E+01	4.92E+12	3.37E-08
	7.17E+05	1.43E+06	9.5	3.57E+05	8990	224755	1.27E+01	5.11E+12	4.39E-08
	3.59E+05	7.17E+05	8	1.79E+05	7571	189267	1.39E+01	8.05E+13	2.35E-09
	0	3.59E+05	207	1.80E+05	195891	4897285	1.39E+01	7.96E+13	6.15E-08
								Total	2.22E-06

Figure 4.11: Reference MP, SS10, Equivalent fatigue damage results.

SS	min amp	max amp	cycle	avg amp	total cycles	design life	log S		Eq. Fatigue dama
10	5.72E+06	6.36E+06	1.5	3.20E+05	1420	35488	1.29E+01	7.88E+12	4.50E-09
	5.09E+06	5.72E+06	0.5	3.15E+05	473	11829	1.29E+01	8.39E+12	1.41E-09
	4.45E+06	5.09E+06	0	3.20E+05	0	0	1.29E+01	7.88E+12	0.00E+00
	3.82E+06	4.45E+06	2	3.15E+05	1893	47317	1.29E+01	8.39E+12	5.64E-09
	3.18E+06	3.82E+06	1	3.20E+05	946	23658	1.29E+01	7.88E+12	3.00E-09
	2.54E+06	3.18E+06	5	3.20E+05	4732	118292	1.29E+01	7.88E+12	1.50E-08
	1.91E+06	2.54E+06	5	3.15E+05	4732	118292	1.29E+01	8.39E+12	1.41E-08
	1.27E+06	1.91E+06	5	3.20E+05	4732	118292	1.29E+01	7.88E+12	1.50E-08
	9.54E+05	1.27E+06	4	1.58E+05	3785	94634	1.41E+01	1.33E+14	7.14E-10
	6.36E+05	9.54E+05	5	1.59E+05	4732	118292	1.41E+01	1.29E+14	9.15E-10
	3.18E+05	6.36E+05	10	1.59E+05	9463	236584	1.41E+01	1.29E+14	1.83E-09
	1.59E+05	3.18E+05	41.5	7.95E+04	39273	981823	1.53E+01	2.07E+15	4.75E-10
	0	1.59E+05	304.5	7.95E+04	288159	7203978	1.53E+01	2.07E+15	3.48E-09
				0.00E+00				Total	6.61E-08

Figure 4.12: Perforated MP, SS10, Equivalent fatigue damage results.

5

Results and conclusion

5.1. Model comparisson

The primary objective of this study was to conduct a comparative analysis of the structural behavior of a reference monopile and a perforated monopile under various sea states during power production scenarios with a focus on gathering insight on how the fatigue loads could affect the design life of the structure. Hence, passing the ULS was a basic requirement for this study.

By assesing the performance of both models under extreme conditions, specifically waves with a 50-year and 1-year return period. The study considered Ultimate Limit State (ULS) conditions corresponding to DLC 1.1(tab.- 5.1), with maximum stresses presented after applying a material safety factor (γ_m = 1.1) in accordance with industry standards (DNV-GL, 2016).

Table 5.1: ULS study results.

Design situation	DLC	Wind condition	Waves	Type of analysis	Status
Power production	1.1	NTM	NSS	ULS	Pass
Parked condition	7.2	NTM	NSS	ULS	Pass

Simulations for both monopile designs, encompassing all sea states corresponding to each Design Load Case (DLC) were held, as detailed in Section 4.2, for both structures. Subjecting both the reference and perforated monopiles to a total of 35 distinct sea states, selected to represent the spectrum of conditions encountered during both parked conditions and power production scenarios.

The analysis focused on the computation of maximum stresses at critical locations, specifically at the mudline (fig. 5.1a, 5.1b), within the perforations, and around the splash zone section (fig. 5.2a, 5.2b) of each monopile . To gauge the impact of the perforations, stress reduction, expressed as a percentage, was quantified by contrasting the maximum stresses observed at the mudline between the two monopile designs.

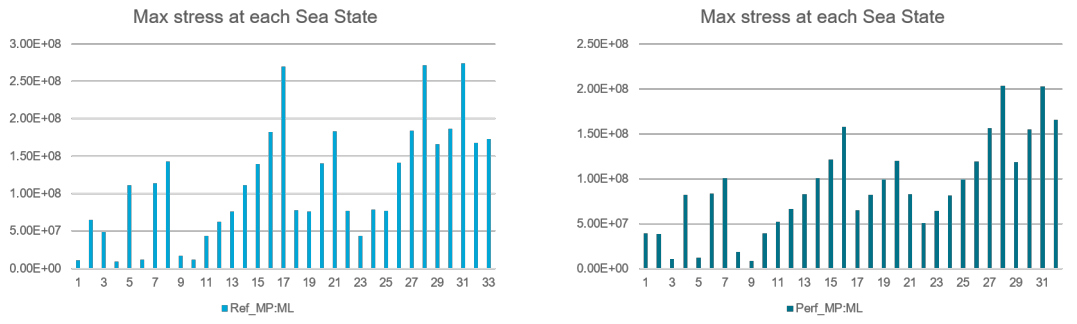

(a) Reference MP

(b) Perforated MP

Figure 5.1: Ansys Mechanical transient analysis stress concentration results.

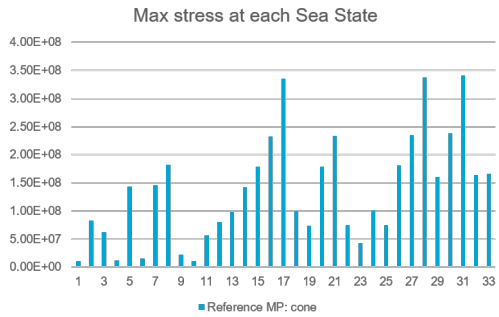

(a) Reference MP, Ansys Mechanical transient analysis stress concentration results.

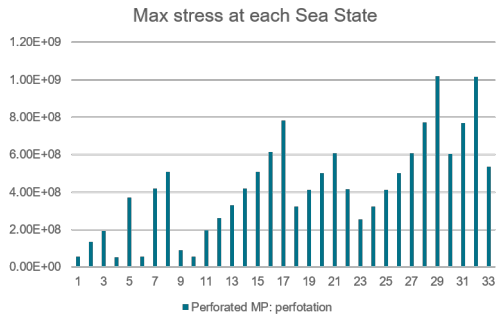

(b) Perforated MP, Ansys Mechanical transient analysis stress concentrations results.

Notably, the maximum stresses which materialized predominantly at two key locations: the cone and mudline for the reference monopile, and at the perforations for the perforated monopile. These outcomes align with the hypotheses stated in Chapter 1, setting the stage for a comparative evaluation based on the maximum stresses reached at the conclusion the simulations. The subsequent sections of the analysis summarize a series of significant findings that contribute insights into the structural behavior of monopile foundations in deep water sites.

5.1.1. Stress comparison

As a result from the simulations, the maximum stresses at the mudline of both models were measured and can be seen in for the reference monopile at each sea state (1-33) in fig. 5.3. An increasing trend in stresses can be seen from sea states 1 to 33 which is to be expected due to how the load cases were lumped based on the 3D scatter diagram (D.1) where the environmental conditions are more rough the higher the sea state (see Appendix B).

Furthermore, a sudden decrease can be seen in the maximum stress found for sea state 8 compared to sea state 9, as well as for sea state 17 to 18 and lastly from sea state 21 to 22. This can also be related to the probability density functions (fig. 5.6), where the presence of certain frequencies could cause resonance with the bending modes of the monopile structures when coupled with increasing mean wind speeds.

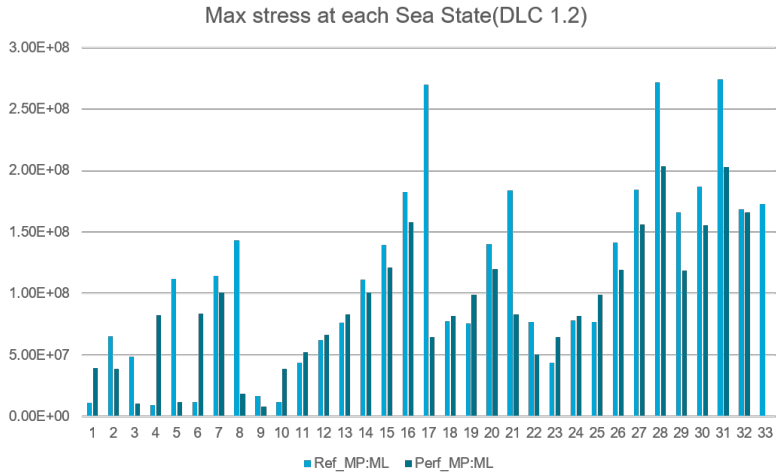

Figure 5.3: DLC 1.2 max. stress comparisson.

Also, a notable trend was observed in the stress distribution along the monopiles. At the mudline, which is a critical region for structural integrity due to its proximity to the seabed, the perforated monopile displayed a marked reduction in maximum stresses compared to the reference monopile. The reduction in maximum stresses can be attributed to the enhanced flow dynamics facilitated by the perforations. The openings in the perforated monopile allow for a more efficient and controlled flow of water, which helps to alleviate some of the lateral loading pressures and subsequent stress concentrations at the mudline.

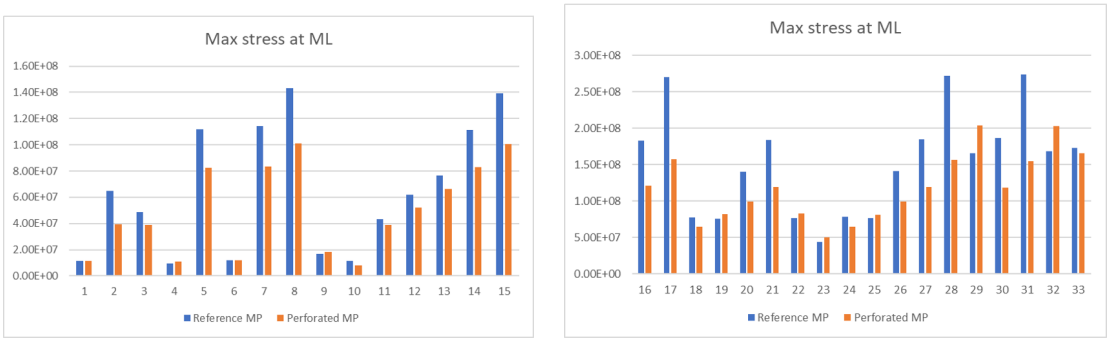

(a) Sea states 1-15 stress concentration results.

(b) Sea states 16-33 stress concentrations results.

Figure 5.4: Max. stress(ML) comparison per sea state

The high fluctuations in resulting stresses in lower sea states (fig. 5.4a) compared to high sea states (fig. 5.4b) can be due to resonance with lower frequency components which are not present in rough sea states. In order to verify this, a frequency analysis of the applied wave force signal was made based on the loads at MSL. By comparing the probability density functions of said sea sea states (5.5a, 5.9b, 5.6a, 5.6b), the peak of the spectrum of lower sea states is closer to the natural frequency of the structure which translates in to a higher probability of occurrence for said frequency within these particular sea states.

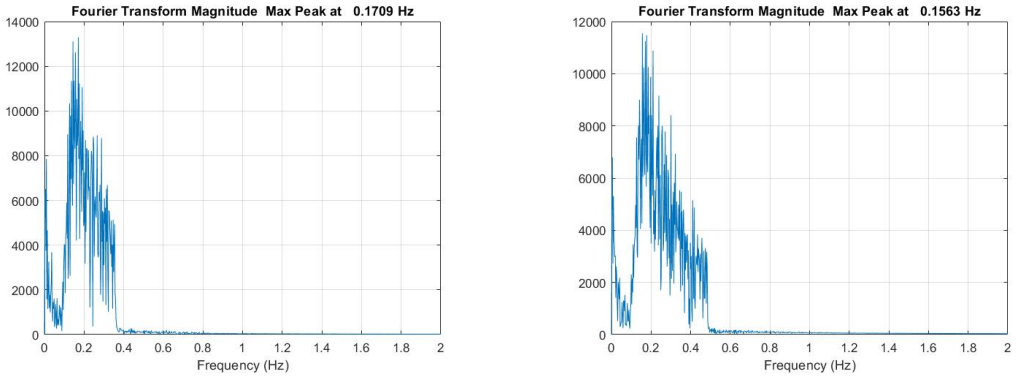

(a) Sea state 5 wave load signal PDF (MSL).

(b) Sea state 6 wave load signal PDF (MSL).

Figure 5.5: Lower sea state, PDF comparisson

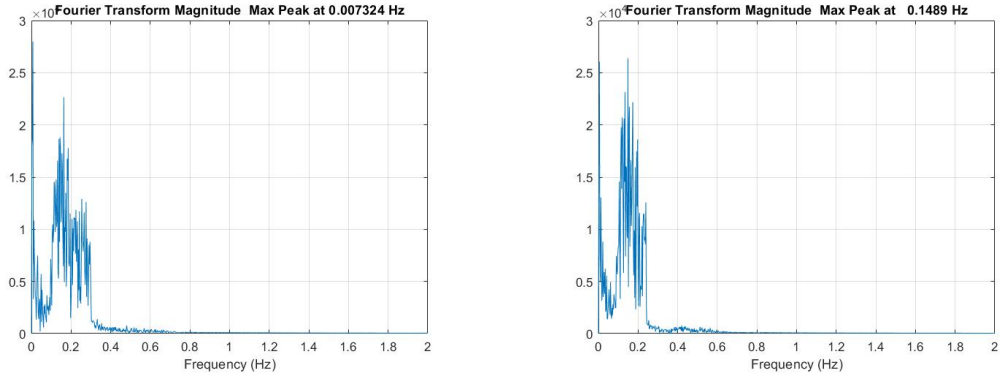

(a) Sea state 21 wave load signal PDF (MSL).

(b) Sea state 22 wave load signal PDF (MSL).

Figure 5.6: Rough sea state, PDF functions

With the results, a stress comparisson was done considering the stress reduction (SR) can be expressed

as:

$$SR = \frac{\Delta\sigma_{ml}}{\sigma_R} \cdot 100 \tag{5.1}$$

Where,

$\Delta\sigma_{ml}$: Difference between resulting maximum stresses
σ_R : Max. ML stress found for the reference monopile

As a result, a decrease of an average of 17% of the stresses at the mudline of the perforated monopile compared to the reference monopile was found. However, a contrasting pattern emerged when examining the stress distribution in the splash zone. In this upper region of the monopiles, where the wave action forces are most pronounced, the perforated monopile exhibited an increase in stresses compared to the reference monopile (fig. 5.7). This phenomenon can be attributed to a higher overturning moment around the area where the perforations are located.

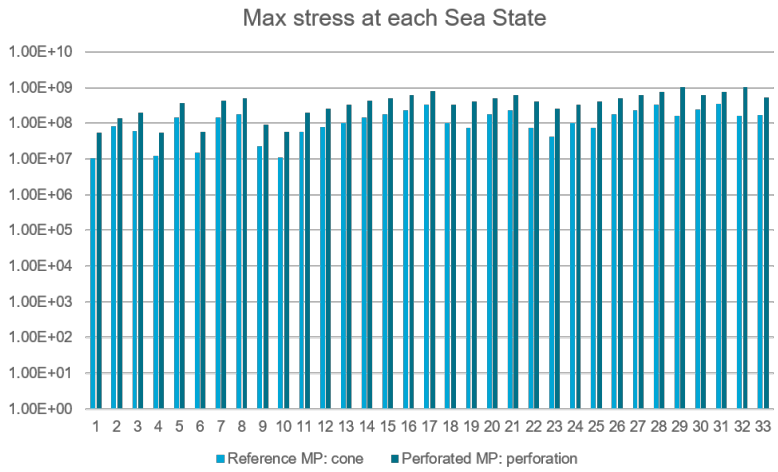

Figure 5.7: Sea states max stress comparisson.

This resulted in an average increase of a factor of 2.9 in the stresses at the perforations. Additionally, a similar trend as the one found for the maximum stresses at the mudline in fluctuations in resulting stresses in lower sea states lower compared to high sea states. This can also be attributed to resonance with lower frequency components which were not present in higher sea states. Furthermore, it is important to understand how the decrease in the natural frequency due to the 5% decrease in mass compared to the reference monopile, increases the probability of resonance for the perforated monopile structure.

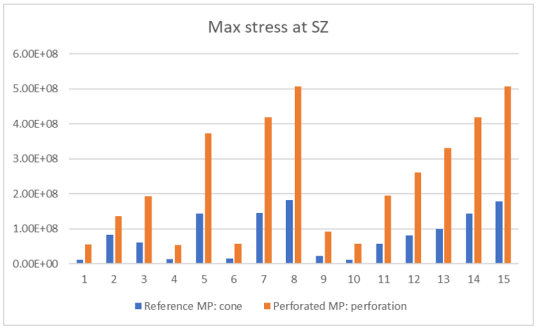

(a) Sea states 1-15 max stress results.

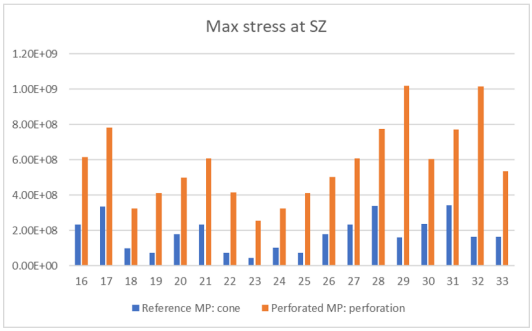

(b) Sea states 16-33 max stress results.

Figure 5.8: Sea states 1-33 max stress results.

As can be seen in fig. 5.8, a sudden increse can be seen in the maximum stress found for sea state 7 compared to sea state 6, as well as for sea state 17 to 18 and lastly from sea state 21 to 22. This can also

be related to the probability density functions in fig. 5.6 with the difference that the perforated monopile is susceptible to frequencies below 0.18Hz as well. An example of this difference can be seen by relating the variation in maximum stresses, to the PDFs of the load signals corresponding to these results. Hence, it can be seen in the frequencies relating to the bending modes of the structure could cause resonance (fig. 5.9).

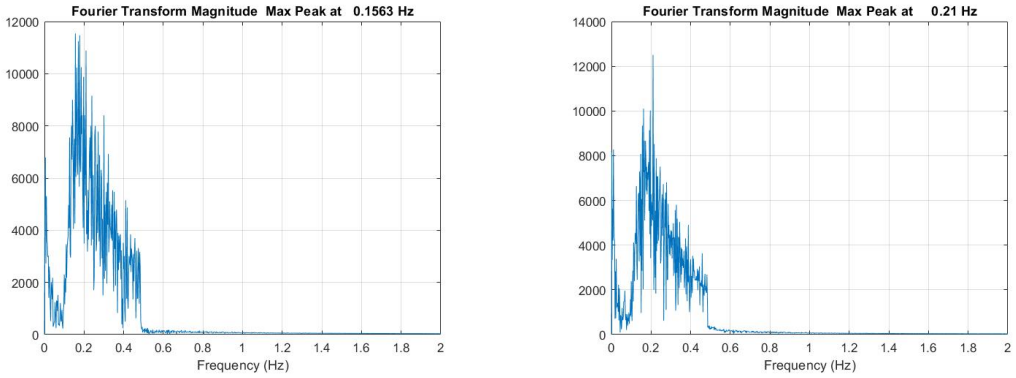

(a) Sea state 6 wave load signal PDF (MSL).

(b) Sea state 7 wave load signal PDF(MSL).

Figure 5.9: Lower sea state, PDF comparisson

These findings underscore the importance of a comprehensive assessment of monopile designs in the context of offshore renewable energy structures. The choice between a conventional monopile and a perforated monopile should be made with careful consideration of the specific environmental conditions at the installation site. While the perforated monopile offers advantages in stress reduction at the mudline, it may necessitate additional design considerations to mitigate the increased stresses in the splash zone.

In order to understand the behaviour of both structures in depth, a dynamic analysis through the analysis of the dynamic response of the structure at the areas which are the most susceptible to fatigue loads. Understanding the significance of the first natural frequency is crucial, especially when it comes to resonance. If the excitation frequency, such as that from fluid forces, closely matches the first natural frequency of the structure, it can lead to resonance, where the structural response is significantly amplified. Thus, in the following section, a frequency analysis of the structural response is introduced to aid answer the research questions stated in 1.

5.1.2. Dynamic analysis

The stress concentrations showed peaks in different sea states for the reference monopile and the perforated monopile (Appendix E). This could be caused by the difference in natural frequency resulting from the decrease in mass due to the perforations. Since the structural response showed a non-linear trend in variations for both low and high sea states, a deeper understanding of the response of the structure by means of a frequency domain analysis was done with the aim of finding which frequencies were excited at critical sea states and if there was resonance occurring with any of the natural frequencies of the monopile structures.

When analyzing the dynamic response of two different structures in a one-way coupled fluid-structure interaction (FSI) model, the Fourier Transform (FT) can be used to understand the behaviour of the structure to environmental loads. With the primary goal being to identify the frequencies that get excited during critical sea states and assess whether any resonance occurs with the natural frequencies of the monopile structures.

The sea states chosen for a comprehensive studdy of the stress response were based on their performance and resonance features explained in previous sections. First, the performance between the reference and the perforated monopile for the same sea state is analyzed.

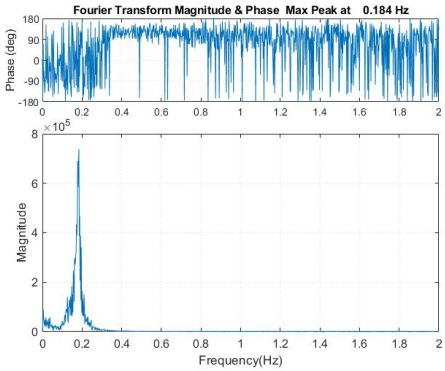

(a) Reference monopile: SS6 stress response FT.

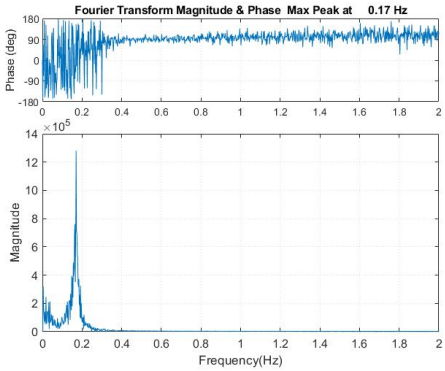

(b) Perforated monopile: SS6 stress response FT.

Figure 5.10: Sea state 6, stress response frequency analysis.

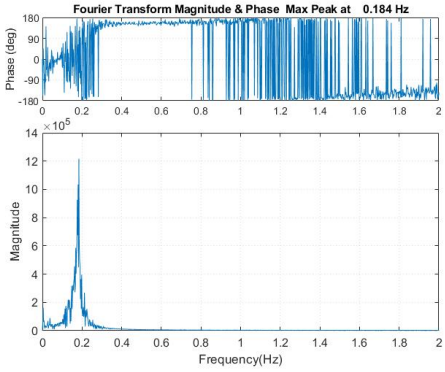

(a) Reference monopile: SS10 stress response FT.

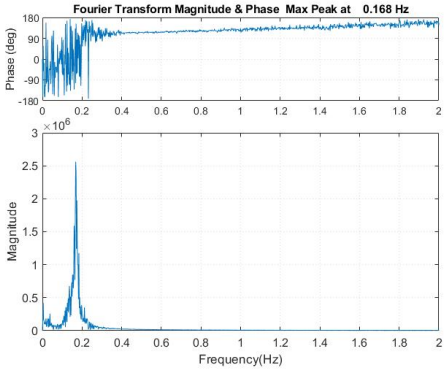

(b) Perforated monopile: SS10 stress response FT.

Figure 5.11: Sea state 10, stress response frequency analysis.

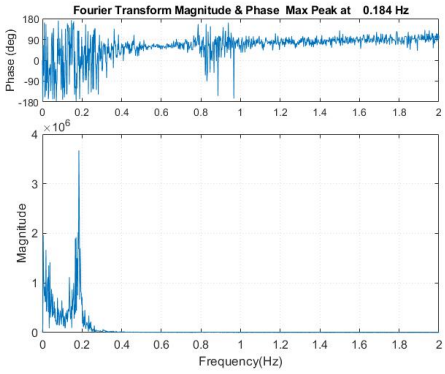

(a) Reference monopile: SS23 stress response FT.

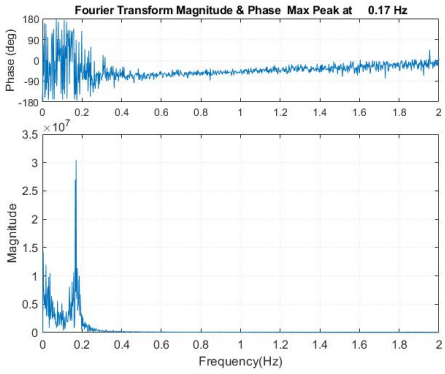

(b) Perforated monopile: SS23 stress response FT.

Figure 5.12: Sea state 23, stress response frequency analysis.

The stress response signal of the monopile to sea states 6, 10, 19 and 23 at the perforations were selected as reference for the analysis. The result can be seen in figs. 5.10, 5.11 and 5.12, from which several observations can be made.

First, the analysis of stress responses reveals that the highest stresses correspond to the natural frequencies of both the reference and perforated monopile structures. This indicates the importance of understanding and accounting for these natural frequencies when designing and assessing the structural integrity of monopiles in offshore environments.

Second, as sea states become more severe, the influence of wind loads, characterized by low frequencies, becomes increasingly significant. This finding highlights the importance of considering both wave-induced and wind-induced loads in the design and analysis of monopile foundations, particularly in harsh offshore conditions.

Third, the phase analysis is a valuable indicator of how the structural response follows the displacement of the structure. Notably, the variation in phase is high for the reference monopile, especially for higher frequencies. In contrast, the phase is more stable for the perforated monopile. This suggests that the perforated monopile may exhibit more predictable and stable behavior in response to environmental loads, which could be advantageous in terms of structural reliability and performance.

Next, the structural response of sea states with similar characteristics but with a significant increase in resulting maximum stress are compared against each other (figs. 5.13, 5.14, 5.15). For this, sea states 6, 5, 19, 17, 21 and 23 were taken as reference.

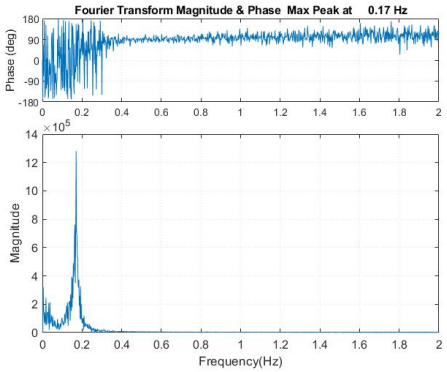

(a) Perforated monopile: SS6 stress response FT.

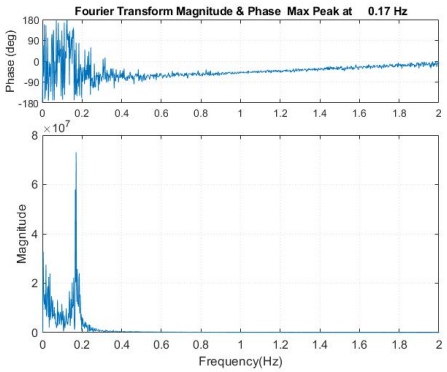

(b) Perforated monopile: SS5 stress response FT.

Figure 5.13: Sea state 5 vs 6, stress response frequency analysis.

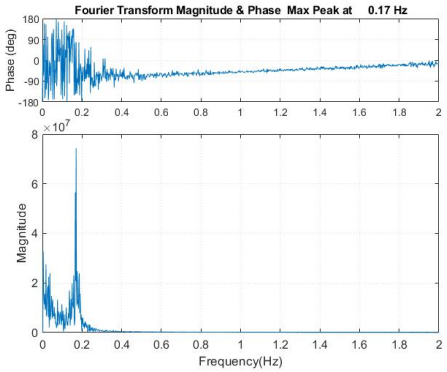

(a) Perforated monopile: SS19 stress response FT.

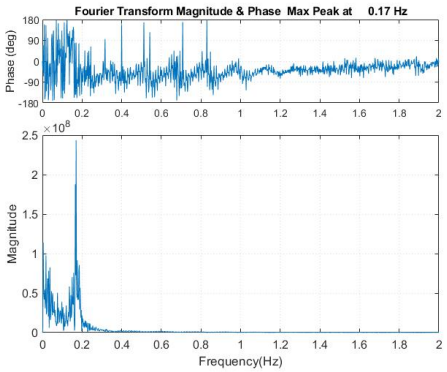

(b) Perforated monopile: SS17 stress response FT.

Figure 5.14: Sea state 17 vs 19, stress response frequency analysis.

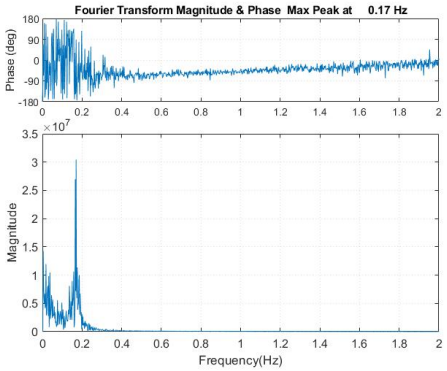

(a) Perforated monopile: SS23 stress response FT.

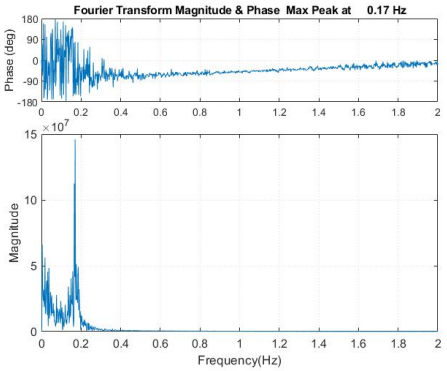

(b) Perforated monopile: SS21 stress response FT.

Figure 5.15: Sea state 21 vs 23, stress response frequency analysis.

As a result, the dominant frequencies present in the structural response can be found to be related to the natural frequency of the structure. A particulary high stress response was found for SS17 compared to SS19. When analyzing the relation between the probability density function and the phase of both sea states, high interaction with bending modes can be seen for SS17.

At this point, a viable solution would be to increase the foundations natural frequency by modifying the parameters that are below the manufacturability limits. Namely, the pile diameter, wall thickness and cone angle. For this, a several modifications were proposed. However, with the tower dimensions as a constraint, obtaining a geometry where the stiffness of the foundation did not shift stress concentrations towards the tower instead of towards the soil proved to be a cumbersome task and was left as a discussion point.

To link these concepts to a one-way coupled FSI model, by comparing the frequency spectra, an understanding of how the excitations affect the structural response, particularly in the vicinity of the structure's first natural frequency can be obtained. This analysis is essential for understanding resonance phenomena, structural integrity, and overall system performance in FSI applications. This comparative analysis provides valuable insights into optimizing monopile designs to ensure their long-term performance and structural reliability in varying sea state conditions during power production scenarios.

5.1.3. Fatigue life assesment

Following the stress analysis, the load stress time series data were exported to initiate the subsequent steps of our investigation. The procedure outlined in Section 4.1, which is pivotal in characterizing the fatigue behavior of structural components, was meticulously repeated. This iterative process was undertaken to ensure a comprehensive assessment of the monopile designs' long-term performance under varying sea state conditions(Appendix C).

The outcome of this analysis is graphically depicted in figs. 5.16, 5.17. In this representation, sea states are color-coded, with those appearing in red indicating a potential risk of structural failure when considering a typical design life of 25 years. This design life duration aligns with industry standards and practices for Offshore Wind Turbines (OWT).

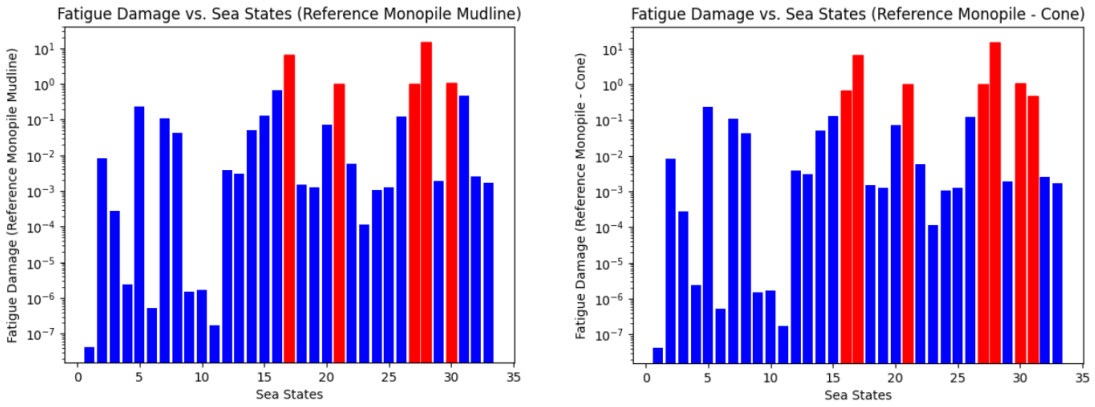

(a) Mudline. (b) Cone.

Figure 5.16: Fatigue damage results: Reference monopile.

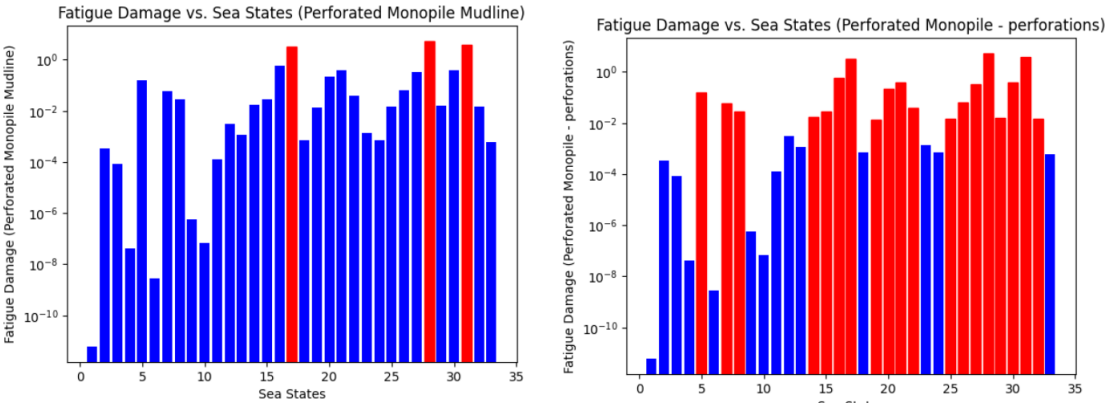

(a) Mudline. (b) Perforations.

Figure 5.17: Fatigue damage results: Perforated monopile

The significance of sea states highlighted in red cannot be understated. They signify conditions that could potentially challenge the structural integrity and longevity of the monopiles over their intended operational lifespan. Thus, this visual representation serves as a crucial reference point for decision-making, design refinement, and risk mitigation strategies in the context of offshore wind energy projects.

However, the shortcomings of the structural modelling should also be taken into consideration when analyzing these results since it doesn't take into considerations aspects such as the potential additional hydrodynamic damping due to the perforations as stated in section 2.7.

5.2. Alternative solutions

In order to asses the viability and the direction of further research on perforated monopiles, alternative solutions for the model in order to potentially reduce the stress concentrations at the sensitive parts of the monopile were studied. Accordingly, critical sea states (fig. 5.18) were selected based on the performance of the structure when exposed to a 600s time domain simulation and the resulting fatigue damage induced for a 25 year design life.

5.2.1. Different thickness parameters at the areas with the highest stress concentrations

An intiutive approach to tackle the high stress concentrations without altering the geometry of the monopile significantly is to increase the plate thickness at the areas which presented a high stress result from the transient analysis simulations.

This was applied with a 10mm increment for the perforated monopile at the splash zone since the perforations failed for multiple sea states for DLC 1.2. The time domain simmulations were repeated for both scenarios taking into consideration the most critical sea states, i.e. the sea states that induced the most amount of damage for a design life of 25 years. This however, did not show a linear trend in terms of the stress concentrations (fig. 5.18).

SS	ML	Perforation(upper)	Perforation(lower)
4	-1%	-11%	-12%
6	0%	-11%	-11%
9	-1%	-11%	-12%
10	-1%	-11%	-12%
19	13%	-1%	-1%
22	14%	-1%	0%
23	0%	0%	0%
25	14%	0%	0%
29	6%	-6%	-6%
32	7%	-6%	-6%

Figure 5.18: Stresss reduction due to 10mm increase of plate thickness at SZ of representative sea states.

As a result of the simulations, the stress reduction was minimal at the perforations for lower sea states with an average of a decrease of 11% in the maximum stress concentrations and little to no change in the maximum stresses found at the mudline (fig. 5.19).

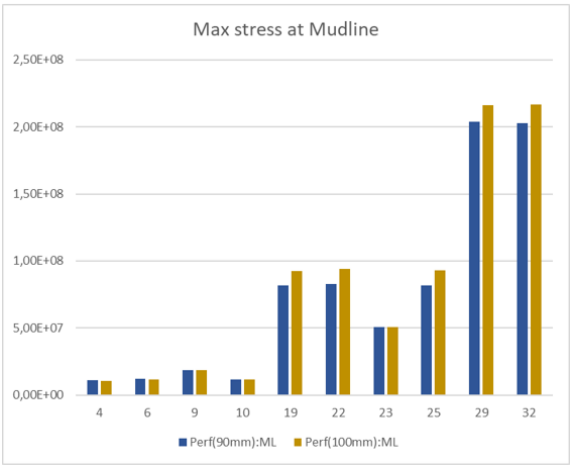

Figure 5.19: Transient stress analysis of representative sea states(ML results).

At the perforations, an increase in maximum stresses was found for rough sea states, while the stresses at the perforations stayed the same 5.20. Thus, this option was not pushed further as an alternative since it should be done together with a sensitivity analysis, together with an thickness optimization algorithm (Liu, 2021), to the increment in thickness throughout the monopile.

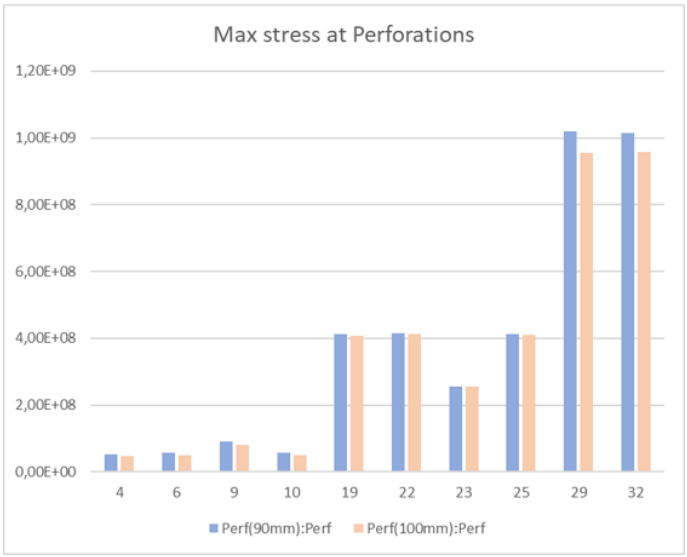

Figure 5.20: Transient stress analysis of representative sea states(ML results).

5.2.2. Increasing the damping of the monopile

The damping of the structure plays an important role in the stress response of the monopile. Initially, the simulations were run assuming 3% damping on all modes. However, this was considered a conservative approach due to the aspects that contribute to the total damping of the structure. To get insight on how these changes would affect the fatigue damage induced by the perforations.

Furthermore, with the monopile being a relatively slender structure in relation to it's height and taking the manufacturability limits into consideration, increasing the structural damping could benefit the structural reliability of the monopile foundation considerably.

As shown in Chapter 4, the fatigue lifetime of the monopile is governed by a variety of external and internal factors, one of them being the dominant wave states. Figures 5.16 and 5.17 show the high variability of fatigue damage due to different sea states, highlighting the importance of reliable met-ocean data.
However, adapting the environment to the monopile is not a realistic approach. Thus, although avoiding the critical sea states by changing the site conditions is considered only alternative for a technical feasibility study for locations for the monopile. On the other hand, the internal factors such as the slenderness and the total damping of the monopile.

Additionally, literature implies that other sources of damping such as structural-, soil- and hydrodynamic damping can be highly uncertain, ranging from an overall damping ratio of 1-3%, which is also variable over time (Kuehn, 2001, Arany et al. 2017).

To asses to suceptibility of the system to a different damping ratio, the simulations were re-run considering 5% of structural damping. The resulting stress responses were analyzed for fatigue damage according to Chapter 4 which resulted in a significant decrease in fatigue damage for most reference sea states (fig. 5.21).

FLS	3% damping		5% damping		Equivalent fatigue damage reduction (at perforation)
MINER SUM SS	Perforated ML Eq. Fatigue damage	Perforated Perf Eq. Fatigue damage	Perforated ML Eq. Fatigue damage	Perforated Perf Eq. Fatigue damage	
4	4.16E-08	2.09E-05	1.36E-08	9.69E-06	-54%
6	2.85E-09	1.07E-06	6.14E-11	1.07E-06	0%
9	5.74E-07	4.63E+01	1.05E-07	1.14E-04	-100%
10	6.61E-08	3.14E-05	1.67E-08	1.53E-05	-51%
19	1.39E-02	5.80E+00	1.67E-03	3.63E+00	-37%
22	3.94E-02	2.15E+01	1.48E-02	7.28E+00	-66%
23	1.34E-03	4.89E-01	6.36E-04	1.51E-01	-69%
25	1.48E-02	9.57E+00	8.76E-03	4.56E+00	-52%
29	1.65E-02	5.00E+00	3.22E-03	4.02E+00	-20%
32	1.44E-02	6.68E+00	1.44E-02	4.82E+00	-28%
Total	0.100396	95.415402	0.043511	24.457470	-74%

Figure 5.21: Equivalent damage per sea state, 5% structural damping.

When plotting these results next to each other, an decrease in fatigue damage for all sea states can be seen at the mudline (fig. 5.22):

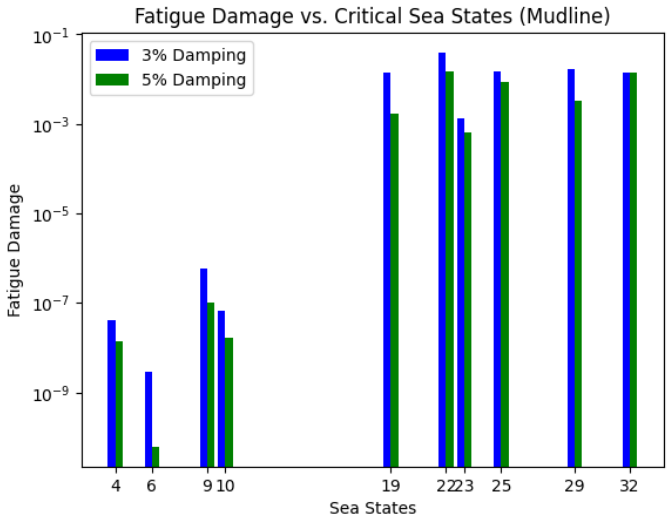

Figure 5.22: 3% damping vs 5% damping, fatigue damage at the mudline.

Furthermore, a drastic decrease in fatigue damage can be seen for SS6 compared to the rest of the reference sea states. Thus, stress response signal was analyzed and compared to the stress response signal of the structure with 3% damping by means of a fourier transform (fig. 5.23).

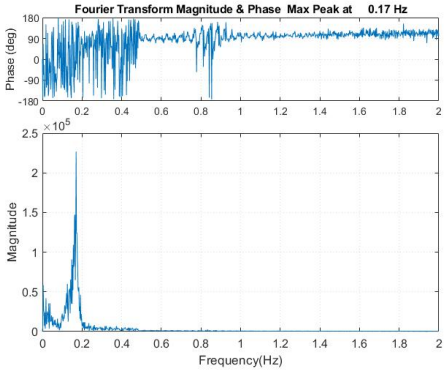

(a) Perforated monopile: 3% damping stress response FT.

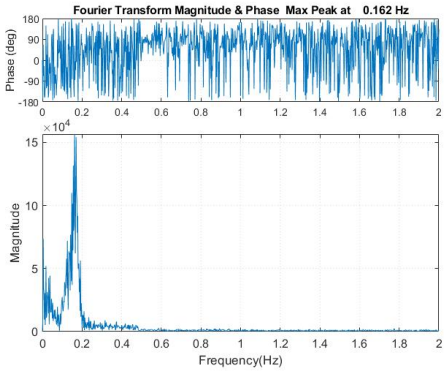

(b) Perforated monopile: 5% damping stress response FT.

Figure 5.23: SS6: 3% vs 5% structural damping, stress response frequency analysis.

From the FT of the stress responses, two main observations can be made. Firstly, the max peak of the simulation with 5% structural damping presents a shift in the max peak from 0.17Hz to 0.162 Hz which indicates less interaction with the natural frequency of the system (fig. 5.23b). And secondly, the phase of the response indicates less resonance features with higher bending modes.

The fatigue damage at the perforations also showed positive results when applying 5% structural damping to the simmulations. Particularly SS9, which indicated failure of the structure when running the simulation with 3% damping, showed significant improvement in terms of fatigue damage (fig. 5.24).

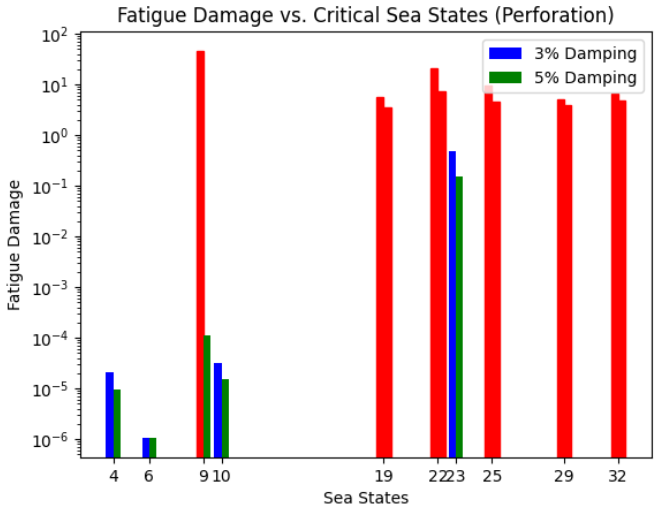

Figure 5.24: 3% damping vs 5% damping, fatigue damage at the perforation.

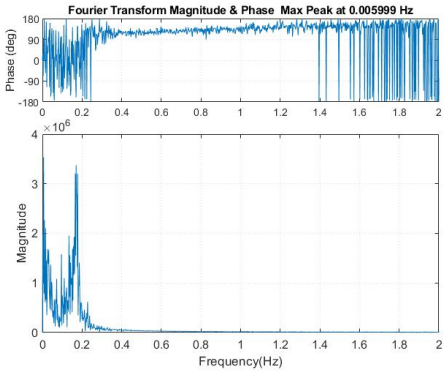

(a) Perforated monopile: 3% damping stress response FT.

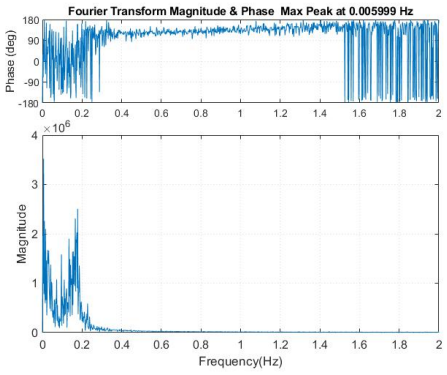

(b) Perforated monopile: 5% damping stress response FT.

Figure 5.25: SS9: 3% vs 5% structural damping, stress response frequency analysis.

The same procedure used for SS6 at the mudline was repeated for SS9. In contrast to the result for SS6, the stress response did not present a significant shift in max peak and phase (fig. 5.25). However, the maximum stress signal around the natural frequency of the monopile did show an important reduction (5.25b).

Hence, the difference in fatigue damage was traced back to the change in stress amplitudes in the stress response time signal (5.2). Where it was found that higher stress amplitudes were reduced and small stress amplitudes (which induce less fatigue damage) increased significantly.

Table 5.2: SS9, 3% vs 5% RFC stress amplitude result comparison

SS	min amp	max amp	cycle
9	6.46×10^8	7.18×10^8	1.5
	5.74×10^8	6.46×10^8	1.5
	5.03×10^8	5.74×10^8	4
	4.31×10^8	5.03×10^8	6.5
	3.59×10^8	4.31×10^8	6.5
	2.87×10^8	3.59×10^8	12.5
	2.15×10^8	2.87×10^8	15
	1.44×10^8	2.15×10^8	15.5
	1.08×10^8	1.44×10^8	8
	7.18×10^7	1.08×10^8	5.5
	3.59×10^7	7.18×10^7	2.5
	1.80×10^7	3.59×10^7	0
	0	1.80×10^7	13

SS	min amp	max amp	cycle
9 (5% damping)	2.75×10^7	3.06×10^7	2
	2.45×10^7	2.75×10^7	1.5
	2.14×10^7	2.45×10^7	5.5
	1.84×10^7	2.14×10^7	2.5
	1.53×10^7	1.84×10^7	2.5
	1.22×10^7	1.53×10^7	4.5
	9.18×10^6	1.22×10^7	13
	6.12×10^6	9.18×10^6	14
	4.59×10^6	6.12×10^6	5.5
	3.06×10^6	4.59×10^6	6.5
	1.53×10^6	3.06×10^6	16
	7.65×10^5	1.53×10^6	94
	0	7.65×10^5	37.5

5.2.3. Different perforation geometries at the splash zone

Alternatively, different shaped of perforations could be used as suggested by Van Der Ploeg, 2021. Since the perforations are elliptical, the holes have two different axes (fig. 5.26). For these types of plates under uni-axial tension, the Inglis Equation is used to describe the relation between ellipse geometry and stress concentration factor.

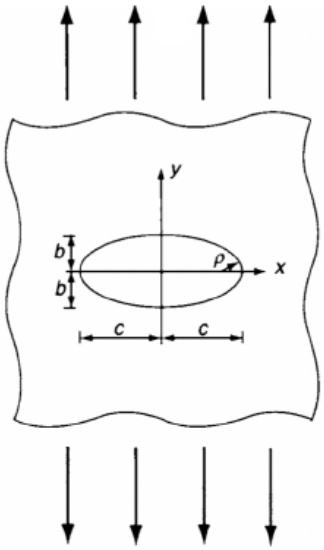

Figure 5.26: Elliptical hole under uni-axial tension loading.

With the geometry presented in 5.26, the highest stress near the perforation can be found with equation 5.2, where ρ is the radius of curvature 5.3. Which, by substitution, results in equation 5.4.

$$\sigma_{max} = \sigma_{nom}\left(1 + 2\sqrt{\frac{c}{\rho}}\right) \tag{5.2}$$

$$\rho = \frac{b^2}{c} \tag{5.3}$$

$$\sigma_{max} = \sigma_{nom}\left(1 + 2\sqrt{\frac{c}{b}}\right) \tag{5.4}$$

Although this equation is meant for an infinite plate, several adaptations and correction factors have been made to the equations presented above to account for the dimensions and shape of the plate

itself Van Der Ploeg, 2021. The one thing to note however is that the influence of the ellipse geometry on the eventual stress concentration factor remains unchanged after including the correction factors for shape and dimension effects or combined loading.

From this relation it is concluded that the stress concentration factor reduces when increasing the value of b. This is a promising realisation for the purposes of this study, as this both increases the size of the perforation and at the same time reduces the expected stress concentration.

Theoretically, this will result in a larger force reduction since pile porosity is increased, whilst stresses could remain within an acceptable range due to reduced stress concentration factors. However, as could be seen throughout the simulations, that as the structure becomes lighter, the natural frequency also lowers, causing the monopile to experience resonance and higher stress amplitude loading.

To test this hypothesis two different options to the perforations (fig. 5.27) were made by increasing the dimensions of b by a factor 2 for option 1 (fig. 5.28); and b by a factor 5 and c by a factor 2 for option 2 (fig. 5.33).

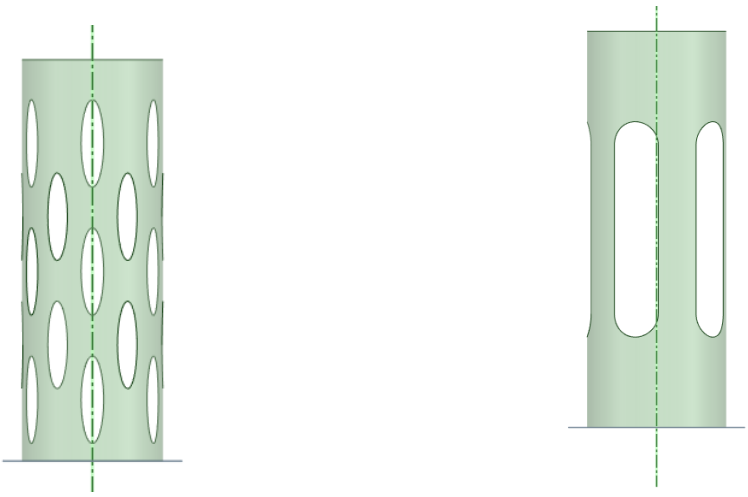

(a) Perforated geometry: option 1.

(b) Perforated geometry: option 2.

Figure 5.27: Perforated geometry alternatives.

The models were set up as shown in fig. and a time domain analysis was run for the reference sea states. The wave load reduction factor used for the initial perforated monopile dimensions since no experimental data was available for these perforation geometries. By doing so, the comparative nature of the simulations is maintained and a stress analysis can be held.

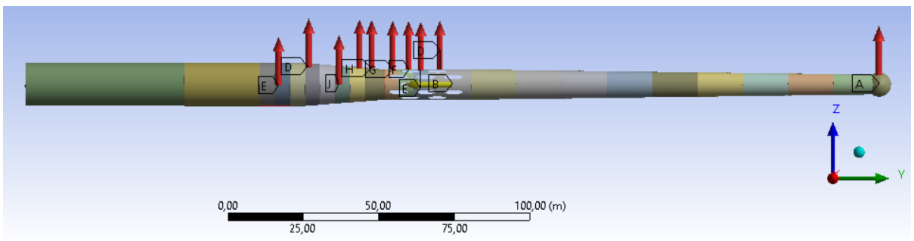

Figure 5.28: Perforated geometry: option 1.

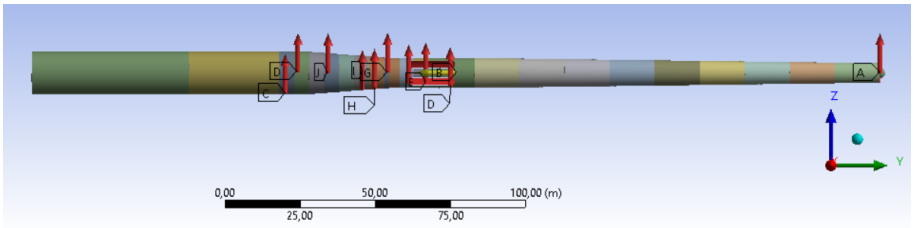

Figure 5.29: Perforated geometry: option 2.

As a result of the simulations for SS6, the maximum stress throughout the model was still at the perforations for both models (figs. 5.30, 5.32). The simulations were repeated for different sea states to understand the behaviour of the structures under different environmental conditions.

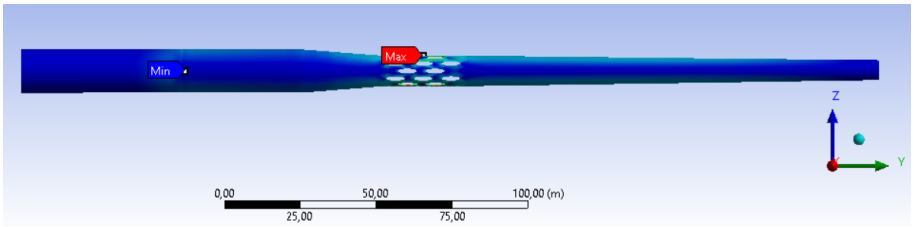

Figure 5.30: Perforated geometry: option 2.

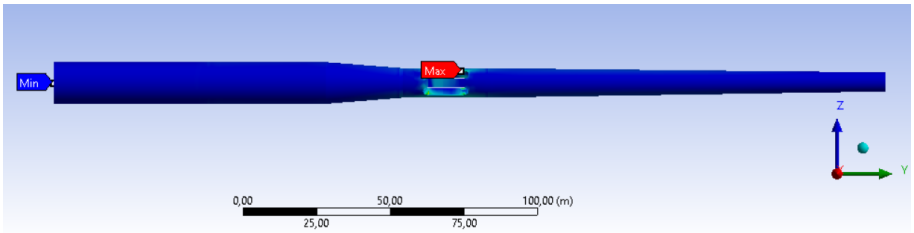

Figure 5.31: Perforated geometry: option 2.

When focusing on the maximum stress at the perforations, the perforation option 1 showed favourable results for SS6 while perforation option 2 showed an increase in maximum stress at the perforations compared to the original perforation geometry.

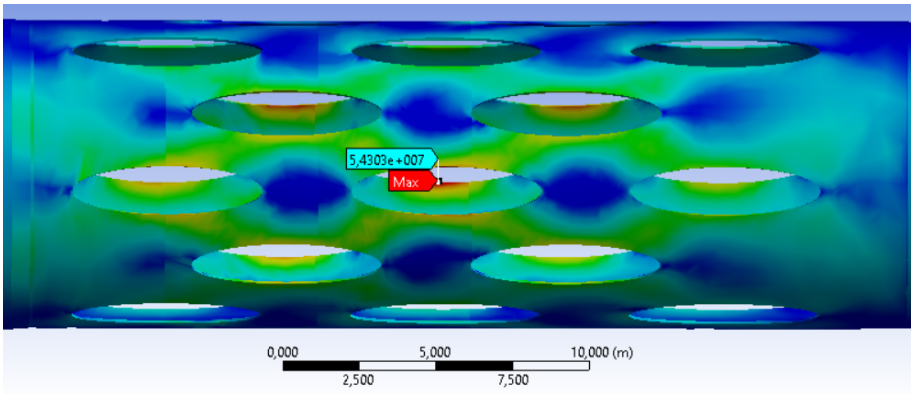

Figure 5.32: Perforated geometry: option 2.

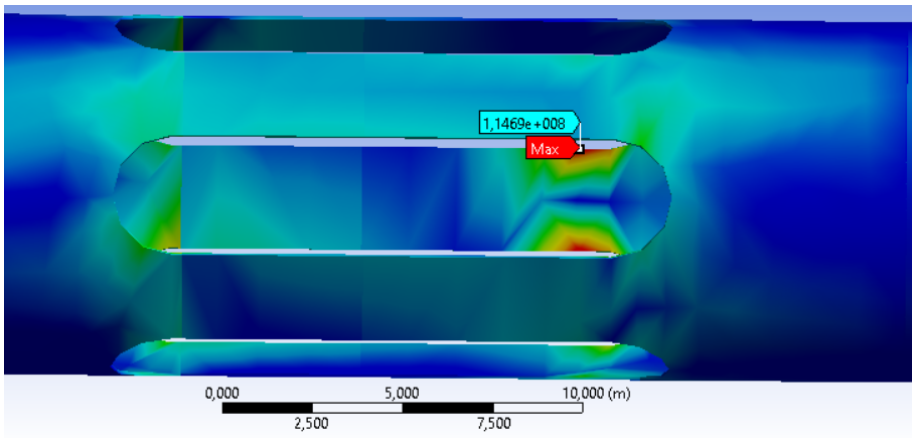

Figure 5.33: Perforated geometry: option 2.

As a result, the maximum stresses showed an decrease in maximum stresses for lower sea states but an increase in them for high sea states for option 1 and a significant increase in maximum stress at the perforations for option 2 (5.34).

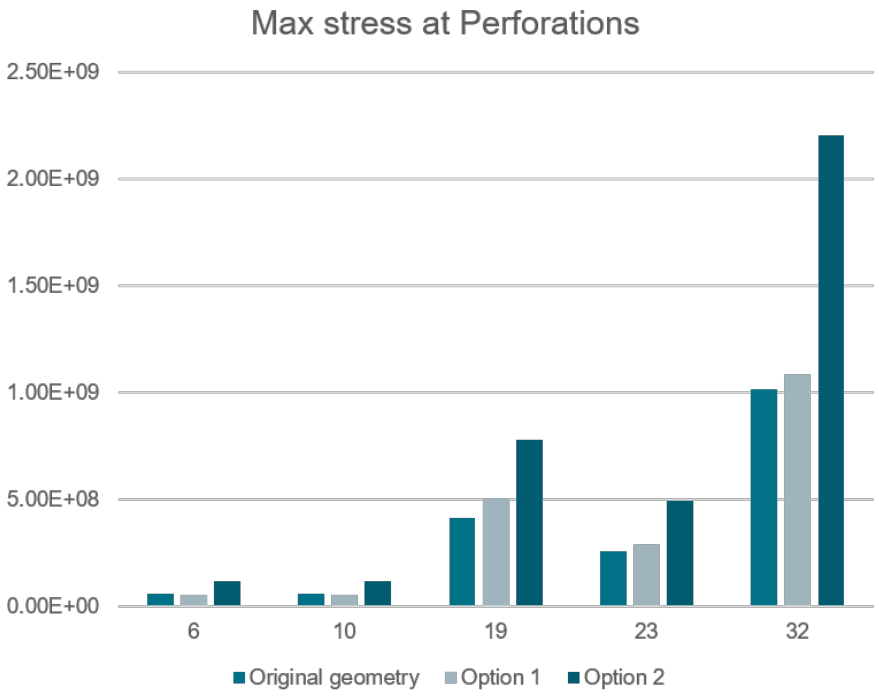

Figure 5.34: Maximum stress comparison at the perforations.

5.3. Conclusions

As the offshore wind industry continues to grow, optimizing the cost-effectiveness of support structures for both fixed-bottom and floating platforms remains a key area of focus. Understanding the cost distribution among different components can identify opportunities to streamline processes, reduce expenses, and advance the deployment of offshore renewable technologies on a global scale.

Ongoing research and technological advancements are expected to play a vital role in driving down costs and making offshore wind energy more competitive with conventional power generation sources.

The presented research focuses on a deeper understanding of one of the emerging technologies in the offshore wind turbine development in deep waters. By choosing a representative water depth of 80 meters and subjecting a monopile structure to environmental loading representative of the conditions of the North Sea (N59 E2.5), the study aims to assess the potential of perforated monopiles in deep water sites and answer the main research question:

Does the structural integrity of a perforated monopile uphold in deepwater conditions when considering a dynamic fluid-structure interaction model?

To answer this question, a comparative FEM analysis was done on both a conventional monopile and a perforated monopile. This analysis provides insights into the limiting factors for these structures in deep water sites.

By the means of manufacturability, ULS (Ultimate Limit State), and FLS (Fatigue Limit State) checks for both power production and parked conditions, we evaluated whether exposure to the environmental conditions at the chosen site induced fatigue failure in the structure. The results indicated that the fatigue damage induced by different sea states could potentially lead to failure of the conventional monopile foundation based on the fatigue curve for non-welded (hollow) sections.
A dynamic analysis showed that the structure experienced the highest loads due to wave loads around the natural frequency of the structure. This observation led to the alternative of adding perforations around the splash zone, where the wave loads are highest. The goal was to allow part of the water to flow through the structure rather than against it.

Running the same sea state simulations on the perforated monopile, the effects and benefits of perforated monopiles were evaluated by comparing the stress concentrations due to each representative sea state and the resulting fatigue damage for a design life of 25 years.

This analysis had two main objectives. The first was to study the stress reduction at the mudline due to the wave load reduction induced by perforations at the splash zone. The second was to analyze if the dynamic response of the structure around the first natural frequency was reduced compared to the reference monopile.

By running the same sea state simulations to the perforated monopile, the effects and benefits of perforated monopiles were evaluated by comparing the stress concentrations due to each of the representative sea states and the resulting fatigue damage for a design life of 25 years of the structure.

The first hypothesis was tested by comparing the maximum stresses at the perforations and at the mudline resulting from the transient FEM simulations. This provided valuable insight into the behavior of the perforated monopile, resulting in an average reduction of 17% in the maximum stresses at the mudline and a significant reduction in fatigue damage at the mudline, a critical area of focus in the design of offshore monopile structures.

However, the stresses at the perforations showed an increase up to above the yield stress of the material and fatigue failure due to multiple single sea states at the perforations. To address this, a comparative analysis between the stress response of the reference monopile and the perforated monopile at the nodes with the highest stresses throughout all sea states was conducted. A Fourier transform was used to check which frequencies were being excited during the simulations.

As a result, it was found that most of the stress responses had their maximum stress response around the natural frequency of the structure. Additionally, interaction with higher bending modes of the monopile was found for lower sea states. Ideally, a model that considers potential hydrodynamic damping due to the addition of the perforations and is fully coupled with the wave loads is needed.

The primary objective of this study was to conduct a comparative analysis of the structural behavior of a reference monopile and a perforated monopile under various sea states during power production scenarios, with a focus on assessing how fatigue loads could affect the design life of the structure.This comparative analysis offers valuable insights into optimizing monopile designs to ensure long-term performance and structural reliability in varying sea state conditions during power production scenarios:

- Dynamic analysis of both structures revealed that the highest stresses corresponded to their natural frequencies, emphasizing the importance of considering these frequencies in design and assessment.
- The influence of wind loads became more significant as sea states became more severe, highlighting the need to consider both wave and wind-induced loads in design.
- Phase analysis indicated that the perforated monopile exhibited more stable behavior in response to environmental loads, suggesting potential advantages in terms of structural reliability.
- Suggestions were made for modifying parameters such as pile diameter, wall thickness, and cone angle to increase the foundation's natural frequency.

Given the answers to the research questions, **alternative solutions** to the perforations at the splash zone were looked into in order to establish towards which direction further research should be made.//
Increasing the plate thickness was proposed which resulted in a non-linear increase of the stress at the perforations with a generalized decrease in stressses for low sea states and an increase in maximum stress for rough sea states. Thus, finding that in order to optimize the stresses by adding material at the splash zone, an optimization algorithm that takes into account the plate thickness along the whole structure should be made.

Structural damping plays a crucial role in the stress response of the monopile, and initially, simulations were conducted with 3% damping on all modes. However, an increase in structural damping to 5% was considered, and it resulted in a significant decrease in fatigue damage for most reference sea states. This change led to a shift in the dominant peak frequencies, indicating less interaction with the natural frequency of the system. Higher structural damping reduced resonance features with higher bending modes, improving structural reliability.

Finally, the study explored the possibility of using different perforation geometries by altering the dimensions of the holes. The goal was to increase the size of the perforations to enhance force reduction while maintaining acceptable stress levels, for which two alternative perforation options were examined.

Simulations revealed that, for SS6, maximum stress still occurred at the perforations for both models. Further simulations for different sea states demonstrated different responses for these alternative geometries. Perforation option 1 showed favorable results for SS6, while option 2 resulted in increased maximum stress at the perforations compared to the original geometry.

The outcomes indicated that the choice of perforation geometry could significantly impact the structural response, with the potential to reduce or increase maximum stresses depending on the sea state and design conditions.

In conclusion, the report explored various strategies to improve the structural performance of the perforated monopile. These included changes in plate thickness, modifications to the damping characteristics, and alterations in perforation geometry. The results demonstrated the complex interplay of these factors in influencing stress concentrations and fatigue damage for different sea states and loading conditions. These findings contribute to a better understanding of the structural behavior of perforated monopiles in offshore environments and provide insights into optimizing their

design for long-term performance and reliability.

6

Discussion

Finally, a discussion on the applicability of the concept and potential usage of perforated monopiles in deep water. Important conclusions can be made from the results obtained from this study bringing deeper insight to the behaviour and response to environmental loading of the structure in deep water sites. It is crucial, however, to consider the scope of the research when determining the potential of the perforated monopile as an OWSS. Thus, several discussion points and recommendations for future research are presented in the following sections.

6.1. Recommendations and Further Analysis

Firstly, ensuring the structural integrity of the monopile is essential. However, focusing solely on structural integrity can lead to over-engineering. To optimize cost-effectiveness, it's crucial to evaluate the structure's potential for material reduction in non-critical areas and consider alternative materials. When the mass of the structure cannot be reduced further without compromising structural integrity, the design can be considered complete. High costs associated with the monopile structure can become a limiting factor, potentially halting further development.

Furthermore, site selection plays a vital role in structural design. Choosing a representative site in the North Sea was based on factors like water depth and readily available environmental data. Modifying the natural frequency to avoid dominant environmental loading frequencies can be challenging, especially for large offshore wind turbine (OWT) structures. Careful selection of offshore sites within deep water locations is recommended to assess the potential of deploying such structures effectively.

An important limitation for this study was the turbine characteristics since they can not be modified. Currently the design of the turbine and the foundation is done separately by different industries. This meant that the foundation, which had to be designed for a natural frequency of 0.2 Hz was limited to thickness adjustments because the adjusting the diameter of the monopile and increasing the thickness to the required values to achieve this was not feasible because the stiffness of the monopile would be such that the load concentrations would shift to the tower.

Ideally, as OWT technologies advance, the industry should move towards an integrated design apporach where flexibility in changes of the tower parameter is possible together with adjustments to the parameters of the foundation.

Enhancing the modeling of environmental conditions is crucial for accuracy. Using smaller water depth intervals can lead to more precise lumping of wave loads. Additionally, employing more accurate wave models is important, especially for deep waters. Examining how the Keulegan-Carpenter (KC) number affects wave load signals for perforated monopiles is essential. Furthermore, considering the variability of the wave reduction factor within each wave time signal is important. Incorporating different load case probabilities, including those related to maintenance and fault conditions, can add depth to the analysis.

Additionally, in principle, two scatter diagrams are required for the production wind speed range: one with the load cases probabilities during actual production and another for failure and repair state. This study considered the turbine to be operational throughout it's design life which is not the case when considering maintenance, fault and the variation in thrust force before the turbine reaches rated wind speed. Establishment of such load case probabilities is quite a cumbersome task and outside of the scope of this research.

Another aspect that could lead to uncertanties is the accuracy of stress distributions. Choosing between solid and shell elements depends on the need for stress distribution accuracy. Solid elements are suitable for capturing complex stress gradients, but shell elements were chosen due to computational efficiency. A comparison between both types of elements to assess stress concentration differences is recommended.

Consideration of damping in the structure is crucial for preventing resonance and high stress variations. Damping aspects should be thoroughly studied and compared to the results obtained in this thesis. Additionally, potential factors like marine growth and ice formations on perforations should be considered when accounting for the design life of an OWT.

Exploring the performance of perforated monopiles in shallow waters, considering the 5% mass reduction due to perforations, and the associated economic benefits is a potential area of future research. Furthermore, an integrated design process that addresses the interaction between turbine design and foundation design should be considered for future OWT projects. Lastly, studying the effectiveness of structural control mechanisms, such as resonant dampers, can lead to advancements in reducing fatigue damage in offshore wind turbines.

Finally, different material at the splash zone (i.e. S40 structural steel) can be beneficial in terms of fatigue load resistance due to its better performance in accordance to the S-N curves. Because of the higher cost of the potentially better performing material however, this should be done carefully and in a cost effective way. By changing the material in specific areas with high stresses, the resistance of the material can be increased thus, the structure could possibly pass the fatigue limit check for the design life of 25 years.

An interesting additional opportunity could be to add strengthening on the inside of the monopile to allow for even further increase of pile porosity. Additional research is required to identify whether the potential gains outweigh the additional manufacturing step required to weld the strengthening parts on the inside of the pile.

References

Andersen, J., Abrahamsen, R., Andersen, T. L., Andersen, M. T., Baun, T. L., & Neubauer, J. L. (2020). Wave load mitigation by perforation of monopiles. *Journal of Marine Science and Engineering, 8*(5). https://doi.org/10.3390/JMSE8050352

Arany, L., Bhattacharya, S., Macdonald, J., & Hogan, S. J. (2017). Design of monopiles for offshore wind turbines in 10 steps. *Soil Dynamics and Earthquake Engineering, 92*, 126–152. https://doi.org/10.1016/j.soildyn.2016.09.024

DNV-GL. (2007). *OFFSHORE STANDARD DESIGN OF OFFSHORE WIND TURBINE STRUCTURES* (tech. rep.). Det Norske Veritas. http://webshop.dnv.com/global/,

DNV-GL. (2010). *DNV-RP-C205: ENVIRONMENTAL CONDITIONS AND ENVIRONMENTAL LOADS* (tech. rep.). Det Norske Veritas. http://www.dnv.com

DNV-GL. (2011). *DNV-RP-C205 Fatigue Design of Offshore Steel Structures* (tech. rep.). Det Norske Varitas. http://www.dnv.com

DNV-GL. (2016). *DNV-GL-ST-0437 Loads and site conditions for wind turbines* (tech. rep.). Det Norske Veritas. http://www.dnvgl.com

European Comission. (2022). RE Power EU Plan.

Fischer, T., De Vries, W., Schmidt, B., Argyriadis, K., Tarp-Johansen, N.-J., Passon, P., & Ploeg, A. (2010). *Upwind Design Basis (WP4: Offshore Foundations and Support Structures)* (tech. rep.). www.golfklimaat.nl

GWEC. (2022a). *FLOATING OFFSHORE WIND-A GLOBAL OPPORTUNITY* (tech. rep.). Global Wind Energy Council. www.gwec.net

GWEC. (2022b). *Offshore Wind Report 2022* (tech. rep.). Global Wind Energy Council. www.gwec.net

Holthuijsen. (2010). *Waves in oceanic and coastal waters* (tech. rep.).

IEA. (2019). *Offshore Wind Outlook 2019: World Energy Outlook Special Report* (tech. rep.). International Energy Agency. www.iea.org/t&c/

K. Hasselmann, W. Sell, D. B. Ross, & P. Müller. (1975). A Parametric Wave Prediction Model.

Kauzlarich, J. J. (1989). *The Palmgren-Miner rule derived* (tech. rep.).

Kuehn, M. (J. (2001). *Dynamics and design optimisation of offshore wind energy conversion systems.* DUWIND, Delft University Wind Energy Research Institute.

Liu, Y. E. (2021). *Monopile Forever Overcoming the Technical Boundaries of Monopile Foundations in Deep Waters* (tech. rep.). http://repository.tudelft.nl/.

MEACP. (2019). *Climate Agreement* (tech. rep.). Ministry of Economic Affairs and Climate Policy.

NEA. (2023). *Dutch Offshore Wind Innovation Guide* (tech. rep.). Netherlands Enterprise Agency. www.windandwaterworks.com

Oh, K. Y., Nam, W., Ryu, M. S., Kim, J. Y., & Epureanu, B. I. (2018). A review of foundations of offshore wind energy convertors: Current status and future perspectives. https://doi.org/10.1016/j.rser.2018.02.005

Santos, A. (2013). Determination of stress concentration factors on flat plates of structural steel. *Journal of Physics: Conference Series, 466*(1). https://doi.org/10.1088/1742-6596/466/1/012035

Sarpkaya. (2010). *Wave Forces on Offshore Structures* (tech. rep.).

Star, J. Q. (2022). *Thesis Surrogate models for the char-acterization of hydrodynamic loads on perforated monopiles* (tech. rep.). http://repository.tudelft.nl/.

Van Der Ploeg, J. F. (2021). *Perforation of Monopiles to Reduce Hydrodynamic Loads and Enable use in Deep Waters* (tech. rep.).

Vergassola, M., Cabboi, A., & Der Male, P. V. (2020). Comparative analysis of offshore support structures for two-bladed large wind turbines (10+MW) in deep waters. *Journal of Physics: Conference Series*, *1618*(5). https://doi.org/10.1088/1742-6596/1618/5/052076

Zaaijer, M. B. (2006). Foundation modelling to assess dynamic behaviour of offshore wind turbines. *Applied Ocean Research*, *28*(1), 45–57. https://doi.org/10.1016/j.apor.2006.03.004

A

Appendix A: Scatter diagrams

Load case study

	lower	00	01	02	03	04	05	06	07	08	09	10	11	12	13	14	15	16	17	18	19	20	21	22	23	24	25	26	27	28	
lower	upper	01	02	03	04	05	06	07	08	09	10	11	12	13	14	15	16	17	18	19	20	21	22	23	24	25	26	27	28	29	total
0.0	0.5	0.1	0.3	0.4	0.5	0.5	0.3	0.1	0.0	0.0	0	0	0	0	0	0	0	0	0	0	0	0	0	0	0	0	0	0	0	0	2.3
0.5	1.0	0.2	1.0	1.6	2.0	2.4	2.3	1.9	1.0	0.4	0.1	0.0	0.0	0.0	0	0	0	0	0	0	0	0	0	0	0	0	0	0	0	0	12.9
1.0	1.5	0.1	0.6	1.2	1.7	2.3	2.8	3.0	2.5	1.7	0.9	0.4	0.1	0.0	0.0	0.0	0.0	0	0	0	0	0	0	0	0	0	0	0	0	0	17.4
1.5	2.0	0.1	0.3	0.6	1.0	1.5	1.8	2.2	2.5	2.4	1.7	1.0	0.6	0.2	0.1	0.0	0.0	0.0	0	0	0	0	0	0	0	0	0	0	0	0	15.9
2.0	2.5	0.0	0.2	0.4	0.5	0.8	1.1	1.3	1.7	1.9	1.9	1.5	1.1	0.6	0.3	0.1	0.1	0.0	0.0	0.0	0.0	0	0	0	0	0	0	0	0	0	13.6
2.5	3.0	0.0	0.1	0.2	0.3	0.4	0.6	0.7	1.0	1.3	1.6	1.6	1.4	0.9	0.6	0.3	0.1	0.1	0.0	0.0	0.0	0	0	0	0	0	0	0	0	0	11.1
3.0	3.5	0.0	0.0	0.1	0.2	0.2	0.3	0.4	0.5	0.6	0.9	1.1	1.2	1.0	0.7	0.5	0.2	0.1	0.1	0.0	0.0	0.0	0.0	0	0	0	0	0	0	0	8.3
3.5	4.0	0.0	0.0	0.0	0.1	0.1	0.2	0.2	0.3	0.4	0.5	0.6	0.9	0.9	0.8	0.6	0.4	0.2	0.1	0.0	0.0	0.0	0.0	0.0	0	0	0	0	0	0	6.3
4.0	4.5	0.0	0.0	0.0	0.0	0.0	0.1	0.1	0.1	0.2	0.2	0.4	0.5	0.5	0.6	0.6	0.4	0.3	0.1	0.1	0.0	0.0	0.0	0.0	0	0.0	0	0	0	0	4.2
4.5	5.0	0	0.0	0.0	0.0	0.0	0.0	0.0	0.1	0.1	0.1	0.2	0.3	0.3	0.3	0.3	0.4	0.3	0.3	0.2	0.1	0.1	0.0	0.0	0.0	0.0	0.0	0	0	0	2.9
5.0	5.5	0	0	0.0	0.0	0.0	0.0	0.0	0.0	0.0	0.0	0.1	0.1	0.2	0.2	0.2	0.2	0.3	0.2	0.1	0.1	0.0	0.0	0.0	0.0	0.0	0.0	0	0	0	2.0
5.5	6.0	0.0	0	0.0	0.0	0.0	0.0	0.0	0.0	0.0	0.0	0.0	0.1	0.1	0.1	0.1	0.2	0.2	0.2	0.1	0.1	0.0	0.0	0.0	0.0	0.0	0	0	0	0	1.3
6.0	6.5	0.0	0	0	0	0	0.0	0.0	0.0	0.0	0.0	0.0	0.0	0.0	0.1	0.1	0.1	0.1	0.1	0.1	0.1	0.0	0.0	0.0	0.0	0.0	0.0	0	0	0	0.7
6.5	7.0	0	0	0	0	0.0	0	0	0.0	0.0	0.0	0.0	0.0	0.0	0.0	0.0	0.0	0.1	0.1	0.0	0.1	0.0	0.0	0.0	0.0	0	0.0	0	0	0	0.5
7.0	7.5	0	0	0	0	0	0	0	0	0	0.0	0.0	0.0	0.0	0.0	0.0	0.0	0.0	0.0	0.0	0.0	0.0	0.0	0.0	0.0	0.0	0	0	0	0	0.3
7.5	8.0	0	0	0	0	0.0	0	0	0.0	0	0	0.0	0	0.0	0.0	0.0	0.0	0.0	0.0	0.0	0.0	0.0	0.0	0.0	0.0	0.0	0.0	0	0.0	0	0.1
8.0	8.5	0	0	0	0	0	0	0	0	0	0	0	0.0	0.0	0.0	0.0	0.0	0.0	0.0	0.0	0.0	0.0	0.0	0.0	0.0	0.0	0	0	0	0	0.1
8.5	9.0	0	0	0	0	0	0	0	0	0	0.0	0	0.0	0.0	0.0	0.0	0.0	0.0	0.0	0.0	0.0	0.0	0.0	0.0	0.0	0.0	0.0	0.0	0	0	0.0
9.0	9.5	0	0	0	0	0	0	0	0	0	0	0	0	0	0.0	0.0	0.0	0.0	0.0	0.0	0.0	0.0	0.0	0.0	0.0	0.0	0.0	0.0	0	0	0.0
9.5	10.0	0	0	0	0	0	0	0	0	0	0	0	0	0	0	0	0.0	0	0.0	0	0.0	0.0	0.0	0.0	0	0	0.0	0	0.0	0	0.0
10.0	10.5	0	0	0	0	0	0	0	0	0	0	0	0	0	0	0	0	0.0	0.0	0.0	0	0	0.0	0	0	0	0	0.0	0.0	0	0.0
10.5	11.0	0	0	0	0	0	0	0	0	0	0	0	0	0	0	0	0	0	0	0.0	0	0	0.0	0	0	0	0	0	0	0	0.0
11.0	11.5	0	0	0	0	0	0	0	0	0	0	0	0	0	0	0	0	0	0	0	0	0	0	0	0.0	0	0	0	0	0	0.0
11.5	12.0	0	0	0	0	0	0	0	0	0	0	0	0	0	0	0	0	0	0	0	0	0	0	0	0	0	0	0	0	0	0.0
total		0.5	2.5	4.6	6.4	8.2	9.4	9.9	9.8	9.1	8.1	7.1	6.2	4.8	3.8	3.0	2.2	1.5	1.1	0.7	0.4	0.3	0.2	0.1	0.0	0.0	0.0	0.0	0.0	0.0	100.0

Your choices :

Model output point is 59° 00'N, 2° 30'E
Season is all year
First and last year analysed 1992-2020
Variables are wave height (m) and wind speed (m/s)
Data source is wavemodel
Results are based on 84744 model records

Figure A.1: Percentage of occurrence of wave height (m) in rows versus wind speed (m/s) in columns. Van Der Ploeg, 2021

	lower	00	01	02	03	04	05	06	07	08	09	10	11	12	13	14	15	16	17	18	19	20	21	
lower	upper	01	02	03	04	05	06	07	08	09	10	11	12	13	14	15	16	17	18	19	20	21	22	total
0.0	0.5	0	0.0	0.1	0.3	0.4	0.3	0.3	0.3	0.4	0.2	0.1	0.1	0.0	0.0	0.0	0.0	0	0.0	0	0	0	0	2.3
0.5	1.0	0	0	0.0	0.8	1.8	2.3	1.4	1.6	1.2	1.3	1.1	0.7	0.4	0.2	0.0	0.1	0.0	0	0.0	0	0.0	0	12.9
1.0	1.5	0	0	0	0.0	2.2	3.8	1.5	2.9	1.6	1.4	1.4	1.3	0.9	0.2	0.1	0.1	0.0	0	0.0	0	0	0	17.4
1.5	2.0	0	0	0	0	0.6	3.6	2.3	2.3	1.4	1.3	1.2	1.1	1.0	0	0.5	0.2	0.0	0.0	0.0	0	0	0	15.9
2.0	2.5	0	0	0	0	0.0	0.4	4.1	1.9	1.8	1.5	1.2	0.8	0.9	0	0.6	0.2	0	0.0	0.0	0	0	0	13.6
2.5	3.0	0	0	0	0	0.0	0.0	2.4	2.5	2.1	0.9	1.1	0.7	0.7	0	0.5	0.2	0	0.0	0	0	0	0	11.1
3.0	3.5	0	0	0	0	0	0.0	0.6	2.3	2.5	0.5	0.8	0.7	0.4	0.0	0.4	0.2	0	0.0	0	0.0	0	0	8.3
3.5	4.0	0	0	0	0	0	0	0.1	1.0	3.1	0.4	0.4	0.5	0	0.3	0.3	0.2	0	0.0	0	0.0	0	0	6.3
4.0	4.5	0	0	0	0	0	0	0.0	0.2	2.6	0.3	0.3	0.3	0	0.2	0.2	0.1	0	0.0	0	0	0	0	4.2
4.5	5.0	0	0	0	0	0	0	0	0.0	1.6	0.4	0.2	0.2	0	0.2	0.1	0.0	0	0.0	0	0	0	0	2.9
5.0	5.5	0	0	0	0	0	0	0	0.0	0.9	0.5	0.2	0.1	0	0.1	0.1	0.0	0	0.0	0	0	0	0	2.0
5.5	6.0	0	0	0	0	0	0	0	0	0.3	0.5	0.2	0.1	0	0.1	0.0	0.0	0	0.0	0	0	0	0	1.3
6.0	6.5	0	0	0	0	0	0	0	0	0.1	0.4	0.1	0.1	0	0.1	0.0	0.0	0	0.0	0	0	0	0	0.7
6.5	7.0	0	0	0	0	0	0	0	0	0.0	0.2	0.1	0.1	0	0.1	0.0	0.0	0	0.0	0	0	0	0	0.5
7.0	7.5	0	0	0	0	0	0	0	0	0	0.1	0.1	0.0	0	0.0	0.0	0.0	0	0.0	0	0	0	0	0.3
7.5	8.0	0	0	0	0	0	0	0	0	0	0.0	0.1	0.0	0	0.0	0.0	0.0	0	0	0	0	0	0	0.1
8.0	8.5	0	0	0	0	0	0	0	0	0	0.0	0.0	0.0	0	0.0	0.0	0.0	0	0	0	0	0	0	0.1
8.5	9.0	0	0	0	0	0	0	0	0	0	0	0.0	0.0	0	0.0	0.0	0	0	0	0	0	0	0	0.0
9.0	9.5	0	0	0	0	0	0	0	0	0	0	0	0.0	0	0.0	0.0	0.0	0	0	0	0	0	0	0.0
9.5	10.0	0	0	0	0	0	0	0	0	0	0	0	0.0	0	0.0	0.0	0	0	0	0	0	0	0	0.0
10.0	10.5	0	0	0	0	0	0	0	0	0	0	0	0.0	0	0.0	0.0	0.0	0	0	0	0	0	0	0.0
10.5	11.0	0	0	0	0	0	0	0	0	0	0	0	0	0	0	0.0	0	0	0	0	0	0	0	0.0
11.0	11.5	0	0	0	0	0	0	0	0	0	0	0	0	0	0	0.0	0	0	0	0	0	0	0	0.0
11.5	12.0	0	0	0	0	0	0	0	0	0	0	0	0	0	0	0	0	0	0	0	0	0	0	0.0
total		0.0	0.0	0.1	1.1	5.0	10.4	12.6	15.1	19.5	10.1	8.5	7.0	4.3	1.7	3.0	1.2	0.1	0.2	0.0	0.0	0.0	0.0	100.0

Your choices :

Model output point is 59° 00'N, 2° 30'E
Season is all year
First and last year analysed 1992-2020
Variables are wave height (m) and peak wave period (s)
Data source is wavemodel
Results are based on 84744 model records

Figure A.2: Percentage of occurrence of wave height (m) in rows versus peak wave period (s) in columns.Van Der Ploeg, 2021

	lower	01	02	03	04	05	06	07	08	09	10	11	12	
lower	upper	02	03	04	05	06	07	08	09	10	11	12	13	total
0.0	0.5	0	0.1	1.0	0.9	0.2	0.0	0.0	0	0	0	0	0	2.3
0.5	1.0	0	0.0	2.2	7.1	2.6	0.7	0.2	0.1	0.0	0.0	0	0	12.9
1.0	1.5	0	0	0.2	8.5	6.1	1.9	0.4	0.2	0.0	0.0	0	0	17.4
1.5	2.0	0	0	0	3.8	8.3	2.9	0.8	0.1	0.1	0.0	0	0	15.9
2.0	2.5	0	0	0	0.2	8.3	3.6	1.2	0.2	0.0	0.0	0.0	0	13.6
2.5	3.0	0	0	0	0	4.6	5.1	1.2	0.3	0.0	0.0	0	0	11.1
3.0	3.5	0	0	0	0	0.6	6.2	1.2	0.3	0.0	0.0	0	0	8.3
3.5	4.0	0	0	0	0	0.0	4.4	1.6	0.3	0.0	0.0	0	0	6.3
4.0	4.5	0	0	0	0	0	1.6	2.3	0.2	0.0	0.0	0	0	4.2
4.5	5.0	0	0	0	0	0	0.3	2.3	0.2	0.0	0.0	0	0	2.9
5.0	5.5	0	0	0	0	0	0.0	1.5	0.4	0.0	0.0	0	0	2.0
5.5	6.0	0	0	0	0	0	0	0.6	0.6	0.0	0.0	0	0	1.3
6.0	6.5	0	0	0	0	0	0	0.2	0.5	0.0	0	0	0	0.7
6.5	7.0	0	0	0	0	0	0	0.0	0.4	0.1	0.0	0	0	0.5
7.0	7.5	0	0	0	0	0	0	0.0	0.2	0.1	0.0	0	0	0.3
7.5	8.0	0	0	0	0	0	0	0	0.1	0.1	0.0	0	0	0.1
8.0	8.5	0	0	0	0	0	0	0	0.0	0.1	0.0	0	0	0.1
8.5	9.0	0	0	0	0	0	0	0	0.0	0.0	0.0	0	0	0.0
9.0	9.5	0	0	0	0	0	0	0	0	0.0	0.0	0	0	0.0
9.5	10.0	0	0	0	0	0	0	0	0	0.0	0.0	0.0	0	0.0
10.0	10.5	0	0	0	0	0	0	0	0	0.0	0.0	0.0	0	0.0
10.5	11.0	0	0	0	0	0	0	0	0	0	0.0	0.0	0	0.0
11.0	11.5	0	0	0	0	0	0	0	0	0	0	0.0	0	0.0
11.5	12.0	0	0	0	0	0	0	0	0	0	0	0	0	0.0
total		0.0	0.1	3.4	20.5	30.8	26.8	13.6	4.0	0.7	0.1	0.0	0.0	100.0

Your choices :

Model output point is 59° 00'N, 2° 30'E
Season is all year
First and last year analysed 1992-2020
Variables are wave height (m) and zero-crossing wave period (s)
Data source is wavemodel
Results are based on 84744 model records

Figure A.3: Percentage of occurrence of wave height (m) in rows versus zerocrossing wave period (s) in columns. Van Der Ploeg, 2021

B

Appendix B: DLC's

SS	Hs	Tp	U(h)	Prob
1	$0 < Hs < 1$	5.5	5.1	6.82
2	$0 < Hs < 1$	5.5	11.0	8.59
3	$1 < Hs < 2$	12.8	9.5	1.48
4	$1 < Hs < 2$	8.4	8.0	10.27
5	$1 < Hs < 2$	8.4	13.9	10.35
6	$1 < Hs < 2$	6.2	8.0	5.38
7	$1 < Hs < 2$	6.2	13.9	6.34
8	$1 < Hs < 2$	6.2	15.3	0.79
9	$2 < Hs < 3$	7.5	6.6	2.29
10	$2 < Hs < 3$	7.5	8.0	1.50
11	$2 < Hs < 3$	7.5	9.5	1.77
12	$2 < Hs < 3$	7.5	11.0	2.65
13	$2 < Hs < 3$	7.5	12.4	1.67
14	$2 < Hs < 3$	7.5	13.9	1.83
15	$2 < Hs < 3$	7.5	15.3	1.62
16	$2 < Hs < 3$	7.5	16.8	1.31
17	$2 < Hs < 3$	7.5	19.0	1.57
18	$2 < Hs < 3$	10	12.4	1.13
19	$2 < Hs < 3$	10	13.9	1.23
20	$2 < Hs < 3$	10	15.3	1.09
21	$2 < Hs < 3$	10	16.8	1.94
22	$2 < Hs < 3$	12.5	13.9	2.85
23	$3 < Hs < 4$	9	11.0	2.50
24	$3 < Hs < 4$	9	12.4	1.00
25	$3 < Hs < 4$	9	13.9	1.40
26	$3 < Hs < 4$	9	15.3	1.70
27	$3 < Hs < 4$	9	16.8	2.10
28	$3 < Hs < 4$	9	19.0	3.40
29	$3 < Hs < 4$	9	21.9	1.70
30	$4 < Hs < 5$	11.5	16.8	1.94
31	$4 < Hs < 5$	11.5	19.0	1.65
32	$4 < Hs < 5$	11.5	21.9	2.53
33	$5 < Hs < 7$	8	21.9	1.70
34	$5 < Hs < 7$	8	26.3	0.97
35	$5 < Hs < 7$	11	26.3	0.93

C

Appendix C: FLS analysis

C.1. Reference monopile, mudline fatigue damage calculations

SS	min amp	max amp	cycle	avg amp	total cycles	design life	log S		Eq. Fatigue da
	3.81E+06	4.23E+06	0.5	2.10E+05	2150	53762	1.36E+01	4.25E+13	0.000000
	3.38E+06	3.81E+06	0	2.15E+05	0	0	1.36E+01	3.87E+13	0.000000
	2.96E+06	3.38E+06	1	2.10E+05	4301	107523	1.36E+01	4.25E+13	0.000000
	2.54E+06	2.96E+06	0.5	2.10E+05	2150	53762	1.36E+01	4.25E+13	0.000000
	2.12E+06	2.54E+06	1	2.10E+05	4301	107523	1.36E+01	4.25E+13	0.000000
	1.69E+06	2.12E+06	3	2.15E+05	12903	322570	1.36E+01	3.87E+13	0.000000
1	1.27E+06	1.69E+06	6	2.10E+05	25806	645139	1.36E+01	4.25E+13	0.000000
	8.46E+05	1.27E+06	0.5	2.12E+05	2150	53762	1.36E+01	4.09E+13	0.000000
	6.35E+05	8.46E+05	2	1.06E+05	8602	215046	1.48E+01	6.67E+14	0.000000
	4.23E+05	6.35E+05	6	1.06E+05	25806	645139	1.48E+01	6.54E+14	0.000000
	2.12E+05	4.23E+05	25.5	1.06E+05	109674	2741843	1.48E+01	6.67E+14	0.000000
	1.06E+05	2.12E+05	47.5	5.30E+04	204294	5107354	1.60E+01	1.05E+16	0.000000
	0	1.06E+05	397.5	5.30E+04	1709619	42740487	1.60E+01	1.05E+16	0.000000
				0.00E+00					0.000000
	5.29E+07	5.88E+07	0.5	2.95E+06	2710	67756	9.04E+00	1.09E+09	0.000062
	4.70E+07	5.29E+07	1.5	2.95E+06	8131	203267	9.04E+00	1.09E+09	0.000186
	4.12E+07	4.70E+07	5	2.90E+06	27102	677557	9.07E+00	1.17E+09	0.000580
	3.53E+07	4.12E+07	4	2.95E+06	21682	542046	9.04E+00	1.09E+09	0.000497
	2.94E+07	3.53E+07	7	2.95E+06	37943	948580	9.04E+00	1.09E+09	0.000870
	2.35E+07	2.94E+07	8	2.95E+06	43364	1084091	9.04E+00	1.09E+09	0.000994
	1.76E+07	2.35E+07	17.5	2.95E+06	94858	2371450	9.04E+00	1.09E+09	0.002174
2	1.18E+07	1.76E+07	22.5	2.90E+06	121960	3049007	9.07E+00	1.17E+09	0.002611
	8.82E+06	1.18E+07	9.5	1.49E+06	51494	1287359	1.02E+01	1.68E+10	0.000077
	5.88E+06	8.82E+06	3	1.47E+06	16261	406534	1.02E+01	1.77E+10	0.000023
	2.94E+06	5.88E+06	2	1.47E+06	10841	271023	1.02E+01	1.77E+10	0.000015
	1.47E+06	2.94E+06	3	7.35E+05	16261	406534	1.15E+01	2.83E+11	0.000001
	0	1.47E+06	24	7.35E+05	130091	3252274	1.15E+01	2.83E+11	0.000011
				0.00E+00					0.008102
	3.98E+07	4.42E+07	1	2.20E+06	932	23297	9.55E+00	3.53E+09	0.000007
	3.54E+07	3.98E+07	2	2.20E+06	1864	46594	9.55E+00	3.53E+09	0.000013
	3.09E+07	3.54E+07	3	2.25E+06	2796	69891	9.51E+00	3.22E+09	0.000022
	2.65E+07	3.09E+07	3	2.20E+06	2796	69891	9.55E+00	3.53E+09	0.000020
	2.21E+07	2.65E+07	4.5	2.20E+06	4193	104836	9.55E+00	3.53E+09	0.000030
	1.77E+07	2.21E+07	4	2.20E+06	3727	93187	9.55E+00	3.53E+09	0.000026
3	1.33E+07	1.77E+07	9	2.20E+06	8387	209672	9.55E+00	3.53E+09	0.000059
	8.84E+06	1.33E+07	12.5	2.23E+06	11648	291211	9.52E+00	3.34E+09	0.000087
	6.63E+06	8.84E+06	7.5	1.11E+06	6989	174726	1.07E+01	5.54E+10	0.000003
	4.42E+06	6.63E+06	11	1.11E+06	10251	256266	1.07E+01	5.54E+10	0.000005
	2.21E+06	4.42E+06	9.5	1.11E+06	8853	221320	1.07E+01	5.54E+10	0.000004
	1.11E+06	2.21E+06	6	5.50E+05	5591	139781	1.20E+01	9.03E+11	0.000000
	0	1.11E+06	56	5.55E+05	52185	1304624	1.19E+01	8.71E+11	0.000001
				0.00E+00					0.000278
	8.99E+06	9.99E+06	1.5	5.00E+05	9716	242912	1.21E+01	1.32E+12	0.000000
	7.99E+06	8.99E+06	0.5	5.00E+05	3239	80971	1.21E+01	1.32E+12	0.000000
	6.99E+06	7.99E+06	0	5.00E+05	0	0	1.21E+01	1.32E+12	0.000000
	5.99E+06	6.99E+06	0	5.00E+05	0	0	1.21E+01	1.32E+12	0.000000
	5.00E+06	5.99E+06	0.5	4.95E+05	3239	80971	1.21E+01	1.38E+12	0.000000
	4.00E+06	5.00E+06	0.5	5.00E+05	3239	80971	1.21E+01	1.32E+12	0.000000
	3.00E+06	4.00E+06	8	5.00E+05	51821	1295533	1.21E+01	1.32E+12	0.000001
4	2.00E+06	3.00E+06	5.5	5.00E+05	35627	890679	1.21E+01	1.32E+12	0.000001
	1.50E+06	2.00E+06	8.5	2.50E+05	55060	1376504	1.33E+01	2.11E+13	0.000000
	9.99E+05	1.50E+06	7	2.51E+05	45344	1133591	1.33E+01	2.10E+13	0.000000
	5.00E+05	9.99E+05	10.5	2.50E+05	68015	1700387	1.33E+01	2.13E+13	0.000000
	2.50E+05	5.00E+05	16.5	1.25E+05	106881	2672037	1.45E+01	3.38E+14	0.000000
	0	2.50E+05	260	1.25E+05	1684193	42104822	1.45E+01	3.38E+14	0.000000
				0.00E+00					0.000002
	1.29E+08	1.44E+08	0.5	7.50E+06	3265	81624	7.42E+00	2.61E+07	0.003127
	1.15E+08	1.29E+08	1	7.00E+06	6530	163249	7.54E+00	3.44E+07	0.004745
	1.01E+08	1.15E+08	4	7.00E+06	26120	652994	7.54E+00	3.44E+07	0.018980
	8.63E+07	1.01E+08	0.5	7.35E+06	3265	81624	7.45E+00	2.83E+07	0.002884
	7.19E+07	8.63E+07	4	7.20E+06	26120	652994	7.49E+00	3.07E+07	0.021244
	5.75E+07	7.19E+07	7	7.20E+06	45710	1142740	7.49E+00	3.07E+07	0.037177
5	4.31E+07	5.75E+07	11.5	7.20E+06	75094	1877358	7.49E+00	3.07E+07	0.061077
	2.88E+07	4.31E+07	14.5	7.15E+06	94684	2367104	7.50E+00	3.16E+07	0.074893
	2.16E+07	2.88E+07	6	3.60E+06	39180	979491	8.69E+00	4.92E+08	0.001992
	1.44E+07	2.16E+07	7.5	3.60E+06	48975	1224364	8.69E+00	4.92E+08	0.002490
	7.19E+06	1.44E+07	10	3.61E+06	65299	1632485	8.69E+00	4.89E+08	0.003338
	3.60E+06	7.19E+06	7.5	1.80E+06	48975	1224364	9.90E+00	7.96E+09	0.000154
	0	3.60E+06	56.5	1.80E+06	368942	9223541	9.90E+00	7.87E+09	0.001172
				0.00E+00					0.233272

Figure C.1: Reference monopile, Rainflow analysis result and fatigue damage calculation(ML), SS1-SS5

SS	min amp	max amp	cycle	avg amp	total cycles	design life	log S		Eq. Fatigue da
6	6.72E+06	7.47E+06	1.5	3.75E+05	5088	127188	1.26E+01	4.18E+12	0.000000
	5.98E+06	6.72E+06	0.5	3.70E+05	1696	42396	1.26E+01	4.41E+12	0.000000
	5.23E+06	5.98E+06	0	3.75E+05	0	0	1.26E+01	4.18E+12	0.000000
	4.48E+06	5.23E+06	0.5	3.75E+05	1696	42396	1.26E+01	4.18E+12	0.000000
	3.74E+06	4.48E+06	4.5	3.70E+05	15263	381564	1.26E+01	4.41E+12	0.000000
	2.99E+06	3.74E+06	3	3.75E+05	10175	254376	1.26E+01	4.18E+12	0.000000
	2.24E+06	2.99E+06	5.5	3.75E+05	18654	466356	1.26E+01	4.18E+12	0.000000
	1.49E+06	2.24E+06	7.5	3.75E+05	25438	635940	1.26E+01	4.18E+12	0.000000
	1.12E+06	1.49E+06	4	1.85E+05	13567	339168	1.38E+01	7.05E+13	0.000000
	7.47E+05	1.12E+06	7.5	1.87E+05	25438	635940	1.38E+01	6.83E+13	0.000000
	3.74E+05	7.47E+05	16	1.87E+05	54267	1356673	1.38E+01	6.83E+13	0.000000
	1.87E+05	3.74E+05	34	9.35E+04	115317	2882930	1.50E+01	1.08E+15	0.000000
	0	1.87E+05	213	9.35E+04	722428	18060710	1.50E+01	1.08E+15	0.000000
				0.00E+00					0.000001
7	1.21E+08	1.34E+08	0.5	6.50E+06	2001	50015	7.67E+00	4.63E+07	0.001081
	1.07E+08	1.21E+08	0	7.00E+06	0	0	7.54E+00	3.44E+07	0.000000
	9.39E+07	1.07E+08	3	6.55E+06	12004	300089	7.65E+00	4.49E+07	0.006687
	8.05E+07	9.39E+07	1	6.70E+06	4001	100030	7.61E+00	4.10E+07	0.002440
	6.71E+07	8.05E+07	4.5	6.70E+06	18005	450134	7.61E+00	4.10E+07	0.010981
	5.37E+07	6.71E+07	6.5	6.70E+06	26008	650193	7.61E+00	4.10E+07	0.015861
	4.03E+07	5.37E+07	12	6.70E+06	48014	1200357	7.61E+00	4.10E+07	0.029283
	2.68E+07	4.03E+07	15	6.75E+06	60018	1500446	7.60E+00	3.98E+07	0.037708
	2.01E+07	2.68E+07	8.5	3.35E+06	34010	850253	8.82E+00	6.56E+08	0.001296
	1.34E+07	2.01E+07	3	3.35E+06	12004	300089	8.82E+00	6.56E+08	0.000458
	6.71E+06	1.34E+07	11.5	3.35E+06	46014	1150342	8.82E+00	6.60E+08	0.001743
	3.36E+06	6.71E+06	4.5	1.68E+06	18005	450134	1.00E+01	1.05E+10	0.000043
	0	3.36E+06	63.5	1.68E+06	254076	6351888	1.00E+01	1.04E+10	0.000613
				0.00E+00					0.108194
8	1.67E+08	1.86E+08	1	9.50E+06	497	12430	7.01E+00	1.01E+07	0.001226
	1.49E+08	1.67E+08	0	9.00E+06	0	0	7.10E+00	1.26E+07	0.000000
	1.30E+08	1.49E+08	4.5	9.50E+06	2237	55934	7.01E+00	1.01E+07	0.005515
	1.11E+08	1.30E+08	2	9.50E+06	994	24859	7.01E+00	1.01E+07	0.002451
	9.29E+07	1.11E+08	5	9.05E+06	2486	62149	7.09E+00	1.23E+07	0.005047
	7.43E+07	9.29E+07	10	9.30E+06	4972	124297	7.04E+00	1.10E+07	0.011256
	5.57E+07	7.43E+07	7	9.30E+06	3480	87008	7.04E+00	1.10E+07	0.007879
	3.71E+07	5.57E+07	7	9.30E+06	3480	87008	7.04E+00	1.10E+07	0.007879
	2.79E+07	3.71E+07	8.5	4.60E+06	4226	105653	8.27E+00	1.84E+08	0.000573
	1.86E+07	2.79E+07	4.5	4.65E+06	2237	55934	8.25E+00	1.77E+08	0.000317
	9.29E+06	1.86E+07	9.5	4.66E+06	4723	118082	8.25E+00	1.76E+08	0.000671
	4.64E+06	9.29E+06	9	2.33E+06	4475	111868	9.45E+00	2.83E+09	0.000040
	0	4.64E+06	87.5	2.32E+06	43504	1087601	9.46E+00	2.85E+09	0.000381
				0.00E+00					0.043236
9	1.02E+07	1.13E+07	1.5	5.50E+05	2171	54275	1.20E+01	9.03E+11	0.000000
	9.04E+06	1.02E+07	1	5.80E+05	1447	36183	1.19E+01	7.30E+11	0.000000
	7.91E+06	9.04E+06	1	5.65E+05	1447	36183	1.19E+01	8.11E+11	0.000000
	6.78E+06	7.91E+06	4	5.65E+05	5789	144734	1.19E+01	8.11E+11	0.000000
	5.65E+06	6.78E+06	6	5.65E+05	8684	217100	1.19E+01	8.11E+11	0.000000
	4.52E+06	5.65E+06	2.5	5.65E+05	3618	90459	1.19E+01	8.11E+11	0.000000
	3.39E+06	4.52E+06	5.5	5.65E+05	7960	199009	1.19E+01	8.11E+11	0.000000
	2.26E+06	3.39E+06	11	5.65E+05	15921	398018	1.19E+01	8.11E+11	0.000000
	1.70E+06	2.26E+06	6.5	2.80E+05	9408	235192	1.31E+01	1.34E+13	0.000000
	1.13E+06	1.70E+06	5.5	2.85E+05	7960	199009	1.31E+01	1.25E+13	0.000000
	5.65E+05	1.13E+06	9.5	2.83E+05	13750	343742	1.31E+01	1.30E+13	0.000000
	2.83E+05	5.65E+05	14.5	1.41E+05	20986	524659	1.43E+01	2.09E+14	0.000000
	0	2.83E+05	156	1.42E+05	225784	5644612	1.43E+01	2.06E+14	0.000000
				0.00E+00					0.000002
10	1.18E+07	1.31E+07	2.5	6.50E+05	2366	59146	1.17E+01	4.63E+11	0.000000
	1.05E+07	1.18E+07	1	6.50E+05	946	23658	1.17E+01	4.63E+11	0.000000
	9.15E+06	1.05E+07	1	6.75E+05	946	23658	1.16E+01	3.98E+11	0.000000
	7.84E+06	9.15E+06	1.5	6.55E+05	1420	35488	1.17E+01	4.49E+11	0.000000
	6.54E+06	7.84E+06	0.5	6.50E+05	473	11829	1.17E+01	4.63E+11	0.000000
	5.23E+06	6.54E+06	1.5	6.55E+05	1420	35488	1.17E+01	4.49E+11	0.000000
	3.92E+06	5.23E+06	6.5	6.55E+05	6151	153779	1.17E+01	4.49E+11	0.000000
	2.61E+06	3.92E+06	15	6.55E+05	14195	354876	1.17E+01	4.49E+11	0.000001
	1.96E+06	2.61E+06	0.5	3.25E+05	473	11829	1.29E+01	7.40E+12	0.000000
	1.31E+06	1.96E+06	6	3.25E+05	5678	141950	1.29E+01	7.40E+12	0.000000
	6.54E+05	1.31E+06	11.5	3.28E+05	10883	272071	1.29E+01	7.14E+12	0.000000
	3.27E+05	6.54E+05	10.5	1.64E+05	9937	248413	1.41E+01	1.16E+14	0.000000
	0	3.27E+05	218.5	1.64E+05	206774	5169357	1.41E+01	1.16E+14	0.000000
				0.00E+00					0.000002

Figure C.2: Reference monopile, Rainflow analysis result and fatigue damage calculation(ML), SS6-SS10

SS	min amp	max amp	cycle	avg amp	total cycles	design life	log S		Eq. Fatigue da
	6.72E+06	7.47E+06	1.5	3.75E+05	1670	41750	1.26E+01	4.18E+12	0.000000
	5.98E+06	6.72E+06	0.5	3.70E+05	557	13917	1.26E+01	4.41E+12	0.000000
	5.23E+06	5.98E+06	0	3.75E+05	0	0	1.26E+01	4.18E+12	0.000000
	4.48E+06	5.23E+06	0.5	3.75E+05	557	13917	1.26E+01	4.18E+12	0.000000
	3.74E+06	4.48E+06	4.5	3.70E+05	5010	125250	1.26E+01	4.41E+12	0.000000
	2.99E+06	3.74E+06	3	3.75E+05	3340	83500	1.26E+01	4.18E+12	0.000000
11	2.24E+06	2.99E+06	5.5	3.75E+05	6123	153084	1.26E+01	4.18E+12	0.000000
	1.49E+06	2.24E+06	7.5	3.75E+05	8350	208750	1.26E+01	4.18E+12	0.000000
	1.12E+06	1.49E+06	4	1.85E+05	4453	111334	1.38E+01	7.05E+13	0.000000
	7.47E+05	1.12E+06	7.5	1.87E+05	8350	208750	1.38E+01	6.83E+13	0.000000
	3.74E+05	7.47E+05	16	1.87E+05	17813	445334	1.38E+01	6.83E+13	0.000000
	1.87E+05	3.74E+05	34	9.35E+04	37853	946335	1.50E+01	1.08E+15	0.000000
	0	1.87E+05	213	9.35E+04	237141	5928513	1.50E+01	1.08E+15	0.000000
				0.00E+00					0.000000
	6.02E+07	6.69E+07	1	3.35E+06	1668	41712	8.82E+00	6.56E+08	0.000064
	5.35E+07	6.02E+07	2	3.35E+06	3337	83424	8.82E+00	6.56E+08	0.000127
	4.68E+07	5.35E+07	2.5	3.35E+06	4171	104279	8.82E+00	6.56E+08	0.000159
	4.01E+07	4.68E+07	5	3.35E+06	8342	208559	8.82E+00	6.56E+08	0.000318
	3.35E+07	4.01E+07	3.5	3.30E+06	5840	145991	8.84E+00	6.97E+08	0.000210
	2.68E+07	3.35E+07	12	3.35E+06	20022	500541	8.82E+00	6.56E+08	0.000763
12	2.01E+07	2.68E+07	11.5	3.35E+06	19187	479686	8.82E+00	6.56E+08	0.000731
	1.34E+07	2.01E+07	23	3.35E+06	38375	959371	8.82E+00	6.56E+08	0.001463
	1.00E+07	1.34E+07	9	1.70E+06	15016	375406	1.00E+01	9.89E+09	0.000038
	6.69E+06	1.00E+07	8.5	1.66E+06	14182	354550	1.00E+01	1.10E+10	0.000032
	3.35E+06	6.69E+06	4	1.67E+06	6674	166847	1.00E+01	1.06E+10	0.000016
	1.67E+06	3.35E+06	3	8.40E+05	5005	125135	1.12E+01	1.66E+11	0.000001
	0	1.67E+06	25	8.35E+05	41712	1042795	1.12E+01	1.70E+11	0.000006
				0.00E+00					0.003927
	6.37E+07	7.08E+07	0.5	3.55E+06	527	13176	8.72E+00	5.20E+08	0.000025
	5.66E+07	6.37E+07	1	3.55E+06	1054	26352	8.72E+00	5.20E+08	0.000051
	4.96E+07	5.66E+07	3	3.50E+06	3162	79057	8.74E+00	5.50E+08	0.000144
	4.25E+07	4.96E+07	6	3.55E+06	6325	158114	8.72E+00	5.20E+08	0.000304
	3.54E+07	4.25E+07	2	3.55E+06	2108	52705	8.72E+00	5.20E+08	0.000101
	2.83E+07	3.54E+07	14	3.55E+06	14757	368933	8.72E+00	5.20E+08	0.000709
13	2.12E+07	2.83E+07	11.5	3.55E+06	12122	303052	8.72E+00	5.20E+08	0.000583
	1.42E+07	2.12E+07	23	3.50E+06	24244	606104	8.74E+00	5.50E+08	0.001101
	1.06E+07	1.42E+07	6.5	1.80E+06	6852	171290	9.90E+00	7.87E+09	0.000022
	7.08E+06	1.06E+07	5.5	1.76E+06	5798	144938	9.93E+00	8.61E+09	0.000017
	3.54E+06	7.08E+06	5	1.77E+06	5270	131762	9.93E+00	8.42E+09	0.000016
	1.77E+06	3.54E+06	5.5	8.85E+05	5798	144938	1.11E+01	1.35E+11	0.000001
	0	1.77E+06	27	8.85E+05	28461	711513	1.11E+01	1.35E+11	0.000005
				0.00E+00					0.003079
	1.31E+08	1.45E+08	0.5	7.00E+06	576	14411	7.54E+00	3.44E+07	0.000419
	1.16E+08	1.31E+08	1.5	7.50E+06	1729	43234	7.42E+00	2.61E+07	0.001656
	1.02E+08	1.16E+08	3	7.00E+06	3459	86469	7.54E+00	3.44E+07	0.002513
	8.72E+07	1.02E+08	3	7.40E+06	3459	86469	7.44E+00	2.75E+07	0.003139
	7.27E+07	8.72E+07	3.5	7.25E+06	4035	100880	7.48E+00	2.99E+07	0.003374
	5.82E+07	7.27E+07	8	7.25E+06	9223	230583	7.48E+00	2.99E+07	0.007712
14	4.36E+07	5.82E+07	15	7.30E+06	17294	432343	7.46E+00	2.91E+07	0.014863
	2.91E+07	4.36E+07	16	7.25E+06	18447	461166	7.48E+00	2.99E+07	0.015424
	2.18E+07	2.91E+07	6.5	3.65E+06	7494	187349	8.67E+00	4.65E+08	0.000403
	1.45E+07	2.18E+07	6.5	3.65E+06	7494	187349	8.67E+00	4.65E+08	0.000403
	7.27E+06	1.45E+07	9.5	3.62E+06	10953	273817	8.68E+00	4.84E+08	0.000566
	3.64E+06	7.27E+06	5	1.82E+06	5765	144114	9.88E+00	7.61E+09	0.000019
	0	3.64E+06	58	1.82E+06	66869	1671727	9.88E+00	7.53E+09	0.000222
				0.00E+00					0.050714
	1.77E+08	1.97E+08	0.5	1.00E+07	511	12764	6.92E+00	8.26E+06	0.001545
	1.57E+08	1.77E+08	2	1.00E+07	2042	51058	6.92E+00	8.26E+06	0.006181
	1.38E+08	1.57E+08	4.5	9.50E+06	4595	114880	7.01E+00	1.01E+07	0.011328
	1.18E+08	1.38E+08	3.5	1.00E+07	3574	89351	6.92E+00	8.26E+06	0.010817
	9.83E+07	1.18E+08	3	9.85E+06	3063	76587	6.94E+00	8.78E+06	0.008728
	7.86E+07	9.83E+07	9.5	9.85E+06	9701	242524	6.94E+00	8.78E+06	0.027638
15	5.90E+07	7.86E+07	9	9.80E+06	9190	229760	6.95E+00	8.96E+06	0.025655
	3.93E+07	5.90E+07	12.5	9.85E+06	12764	319110	6.94E+00	8.78E+06	0.036365
	2.95E+07	3.93E+07	6	4.90E+06	6127	153173	8.16E+00	1.43E+08	0.001069
	1.97E+07	2.95E+07	4.5	4.90E+06	4595	114880	8.16E+00	1.43E+08	0.000802
	9.83E+06	1.97E+07	10	4.94E+06	10212	255288	8.14E+00	1.39E+08	0.001833
	4.91E+06	9.83E+06	7	2.46E+06	7148	178702	9.35E+00	2.26E+09	0.000079
	0	4.91E+06	62	2.46E+06	63312	1582788	9.36E+00	2.27E+09	0.000696
				0.00E+00					0.132735

Figure C.3: Reference monopile, Rainflow analysis result and fatigue damage calculation(ML), SS11-SS15

SS	min amp	max amp	cycle	avg amp	total cycles	design life	log S		Eq. Fatigue da
16	2.67E+08	2.97E+08	0.5	1.50E+07	412	10294	6.21E+00	1.63E+06	0.006309
	2.38E+08	2.67E+08	1	1.45E+07	824	20588	6.27E+00	1.87E+06	0.011017
	2.08E+08	2.38E+08	4.5	1.50E+07	3706	92645	6.21E+00	1.63E+06	0.056779
	1.78E+08	2.08E+08	2.5	1.50E+07	2059	51469	6.21E+00	1.63E+06	0.031544
	1.48E+08	1.78E+08	4.5	1.50E+07	3706	92645	6.21E+00	1.63E+06	0.056779
	1.19E+08	1.48E+08	8	1.45E+07	6588	164702	6.27E+00	1.87E+06	0.088140
	8.91E+07	1.19E+08	13.5	1.50E+07	11117	277935	6.22E+00	1.65E+06	0.168077
	5.94E+07	8.91E+07	18	1.49E+07	14823	370580	6.23E+00	1.70E+06	0.218166
	4.45E+07	5.94E+07	10.5	7.45E+06	8647	216172	7.43E+00	2.68E+07	0.008062
	2.97E+07	4.45E+07	5	7.40E+06	4118	102939	7.44E+00	2.75E+07	0.003737
	1.48E+07	2.97E+07	6	7.45E+06	4941	123527	7.43E+00	2.68E+07	0.004607
	7.42E+06	1.48E+07	5	3.69E+06	4118	102939	8.65E+00	4.46E+08	0.000231
	0	7.42E+06	51	3.71E+06	41999	1049976	8.64E+00	4.36E+08	0.002408
				0.00E+00					0.655855
17	4.49E+08	4.99E+08	0.5	2.50E+07	494	12353	5.33E+00	2.11E+05	0.058414
	3.99E+08	4.49E+08	3	2.50E+07	2965	74116	5.33E+00	2.11E+05	0.350487
	3.49E+08	3.99E+08	4	2.50E+07	3953	98821	5.33E+00	2.11E+05	0.467316
	2.99E+08	3.49E+08	4	2.50E+07	3953	98821	5.33E+00	2.11E+05	0.467316
	2.50E+08	2.99E+08	5	2.45E+07	4941	123527	5.36E+00	2.29E+05	0.538797
	2.00E+08	2.50E+08	10.5	2.50E+07	10376	259406	5.33E+00	2.11E+05	1.226704
	1.50E+08	2.00E+08	16	2.50E+07	15811	395285	5.33E+00	2.11E+05	1.869264
	9.98E+07	1.50E+08	13.5	2.51E+07	13341	333522	5.32E+00	2.08E+05	1.602578
	7.49E+07	9.98E+07	8	1.25E+07	7906	197643	6.54E+00	3.44E+06	0.057485
	4.99E+07	7.49E+07	3	1.25E+07	2965	74116	6.53E+00	3.38E+06	0.021905
	2.50E+07	4.99E+07	10	1.25E+07	9882	247053	6.54E+00	3.44E+06	0.071857
	1.25E+07	2.50E+07	8.5	6.25E+06	8400	209995	7.73E+00	5.41E+07	0.003879
	0	1.25E+07	41	6.25E+06	40517	1012918	7.73E+00	5.41E+07	0.018711
				0.00E+00					6.754715
18	5.79E+07	6.43E+07	0.5	3.20E+06	355	8886	8.90E+00	7.88E+08	0.000011
	5.14E+07	5.79E+07	2.5	3.25E+06	1777	44431	8.87E+00	7.40E+08	0.000060
	4.50E+07	5.14E+07	2.5	3.20E+06	1777	44431	8.90E+00	7.88E+08	0.000056
	3.86E+07	4.50E+07	5.5	3.20E+06	3910	97749	8.90E+00	7.88E+08	0.000124
	3.22E+07	3.86E+07	7	3.20E+06	4976	124408	8.90E+00	7.88E+08	0.000158
	2.57E+07	3.22E+07	13.5	3.25E+06	9597	239929	8.87E+00	7.40E+08	0.000324
	1.93E+07	2.57E+07	13.5	3.20E+06	9597	239929	8.90E+00	7.88E+08	0.000305
	1.29E+07	1.93E+07	18	3.20E+06	12796	319905	8.90E+00	7.88E+08	0.000406
	9.65E+06	1.29E+07	11	1.63E+06	7820	195498	1.01E+01	1.18E+10	0.000017
	6.43E+06	9.65E+06	5	1.61E+06	3555	88863	1.01E+01	1.23E+10	0.000007
	3.22E+06	6.43E+06	6	1.61E+06	4265	106635	1.01E+01	1.24E+10	0.000009
	1.61E+06	3.22E+06	3	8.05E+05	2133	53318	1.13E+01	1.97E+11	0.000000
	0	1.61E+06	17	8.05E+05	12085	302133	1.13E+01	1.97E+11	0.000002
				0.00E+00					0.001479
19	5.63E+07	6.25E+07	0.5	3.10E+06	389	9719	8.95E+00	8.94E+08	0.000011
	5.00E+07	5.63E+07	4	3.15E+06	3110	77755	8.92E+00	8.39E+08	0.000093
	4.38E+07	5.00E+07	2.5	3.10E+06	1944	48597	8.95E+00	8.94E+08	0.000054
	3.75E+07	4.38E+07	4	3.15E+06	3110	77755	8.92E+00	8.39E+08	0.000093
	3.13E+07	3.75E+07	3.5	3.10E+06	2721	68035	8.95E+00	8.94E+08	0.000076
	2.50E+07	3.13E+07	11	3.15E+06	8553	213826	8.92E+00	8.39E+08	0.000255
	1.88E+07	2.50E+07	12.5	3.10E+06	9719	242984	8.95E+00	8.94E+08	0.000272
	1.25E+07	1.88E+07	15.5	3.15E+06	12052	301300	8.92E+00	8.39E+08	0.000359
	9.38E+06	1.25E+07	10	1.56E+06	7775	194387	1.01E+01	1.39E+10	0.000014
	6.25E+06	9.38E+06	5	1.57E+06	3888	97193	1.01E+01	1.38E+10	0.000007
	3.13E+06	6.25E+06	8	1.56E+06	6220	155510	1.01E+01	1.39E+10	0.000011
	1.56E+06	3.13E+06	10	7.85E+05	7775	194387	1.13E+01	2.18E+11	0.000001
	0	1.56E+06	33	7.80E+05	25659	641477	1.13E+01	2.23E+11	0.000003
				0.00E+00					0.001248
20	1.72E+08	1.91E+08	0.5	9.50E+06	344	8609	7.01E+00	1.01E+07	0.000849
	1.53E+08	1.72E+08	0.5	9.50E+06	344	8609	7.01E+00	1.01E+07	0.000849
	1.34E+08	1.53E+08	3	9.50E+06	2066	51651	7.01E+00	1.01E+07	0.005093
	1.14E+08	1.34E+08	4.5	1.00E+07	3099	77477	6.92E+00	8.26E+06	0.009379
	9.54E+07	1.14E+08	3	9.30E+06	2066	51651	7.04E+00	1.10E+07	0.004677
	7.63E+07	9.54E+07	6	9.55E+06	4132	103303	7.00E+00	9.93E+06	0.010402
	5.72E+07	7.63E+07	14.5	9.55E+06	9986	249648	7.00E+00	9.93E+06	0.025139
	3.82E+07	5.72E+07	8.5	9.50E+06	5854	146346	7.01E+00	1.01E+07	0.014430
	2.86E+07	3.82E+07	5	4.80E+06	3443	86086	8.19E+00	1.56E+08	0.000553
	1.91E+07	2.86E+07	9	4.75E+06	6198	154954	8.21E+00	1.62E+08	0.000955
	9.54E+06	1.91E+07	10.5	4.78E+06	7231	180780	8.20E+00	1.58E+08	0.001143
	4.77E+06	9.54E+06	10.5	2.39E+06	7231	180780	9.41E+00	2.55E+09	0.000071
	0	4.77E+06	72.5	2.39E+06	49930	1248241	9.41E+00	2.55E+09	0.000489
				0.00E+00					0.074029

Figure C.4: Reference monopile, Rainflow analysis result and fatigue damage calculation(ML), SS16-SS20

SS	min amp	max amp	cycle	avg amp	total cycles	design life	log S		Eq. Fatigue da
21	2.63E+08	2.92E+08	0.5	1.45E+07	611	15273	6.27E+00	1.87E+06	0.008173
	2.34E+08	2.63E+08	0.5	1.45E+07	611	15273	6.27E+00	1.87E+06	0.008173
	2.05E+08	2.34E+08	3	1.45E+07	3666	91640	6.27E+00	1.87E+06	0.049040
	1.75E+08	2.05E+08	6.5	1.50E+07	7942	198552	6.21E+00	1.63E+06	0.121686
	1.46E+08	1.75E+08	2.5	1.45E+07	3055	76366	6.27E+00	1.87E+06	0.040867
	1.17E+08	1.46E+08	9.5	1.45E+07	11608	290192	6.27E+00	1.87E+06	0.155295
	8.77E+07	1.17E+08	16	1.47E+07	19550	488744	6.25E+00	1.79E+06	0.272541
	5.84E+07	8.77E+07	18	1.47E+07	21993	549837	6.25E+00	1.79E+06	0.306609
	4.38E+07	5.84E+07	6	7.30E+06	7331	183279	7.46E+00	2.91E+07	0.006301
	2.92E+07	4.38E+07	5.5	7.30E+06	6720	168006	7.46E+00	2.91E+07	0.005776
	1.46E+07	2.92E+07	4	7.30E+06	4887	122186	7.46E+00	2.91E+07	0.004201
	7.31E+06	1.46E+07	6	3.65E+06	7331	183279	8.67E+00	4.68E+08	0.000392
	0	7.31E+06	57.5	3.66E+06	70257	1756424	8.67E+00	4.63E+08	0.003795
				0.00E+00					0.982849
22	6.69E+07	7.43E+07	1.5	3.70E+06	2699	67480	8.64E+00	4.41E+08	0.000153
	5.94E+07	6.69E+07	0	3.75E+06	0	0	8.62E+00	4.18E+08	0.000000
	5.20E+07	5.94E+07	3.5	3.70E+06	6298	157453	8.64E+00	4.41E+08	0.000357
	4.46E+07	5.20E+07	7	3.70E+06	12596	314907	8.64E+00	4.41E+08	0.000714
	3.72E+07	4.46E+07	5.5	3.70E+06	9897	247427	8.64E+00	4.41E+08	0.000561
	2.97E+07	3.72E+07	5.5	3.75E+06	9897	247427	8.62E+00	4.18E+08	0.000592
	2.23E+07	2.97E+07	15	3.70E+06	26992	674800	8.64E+00	4.41E+08	0.001531
	1.49E+07	2.23E+07	16.5	3.70E+06	29691	742280	8.64E+00	4.41E+08	0.001684
	1.11E+07	1.49E+07	8.5	1.90E+06	15295	382387	9.80E+00	6.34E+09	0.000060
	7.43E+06	1.11E+07	6	1.84E+06	10797	269920	9.86E+00	7.29E+09	0.000037
	3.72E+06	7.43E+06	5	1.86E+06	8997	224933	9.84E+00	6.98E+09	0.000032
	1.86E+06	3.72E+06	9	9.30E+05	16195	404880	1.10E+01	1.10E+11	0.000004
	0	1.86E+06	41	9.30E+05	73778	1844454	1.10E+01	1.10E+11	0.000017
				0.00E+00					0.005744
23	2.67E+07	2.97E+07	2	1.50E+06	3154	78840	1.02E+01	1.63E+10	0.000005
	2.38E+07	2.67E+07	1	1.45E+06	1577	39420	1.03E+01	1.87E+10	0.000002
	2.08E+07	2.38E+07	3	1.50E+06	4730	118260	1.02E+01	1.63E+10	0.000007
	1.78E+07	2.08E+07	3.5	1.50E+06	5519	137970	1.02E+01	1.63E+10	0.000008
	1.49E+07	1.78E+07	5	1.45E+06	7884	197100	1.03E+01	1.87E+10	0.000011
	1.19E+07	1.49E+07	8.5	1.50E+06	13403	335070	1.02E+01	1.63E+10	0.000021
	8.91E+06	1.19E+07	10	1.50E+06	15768	394200	1.02E+01	1.65E+10	0.000024
	5.94E+06	8.91E+06	13.5	1.49E+06	21287	532170	1.02E+01	1.70E+10	0.000031
	4.46E+06	5.94E+06	7.5	7.40E+05	11826	295650	1.14E+01	2.75E+11	0.000001
	2.97E+06	4.46E+06	0.5	7.45E+05	788	19710	1.14E+01	2.68E+11	0.000000
	1.49E+06	2.97E+06	13.5	7.40E+05	21287	532170	1.14E+01	2.75E+11	0.000002
	7.43E+05	1.49E+06	11.5	3.74E+05	18133	453330	1.26E+01	4.24E+12	0.000000
	0	7.43E+05	70	3.72E+05	110376	2759400	1.26E+01	4.34E+12	0.000001
				0.00E+00					0.000113
24	5.48E+07	6.09E+07	1.5	3.05E+06	946	23652	8.98E+00	9.55E+08	0.000025
	4.87E+07	5.48E+07	2	3.05E+06	1261	31536	8.98E+00	9.55E+08	0.000033
	4.26E+07	4.87E+07	4.5	3.05E+06	2838	70956	8.98E+00	9.55E+08	0.000074
	3.65E+07	4.26E+07	4	3.05E+06	2523	63072	8.98E+00	9.55E+08	0.000066
	3.05E+07	3.65E+07	5.5	3.00E+06	3469	86724	9.01E+00	1.02E+09	0.000085
	2.44E+07	3.05E+07	14	3.05E+06	8830	220752	8.98E+00	9.55E+08	0.000231
	1.83E+07	2.44E+07	10.5	3.05E+06	6623	165564	8.98E+00	9.55E+08	0.000173
	1.22E+07	1.83E+07	20.5	3.05E+06	12930	323244	8.98E+00	9.55E+08	0.000339
	9.14E+06	1.22E+07	9	1.53E+06	5676	141912	1.02E+01	1.51E+10	0.000009
	6.09E+06	9.14E+06	3	1.53E+06	1892	47304	1.02E+01	1.53E+10	0.000003
	3.05E+06	6.09E+06	3	1.52E+06	1892	47304	1.02E+01	1.55E+10	0.000003
	1.52E+06	3.05E+06	4	7.65E+05	2523	63072	1.14E+01	2.41E+11	0.000000
	0	1.52E+06	36	7.60E+05	22706	567648	1.14E+01	2.48E+11	0.000002
				0.00E+00					0.001045
25	5.42E+07	6.02E+07	5	3.00E+06	4415	110376	9.01E+00	1.02E+09	0.000108
	4.82E+07	5.42E+07	2.5	3.00E+06	2208	55188	9.01E+00	1.02E+09	0.000054
	4.21E+07	4.82E+07	6	3.05E+06	5298	132451	8.98E+00	9.55E+08	0.000139
	3.61E+07	4.21E+07	3.5	3.00E+06	3091	77263	9.01E+00	1.02E+09	0.000076
	3.01E+07	3.61E+07	4	3.00E+06	3532	88301	9.01E+00	1.02E+09	0.000087
	2.41E+07	3.01E+07	8.5	3.00E+06	7506	187639	9.01E+00	1.02E+09	0.000184
	1.81E+07	2.41E+07	10.5	3.00E+06	9272	231790	9.01E+00	1.02E+09	0.000227
	1.20E+07	1.81E+07	14.5	3.05E+06	12804	320090	8.98E+00	9.55E+08	0.000335
	9.03E+06	1.20E+07	9.5	1.49E+06	8389	209714	1.02E+01	1.70E+10	0.000012
	6.02E+06	9.03E+06	7.5	1.51E+06	6623	165564	1.02E+01	1.61E+10	0.000010
	3.01E+06	6.02E+06	5	1.51E+06	4415	110376	1.02E+01	1.61E+10	0.000007
	1.51E+06	3.01E+06	9	7.50E+05	7947	198677	1.14E+01	2.61E+11	0.000001
	0	1.51E+06	45	7.55E+05	39735	993384	1.14E+01	2.54E+11	0.000004
				0.00E+00					0.001244

Figure C.5: Reference monopile, Rainflow analysis result and fatigue damage calculation(ML), SS21-SS25

SS	min amp	max amp	cycle	avg amp	total cycles	design life	log S		Eq. Fatigue da
26	1.68E+08	1.87E+08	0.5	9.50E+06	536	13403	7.01E+00	1.01E+07	0.001322
	1.50E+08	1.68E+08	0	9.00E+06	0	0	7.10E+00	1.26E+07	0.000000
	1.31E+08	1.50E+08	5.5	9.50E+06	5897	147431	7.01E+00	1.01E+07	0.014537
	1.12E+08	1.31E+08	3.5	9.50E+06	3753	93820	7.01E+00	1.01E+07	0.009251
	9.36E+07	1.12E+08	4.5	9.20E+06	4825	120625	7.06E+00	1.15E+07	0.010461
	7.48E+07	9.36E+07	7.5	9.40E+06	8042	201042	7.02E+00	1.06E+07	0.019002
	5.61E+07	7.48E+07	13.5	9.35E+06	14475	361876	7.03E+00	1.08E+07	0.033482
	3.74E+07	5.61E+07	12.5	9.35E+06	13403	335070	7.03E+00	1.08E+07	0.031001
	2.81E+07	3.74E+07	3	4.65E+06	3217	80417	8.25E+00	1.77E+08	0.000455
	1.87E+07	2.81E+07	7.5	4.70E+06	8042	201042	8.23E+00	1.69E+08	0.001188
	9.36E+06	1.87E+07	13.5	4.67E+06	14475	361876	8.24E+00	1.74E+08	0.002084
	4.68E+06	9.36E+06	4	2.34E+06	4289	107222	9.44E+00	2.76E+09	0.000039
	0	4.68E+06	72.5	2.34E+06	77736	1943406	9.44E+00	2.76E+09	0.000705
				0.00E+00					0.123527
27	2.59E+08	2.88E+08	0.5	1.45E+07	662	16556	6.27E+00	1.87E+06	0.008860
	2.30E+08	2.59E+08	0	1.45E+07	0	0	6.27E+00	1.87E+06	0.000000
	2.01E+08	2.30E+08	5.5	1.45E+07	7285	182120	6.27E+00	1.87E+06	0.097461
	1.73E+08	2.01E+08	2.5	1.40E+07	3311	82782	6.33E+00	2.15E+06	0.038499
	1.44E+08	1.73E+08	3	1.45E+07	3974	99338	6.27E+00	1.87E+06	0.053161
	1.15E+08	1.44E+08	9	1.45E+07	11921	298015	6.27E+00	1.87E+06	0.159482
	8.63E+07	1.15E+08	13.5	1.44E+07	17881	447023	6.29E+00	1.95E+06	0.229476
	5.75E+07	8.63E+07	24.5	1.44E+07	32451	811264	6.28E+00	1.92E+06	0.422291
	4.31E+07	5.75E+07	7	7.20E+06	9272	231790	7.49E+00	3.07E+07	0.007541
	2.88E+07	4.31E+07	9	7.15E+06	11921	298015	7.50E+00	3.16E+07	0.009429
	1.44E+07	2.88E+07	3	7.20E+06	3974	99338	7.49E+00	3.07E+07	0.003232
	7.19E+06	1.44E+07	3	3.61E+06	3974	99338	8.69E+00	4.89E+08	0.000203
	0	7.19E+06	55.5	3.60E+06	73510	1837760	8.69E+00	4.95E+08	0.003716
				0.00E+00					1.033350
28	4.43E+08	4.92E+08	0.5	2.45E+07	1072	26806	5.36E+00	2.29E+05	0.116920
	3.94E+08	4.43E+08	2.5	2.45E+07	5361	134028	5.36E+00	2.29E+05	0.584601
	3.44E+08	3.94E+08	4	2.50E+07	8578	214445	5.33E+00	2.11E+05	1.014088
	2.95E+08	3.44E+08	4	2.45E+07	8578	214445	5.36E+00	2.29E+05	0.935362
	2.46E+08	2.95E+08	7.5	2.45E+07	16083	402084	5.36E+00	2.29E+05	1.753804
	1.97E+08	2.46E+08	10	2.45E+07	21444	536112	5.36E+00	2.29E+05	2.338406
	1.48E+08	1.97E+08	15.5	2.45E+07	33239	830974	5.36E+00	2.29E+05	3.624529
	9.84E+07	1.48E+08	17.5	2.48E+07	37528	938196	5.34E+00	2.18E+05	4.296356
	7.38E+07	9.84E+07	5	1.23E+07	10722	268056	6.56E+00	3.61E+06	0.074276
	4.92E+07	7.38E+07	8	1.23E+07	17156	428890	6.56E+00	3.61E+06	0.118841
	2.46E+07	4.92E+07	7	1.23E+07	15011	375278	6.56E+00	3.61E+06	0.103986
	1.23E+07	2.46E+07	8	6.15E+06	17156	428890	7.76E+00	5.77E+07	0.007428
	0	1.23E+07	38	6.15E+06	81489	2037226	7.76E+00	5.77E+07	0.035281
				0.00E+00					15.003878
29	7.20E+07	8.00E+07	2	4.00E+06	2144	53611	8.51E+00	3.23E+08	0.000166
	6.40E+07	7.20E+07	0	4.00E+06	0	0	8.51E+00	3.23E+08	0.000000
	5.60E+07	6.40E+07	2	4.00E+06	2144	53611	8.51E+00	3.23E+08	0.000166
	4.80E+07	5.60E+07	3	4.00E+06	3217	80417	8.51E+00	3.23E+08	0.000249
	4.00E+07	4.80E+07	1	4.00E+06	1072	26806	8.51E+00	3.23E+08	0.000083
	3.20E+07	4.00E+07	2.5	4.00E+06	2681	67014	8.51E+00	3.23E+08	0.000208
	2.40E+07	3.20E+07	3	4.00E+06	3217	80417	8.51E+00	3.23E+08	0.000249
	1.60E+07	2.40E+07	7	4.00E+06	7506	187639	8.51E+00	3.23E+08	0.000582
	1.20E+07	1.60E+07	2.5	2.00E+06	2681	67014	9.71E+00	5.16E+09	0.000013
	8.00E+06	1.20E+07	6	2.00E+06	6433	160834	9.71E+00	5.16E+09	0.000031
	4.00E+06	8.00E+06	17	2.00E+06	18228	455695	9.71E+00	5.16E+09	0.000088
	2.00E+06	4.00E+06	17	1.00E+06	18228	455695	1.09E+01	8.26E+10	0.000006
	0	2.00E+06	299.5	1.00E+06	321131	8028277	1.09E+01	8.26E+10	0.000097
				0.00E+00					0.001938
30	2.62E+08	2.91E+08	0.5	1.45E+07	613	15324	6.27E+00	1.87E+06	0.008200
	2.33E+08	2.62E+08	1.5	1.45E+07	1839	45971	6.27E+00	1.87E+06	0.024601
	2.04E+08	2.33E+08	5.5	1.45E+07	6742	168562	6.27E+00	1.87E+06	0.090205
	1.75E+08	2.04E+08	5.5	1.45E+07	6742	168562	6.27E+00	1.87E+06	0.090205
	1.46E+08	1.75E+08	6	1.45E+07	7355	183886	6.27E+00	1.87E+06	0.098406
	1.16E+08	1.46E+08	11	1.50E+07	13485	337124	6.21E+00	1.63E+06	0.206612
	8.73E+07	1.16E+08	12	1.44E+07	14711	367772	6.29E+00	1.95E+06	0.188793
	5.82E+07	8.73E+07	20.5	1.46E+07	25131	628277	6.27E+00	1.84E+06	0.340881
	4.37E+07	5.82E+07	3.5	7.25E+06	4291	107267	7.48E+00	2.99E+07	0.003588
	2.91E+07	4.37E+07	4	7.30E+06	4904	122591	7.46E+00	2.91E+07	0.004215
	1.46E+07	2.91E+07	6	7.25E+06	7355	183886	7.48E+00	2.99E+07	0.006150
	7.28E+06	1.46E+07	2.5	3.66E+06	3065	76619	8.66E+00	4.60E+08	0.000166
	0	7.28E+06	49.5	3.64E+06	60682	1517059	8.67E+00	4.71E+08	0.003224
				0.00E+00					1.065248

Figure C.6: Reference monopile, Rainflow analysis result and fatigue damage calculation(ML), SS26-SS30

SS	min amp	max amp	cycle	avg amp	total cycles	design life	log S		Eq. Fatigue da
31	2.49E+08	2.77E+08	0.5	1.40E+07	521	13025	6.33E+00	2.15E+06	0.006058
	2.22E+08	2.49E+08	0	1.35E+07	0	0	6.40E+00	2.49E+06	0.000000
	1.94E+08	2.22E+08	1.5	1.40E+07	1563	39076	6.33E+00	2.15E+06	0.018173
	1.66E+08	1.94E+08	4.5	1.40E+07	4689	117227	6.33E+00	2.15E+06	0.054518
	1.39E+08	1.66E+08	3	1.35E+07	3126	78152	6.40E+00	2.49E+06	0.031425
	1.11E+08	1.39E+08	6	1.40E+07	6252	156303	6.33E+00	2.15E+06	0.072691
	8.31E+07	1.11E+08	11.5	1.40E+07	11983	299581	6.34E+00	2.18E+06	0.137344
	5.54E+07	8.31E+07	10	1.39E+07	10420	260505	6.35E+00	2.24E+06	0.116042
	4.16E+07	5.54E+07	12.5	6.90E+06	13025	325631	7.56E+00	3.64E+07	0.008936
	2.77E+07	4.16E+07	10	6.95E+06	10420	260505	7.55E+00	3.54E+07	0.007358
	1.39E+07	2.77E+07	4	6.90E+06	4168	104202	7.56E+00	3.64E+07	0.002859
	6.93E+06	1.39E+07	13	3.49E+06	13546	338657	8.75E+00	5.60E+08	0.000605
	0	6.93E+06	75	3.47E+06	78152	1953788	8.76E+00	5.73E+08	0.003409
				0.00E+00					0.459418
32	7.11E+07	7.90E+07	0.5	3.95E+06	797	19921	8.53E+00	3.39E+08	0.000059
	6.32E+07	7.11E+07	1	3.95E+06	1594	39842	8.53E+00	3.39E+08	0.000117
	5.53E+07	6.32E+07	0	3.95E+06	0	0	8.53E+00	3.39E+08	0.000000
	4.74E+07	5.53E+07	3.5	3.95E+06	5578	139447	8.53E+00	3.39E+08	0.000411
	3.95E+07	4.74E+07	1	3.95E+06	1594	39842	8.53E+00	3.39E+08	0.000117
	3.16E+07	3.95E+07	3	3.95E+06	4781	119526	8.53E+00	3.39E+08	0.000352
	2.37E+07	3.16E+07	4	3.95E+06	6375	159368	8.53E+00	3.39E+08	0.000470
	1.58E+07	2.37E+07	5.5	3.95E+06	8765	219131	8.53E+00	3.39E+08	0.000646
	1.19E+07	1.58E+07	3.5	1.95E+06	5578	139447	9.76E+00	5.71E+09	0.000024
	7.90E+06	1.19E+07	11	2.00E+06	17530	438262	9.71E+00	5.16E+09	0.000085
	3.95E+06	7.90E+06	18.5	1.98E+06	29483	737076	9.73E+00	5.43E+09	0.000136
	1.98E+06	3.95E+06	41.5	9.85E+05	66138	1653441	1.09E+01	8.78E+10	0.000019
	0	1.98E+06	252	9.90E+05	401607	10040174	1.09E+01	8.60E+10	0.000117
				0.00E+00					0.002553
33	7.02E+07	7.80E+07	0.5	3.90E+06	536	13403	8.55E+00	3.57E+08	0.000038
	6.24E+07	7.02E+07	0	3.90E+06	0	0	8.55E+00	3.57E+08	0.000000
	5.46E+07	6.24E+07	2.5	3.90E+06	2681	67014	8.55E+00	3.57E+08	0.000188
	4.68E+07	5.46E+07	3	3.90E+06	3217	80417	8.55E+00	3.57E+08	0.000225
	3.90E+07	4.68E+07	0.5	3.90E+06	536	13403	8.55E+00	3.57E+08	0.000038
	3.12E+07	3.90E+07	1	3.90E+06	1072	26806	8.55E+00	3.57E+08	0.000075
	2.34E+07	3.12E+07	2.5	3.90E+06	2681	67014	8.55E+00	3.57E+08	0.000188
	1.56E+07	2.34E+07	9	3.90E+06	9650	241250	8.55E+00	3.57E+08	0.000676
	1.17E+07	1.56E+07	4.5	1.95E+06	4825	120625	9.76E+00	5.71E+09	0.000021
	7.80E+06	1.17E+07	12	1.95E+06	12867	321667	9.76E+00	5.71E+09	0.000056
	3.90E+06	7.80E+06	15.5	1.95E+06	16619	415487	9.76E+00	5.71E+09	0.000073
	1.95E+06	3.90E+06	42	9.75E+05	45033	1125835	1.10E+01	9.14E+10	0.000012
	0	1.95E+06	283.5	9.75E+05	303976	7599388	1.10E+01	9.14E+10	0.000083
				0.00E+00					0.001672
34	2.43E+07	2.70E+07	2.5	1.35E+06	1531	38281	1.04E+01	2.49E+10	0.000002
	2.16E+07	2.43E+07	1.5	1.35E+06	919	22969	1.04E+01	2.49E+10	0.000001
	1.89E+07	2.16E+07	4	1.35E+06	2450	61250	1.04E+01	2.49E+10	0.000002
	1.62E+07	1.89E+07	6	1.35E+06	3675	91875	1.04E+01	2.49E+10	0.000004
	1.35E+07	1.62E+07	3.5	1.35E+06	2144	53594	1.04E+01	2.49E+10	0.000002
	1.08E+07	1.35E+07	10.5	1.35E+06	6431	160781	1.04E+01	2.49E+10	0.000006
	8.09E+06	1.08E+07	11	1.36E+06	6737	168437	1.04E+01	2.45E+10	0.000007
	5.39E+06	8.09E+06	15	1.35E+06	9187	229687	1.04E+01	2.49E+10	0.000009
	4.04E+06	5.39E+06	9	6.75E+05	5512	137812	1.16E+01	3.98E+11	0.000000
	2.70E+06	4.04E+06	11	6.70E+05	6737	168437	1.16E+01	4.10E+11	0.000000
	1.35E+06	2.70E+06	9	6.75E+05	5512	137812	1.16E+01	3.98E+11	0.000000
	6.74E+05	1.35E+06	5.5	3.38E+05	3369	84219	1.28E+01	6.33E+12	0.000000
	0	6.74E+05	49.5	3.37E+05	30319	757968	1.28E+01	6.40E+12	0.000000
				0.00E+00					0.000035
35	2.36E+07	2.62E+07	2	1.30E+06	1172	29293	1.05E+01	2.89E+10	0.000001
	2.10E+07	2.36E+07	1	1.30E+06	586	14647	1.05E+01	2.89E+10	0.000001
	1.83E+07	2.10E+07	2	1.35E+06	1172	29293	1.04E+01	2.49E+10	0.000001
	1.57E+07	1.83E+07	7	1.30E+06	4101	102527	1.05E+01	2.89E+10	0.000004
	1.31E+07	1.57E+07	6.5	1.30E+06	3808	95204	1.05E+01	2.89E+10	0.000003
	1.05E+07	1.31E+07	14.5	1.30E+06	8495	212377	1.05E+01	2.89E+10	0.000007
	7.86E+06	1.05E+07	9	1.32E+06	5273	131820	1.04E+01	2.72E+10	0.000005
	5.24E+06	7.86E+06	14	1.31E+06	8202	205054	1.04E+01	2.80E+10	0.000007
	3.93E+06	5.24E+06	7.5	6.55E+05	4394	109850	1.17E+01	4.49E+11	0.000000
	2.62E+06	3.93E+06	15.5	6.55E+05	9081	227024	1.17E+01	4.49E+11	0.000001
	1.31E+06	2.62E+06	12	6.55E+05	7030	175761	1.17E+01	4.49E+11	0.000000
	6.55E+05	1.31E+06	8.5	3.28E+05	4980	124497	1.29E+01	7.18E+12	0.000000
	0	6.55E+05	39	3.28E+05	22849	571222	1.29E+01	7.18E+12	0.000000
									0.000030

Figure C.7: Reference monopile, Rainflow analysis result and fatigue damage calculation(ML), SS30-SS35

C.2. Reference monopile, cone: fatigue damage calculations

SS	min amp	max amp	cycle	avg amp	total cycles/y	Total cycles[D	Log N	N	Eq. Fatigue da
	3.15E+06	3.50E+06	0.5	1.75E+05	2150	53762	1.39E+01	8.81E+13	0.000000
	2.80E+06	3.15E+06	1	1.75E+05	4301	107523	1.39E+01	8.81E+13	0.000000
	2.45E+06	2.80E+06	2	1.75E+05	8602	215046	1.39E+01	8.81E+13	0.000000
	2.10E+06	2.45E+06	2	1.75E+05	8602	215046	1.39E+01	8.81E+13	0.000000
	1.75E+06	2.10E+06	8	1.75E+05	34407	860186	1.39E+01	8.81E+13	0.000000
	1.40E+06	1.75E+06	1.5	1.75E+05	6451	161285	1.39E+01	8.81E+13	0.000000
1	1.05E+06	1.40E+06	3	1.75E+05	12903	322570	1.39E+01	8.81E+13	0.000000
	7.00E+05	1.05E+06	5	1.75E+05	21505	537616	1.39E+01	8.81E+13	0.000000
	5.25E+05	7.00E+05	4.5	8.75E+04	19354	483855	1.51E+01	1.41E+15	0.000000
	3.50E+05	5.25E+05	15	8.75E+04	64514	1612849	1.51E+01	1.41E+15	0.000000
	1.75E+05	3.50E+05	43.5	8.75E+04	187090	4677261	1.51E+01	1.41E+15	0.000000
	8.75E+04	1.75E+05	392	4.38E+04	1685964	42149109	1.64E+01	2.25E+16	0.000000
	0	8.75E+04	0	4.38E+04	0	0	1.64E+01	2.25E+16	0.000000
				0.00E+00					0.000000
	6.29E+07	6.99E+07	0.5	3.50E+06	2710	67756	8.74E+00	5.50E+08	0.000123
	5.59E+07	6.29E+07	1	3.50E+06	5420	135511	8.74E+00	5.50E+08	0.000246
	4.89E+07	5.59E+07	4.5	3.50E+06	24392	609801	8.74E+00	5.50E+08	0.001108
	4.19E+07	4.89E+07	6.5	3.50E+06	35233	880824	8.74E+00	5.50E+08	0.001600
	3.50E+07	4.19E+07	6	3.45E+06	32523	813069	8.77E+00	5.83E+08	0.001394
	2.80E+07	3.50E+07	9.5	3.50E+06	51494	1287359	8.74E+00	5.50E+08	0.002339
2	2.10E+07	2.80E+07	14.5	3.50E+06	78597	1964916	8.74E+00	5.50E+08	0.003570
	1.40E+07	2.10E+07	23.5	3.50E+06	127381	3184519	8.74E+00	5.50E+08	0.005785
	1.05E+07	1.40E+07	10	1.75E+06	54205	1355114	9.94E+00	8.81E+09	0.000154
	6.99E+06	1.05E+07	3	1.76E+06	16261	406534	9.94E+00	8.71E+09	0.000047
	3.50E+06	6.99E+06	5	1.75E+06	27102	677557	9.95E+00	8.91E+09	0.000076
	1.75E+06	3.50E+06	3	8.75E+05	16261	406534	1.11E+01	1.41E+11	0.000003
	0	1.75E+06	14	8.75E+05	75886	1897160	1.11E+01	1.41E+11	0.000013
				0.00E+00					0.016458
	4.67E+07	5.19E+07	0.5	2.60E+06	466	11648	9.26E+00	1.81E+09	0.000006
	4.15E+07	4.67E+07	1.5	2.60E+06	1398	34945	9.26E+00	1.81E+09	0.000019
	3.63E+07	4.15E+07	3	2.60E+06	2796	69891	9.26E+00	1.81E+09	0.000039
	3.11E+07	3.63E+07	4.5	2.60E+06	4193	104836	9.26E+00	1.81E+09	0.000058
	2.60E+07	3.11E+07	3	2.55E+06	2796	69891	9.29E+00	1.95E+09	0.000036
	2.08E+07	2.60E+07	9	2.60E+06	8387	209672	9.26E+00	1.81E+09	0.000116
3	1.56E+07	2.08E+07	11	2.60E+06	10251	256266	9.26E+00	1.81E+09	0.000142
	1.04E+07	1.56E+07	20	2.60E+06	18637	465937	9.26E+00	1.81E+09	0.000258
	7.79E+06	1.04E+07	8.5	1.31E+06	7921	198023	1.05E+01	2.85E+10	0.000007
	5.19E+06	7.79E+06	7	1.30E+06	6523	163078	1.05E+01	2.89E+10	0.000006
	2.60E+06	5.19E+06	4	1.30E+06	3727	93187	1.05E+01	2.94E+10	0.000003
	1.30E+06	2.60E+06	4	6.50E+05	3727	93187	1.17E+01	4.63E+11	0.000000
	0	1.30E+06	45	6.50E+05	41934	1048359	1.17E+01	4.63E+11	0.000002
				0.00E+00					0.000692
	9.67E+06	1.07E+07	3	5.15E+05	19433	485825	1.21E+01	1.17E+12	0.000000
	8.59E+06	9.67E+06	0	5.40E+05	0	0	1.20E+01	9.71E+11	0.000000
	7.52E+06	8.59E+06	0	5.35E+05	0	0	1.20E+01	1.01E+12	0.000000
	6.44E+06	7.52E+06	0.5	5.40E+05	3239	80971	1.20E+01	9.71E+11	0.000000
	5.37E+06	6.44E+06	1.5	5.35E+05	9716	242912	1.20E+01	1.01E+12	0.000000
	4.30E+06	5.37E+06	3.5	5.35E+05	22672	566796	1.20E+01	1.01E+12	0.000001
4	3.22E+06	4.30E+06	4.5	5.40E+05	29149	728737	1.20E+01	9.71E+11	0.000001
	2.15E+06	3.22E+06	4.5	5.35E+05	29149	728737	1.20E+01	1.01E+12	0.000001
	1.61E+06	2.15E+06	3.5	2.70E+05	22672	566796	1.32E+01	1.55E+13	0.000000
	1.07E+06	1.61E+06	6	2.70E+05	38866	971650	1.32E+01	1.55E+13	0.000000
	5.37E+05	1.07E+06	6	2.67E+05	38866	971650	1.32E+01	1.64E+13	0.000000
	2.69E+05	5.37E+05	24	1.34E+05	155464	3886599	1.44E+01	2.56E+14	0.000000
	0	2.69E+05	262	1.35E+05	1697148	42428705	1.44E+01	2.52E+14	0.000000
				0.00E+00					0.000003
	1.54E+08	1.71E+08	0.5	8.50E+06	3265	81624	7.20E+00	1.58E+07	0.005158
	1.37E+08	1.54E+08	0	8.50E+06	0	0	7.20E+00	1.58E+07	0.000000
	1.19E+08	1.37E+08	3.5	9.00E+06	22855	571370	7.10E+00	1.26E+07	0.045382
	1.02E+08	1.19E+08	2	8.50E+06	13060	326497	7.20E+00	1.58E+07	0.020633
	8.54E+07	1.02E+08	2	8.30E+06	13060	326497	7.24E+00	1.74E+07	0.018758
	6.83E+07	8.54E+07	10	8.55E+06	65299	1632485	7.19E+00	1.55E+07	0.105612
5	5.12E+07	6.83E+07	12.5	8.55E+06	81624	2040606	7.19E+00	1.55E+07	0.132015
	3.41E+07	5.12E+07	10	8.55E+06	65299	1632485	7.19E+00	1.55E+07	0.105612
	2.56E+07	3.41E+07	7.5	4.25E+06	48975	1224364	8.40E+00	2.53E+08	0.004836
	1.71E+07	2.56E+07	5	4.25E+06	32650	816243	8.40E+00	2.53E+08	0.003224
	8.54E+06	1.71E+07	9	4.28E+06	58769	1469237	8.39E+00	2.46E+08	0.005969
	4.27E+06	8.54E+06	7.5	2.14E+06	48975	1224364	9.60E+00	3.98E+09	0.000308
	0	4.27E+06	94.5	2.14E+06	617079	15426985	9.60E+00	3.98E+09	0.003880
				0.00E+00					0.451387

Figure C.8: Reference monopile, Rainflow analysis result and fatigue damage calculation(cone), SS1-SS5

SS	min amp	max amp	cycle	avg amp	total cycles/y	Total cycles(L	Log N	N	Eq. Fatigue da
6	7.83E+06	8.70E+06	1	4.35E+05	3392	84792	1.24E+01	2.31E+12	0.000000
	6.96E+06	7.83E+06	0.5	4.35E+05	1696	42396	1.24E+01	2.31E+12	0.000000
	6.09E+06	6.96E+06	1	4.35E+05	3392	84792	1.24E+01	2.31E+12	0.000000
	5.22E+06	6.09E+06	1	4.35E+05	3392	84792	1.24E+01	2.31E+12	0.000000
	4.35E+06	5.22E+06	3.5	4.35E+05	11871	296772	1.24E+01	2.31E+12	0.000000
	3.48E+06	4.35E+06	2.5	4.35E+05	8479	211980	1.24E+01	2.31E+12	0.000000
	2.61E+06	3.48E+06	5	4.35E+05	16958	423960	1.24E+01	2.31E+12	0.000000
	1.74E+06	2.61E+06	4	4.35E+05	13567	339168	1.24E+01	2.31E+12	0.000000
	1.31E+06	1.74E+06	2	2.15E+05	6783	169584	1.36E+01	3.87E+13	0.000000
	8.70E+05	1.31E+06	7	2.20E+05	23742	593544	1.35E+01	3.53E+13	0.000000
	4.35E+05	8.70E+05	11	2.18E+05	37309	932713	1.36E+01	3.69E+13	0.000000
	2.18E+05	4.35E+05	11	1.09E+05	37309	932713	1.48E+01	5.96E+14	0.000000
	0	2.18E+05	248.5	1.09E+05	842833	21070828	1.48E+01	5.85E+14	0.000000
				0.00E+00					0.000001
7	1.43E+08	1.59E+08	0.5	8.00E+06	2001	50015	7.30E+00	2.02E+07	0.002480
	1.27E+08	1.43E+08	0	8.00E+06	0	0	7.30E+00	2.02E+07	0.000000
	1.11E+08	1.27E+08	4	8.00E+06	16005	400119	7.30E+00	2.02E+07	0.019840
	9.55E+07	1.11E+08	1.5	7.75E+06	6002	150045	7.36E+00	2.29E+07	0.006553
	7.96E+07	9.55E+07	3.5	7.95E+06	14004	350104	7.32E+00	2.07E+07	0.016930
	6.37E+07	7.96E+07	8	7.95E+06	32010	800238	7.32E+00	2.07E+07	0.038698
	4.78E+07	6.37E+07	10.5	7.95E+06	42012	1050312	7.32E+00	2.07E+07	0.050791
	3.18E+07	4.78E+07	9	8.00E+06	36011	900268	7.30E+00	2.02E+07	0.044641
	2.39E+07	3.18E+07	9.5	3.95E+06	38011	950282	8.53E+00	3.39E+08	0.002801
	1.59E+07	2.39E+07	8	4.00E+06	32010	800238	8.51E+00	3.23E+08	0.002480
	7.96E+06	1.59E+07	9	3.97E+06	36011	900268	8.52E+00	3.33E+08	0.002707
	3.98E+06	7.96E+06	7.5	1.99E+06	30009	750223	9.72E+00	5.27E+09	0.000142
	0	3.98E+06	95	1.99E+06	380113	9502824	9.72E+00	5.27E+09	0.001804
				0.00E+00					0.189868
8	1.98E+08	2.20E+08	1.5	1.10E+07	746	18645	6.75E+00	5.64E+06	0.003305
	1.76E+08	1.98E+08	0	1.10E+07	0	0	6.75E+00	5.64E+06	0.000000
	1.54E+08	1.76E+08	4.5	1.10E+07	2237	55934	6.75E+00	5.64E+06	0.009914
	1.32E+08	1.54E+08	4	1.10E+07	1989	49719	6.75E+00	5.64E+06	0.008812
	1.10E+08	1.32E+08	6	1.10E+07	2983	74578	6.75E+00	5.64E+06	0.013219
	8.80E+07	1.10E+08	8.5	1.10E+07	4226	105653	6.75E+00	5.64E+06	0.018726
	6.60E+07	8.80E+07	12	1.10E+07	5966	149157	6.75E+00	5.64E+06	0.026437
	4.40E+07	6.60E+07	16	1.10E+07	7955	198876	6.75E+00	5.64E+06	0.035249
	3.30E+07	4.40E+07	6.5	5.50E+06	3232	80793	7.96E+00	9.03E+07	0.000895
	2.20E+07	3.30E+07	6	5.50E+06	2983	74578	7.96E+00	9.03E+07	0.000826
	1.10E+07	2.20E+07	6	5.50E+06	2983	74578	7.96E+00	9.03E+07	0.000826
	5.50E+06	1.10E+07	2	2.75E+06	994	24859	9.16E+00	1.44E+09	0.000017
	0	5.50E+06	86	2.75E+06	42758	1068957	9.16E+00	1.44E+09	0.000740
				0.00E+00					0.118967
9	1.25E+07	1.39E+07	1	7.00E+05	1447	36183	1.15E+01	3.44E+11	0.000000
	1.11E+07	1.25E+07	3	7.00E+05	4342	108550	1.15E+01	3.44E+11	0.000000
	9.73E+06	1.11E+07	2.5	6.85E+05	3618	90459	1.16E+01	3.75E+11	0.000000
	8.34E+06	9.73E+06	1.5	6.95E+05	2171	54275	1.15E+01	3.54E+11	0.000000
	6.95E+06	8.34E+06	8	6.95E+05	11579	289467	1.15E+01	3.54E+11	0.000001
	5.56E+06	6.95E+06	2.5	6.95E+05	3618	90459	1.15E+01	3.54E+11	0.000000
	4.17E+06	5.56E+06	5.5	6.95E+05	7960	199009	1.15E+01	3.54E+11	0.000001
	2.78E+06	4.17E+06	7.5	6.95E+05	10855	271376	1.15E+01	3.54E+11	0.000001
	2.09E+06	2.78E+06	6	3.45E+05	8684	217100	1.28E+01	5.83E+12	0.000000
	1.39E+06	2.09E+06	7	3.50E+05	10131	253284	1.27E+01	5.50E+12	0.000000
	6.95E+05	1.39E+06	12	3.48E+05	17368	434201	1.28E+01	5.66E+12	0.000000
	3.48E+05	6.95E+05	7	1.74E+05	10131	253284	1.40E+01	9.12E+13	0.000000
	0	3.48E+05	135	1.74E+05	195390	4884760	1.40E+01	9.01E+13	0.000000
				0.00E+00					0.000003
10	1.29E+07	1.43E+07	3	7.00E+05	2839	70975	1.15E+01	3.44E+11	0.000000
	1.15E+07	1.29E+07	1.5	7.00E+05	1420	35488	1.15E+01	3.44E+11	0.000000
	1.00E+07	1.15E+07	1	7.50E+05	946	23658	1.14E+01	2.61E+11	0.000000
	8.60E+06	1.00E+07	0.5	7.00E+05	473	11829	1.15E+01	3.44E+11	0.000000
	7.17E+06	8.60E+06	1.5	7.15E+05	1420	35488	1.15E+01	3.16E+11	0.000000
	5.74E+06	7.17E+06	0.5	7.15E+05	473	11829	1.15E+01	3.16E+11	0.000000
	4.30E+06	5.74E+06	6	7.20E+05	5678	141950	1.15E+01	3.07E+11	0.000000
	2.87E+06	4.30E+06	13.5	7.15E+05	12776	319388	1.15E+01	3.16E+11	0.000001
	2.15E+06	2.87E+06	5	3.60E+05	4732	118292	1.27E+01	4.92E+12	0.000000
	1.43E+06	2.15E+06	7	3.60E+05	6624	165609	1.27E+01	4.92E+12	0.000000
	7.17E+05	1.43E+06	9.5	3.57E+05	8990	224755	1.27E+01	5.11E+12	0.000000
	3.59E+05	7.17E+05	8	1.79E+05	7571	189267	1.39E+01	8.05E+13	0.000000
	0	3.59E+05	207	1.80E+05	195891	4897285	1.39E+01	7.96E+13	0.000000
								Total	0.000002

Figure C.9: Reference monopile, Rainflow analysis result and fatigue damage calculation(cone), SS6-SS10

SS	min amp	max amp	cycle	avg amp	total cycles/y	Total cycles(L	Log N	N	Eq. Fatigue da
11	7.83E+06	8.70E+06	1	4.35E+05	1113	27833	1.24E+01	2.31E+12	0.000000
	6.96E+06	7.83E+06	0.5	4.35E+05	557	13917	1.24E+01	2.31E+12	0.000000
	6.09E+06	6.96E+06	1	4.35E+05	1113	27833	1.24E+01	2.31E+12	0.000000
	5.22E+06	6.09E+06	1	4.35E+05	1113	27833	1.24E+01	2.31E+12	0.000000
	4.35E+06	5.22E+06	3.5	4.35E+05	3897	97417	1.24E+01	2.31E+12	0.000000
	3.48E+06	4.35E+06	2.5	4.35E+05	2783	69583	1.24E+01	2.31E+12	0.000000
	2.61E+06	3.48E+06	5	4.35E+05	5567	139167	1.24E+01	2.31E+12	0.000000
	1.74E+06	2.61E+06	4	4.35E+05	4453	111334	1.24E+01	2.31E+12	0.000000
	1.31E+06	1.74E+06	2	2.15E+05	2227	55667	1.36E+01	3.87E+13	0.000000
	8.70E+05	1.31E+06	7	2.20E+05	7793	194834	1.35E+01	3.53E+13	0.000000
	4.35E+05	8.70E+05	11	2.18E+05	12247	306167	1.36E+01	3.69E+13	0.000000
	2.18E+05	4.35E+05	11	1.09E+05	12247	306167	1.48E+01	5.96E+14	0.000000
	0	2.18E+05	248.5	1.09E+05	276664	6916598	1.48E+01	5.85E+14	0.000000
				0.00E+00					0.000000
12	7.02E+07	7.80E+07	0.5	3.90E+06	834	20856	8.55E+00	3.57E+08	0.000058
	6.24E+07	7.02E+07	3	3.90E+06	5005	125135	8.55E+00	3.57E+08	0.000350
	5.46E+07	6.24E+07	2.5	3.90E+06	4171	104279	8.55E+00	3.57E+08	0.000292
	4.68E+07	5.46E+07	4.5	3.90E+06	7508	187703	8.55E+00	3.57E+08	0.000526
	3.90E+07	4.68E+07	3.5	3.90E+06	5840	145991	8.55E+00	3.57E+08	0.000409
	3.12E+07	3.90E+07	12	3.90E+06	20022	500541	8.55E+00	3.57E+08	0.001402
	2.34E+07	3.12E+07	12	3.90E+06	20022	500541	8.55E+00	3.57E+08	0.001402
	1.56E+07	2.34E+07	24.5	3.90E+06	40878	1021939	8.55E+00	3.57E+08	0.002862
	1.17E+07	1.56E+07	9.5	1.95E+06	15850	396262	9.76E+00	5.71E+09	0.000069
	7.80E+06	1.17E+07	5.5	1.95E+06	9177	229415	9.76E+00	5.71E+09	0.000040
	3.90E+06	7.80E+06	6	1.95E+06	10011	250271	9.76E+00	5.71E+09	0.000044
	1.95E+06	3.90E+06	3	9.75E+05	5005	125135	1.10E+01	9.14E+10	0.000001
	0	1.95E+06	16	9.75E+05	26696	667389	1.10E+01	9.14E+10	0.000007
				0.00E+00					0.007463
13	6.44E+07	7.15E+07	0.5	3.55E+06	527	13176	8.72E+00	5.20E+08	0.000025
	5.72E+07	6.44E+07	1.5	3.60E+06	1581	39529	8.69E+00	4.92E+08	0.000080
	5.01E+07	5.72E+07	2	3.55E+06	2108	52705	8.72E+00	5.20E+08	0.000101
	4.29E+07	5.01E+07	1.5	3.60E+06	1581	39529	8.69E+00	4.92E+08	0.000080
	3.58E+07	4.29E+07	3.5	3.55E+06	3689	92233	8.72E+00	5.20E+08	0.000177
	2.86E+07	3.58E+07	15	3.60E+06	15811	395285	8.69E+00	4.92E+08	0.000804
	2.15E+07	2.86E+07	11	3.55E+06	11595	289876	8.72E+00	5.20E+08	0.000557
	1.43E+07	2.15E+07	22.5	3.60E+06	23717	592928	8.69E+00	4.92E+08	0.001206
	1.07E+07	1.43E+07	7	1.80E+06	7379	184466	9.90E+00	7.87E+09	0.000023
	7.15E+06	1.07E+07	2	1.78E+06	2108	52705	9.92E+00	8.32E+09	0.000006
	3.58E+06	7.15E+06	6	1.79E+06	6325	158114	9.91E+00	8.14E+09	0.000019
	1.79E+06	3.58E+06	5.5	8.95E+05	5798	144938	1.11E+01	1.29E+11	0.000001
	0	1.79E+06	55.5	8.95E+05	58502	1462555	1.11E+01	1.29E+11	0.000011
				0.00E+00					0.003093
14	1.56E+08	1.73E+08	0.5	8.50E+06	576	14411	7.20E+00	1.58E+07	0.000911
	1.38E+08	1.56E+08	1.5	9.00E+06	1729	43234	7.10E+00	1.26E+07	0.003434
	1.21E+08	1.38E+08	4	8.50E+06	4612	115292	7.20E+00	1.58E+07	0.007286
	1.04E+08	1.21E+08	2.5	8.50E+06	2882	72057	7.20E+00	1.58E+07	0.004554
	8.65E+07	1.04E+08	2	8.75E+06	2306	57646	7.15E+00	1.41E+07	0.004091
	6.92E+07	8.65E+07	8.5	8.65E+06	9800	244995	7.17E+00	1.48E+07	0.016604
	5.19E+07	6.92E+07	11	8.65E+06	12682	317052	7.17E+00	1.48E+07	0.021488
	3.46E+07	5.19E+07	14.5	8.65E+06	16717	417932	7.17E+00	1.48E+07	0.028325
	2.59E+07	3.46E+07	4	4.35E+06	4612	115292	8.36E+00	2.31E+08	0.000500
	1.73E+07	2.59E+07	3	4.30E+06	3459	86469	8.38E+00	2.42E+08	0.000358
	8.65E+06	1.73E+07	15	4.33E+06	17294	432343	8.37E+00	2.36E+08	0.001831
	4.32E+06	8.65E+06	2.5	2.17E+06	2882	72057	9.58E+00	3.76E+09	0.000019
	0	4.32E+06	94	2.16E+06	108374	2709351	9.58E+00	3.79E+09	0.000714
				0.00E+00					0.090114
15	2.10E+08	2.33E+08	0.5	1.15E+07	511	12764	6.67E+00	4.72E+06	0.002703
	1.87E+08	2.10E+08	0	1.15E+07	0	0	6.67E+00	4.72E+06	0.000000
	1.63E+08	1.87E+08	6	1.20E+07	6127	153173	6.60E+00	3.98E+06	0.038451
	1.40E+08	1.63E+08	2.5	1.15E+07	2553	63822	6.67E+00	4.72E+06	0.013513
	1.17E+08	1.40E+08	7	1.15E+07	7148	178702	6.67E+00	4.72E+06	0.037837
	9.34E+07	1.17E+08	10	1.18E+07	10212	255288	6.63E+00	4.26E+06	0.059918
	7.00E+07	9.34E+07	13	1.17E+07	13275	331875	6.64E+00	4.41E+06	0.075287
	4.67E+07	7.00E+07	15	1.17E+07	15317	382933	6.65E+00	4.48E+06	0.085394
	3.50E+07	4.67E+07	5.5	5.85E+06	5616	140409	7.85E+00	7.05E+07	0.001991
	2.33E+07	3.50E+07	5	5.85E+06	5106	127644	7.85E+00	7.05E+07	0.001810
	1.17E+07	2.33E+07	4.5	5.80E+06	4595	114880	7.86E+00	7.30E+07	0.001574
	5.84E+06	1.17E+07	4	2.93E+06	4085	102115	9.05E+00	1.12E+09	0.000091
	0	5.84E+06	75	2.92E+06	76587	1914663	9.06E+00	1.14E+09	0.001685
				0.00E+00					0.320253

Figure C.10: Reference monopile, Rainflow analysis result and fatigue damage calculation(cone), SS11-SS15

SS	min amp	max amp	cycle	avg amp	total cycles/	Total cycles/[	Log N	N	Eq. Fatigue d
16	3.18E+08	3.53E+08	1	1.75E+07	824	20588	5.94E+00	8.81E+05	0.023376
	2.82E+08	3.18E+08	1	1.80E+07	824	20588	5.90E+00	7.87E+05	0.026164
	2.47E+08	2.82E+08	5.5	1.75E+07	4529	113233	5.94E+00	8.81E+05	0.128565
	2.12E+08	2.47E+08	1.5	1.75E+07	1235	30882	5.94E+00	8.81E+05	0.035063
	1.77E+08	2.12E+08	5.5	1.75E+07	4529	113233	5.94E+00	8.81E+05	0.128565
	1.41E+08	1.77E+08	9.5	1.80E+07	7823	195584	5.90E+00	7.87E+05	0.248555
	1.06E+08	1.41E+08	14.5	1.75E+07	11941	298523	5.94E+00	8.81E+05	0.338945
	7.06E+07	1.06E+08	18.5	1.77E+07	15235	380874	5.93E+00	8.42E+05	0.452558
	5.30E+07	7.06E+07	6.5	8.80E+06	5353	133821	7.14E+00	1.38E+07	0.009715
	3.53E+07	5.30E+07	5.5	8.85E+06	4529	113233	7.13E+00	1.35E+07	0.008409
	1.77E+07	3.53E+07	7	8.80E+06	5765	144114	7.14E+00	1.38E+07	0.010463
	8.83E+06	1.77E+07	3	4.44E+06	2471	61763	8.33E+00	2.14E+08	0.000289
	0	8.83E+06	43.5	4.42E+06	35823	895568	8.34E+00	2.17E+08	0.004119
				0.00E+00					1.414787
17	5.55E+08	6.16E+08	1	3.05E+07	988	24705	4.98E+00	9.55E+04	0.258815
	4.93E+08	5.55E+08	1	3.10E+07	988	24705	4.95E+00	8.94E+04	0.276209
	4.31E+08	4.93E+08	5	3.10E+07	4941	123527	4.95E+00	8.94E+04	1.381044
	3.70E+08	4.31E+08	4.5	3.05E+07	4447	111174	4.98E+00	9.55E+04	1.164669
	3.08E+08	3.70E+08	6	3.10E+07	5929	148232	4.95E+00	8.94E+04	1.657252
	2.47E+08	3.08E+08	8	3.05E+07	7906	197643	4.98E+00	9.55E+04	2.070523
	1.85E+08	2.47E+08	15	3.10E+07	14823	370580	4.95E+00	8.94E+04	4.143131
	1.23E+08	1.85E+08	18	3.10E+07	17788	444696	4.95E+00	8.94E+04	4.971757
	9.24E+07	1.23E+08	11.5	1.53E+07	11364	284111	6.18E+00	1.51E+06	0.188475
	6.16E+07	9.24E+07	3	1.54E+07	2965	74116	6.17E+00	1.47E+06	0.050466
	3.08E+07	6.16E+07	6	1.54E+07	5929	148232	6.17E+00	1.47E+06	0.100931
	1.54E+07	3.08E+07	3	7.70E+06	2965	74116	7.37E+00	2.35E+07	0.003154
	0	1.54E+07	34	7.70E+06	33599	839981	7.37E+00	2.35E+07	0.035746
				0.00E+00					16.302172
18	5.62E+07	6.24E+07	0.5	3.10E+06	355	8886	8.95E+00	8.94E+08	0.000010
	4.99E+07	5.62E+07	0.5	3.15E+06	355	8886	8.92E+00	8.39E+08	0.000011
	4.37E+07	4.99E+07	3.5	3.10E+06	2488	62204	8.95E+00	8.94E+08	0.000070
	3.74E+07	4.37E+07	5	3.15E+06	3555	88863	8.92E+00	8.39E+08	0.000106
	3.12E+07	3.74E+07	5	3.10E+06	3555	88863	8.95E+00	8.94E+08	0.000099
	2.50E+07	3.12E+07	13	3.10E+06	9242	231043	8.95E+00	8.94E+08	0.000258
	1.87E+07	2.50E+07	15	3.15E+06	10664	266588	8.92E+00	8.39E+08	0.000318
	1.25E+07	1.87E+07	16	3.10E+06	11374	284360	8.95E+00	8.94E+08	0.000318
	9.36E+06	1.25E+07	8	1.57E+06	5687	142180	1.01E+01	1.36E+10	0.000010
	6.24E+06	9.36E+06	6	1.56E+06	4265	106635	1.01E+01	1.39E+10	0.000008
	3.12E+06	6.24E+06	7	1.56E+06	4976	124408	1.01E+01	1.39E+10	0.000009
	1.56E+06	3.12E+06	4	7.80E+05	2844	71090	1.13E+01	2.23E+11	0.000000
	0	1.56E+06	43	7.80E+05	30569	764218	1.13E+01	2.23E+11	0.000003
				0.00E+00					0.001220
19	6.20E+07	6.89E+07	1.5	3.45E+06	1166	29158	8.77E+00	5.83E+08	0.000050
	5.51E+07	6.20E+07	5	3.45E+06	3888	97193	8.77E+00	5.83E+08	0.000167
	4.82E+07	5.51E+07	4.5	3.45E+06	3499	87474	8.77E+00	5.83E+08	0.000150
	4.13E+07	4.82E+07	5.5	3.45E+06	4277	106913	8.77E+00	5.83E+08	0.000183
	3.45E+07	4.13E+07	5	3.40E+06	3888	97193	8.79E+00	6.18E+08	0.000157
	2.76E+07	3.45E+07	13	3.45E+06	10108	252703	8.77E+00	5.83E+08	0.000433
	2.07E+07	2.76E+07	14	3.45E+06	10886	272142	8.77E+00	5.83E+08	0.000467
	1.38E+07	2.07E+07	17	3.45E+06	13218	330458	8.77E+00	5.83E+08	0.000567
	1.03E+07	1.38E+07	10.5	1.75E+06	8164	204106	9.94E+00	8.81E+09	0.000023
	6.89E+06	1.03E+07	3	1.71E+06	2333	58316	9.99E+00	9.77E+09	0.000006
	3.45E+06	6.89E+06	4	1.72E+06	3110	77755	9.97E+00	9.44E+09	0.000008
	1.72E+06	3.45E+06	3	8.65E+05	2333	58316	1.12E+01	1.48E+11	0.000000
	0	1.72E+06	13	8.60E+05	10108	252703	1.12E+01	1.51E+11	0.000002
				0.00E+00					0.002214
20	2.04E+08	2.27E+08	0.5	1.15E+07	344	8609	6.67E+00	4.72E+06	0.001823
	1.81E+08	2.04E+08	0	1.15E+07	0	0	6.67E+00	4.72E+06	0.000000
	1.59E+08	1.81E+08	3.5	1.10E+07	2410	60260	6.75E+00	5.64E+06	0.010681
	1.36E+08	1.59E+08	4.5	1.15E+07	3099	77477	6.67E+00	4.72E+06	0.016405
	1.13E+08	1.36E+08	6.5	1.15E+07	4476	111911	6.67E+00	4.72E+06	0.023695
	9.07E+07	1.13E+08	5.5	1.12E+07	3788	94694	6.73E+00	5.34E+06	0.017718
	6.80E+07	9.07E+07	12	1.14E+07	8264	206605	6.70E+00	4.98E+06	0.041507
	4.54E+07	6.80E+07	13	1.13E+07	8953	223823	6.70E+00	5.07E+06	0.044179
	3.40E+07	4.54E+07	5	5.70E+06	3443	86086	7.89E+00	7.83E+07	0.001100
	2.27E+07	3.40E+07	9.5	5.65E+06	6543	163563	7.91E+00	8.11E+07	0.002018
	1.13E+07	2.27E+07	6	5.70E+06	4132	103303	7.89E+00	7.83E+07	0.001320
	5.67E+06	1.13E+07	3.5	2.82E+06	2410	60260	9.12E+00	1.32E+09	0.000046
	0	5.67E+06	90	2.84E+06	61982	1549541	9.11E+00	1.28E+09	0.001212
				0.00E+00					0.161704

Figure C.11: Reference monopile, Rainflow analysis result and fatigue damage calculation(cone), SS16-SS20

SS	min amp	max amp	cycle	avg amp	total cycles/y	Total cycles(L	Log N	N	Eq. Fatigue da
	3.12E+08	3.46E+08	1	1.70E+07	1222	30547	6.00E+00	9.89E+05	0.030886
	2.77E+08	3.12E+08	0	1.75E+07	0	0	5.94E+00	8.81E+05	0.000000
	2.42E+08	2.77E+08	3.5	1.75E+07	4277	106913	5.94E+00	8.81E+05	0.121390
	2.08E+08	2.42E+08	5.5	1.70E+07	6720	168006	6.00E+00	9.89E+05	0.169871
	1.73E+08	2.08E+08	4	1.75E+07	4887	122186	5.94E+00	8.81E+05	0.138731
	1.38E+08	1.73E+08	6.5	1.75E+07	7942	198552	5.94E+00	8.81E+05	0.225438
21	1.04E+08	1.38E+08	14	1.70E+07	17106	427651	6.00E+00	9.89E+05	0.432400
	6.92E+07	1.04E+08	15.5	1.74E+07	18939	473471	5.95E+00	9.01E+05	0.525400
	5.19E+07	6.92E+07	9.5	8.65E+06	11608	290192	7.17E+00	1.48E+07	0.019668
	3.46E+07	5.19E+07	4	8.65E+06	4887	122186	7.17E+00	1.48E+07	0.008281
	1.73E+07	3.46E+07	8	8.65E+06	9775	244372	7.17E+00	1.48E+07	0.016562
	8.66E+06	1.73E+07	5	4.32E+06	6109	152733	8.38E+00	2.37E+08	0.000644
	0	8.66E+06	54	4.33E+06	65980	1649512	8.37E+00	2.35E+08	0.007020
				0.00E+00					1.696290
	7.97E+07	8.85E+07	1	4.40E+06	1799	44987	8.34E+00	2.20E+08	0.000204
	7.08E+07	7.97E+07	1.5	4.45E+06	2699	67480	8.32E+00	2.11E+08	0.000320
	6.20E+07	7.08E+07	1.5	4.40E+06	2699	67480	8.34E+00	2.20E+08	0.000306
	5.31E+07	6.20E+07	8.5	4.45E+06	15295	382387	8.32E+00	2.11E+08	0.001815
	4.43E+07	5.31E+07	8	4.40E+06	14396	359893	8.34E+00	2.20E+08	0.001633
	3.54E+07	4.43E+07	6	4.45E+06	10797	269920	8.32E+00	2.11E+08	0.001281
22	2.66E+07	3.54E+07	15	4.40E+06	26992	674800	8.34E+00	2.20E+08	0.003062
	1.77E+07	2.66E+07	16.5	4.45E+06	29691	742280	8.32E+00	2.11E+08	0.003524
	1.33E+07	1.77E+07	14	2.20E+06	25193	629813	9.55E+00	3.53E+09	0.000179
	8.85E+06	1.33E+07	6.5	2.23E+06	11697	292413	9.53E+00	3.37E+09	0.000087
	4.43E+06	8.85E+06	5	2.21E+06	8997	224933	9.54E+00	3.46E+09	0.000065
	2.21E+06	4.43E+06	1	1.11E+06	1799	44987	1.07E+01	5.44E+10	0.000001
	0	2.21E+06	17	1.11E+06	30591	764774	1.07E+01	5.54E+10	0.000014
				0.00E+00					0.012491
	2.98E+07	3.31E+07	0.5	1.65E+06	788	19710	1.00E+01	1.11E+10	0.000002
	2.65E+07	2.98E+07	2	1.65E+06	3154	78840	1.00E+01	1.11E+10	0.000007
	2.32E+07	2.65E+07	3.5	1.65E+06	5519	137970	1.00E+01	1.11E+10	0.000012
	1.99E+07	2.32E+07	4.5	1.65E+06	7096	177390	1.00E+01	1.11E+10	0.000016
	1.66E+07	1.99E+07	6.5	1.65E+06	10249	256230	1.00E+01	1.11E+10	0.000023
	1.32E+07	1.66E+07	8.5	1.70E+06	13403	335070	1.00E+01	9.89E+09	0.000034
23	9.93E+06	1.32E+07	10	1.64E+06	15768	394200	1.01E+01	1.16E+10	0.000034
	6.62E+06	9.93E+06	17	1.66E+06	26806	670140	1.00E+01	1.10E+10	0.000061
	4.97E+06	6.62E+06	4.5	8.25E+05	7096	177390	1.13E+01	1.78E+11	0.000001
	3.31E+06	4.97E+06	9	8.30E+05	14191	354780	1.12E+01	1.74E+11	0.000002
	1.66E+06	3.31E+06	6.5	8.25E+05	10249	256230	1.13E+01	1.78E+11	0.000001
	8.28E+05	1.66E+06	4	4.16E+05	6307	157680	1.24E+01	2.76E+12	0.000000
	0	8.28E+05	47	4.14E+05	74110	1852740	1.24E+01	2.81E+12	0.000001
				0.00E+00					0.000194
	5.22E+07	5.80E+07	4	2.90E+06	2523	63072	9.07E+00	1.17E+09	0.000054
	4.64E+07	5.22E+07	3	2.90E+06	1892	47304	9.07E+00	1.17E+09	0.000041
	4.06E+07	4.64E+07	1.5	2.90E+06	946	23652	9.07E+00	1.17E+09	0.000020
	3.48E+07	4.06E+07	2	2.90E+06	1261	31536	9.07E+00	1.17E+09	0.000027
	2.90E+07	3.48E+07	8.5	2.90E+06	5361	134028	9.07E+00	1.17E+09	0.000115
	2.32E+07	2.90E+07	6	2.90E+06	3784	94608	9.07E+00	1.17E+09	0.000081
24	1.74E+07	2.32E+07	15	2.90E+06	9461	236520	9.07E+00	1.17E+09	0.000203
	1.16E+07	1.74E+07	17.5	2.90E+06	11038	275940	9.07E+00	1.17E+09	0.000236
	8.70E+06	1.16E+07	4	1.45E+06	2523	63072	1.03E+01	1.87E+10	0.000003
	5.80E+06	8.70E+06	5.5	1.45E+06	3469	86724	1.03E+01	1.87E+10	0.000005
	2.90E+06	5.80E+06	9	1.45E+06	5676	141912	1.03E+01	1.87E+10	0.000008
	1.45E+06	2.90E+06	3	7.25E+05	1892	47304	1.15E+01	2.99E+11	0.000000
	0	1.45E+06	60	7.25E+05	37843	946080	1.15E+01	2.99E+11	0.000003
				0.00E+00					0.000795
	7.19E+07	7.99E+07	1.5	4.00E+06	1325	33113	8.51E+00	3.23E+08	0.000103
	6.39E+07	7.19E+07	0.5	4.00E+06	442	11038	8.51E+00	3.23E+08	0.000034
	5.59E+07	6.39E+07	5.5	4.00E+06	4857	121414	8.51E+00	3.23E+08	0.000376
	4.79E+07	5.59E+07	6.5	4.00E+06	5740	143489	8.51E+00	3.23E+08	0.000445
	4.00E+07	4.79E+07	4.5	3.95E+06	3974	99338	8.53E+00	3.39E+08	0.000293
	3.20E+07	4.00E+07	11	4.00E+06	9713	242827	8.51E+00	3.23E+08	0.000753
25	2.40E+07	3.20E+07	10.5	4.00E+06	9272	231790	8.51E+00	3.23E+08	0.000718
	1.60E+07	2.40E+07	21	4.00E+06	18543	463579	8.51E+00	3.23E+08	0.001437
	1.20E+07	1.60E+07	10.5	2.00E+06	9272	231790	9.71E+00	5.16E+09	0.000045
	7.99E+06	1.20E+07	3.5	2.01E+06	3091	77263	9.71E+00	5.11E+09	0.000015
	4.00E+06	7.99E+06	6	2.00E+06	5298	132451	9.72E+00	5.21E+09	0.000025
	2.00E+06	4.00E+06	2	1.00E+06	1766	44150	1.09E+01	8.26E+10	0.000001
	0	2.00E+06	22	1.00E+06	19426	485654	1.09E+01	8.26E+10	0.000006
				0.00E+00					0.004250

Figure C.12: Reference monopile, Rainflow analysis result and fatigue damage calculation(cone), SS21-SS25

SS	min amp	max amp	cycle	avg amp	total cycles/ y	Total cycles(D	Log N	N	Eq. Fatigue da
26	2.00E+08	2.22E+08	0.5	1.10E+07	536	13403	6.75E+00	5.64E+06	0.002376
	1.78E+08	2.00E+08	0.5	1.10E+07	536	13403	6.75E+00	5.64E+06	0.002376
	1.55E+08	1.78E+08	4	1.15E+07	4289	107222	6.67E+00	4.72E+06	0.022703
	1.33E+08	1.55E+08	3	1.10E+07	3217	80417	6.75E+00	5.64E+06	0.014253
	1.11E+08	1.33E+08	5	1.10E+07	5361	134028	6.75E+00	5.64E+06	0.023756
	8.88E+07	1.11E+08	8	1.11E+07	8578	214445	6.74E+00	5.44E+06	0.039410
	6.66E+07	8.88E+07	12	1.11E+07	12867	321667	6.74E+00	5.44E+06	0.059115
	4.44E+07	6.66E+07	12	1.11E+07	12867	321667	6.74E+00	5.44E+06	0.059115
	3.33E+07	4.44E+07	5	5.55E+06	5361	134028	7.94E+00	8.71E+07	0.001539
	2.22E+07	3.33E+07	9	5.55E+06	9650	241250	7.94E+00	8.71E+07	0.002771
	1.11E+07	2.22E+07	7.5	5.55E+06	8042	201042	7.94E+00	8.71E+07	0.002309
	5.55E+06	1.11E+07	5	2.78E+06	5361	134028	9.14E+00	1.39E+09	0.000096
	0	5.55E+06	82.5	2.78E+06	88458	2211462	9.14E+00	1.39E+09	0.001588
				0.00E+00					0.231407
27	3.07E+08	3.41E+08	1.5	1.70E+07	1987	49669	6.00E+00	9.89E+05	0.050221
	2.73E+08	3.07E+08	0	1.70E+07	0	0	6.00E+00	9.89E+05	0.000000
	2.39E+08	2.73E+08	5	1.70E+07	6623	165564	6.00E+00	9.89E+05	0.167402
	2.05E+08	2.39E+08	3.5	1.70E+07	4636	115895	6.00E+00	9.89E+05	0.117182
	1.71E+08	2.05E+08	4.5	1.70E+07	5960	149008	6.00E+00	9.89E+05	0.150662
	1.37E+08	1.71E+08	7	1.70E+07	9272	231790	6.00E+00	9.89E+05	0.234363
	1.02E+08	1.37E+08	13.5	1.75E+07	17881	447023	5.94E+00	8.81E+05	0.507554
	6.83E+07	1.02E+08	14.5	1.69E+07	19205	480136	6.01E+00	1.02E+06	0.468558
	5.12E+07	6.83E+07	8.5	8.55E+06	11258	281459	7.19E+00	1.55E+07	0.018209
	3.41E+07	5.12E+07	6	8.55E+06	7947	198677	7.19E+00	1.55E+07	0.012853
	1.71E+07	3.41E+07	6	8.50E+06	7947	198677	7.20E+00	1.58E+07	0.012555
	8.54E+06	1.71E+07	3.5	4.28E+06	4636	115895	8.39E+00	2.46E+08	0.000471
	0	8.54E+06	57	4.27E+06	75497	1887430	8.40E+00	2.48E+08	0.007596
				0.00E+00					1.747626
28	5.49E+08	6.10E+08	1	3.05E+07	2144	53611	4.98E+00	9.55E+04	0.561636
	4.88E+08	5.49E+08	1	3.05E+07	2144	53611	4.98E+00	9.55E+04	0.561636
	4.27E+08	4.88E+08	4	3.05E+07	8578	214445	4.98E+00	9.55E+04	2.246544
	3.66E+08	4.27E+08	5	3.05E+07	10722	268056	4.98E+00	9.55E+04	2.808180
	3.05E+08	3.66E+08	5.5	3.05E+07	11794	294862	4.98E+00	9.55E+04	3.088998
	2.44E+08	3.05E+08	7	3.05E+07	15011	375278	4.98E+00	9.55E+04	3.931452
	1.83E+08	2.44E+08	17	3.05E+07	36456	911390	4.98E+00	9.55E+04	9.547811
	1.22E+08	1.83E+08	20.5	3.05E+07	43961	1099030	4.98E+00	9.55E+04	11.513537
	9.14E+07	1.22E+08	10	1.53E+07	21444	536112	6.18E+00	1.51E+06	0.355649
	6.10E+07	9.14E+07	5.5	1.52E+07	11794	294862	6.19E+00	1.55E+06	0.190543
	3.05E+07	6.10E+07	5	1.53E+07	10722	268056	6.18E+00	1.53E+06	0.175511
	1.52E+07	3.05E+07	4	7.65E+06	8578	214445	7.38E+00	2.41E+07	0.008891
	0	1.52E+07	27	7.60E+06	57900	1447502	7.39E+00	2.48E+07	0.058462
				0.00E+00					35.048848
29	6.39E+07	7.10E+07	0.5	3.55E+06	536	13403	8.72E+00	5.20E+08	0.000026
	5.68E+07	6.39E+07	2	3.55E+06	2144	53611	8.72E+00	5.20E+08	0.000103
	4.97E+07	5.68E+07	1.5	3.55E+06	1608	40208	8.72E+00	5.20E+08	0.000077
	4.26E+07	4.97E+07	3	3.55E+06	3217	80417	8.72E+00	5.20E+08	0.000155
	3.55E+07	4.26E+07	0.5	3.55E+06	536	13403	8.72E+00	5.20E+08	0.000026
	2.84E+07	3.55E+07	11	3.55E+06	11794	294862	8.72E+00	5.20E+08	0.000567
	2.13E+07	2.84E+07	3.5	3.55E+06	3753	93820	8.72E+00	5.20E+08	0.000180
	1.42E+07	2.13E+07	11.5	3.55E+06	12331	308264	8.72E+00	5.20E+08	0.000593
	1.07E+07	1.42E+07	3.5	1.75E+06	3753	93820	9.94E+00	8.81E+09	0.000011
	7.10E+06	1.07E+07	5	1.80E+06	5361	134028	9.90E+00	7.87E+09	0.000017
	3.55E+06	7.10E+06	9	1.78E+06	9650	241250	9.92E+00	8.32E+09	0.000029
	1.78E+06	3.55E+06	27.5	8.85E+05	29486	737154	1.11E+01	1.35E+11	0.000005
	0	1.78E+06	234.5	8.90E+05	251437	6285913	1.11E+01	1.32E+11	0.000048
				0.00E+00					0.001836
30	3.10E+08	3.45E+08	0.5	1.75E+07	613	15324	5.94E+00	8.81E+05	0.017399
	2.76E+08	3.10E+08	0	1.70E+07	0	0	6.00E+00	9.89E+05	0.000000
	2.41E+08	2.76E+08	5	1.75E+07	6130	153238	5.94E+00	8.81E+05	0.173988
	2.07E+08	2.41E+08	2.5	1.70E+07	3065	76619	6.00E+00	9.89E+05	0.077470
	1.72E+08	2.07E+08	6.5	1.75E+07	7968	199210	5.94E+00	8.81E+05	0.226185
	1.38E+08	1.72E+08	5	1.70E+07	6130	153238	6.00E+00	9.89E+05	0.154940
	1.03E+08	1.38E+08	14.5	1.75E+07	17776	444391	5.94E+00	8.81E+05	0.504565
	6.90E+07	1.03E+08	16	1.70E+07	19615	490363	6.00E+00	9.89E+05	0.495807
	5.17E+07	6.90E+07	6	8.65E+06	7355	183886	7.17E+00	1.48E+07	0.012463
	3.45E+07	5.17E+07	5	8.60E+06	6130	153238	7.18E+00	1.51E+07	0.010148
	1.72E+07	3.45E+07	6	8.65E+06	7355	183886	7.17E+00	1.48E+07	0.012463
	8.62E+06	1.72E+07	3.5	4.29E+06	4291	107267	8.39E+00	2.44E+08	0.000440
	0	8.62E+06	59	4.31E+06	72328	1808212	8.38E+00	2.39E+08	0.007554
				0.00E+00					1.693421

Figure C.13: Reference monopile, Rainflow analysis result and fatigue damage calculation(cone), SS26-SS30

SS	min amp	max amp	cycle	avg amp	total cycles/y	Total cycles(L	Log N	N	Eq. Fatigue da
31	2.80E+08	3.11E+08	1.5	1.55E+07	1563	39076	6.16E+00	1.43E+06	0.027305
	2.49E+08	2.80E+08	0	1.55E+07	0	0	6.16E+00	1.43E+06	0.000000
	2.18E+08	2.49E+08	5	1.55E+07	5210	130253	6.16E+00	1.43E+06	0.091015
	1.87E+08	2.18E+08	2.5	1.55E+07	2605	65126	6.16E+00	1.43E+06	0.045508
	1.56E+08	1.87E+08	5.5	1.55E+07	5731	143278	6.16E+00	1.43E+06	0.100117
	1.24E+08	1.56E+08	6	1.60E+07	6252	156303	6.10E+00	1.26E+06	0.124007
	9.34E+07	1.24E+08	16	1.53E+07	16672	416808	6.18E+00	1.51E+06	0.276504
	6.22E+07	9.34E+07	16.5	1.56E+07	17193	429833	6.14E+00	1.39E+06	0.308176
	4.67E+07	6.22E+07	10	7.75E+06	10420	260505	7.36E+00	2.29E+07	0.011377
	3.11E+07	4.67E+07	7.5	7.80E+06	7815	195379	7.35E+00	2.23E+07	0.008755
	1.56E+07	3.11E+07	9	7.75E+06	9378	234455	7.36E+00	2.29E+07	0.010239
	7.78E+06	1.56E+07	2.5	3.91E+06	2605	65126	8.55E+00	3.53E+08	0.000184
	0	7.78E+06	45	3.89E+06	46891	1172273	8.56E+00	3.61E+08	0.003250
				0.00E+00					1.006436
32	5.85E+07	6.50E+07	4	3.25E+06	6375	159368	8.87E+00	7.40E+08	0.000215
	5.20E+07	5.85E+07	1.5	3.25E+06	2391	59763	8.87E+00	7.40E+08	0.000081
	4.55E+07	5.20E+07	3	3.25E+06	4781	119526	8.87E+00	7.40E+08	0.000161
	3.90E+07	4.55E+07	3	3.25E+06	4781	119526	8.87E+00	7.40E+08	0.000161
	3.25E+07	3.90E+07	6	3.25E+06	9562	239052	8.87E+00	7.40E+08	0.000323
	2.60E+07	3.25E+07	5	3.25E+06	7968	199210	8.87E+00	7.40E+08	0.000269
	1.95E+07	2.60E+07	2.5	3.25E+06	3984	99605	8.87E+00	7.40E+08	0.000135
	1.30E+07	1.95E+07	7.5	3.25E+06	11953	298815	8.87E+00	7.40E+08	0.000404
	9.75E+06	1.30E+07	5	1.63E+06	7968	199210	1.01E+01	1.18E+10	0.000017
	6.50E+06	9.75E+06	9.5	1.63E+06	15140	378499	1.01E+01	1.18E+10	0.000032
	3.25E+06	6.50E+06	9	1.63E+06	14343	358578	1.01E+01	1.18E+10	0.000030
	1.63E+06	3.25E+06	22	8.10E+05	35061	876523	1.13E+01	1.92E+11	0.000005
	0	1.63E+06	211	8.15E+05	336266	8406654	1.13E+01	1.87E+11	0.000045
				0.00E+00					0.001877
33	6.39E+07	7.10E+07	1	3.55E+06	1072	26806	8.72E+00	5.20E+08	0.000052
	5.68E+07	6.39E+07	2	3.55E+06	2144	53611	8.72E+00	5.20E+08	0.000103
	4.97E+07	5.68E+07	1	3.55E+06	1072	26806	8.72E+00	5.20E+08	0.000052
	4.26E+07	4.97E+07	1	3.55E+06	1072	26806	8.72E+00	5.20E+08	0.000052
	3.55E+07	4.26E+07	3	3.55E+06	3217	80417	8.72E+00	5.20E+08	0.000155
	2.84E+07	3.55E+07	6	3.55E+06	6433	160834	8.72E+00	5.20E+08	0.000309
	2.13E+07	2.84E+07	4.5	3.55E+06	4825	120625	8.72E+00	5.20E+08	0.000232
	1.42E+07	2.13E+07	5.5	3.55E+06	5897	147431	8.72E+00	5.20E+08	0.000283
	1.07E+07	1.42E+07	5.5	1.75E+06	5897	147431	9.94E+00	8.81E+09	0.000017
	7.10E+06	1.07E+07	4.5	1.80E+06	4825	120625	9.90E+00	7.87E+09	0.000015
	3.55E+06	7.10E+06	15.5	1.78E+06	16619	415487	9.92E+00	8.32E+09	0.000050
	1.78E+06	3.55E+06	40	8.85E+05	42889	1072224	1.11E+01	1.35E+11	0.000008
	0	1.78E+06	251.5	8.90E+05	269664	6741608	1.11E+01	1.32E+11	0.000051
				0.00E+00					0.001378
34	2.38E+07	2.64E+07	1	1.30E+06	612	15312	1.05E+01	2.89E+10	0.000001
	2.11E+07	2.38E+07	3	1.35E+06	1837	45937	1.04E+01	2.49E+10	0.000002
	1.85E+07	2.11E+07	4.5	1.30E+06	2756	68906	1.05E+01	2.89E+10	0.000002
	1.59E+07	1.85E+07	4	1.30E+06	2450	61250	1.05E+01	2.89E+10	0.000002
	1.32E+07	1.59E+07	7	1.35E+06	4287	107187	1.04E+01	2.49E+10	0.000004
	1.06E+07	1.32E+07	15.5	1.30E+06	9494	237343	1.05E+01	2.89E+10	0.000008
	7.93E+06	1.06E+07	9	1.34E+06	5512	137812	1.04E+01	2.60E+10	0.000005
	5.29E+06	7.93E+06	17	1.32E+06	10412	260312	1.04E+01	2.72E+10	0.000010
	3.96E+06	5.29E+06	6	6.65E+05	3675	91875	1.16E+01	4.22E+11	0.000000
	2.64E+06	3.96E+06	14.5	6.60E+05	8881	222031	1.16E+01	4.35E+11	0.000001
	1.32E+06	2.64E+06	14	6.60E+05	8575	214375	1.16E+01	4.35E+11	0.000000
	6.61E+05	1.32E+06	6	3.30E+05	3675	91875	1.28E+01	7.01E+12	0.000000
	0	6.61E+05	31.5	3.31E+05	19294	482343	1.28E+01	6.92E+12	0.000000
				0.00E+00					0.000036
35	2.07E+07	2.31E+07	1	1.20E+06	586	14647	1.06E+01	3.98E+10	0.000000
	1.84E+07	2.07E+07	3.5	1.15E+06	2051	51264	1.07E+01	4.72E+10	0.000001
	1.61E+07	1.84E+07	3.5	1.15E+06	2051	51264	1.07E+01	4.72E+10	0.000001
	1.38E+07	1.61E+07	11	1.15E+06	6445	161114	1.07E+01	4.72E+10	0.000003
	1.15E+07	1.38E+07	11.5	1.15E+06	6737	168437	1.07E+01	4.72E+10	0.000004
	9.22E+06	1.15E+07	13.5	1.14E+06	7909	197731	1.07E+01	4.89E+10	0.000004
	6.92E+06	9.22E+06	11	1.15E+06	6445	161114	1.07E+01	4.72E+10	0.000003
	4.61E+06	6.92E+06	17.5	1.16E+06	10253	256318	1.07E+01	4.64E+10	0.000006
	3.46E+06	4.61E+06	7	5.75E+05	4101	102527	1.19E+01	7.56E+11	0.000000
	2.31E+06	3.46E+06	19.5	5.75E+05	11424	285611	1.19E+01	7.56E+11	0.000000
	1.15E+06	2.31E+06	8	5.80E+05	4687	117174	1.19E+01	7.30E+11	0.000000
	5.76E+05	1.15E+06	3	2.87E+05	1758	43940	1.31E+01	1.22E+13	0.000000
	0	5.76E+05	14.5	2.88E+05	8495	212377	1.31E+01	1.20E+13	0.000000
									0.000023

Figure C.14: Reference monopile, Rainflow analysis result and fatigue damage calculation(cone), SS31-SS35

C.3. Perforated monopile, perforation fatigue damage calculations

SS	min amp	max amp	cycle	avg amp	total cycles	design life	log S		Eq. Fatigue da
	3.69E+06	4.10E+06	2	2.05E+05	8602	215046	1.37E+01	4.68E+13	0.000000
	3.28E+06	3.69E+06	0	2.05E+05	0	0	1.37E+01	4.68E+13	0.000000
	2.87E+06	3.28E+06	1	2.05E+05	4301	107523	1.37E+01	4.68E+13	0.000000
	2.46E+06	2.87E+06	2.5	2.05E+05	10752	268808	1.37E+01	4.68E+13	0.000000
	2.05E+06	2.46E+06	2	2.05E+05	8602	215046	1.37E+01	4.68E+13	0.000000
	1.64E+06	2.05E+06	3	2.05E+05	12903	322570	1.37E+01	4.68E+13	0.000000
1	1.23E+06	1.64E+06	3	2.05E+05	12903	322570	1.37E+01	4.68E+13	0.000000
	8.20E+05	1.23E+06	5	2.05E+05	21505	537616	1.37E+01	4.68E+13	0.000000
	6.15E+05	8.20E+05	1.5	1.03E+05	6451	161285	1.49E+01	7.48E+14	0.000000
	4.10E+05	6.15E+05	8.5	1.03E+05	36558	913948	1.49E+01	7.48E+14	0.000000
	2.05E+05	4.10E+05	25.5	1.03E+05	109674	2741843	1.49E+01	7.48E+14	0.000000
	1.03E+05	2.05E+05	51.5	5.10E+04	221498	5537447	1.61E+01	1.22E+16	0.000000
	0	1.03E+05	325.5	5.15E+04	1399953	34998814	1.61E+01	1.17E+16	0.000000
				0.00E+00					0.000000
	9.61E+07	1.07E+08	1	5.45E+06	5420	135511	7.97E+00	9.36E+07	0.001447
	8.54E+07	9.61E+07	0.5	5.35E+06	2710	67756	8.00E+00	1.01E+08	0.000672
	7.48E+07	8.54E+07	4	5.30E+06	21682	542046	8.02E+00	1.05E+08	0.005178
	6.41E+07	7.48E+07	4	5.35E+06	21682	542046	8.00E+00	1.01E+08	0.005376
	5.34E+07	6.41E+07	2.5	5.35E+06	13551	338779	8.00E+00	1.01E+08	0.003360
	4.27E+07	5.34E+07	2	5.35E+06	10841	271023	8.00E+00	1.01E+08	0.002688
	3.20E+07	4.27E+07	12	5.35E+06	65045	1626137	8.00E+00	1.01E+08	0.016128
2	2.14E+07	3.20E+07	10.5	5.30E+06	56915	1422870	8.02E+00	1.05E+08	0.013592
	1.60E+07	2.14E+07	7	2.70E+06	37943	948580	9.19E+00	1.55E+09	0.000610
	1.07E+07	1.60E+07	8	2.65E+06	43364	1084091	9.22E+00	1.68E+09	0.000647
	5.34E+06	1.07E+07	3	2.68E+06	16261	406534	9.20E+00	1.60E+09	0.000254
	2.67E+06	5.34E+06	6	1.34E+06	32523	813069	1.04E+01	2.60E+10	0.000031
	0	2.67E+06	158	1.34E+06	856432	21410807	1.04E+01	2.60E+10	0.000823
				0.00E+00					0.050806
	1.32E+08	1.47E+08	0.5	7.50E+06	466	11648	7.42E+00	2.61E+07	0.000446
	1.18E+08	1.32E+08	0.5	7.00E+06	466	11648	7.54E+00	3.44E+07	0.000339
	1.03E+08	1.18E+08	3	7.50E+06	2796	69891	7.42E+00	2.61E+07	0.002677
	8.82E+07	1.03E+08	6.5	7.40E+06	6057	151430	7.44E+00	2.75E+07	0.005497
	7.35E+07	8.82E+07	0.5	7.35E+06	466	11648	7.45E+00	2.83E+07	0.000412
	5.88E+07	7.35E+07	3.5	7.35E+06	3262	81539	7.45E+00	2.83E+07	0.002881
	4.41E+07	5.88E+07	6	7.35E+06	5591	139781	7.45E+00	2.83E+07	0.004939
3	2.94E+07	4.41E+07	11	7.35E+06	10251	256266	7.45E+00	2.83E+07	0.009054
	2.21E+07	2.94E+07	6	3.65E+06	5591	139781	8.67E+00	4.65E+08	0.000300
	1.47E+07	2.21E+07	6.5	3.70E+06	6057	151430	8.64E+00	4.41E+08	0.000344
	7.35E+06	1.47E+07	8.5	3.68E+06	7921	198023	8.66E+00	4.53E+08	0.000437
	3.68E+06	7.35E+06	6	1.84E+06	5591	139781	9.86E+00	7.29E+09	0.000019
	0	3.68E+06	138.5	1.84E+06	129065	3226616	9.86E+00	7.21E+09	0.000448
				0.00E+00					0.027792
	1.45E+07	1.61E+07	2.5	8.00E+05	16194	404854	1.13E+01	2.02E+11	0.000002
	1.29E+07	1.45E+07	0	8.00E+05	0	0	1.13E+01	2.02E+11	0.000000
	1.13E+07	1.29E+07	1.5	8.00E+05	9716	242912	1.13E+01	2.02E+11	0.000001
	9.66E+06	1.13E+07	4	8.20E+05	25911	647766	1.13E+01	1.83E+11	0.000004
	8.05E+06	9.66E+06	5	8.05E+05	32388	809708	1.13E+01	1.97E+11	0.000004
	6.44E+06	8.05E+06	3	8.05E+05	19433	485825	1.13E+01	1.97E+11	0.000002
	4.83E+06	6.44E+06	2.5	8.05E+05	16194	404854	1.13E+01	1.97E+11	0.000002
4	3.22E+06	4.83E+06	4.5	8.05E+05	29149	728737	1.13E+01	1.97E+11	0.000004
	2.42E+06	3.22E+06	7	4.00E+05	45344	1133591	1.25E+01	3.23E+12	0.000000
	1.61E+06	2.42E+06	7.5	4.05E+05	48582	1214562	1.25E+01	3.07E+12	0.000000
	8.05E+05	1.61E+06	10	4.03E+05	64777	1619416	1.25E+01	3.15E+12	0.000001
	4.03E+05	8.05E+05	5.5	2.01E+05	35627	890679	1.37E+01	5.06E+13	0.000000
	0	4.03E+05	151.5	2.02E+05	981366	24534156	1.37E+01	5.01E+13	0.000000
				0.00E+00					0.000021
	1.23E+07	1.37E+07	0.5	7.00E+05	3239	80971	1.15E+01	3.44E+11	0.000000
	1.10E+07	1.23E+07	0.5	6.50E+05	3239	80971	1.17E+01	4.63E+11	0.000000
	9.59E+06	1.10E+07	0.5	7.05E+05	3239	80971	1.15E+01	3.34E+11	0.000000
	8.22E+06	9.59E+06	1.5	6.85E+05	9716	242912	1.16E+01	3.75E+11	0.000001
	6.85E+06	8.22E+06	1	6.85E+05	6478	161942	1.16E+01	3.75E+11	0.000000
	5.48E+06	6.85E+06	1.5	6.85E+05	9716	242912	1.16E+01	3.75E+11	0.000001
	4.11E+06	5.48E+06	4.5	6.85E+05	29149	728737	1.16E+01	3.75E+11	0.000002
4	2.74E+06	4.11E+06	10	6.85E+05	64777	1619416	1.16E+01	3.75E+11	0.000004
	2.06E+06	2.74E+06	11	3.40E+05	71254	1781358	1.28E+01	6.18E+12	0.000000
	1.37E+06	2.06E+06	6	3.45E+05	38866	971650	1.28E+01	5.83E+12	0.000000
	6.85E+05	1.37E+06	8	3.43E+05	51821	1295533	1.28E+01	6.00E+12	0.000000
	3.43E+05	6.85E+05	5.5	1.71E+05	35627	890679	1.40E+01	9.66E+13	0.000000
	0	3.43E+05	218	1.72E+05	1412131	35303274	1.40E+01	9.55E+13	0.000000
				0.00E+00					0.000010
	5.16E+08	5.73E+08	1	2.85E+07	6530	163249	5.10E+00	1.25E+05	1.303853
	4.58E+08	5.16E+08	1	2.90E+07	6530	163249	5.07E+00	1.17E+05	1.397788
	4.01E+08	4.58E+08	1.5	2.85E+07	9795	244873	5.10E+00	1.25E+05	1.955780
	3.44E+08	4.01E+08	8.5	2.85E+07	55504	1387612	5.10E+00	1.25E+05	11.082752
	2.87E+08	3.44E+08	6.5	2.85E+07	42445	1061115	5.10E+00	1.25E+05	8.475046
	2.29E+08	2.87E+08	13	2.90E+07	84889	2122231	5.07E+00	1.17E+05	18.171241
5	1.72E+08	2.29E+08	13.5	2.85E+07	88154	2203855	5.10E+00	1.25E+05	17.602018
	1.15E+08	1.72E+08	18	2.85E+07	117539	2938473	5.10E+00	1.25E+05	23.469357
	8.60E+07	1.15E+08	10	1.45E+07	65299	1632485	6.27E+00	1.87E+06	0.873617
	5.73E+07	8.60E+07	2	1.44E+07	13060	326497	6.29E+00	1.95E+06	0.167605
	2.87E+07	5.73E+07	2	1.43E+07	13060	326497	6.30E+00	1.98E+06	0.165281
	1.43E+07	2.87E+07	1	7.20E+06	6530	163249	7.49E+00	3.07E+07	0.005311
	0	1.43E+07	19.5	7.15E+06	127334	3183346	7.50E+00	3.16E+07	0.100718
				0.00E+00					84.770367

Figure C.15: Perforated monopile, Rainflow analysis result and fatigue damage calculation(SZ), SS6-SS9

SS	min amp	max amp	cycle	avg amp	total cycles	design life	log S		Eq. Fatigue da
6	7.74E+06	8.60E+06	1	4.30E+05	3392	84792	1.24E+01	2.42E+12	0.000000
	6.88E+06	7.74E+06	2	4.30E+05	6783	169584	1.24E+01	2.42E+12	0.000000
	6.02E+06	6.88E+06	3	4.30E+05	10175	254376	1.24E+01	2.42E+12	0.000000
	5.16E+06	6.02E+06	6.5	4.30E+05	22046	551148	1.24E+01	2.42E+12	0.000000
	4.30E+06	5.16E+06	0.5	4.30E+05	1696	42396	1.24E+01	2.42E+12	0.000000
	3.44E+06	4.30E+06	3.5	4.30E+05	11871	296772	1.24E+01	2.42E+12	0.000000
	2.58E+06	3.44E+06	4	4.30E+05	13567	339168	1.24E+01	2.42E+12	0.000000
	1.72E+06	2.58E+06	8	4.30E+05	27133	678337	1.24E+01	2.42E+12	0.000000
	1.29E+06	1.72E+06	4.5	2.15E+05	15263	381564	1.36E+01	3.87E+13	0.000000
	8.60E+05	1.29E+06	3.5	2.15E+05	11871	296772	1.36E+01	3.87E+13	0.000000
	4.30E+05	8.60E+05	12	2.15E+05	40700	1017505	1.36E+01	3.87E+13	0.000000
	2.15E+05	4.30E+05	10.5	1.08E+05	35613	890317	1.48E+01	6.19E+14	0.000000
	0	2.15E+05	185.5	1.08E+05	629157	15728928	1.48E+01	6.19E+14	0.000000
				0.00E+00					0.000001
6 (5% damping)	6.12E+06	6.80E+06	1	3.40E+05	3392	84792	1.28E+01	6.18E+12	0.000000
	5.44E+06	6.12E+06	0.5	3.40E+05	1696	42396	1.28E+01	6.18E+12	0.000000
	4.76E+06	5.44E+06	3.5	3.40E+05	11871	296772	1.28E+01	6.18E+12	0.000000
	4.08E+06	4.76E+06	5	3.40E+05	16958	423960	1.28E+01	6.18E+12	0.000000
	3.40E+06	4.08E+06	3	3.40E+05	10175	254376	1.28E+01	6.18E+12	0.000000
	2.72E+06	3.40E+06	4	3.40E+05	13567	339168	1.28E+01	6.18E+12	0.000000
	2.04E+06	2.72E+06	4	3.40E+05	13567	339168	1.28E+01	6.18E+12	0.000000
	1.36E+06	2.04E+06	7	3.40E+05	23742	593544	1.28E+01	6.18E+12	0.000000
	1.02E+06	1.36E+06	2	1.70E+05	6783	169584	1.40E+01	9.89E+13	0.000000
	6.80E+05	1.02E+06	8	1.70E+05	27133	678337	1.40E+01	9.89E+13	0.000000
	3.40E+05	6.80E+05	9.5	1.70E+05	32221	805525	1.40E+01	9.89E+13	0.000000
	1.70E+05	3.40E+05	33	8.50E+04	111926	2798138	1.52E+01	1.58E+15	0.000000
	0	1.70E+05	228.5	8.50E+04	774999	19374987	1.52E+01	1.58E+15	0.000000
				0.00E+00					0.000000
7	5.10E+08	5.67E+08	1	2.85E+07	4001	100030	5.10E+00	1.25E+05	0.798930
	4.54E+08	5.10E+08	0	2.80E+07	0	0	5.13E+00	1.34E+05	0.000000
	3.97E+08	4.54E+08	1.5	2.85E+07	6002	150045	5.10E+00	1.25E+05	1.198394
	3.40E+08	3.97E+08	6.5	2.85E+07	26008	650193	5.10E+00	1.25E+05	5.193043
	2.84E+08	3.40E+08	7	2.80E+07	28008	700208	5.13E+00	1.34E+05	5.210258
	2.27E+08	2.84E+08	9.5	2.85E+07	38011	950282	5.10E+00	1.25E+05	7.589832
	1.70E+08	2.27E+08	13.5	2.85E+07	54016	1350401	5.10E+00	1.25E+05	10.785550
	1.13E+08	1.70E+08	22	2.85E+07	88026	2200654	5.10E+00	1.25E+05	17.576452
	8.51E+07	1.13E+08	7	1.40E+07	28008	700208	6.34E+00	2.18E+06	0.321014
	5.67E+07	8.51E+07	3.5	1.42E+07	14004	350104	6.31E+00	2.03E+06	0.172326
	2.84E+07	5.67E+07	5.5	1.42E+07	22007	550164	6.31E+00	2.06E+06	0.267004
	1.42E+07	2.84E+07	2	7.10E+06	8002	200059	7.51E+00	3.25E+07	0.006154
	0	1.42E+07	19.5	7.10E+06	78023	1950580	7.51E+00	3.25E+07	0.060006
				0.00E+00					49.178964
8	6.46E+08	7.18E+08	1.5	3.60E+07	746	18645	4.69E+00	4.92E+04	0.379108
	5.74E+08	6.46E+08	1.5	3.60E+07	746	18645	4.69E+00	4.92E+04	0.379108
	5.03E+08	5.74E+08	4	3.55E+07	1989	49719	4.72E+00	5.20E+04	0.955950
	4.31E+08	5.03E+08	6.5	3.60E+07	3232	80793	4.69E+00	4.92E+04	1.642801
	3.59E+08	4.31E+08	6.5	3.60E+07	3232	80793	4.69E+00	4.92E+04	1.642801
	2.87E+08	3.59E+08	12.5	3.60E+07	6215	155372	4.69E+00	4.92E+04	3.159233
	2.15E+08	2.87E+08	15	3.60E+07	7458	186446	4.69E+00	4.92E+04	3.791080
	1.44E+08	2.15E+08	15.5	3.55E+07	7706	192661	4.72E+00	5.20E+04	3.704305
	1.08E+08	1.44E+08	8	1.80E+07	3978	99438	5.90E+00	7.87E+05	0.126369
	7.18E+07	1.08E+08	5.5	1.81E+07	2735	68364	5.89E+00	7.70E+05	0.088826
	3.59E+07	7.18E+07	2.5	1.80E+07	1243	31074	5.90E+00	7.96E+05	0.039053
	1.80E+07	3.59E+07	0	8.95E+06	0	0	7.11E+00	1.29E+07	0.000000
	0	1.80E+07	13	9.00E+06	6463	161586	7.10E+00	1.26E+07	0.012834
				0.00E+00					15.921470
9	6.46E+08	7.18E+08	1.5	3.60E+07	2171	54275	4.69E+00	4.92E+04	1.103598
	5.74E+08	6.46E+08	1.5	3.60E+07	2171	54275	4.69E+00	4.92E+04	1.103598
	5.03E+08	5.74E+08	4	3.55E+07	5789	144734	4.72E+00	5.20E+04	2.782806
	4.31E+08	5.03E+08	6.5	3.60E+07	9408	235192	4.69E+00	4.92E+04	4.782256
	3.59E+08	4.31E+08	6.5	3.60E+07	9408	235192	4.69E+00	4.92E+04	4.782256
	2.87E+08	3.59E+08	12.5	3.60E+07	18092	452293	4.69E+00	4.92E+04	9.196647
	2.15E+08	2.87E+08	15	3.60E+07	21710	542751	4.69E+00	4.92E+04	11.035976
	1.44E+08	2.15E+08	15.5	3.55E+07	22434	560843	4.72E+00	5.20E+04	10.783373
	1.08E+08	1.44E+08	8	1.80E+07	11579	289467	5.90E+00	7.87E+05	0.367866
	7.18E+07	1.08E+08	5.5	1.81E+07	7960	199009	5.89E+00	7.70E+05	0.258575
	3.59E+07	7.18E+07	2.5	1.80E+07	3618	90459	5.90E+00	7.96E+05	0.113686
	1.80E+07	3.59E+07	0	8.95E+06	0	0	7.11E+00	1.29E+07	0.000000
	0	1.80E+07	13	9.00E+06	18815	470384	7.10E+00	1.26E+07	0.037361
				0.00E+00					46.347998

Figure C.16: Perforated monopile, Rainflow analysis result and fatigue damage calculation(SZ), SS1-SS5

SS	min amp	max amp	cycle	avg amp	total cycles	design life	log S		Eq. Fatigue da
	2.75E+07	3.06E+07	2	1.55E+06	2895	72367	1.02E+01	1.43E+10	0.000005
	2.45E+07	2.75E+07	1.5	1.50E+06	2171	54275	1.02E+01	1.63E+10	0.000003
	2.14E+07	2.45E+07	5.5	1.55E+06	7960	199009	1.02E+01	1.43E+10	0.000014
	1.84E+07	2.14E+07	2.5	1.50E+06	3618	90459	1.02E+01	1.63E+10	0.000006
	1.53E+07	1.84E+07	2.5	1.55E+06	3618	90459	1.02E+01	1.43E+10	0.000006
	1.22E+07	1.53E+07	4.5	1.55E+06	6513	162825	1.02E+01	1.43E+10	0.000011
9 (5%	9.18E+06	1.22E+07	13	1.51E+06	18815	470384	1.02E+01	1.59E+10	0.000030
damping)	6.12E+06	9.18E+06	14	1.53E+06	20263	506568	1.02E+01	1.51E+10	0.000034
	4.59E+06	6.12E+06	5.5	7.65E+05	7960	199009	1.14E+01	2.41E+11	0.000001
	3.06E+06	4.59E+06	6.5	7.65E+05	9408	235192	1.14E+01	2.41E+11	0.000001
	1.53E+06	3.06E+06	16	7.65E+05	23157	578935	1.14E+01	2.41E+11	0.000002
	7.65E+05	1.53E+06	94	3.83E+05	136050	3401241	1.26E+01	3.86E+12	0.000001
	0	7.65E+05	37.5	3.83E+05	54275	1356878	1.26E+01	3.86E+12	0.000000
				0.00E+00					0.000114
	2.53E+07	2.81E+07	2	1.40E+06	1893	47317	1.03E+01	2.15E+10	0.000002
	2.25E+07	2.53E+07	1	1.40E+06	946	23658	1.03E+01	2.15E+10	0.000001
	1.97E+07	2.25E+07	0.5	1.40E+06	473	11829	1.03E+01	2.15E+10	0.000001
	1.69E+07	1.97E+07	1	1.40E+06	946	23658	1.03E+01	2.15E+10	0.000001
	1.41E+07	1.69E+07	3	1.40E+06	2839	70975	1.03E+01	2.15E+10	0.000003
	1.12E+07	1.41E+07	6.5	1.45E+06	6151	153779	1.03E+01	1.87E+10	0.000008
10	8.43E+06	1.12E+07	4.5	1.39E+06	4259	106463	1.04E+01	2.24E+10	0.000005
	5.62E+06	8.43E+06	7.5	1.41E+06	7098	177438	1.03E+01	2.12E+10	0.000008
	4.22E+06	5.62E+06	10.5	7.00E+05	9937	248413	1.15E+01	3.44E+11	0.000001
	2.81E+06	4.22E+06	4	7.05E+05	3785	94634	1.15E+01	3.34E+11	0.000000
	1.41E+06	2.81E+06	6	7.00E+05	5678	141950	1.15E+01	3.44E+11	0.000000
	7.03E+05	1.41E+06	12	3.54E+05	11356	283901	1.27E+01	5.29E+12	0.000000
	0	7.03E+05	78.5	3.52E+05	74287	1857183	1.27E+01	5.41E+12	0.000000
				0.00E+00					0.000031
	2.06E+07	2.29E+07	1	1.15E+06	946	23658	1.07E+01	4.72E+10	0.000001
	1.83E+07	2.06E+07	0	1.15E+06	0	0	1.07E+01	4.72E+10	0.000000
	1.60E+07	1.83E+07	0	1.15E+06	0	0	1.07E+01	4.72E+10	0.000000
	1.37E+07	1.60E+07	0.5	1.15E+06	473	11829	1.07E+01	4.72E+10	0.000000
	1.15E+07	1.37E+07	4.5	1.10E+06	4259	106463	1.08E+01	5.64E+10	0.000002
	9.16E+06	1.15E+07	6.5	1.17E+06	6151	153779	1.06E+01	4.41E+10	0.000003
6	6.87E+06	9.16E+06	6.5	1.15E+06	6151	153779	1.07E+01	4.81E+10	0.000003
	4.58E+06	6.87E+06	10	1.15E+06	9463	236584	1.07E+01	4.81E+10	0.000005
	3.44E+06	4.58E+06	7	5.70E+05	6624	165609	1.19E+01	7.83E+11	0.000000
	2.29E+06	3.44E+06	11.5	5.75E+05	10883	272071	1.19E+01	7.56E+11	0.000000
	1.15E+06	2.29E+06	9.5	5.70E+05	8990	224755	1.19E+01	7.83E+11	0.000000
	5.73E+05	1.15E+06	4	2.89E+05	3785	94634	1.31E+01	1.19E+13	0.000000
	0	5.73E+05	110	2.87E+05	104097	2602422	1.31E+01	1.23E+13	0.000000
				0.00E+00					0.000015
	1.26E+08	1.40E+08	0.5	7.00E+06	557	13917	7.54E+00	3.44E+07	0.000405
	1.12E+08	1.26E+08	1	7.00E+06	1113	27833	7.54E+00	3.44E+07	0.000809
	9.80E+07	1.12E+08	1	7.00E+06	1113	27833	7.54E+00	3.44E+07	0.000809
	8.40E+07	9.80E+07	4.5	7.00E+06	5010	125250	7.54E+00	3.44E+07	0.003641
	7.00E+07	8.40E+07	4	7.00E+06	4453	111334	7.54E+00	3.44E+07	0.003236
	5.60E+07	7.00E+07	5	7.00E+06	5567	139167	7.54E+00	3.44E+07	0.004045
11	4.20E+07	5.60E+07	8.5	7.00E+06	9463	236584	7.54E+00	3.44E+07	0.006877
	2.80E+07	4.20E+07	12	7.00E+06	13360	334001	7.54E+00	3.44E+07	0.009708
	2.10E+07	2.80E+07	9	3.50E+06	10020	250501	8.74E+00	5.50E+08	0.000455
	1.40E+07	2.10E+07	3	3.50E+06	3340	83500	8.74E+00	5.50E+08	0.000152
	7.00E+06	1.40E+07	7.5	3.50E+06	8350	208750	8.74E+00	5.50E+08	0.000379
	3.50E+06	7.00E+06	3.5	1.75E+06	3897	97417	9.94E+00	8.81E+09	0.000011
	0	3.50E+06	123	1.75E+06	136940	3423507	9.94E+00	8.81E+09	0.000389
				0.00E+00					0.030915
	2.06E+08	2.29E+08	0.5	1.15E+07	834	20856	6.67E+00	4.72E+06	0.004416
	1.83E+08	2.06E+08	0	1.15E+07	0	0	6.67E+00	4.72E+06	0.000000
	1.60E+08	1.83E+08	3	1.15E+07	5005	125135	6.67E+00	4.72E+06	0.026495
	1.37E+08	1.60E+08	4.5	1.15E+07	7508	187703	6.67E+00	4.72E+06	0.039743
	1.15E+08	1.37E+08	5.5	1.10E+07	9177	229415	6.75E+00	5.64E+06	0.040662
	9.16E+07	1.15E+08	7.5	1.17E+07	12514	312838	6.64E+00	4.41E+06	0.070968
12	6.87E+07	9.16E+07	4	1.15E+07	6674	166847	6.68E+00	4.81E+06	0.034717
	4.58E+07	6.87E+07	19.5	1.15E+07	32535	813380	6.68E+00	4.81E+06	0.169245
	3.44E+07	4.58E+07	5	5.70E+06	8342	208559	7.89E+00	7.83E+07	0.002665
	2.29E+07	3.44E+07	7.5	5.75E+06	12514	312838	7.88E+00	7.56E+07	0.004140
	1.15E+07	2.29E+07	7	5.70E+06	11679	291983	7.89E+00	7.83E+07	0.003731
	5.73E+06	1.15E+07	2	2.89E+06	3337	83424	9.08E+00	1.19E+09	0.000070
	0	5.73E+06	67.5	2.87E+06	112622	2815546	9.09E+00	1.23E+09	0.002296
				0.00E+00					0.399150

Figure C.17: Perforated monopile, Rainflow analysis result and fatigue damage calculation(SZ), SS9-SS12

SS	min amp	max amp	cycle	avg amp	total cycles	design life	log S		Eq. Fatigue da
13	2.23E+08	2.48E+08	0.5	1.25E+07	527	13176	6.53E+00	3.38E+06	0.003894
	1.98E+08	2.23E+08	2	1.25E+07	2108	52705	6.53E+00	3.38E+06	0.015577
	1.74E+08	1.98E+08	3.5	1.20E+07	3689	92233	6.60E+00	3.98E+06	0.023153
	1.49E+08	1.74E+08	8	1.25E+07	8433	210819	6.53E+00	3.38E+06	0.062309
	1.24E+08	1.49E+08	5	1.25E+07	5270	131762	6.53E+00	3.38E+06	0.038943
	9.92E+07	1.24E+08	7.5	1.24E+07	7906	197643	6.54E+00	3.49E+06	0.056568
	7.44E+07	9.92E+07	12	1.24E+07	12649	316228	6.54E+00	3.49E+06	0.090508
	4.96E+07	7.44E+07	12.5	1.24E+07	13176	329404	6.54E+00	3.49E+06	0.094279
	3.72E+07	4.96E+07	2.5	6.20E+06	2635	65881	7.75E+00	5.59E+07	0.001178
	2.48E+07	3.72E+07	8	6.20E+06	8433	210819	7.75E+00	5.59E+07	0.003771
	1.24E+07	2.48E+07	4	6.20E+06	4216	105409	7.75E+00	5.59E+07	0.001886
	6.20E+06	1.24E+07	2	3.10E+06	2108	52705	8.95E+00	8.94E+08	0.000059
	0	6.20E+06	60	3.10E+06	63246	1581141	8.95E+00	8.94E+08	0.001768
				0.00E+00					0.393893
14	4.43E+08	4.92E+08	0.5	2.45E+07	576	14411	5.36E+00	2.29E+05	0.062860
	3.94E+08	4.43E+08	2	2.45E+07	2306	57646	5.36E+00	2.29E+05	0.251438
	3.44E+08	3.94E+08	6.5	2.50E+07	7494	187349	5.33E+00	2.11E+05	0.885953
	2.95E+08	3.44E+08	7	2.45E+07	8070	201760	5.36E+00	2.29E+05	0.880035
	2.46E+08	2.95E+08	7	2.45E+07	8070	201760	5.36E+00	2.29E+05	0.880035
	1.97E+08	2.46E+08	11	2.45E+07	12682	317052	5.36E+00	2.29E+05	1.382912
	1.48E+08	1.97E+08	16.5	2.45E+07	19023	475578	5.36E+00	2.29E+05	2.074367
	9.84E+07	1.48E+08	12	2.48E+07	13835	345875	5.34E+00	2.18E+05	1.583891
	7.38E+07	9.84E+07	5.5	1.23E+07	6341	158526	6.56E+00	3.61E+06	0.043926
	4.92E+07	7.38E+07	4	1.23E+07	4612	115292	6.56E+00	3.61E+06	0.031946
	2.46E+07	4.92E+07	2	1.23E+07	2306	57646	6.56E+00	3.61E+06	0.015973
	1.23E+07	2.46E+07	1	6.15E+06	1153	28823	7.76E+00	5.77E+07	0.000499
	0	1.23E+07	26	6.15E+06	29976	749395	7.76E+00	5.77E+07	0.012978
				0.00E+00					8.106813
15	7.92E+08	8.80E+08	0.5	4.40E+07	511	12764	4.34E+00	2.20E+04	0.579178
	7.04E+08	7.92E+08	1	4.40E+07	1021	25529	4.34E+00	2.20E+04	1.158355
	6.16E+08	7.04E+08	2.5	4.40E+07	2553	63822	4.34E+00	2.20E+04	2.895888
	5.28E+08	6.16E+08	2	4.40E+07	2042	51058	4.34E+00	2.20E+04	2.316710
	4.40E+08	5.28E+08	10.5	4.40E+07	10722	268053	4.34E+00	2.20E+04	12.162730
	3.52E+08	4.40E+08	7.5	4.40E+07	7659	191466	4.34E+00	2.20E+04	8.687664
	2.64E+08	3.52E+08	14.5	4.40E+07	14807	370168	4.34E+00	2.20E+04	16.796151
	1.76E+08	2.64E+08	18	4.40E+07	18381	459519	4.34E+00	2.20E+04	20.850394
	1.32E+08	1.76E+08	8	2.20E+07	8169	204231	5.55E+00	3.53E+05	0.579178
	8.80E+07	1.32E+08	7.5	2.20E+07	7659	191466	5.55E+00	3.53E+05	0.542979
	4.40E+07	8.80E+07	1	2.20E+07	1021	25529	5.55E+00	3.53E+05	0.072397
	2.20E+07	4.40E+07	3.5	1.10E+07	3574	89351	6.75E+00	5.64E+06	0.015837
	0	2.20E+07	17	1.10E+07	17360	433990	6.75E+00	5.64E+06	0.076922
				0.00E+00					66.734384
16	8.55E+08	9.50E+08	1.5	4.75E+07	1235	30882	4.21E+00	1.62E+04	1.903159
	7.60E+08	8.55E+08	2.5	4.75E+07	2059	51469	4.21E+00	1.62E+04	3.171932
	6.65E+08	7.60E+08	7	4.75E+07	5765	144114	4.21E+00	1.62E+04	8.881409
	5.70E+08	6.65E+08	5	4.75E+07	4118	102939	4.21E+00	1.62E+04	6.343863
	4.75E+08	5.70E+08	11	4.75E+07	9059	226466	4.21E+00	1.62E+04	13.956499
	3.80E+08	4.75E+08	5.5	4.75E+07	4529	113233	4.21E+00	1.62E+04	6.978250
	2.85E+08	3.80E+08	15.5	4.75E+07	12764	319110	4.21E+00	1.62E+04	19.665976
	1.90E+08	2.85E+08	14	4.75E+07	11529	288229	4.21E+00	1.62E+04	17.762817
	1.43E+08	1.90E+08	8	2.35E+07	6588	164702	5.43E+00	2.71E+05	0.608094
	9.50E+07	1.43E+08	5	2.40E+07	4118	102939	5.40E+00	2.49E+05	0.413451
	4.75E+07	9.50E+07	1.5	2.38E+07	1235	30882	5.41E+00	2.60E+05	0.118947
	2.38E+07	4.75E+07	1	1.19E+07	824	20588	6.62E+00	4.19E+06	0.004915
	0	2.38E+07	16.5	1.19E+07	13588	339698	6.61E+00	4.12E+06	0.082467
				0.00E+00					79.891780
17	1.62E+09	1.80E+09	1.5	9.00E+07	1482	37058	3.10E+00	1.26E+03	29.434179
	1.44E+09	1.62E+09	0.5	9.00E+07	494	12353	3.10E+00	1.26E+03	9.811393
	1.26E+09	1.44E+09	2.5	9.00E+07	2471	61763	3.10E+00	1.26E+03	49.056964
	1.08E+09	1.26E+09	6	9.00E+07	5929	148232	3.10E+00	1.26E+03	117.736714
	9.02E+08	1.08E+09	7	8.90E+07	6917	172937	3.12E+00	1.32E+03	131.355629
	7.21E+08	9.02E+08	8	9.05E+07	7906	197643	3.09E+00	1.23E+03	160.499959
	5.41E+08	7.21E+08	14	9.00E+07	13835	345875	3.10E+00	1.26E+03	274.719000
	3.61E+08	5.41E+08	14.5	9.00E+07	14329	358227	3.10E+00	1.26E+03	284.530393
	2.71E+08	3.61E+08	5	4.50E+07	4941	123527	4.30E+00	2.01E+04	6.132121
	1.80E+08	2.71E+08	4.5	4.55E+07	4447	111174	4.28E+00	1.93E+04	5.768312
	9.02E+07	1.80E+08	11.5	4.49E+07	11364	284111	4.31E+00	2.03E+04	13.978927
	4.51E+07	9.02E+07	3	2.26E+07	2965	74116	5.50E+00	3.19E+05	0.232005
	0	4.51E+07	38	2.26E+07	37552	938802	5.50E+00	3.19E+05	2.938735
				0.00E+00					1086.194330

Figure C.18: Perforated monopile, Rainflow analysis result and fatigue damage calculation(SZ), SS13-SS17

SS	min amp	max amp	cycle	avg amp	total cycles	design life	log S		Eq. Fatigue da
	2.20E+08	2.44E+08	1	1.20E+07	711	17773	6.60E+00	3.98E+06	0.004461
	1.95E+08	2.20E+08	0.5	1.25E+07	355	8886	6.53E+00	3.38E+06	0.002626
	1.71E+08	1.95E+08	5	1.20E+07	3555	88863	6.60E+00	3.98E+06	0.022307
	1.46E+08	1.71E+08	5.5	1.25E+07	3910	97749	6.53E+00	3.38E+06	0.028890
	1.22E+08	1.46E+08	6	1.20E+07	4265	106635	6.60E+00	3.98E+06	0.026769
	9.76E+07	1.22E+08	4.5	1.22E+07	3199	79976	6.57E+00	3.73E+06	0.021449
	7.32E+07	9.76E+07	10.5	1.22E+07	7464	186611	6.57E+00	3.73E+06	0.050047
18	4.88E+07	7.32E+07	12.5	1.22E+07	8886	222156	6.57E+00	3.73E+06	0.059580
	3.66E+07	4.88E+07	8.5	6.10E+06	6043	151066	7.78E+00	5.97E+07	0.002532
	2.44E+07	3.66E+07	3.5	6.10E+06	2488	62204	7.78E+00	5.97E+07	0.001043
	1.22E+07	2.44E+07	5	6.10E+06	3555	88863	7.78E+00	5.97E+07	0.001489
	6.10E+06	1.22E+07	3	3.05E+06	2133	53318	8.98E+00	9.55E+08	0.000056
	0	6.10E+06	67	3.05E+06	47630	1190759	8.98E+00	9.55E+08	0.001247
				0.00E+00					0.222497
	4.55E+08	5.06E+08	2	2.55E+07	1555	38877	5.29E+00	1.95E+05	0.199002
	4.05E+08	4.55E+08	1.5	2.50E+07	1166	29158	5.33E+00	2.11E+05	0.137885
	3.54E+08	4.05E+08	5.5	2.55E+07	4277	106913	5.29E+00	1.95E+05	0.547256
	3.04E+08	3.54E+08	6	2.50E+07	4665	116632	5.33E+00	2.11E+05	0.551542
	2.53E+08	3.04E+08	7	2.55E+07	5443	136071	5.29E+00	1.95E+05	0.696507
	2.02E+08	2.53E+08	11	2.55E+07	8553	213826	5.29E+00	1.95E+05	1.094512
	1.52E+08	2.02E+08	15.5	2.50E+07	12052	301300	5.33E+00	2.11E+05	1.424816
19	1.01E+08	1.52E+08	10.5	2.55E+07	8164	204106	5.29E+00	1.95E+05	1.044761
	7.59E+07	1.01E+08	8	1.26E+07	6220	155510	6.52E+00	3.33E+06	0.046702
	5.06E+07	7.59E+07	4.5	1.27E+07	3499	87474	6.51E+00	3.23E+06	0.027117
	2.53E+07	5.06E+07	3	1.27E+07	2333	58316	6.51E+00	3.23E+06	0.018078
	1.27E+07	2.53E+07	2	6.30E+06	1555	38877	7.72E+00	5.24E+07	0.000741
	0	1.27E+07	21	6.35E+06	16328	408212	7.71E+00	5.08E+07	0.008035
				0.00E+00					5.796953
	4.30E+08	4.78E+08	0.5	2.40E+07	389	9719	5.40E+00	2.49E+05	0.039037
	3.82E+08	4.30E+08	0	2.40E+07	0	0	5.40E+00	2.49E+05	0.000000
	3.35E+08	3.82E+08	1	2.35E+07	778	19439	5.43E+00	2.71E+05	0.071769
	2.87E+08	3.35E+08	3	2.40E+07	2333	58316	5.40E+00	2.49E+05	0.234225
	2.39E+08	2.87E+08	7	2.40E+07	5443	136071	5.40E+00	2.49E+05	0.546525
	1.91E+08	2.39E+08	6	2.40E+07	4665	116632	5.40E+00	2.49E+05	0.468450
19 5%	1.43E+08	1.91E+08	11.5	2.40E+07	8942	223545	5.40E+00	2.49E+05	0.897862
damping	9.56E+07	1.43E+08	16.5	2.37E+07	12830	320738	5.42E+00	2.62E+05	1.225023
	7.17E+07	9.56E+07	10	1.20E+07	7775	194387	6.61E+00	4.05E+06	0.047989
	4.78E+07	7.17E+07	7.5	1.20E+07	5832	145790	6.61E+00	4.05E+06	0.035991
	2.39E+07	4.78E+07	9.5	1.20E+07	7387	184668	6.61E+00	4.05E+06	0.045589
	1.20E+07	2.39E+07	2	5.95E+06	1555	38877	7.82E+00	6.59E+07	0.000590
	0	1.20E+07	44	6.00E+06	34212	855302	7.80E+00	6.37E+07	0.013419
				0.00E+00					3.626470
	6.96E+08	7.73E+08	1	3.85E+07	689	17217	4.58E+00	3.76E+04	0.457935
	6.18E+08	6.96E+08	1.5	3.90E+07	1033	25826	4.55E+00	3.57E+04	0.723286
	5.41E+08	6.18E+08	1.5	3.85E+07	1033	25826	4.58E+00	3.76E+04	0.686902
	4.64E+08	5.41E+08	7	3.85E+07	4821	120520	4.58E+00	3.76E+04	3.205543
	3.87E+08	4.64E+08	7.5	3.85E+07	5165	129128	4.58E+00	3.76E+04	3.434510
	3.09E+08	3.87E+08	11.5	3.90E+07	7920	197997	4.55E+00	3.57E+04	5.545196
	2.32E+08	3.09E+08	14.5	3.85E+07	9986	249648	4.58E+00	3.76E+04	6.640053
20	1.55E+08	2.32E+08	18	3.85E+07	12396	309908	4.58E+00	3.76E+04	8.242824
	1.16E+08	1.55E+08	7.5	1.95E+07	5165	129128	5.76E+00	5.71E+05	0.226027
	7.73E+07	1.16E+08	4	1.94E+07	2755	68868	5.77E+00	5.89E+05	0.116881
	3.87E+07	7.73E+07	4.5	1.93E+07	3099	77477	5.77E+00	5.95E+05	0.130137
	1.93E+07	3.87E+07	1	9.70E+06	689	17217	6.97E+00	9.33E+06	0.001845
	0	1.93E+07	11.5	9.65E+06	7920	197997	6.98E+00	9.53E+06	0.020786
				0.00E+00					29.431925
	8.72E+08	9.69E+08	1.5	4.85E+07	1833	45820	4.17E+00	1.49E+04	3.069162
	7.75E+08	8.72E+08	3	4.85E+07	3666	91640	4.17E+00	1.49E+04	6.138324
	6.78E+08	7.75E+08	4.5	4.85E+07	5498	137459	4.17E+00	1.49E+04	9.207486
	5.81E+08	6.78E+08	4.5	4.85E+07	5498	137459	4.17E+00	1.49E+04	9.207486
	4.85E+08	5.81E+08	13	4.80E+07	15884	397105	4.19E+00	1.56E+04	25.519367
	3.88E+08	4.85E+08	11	4.85E+07	13440	336012	4.17E+00	1.49E+04	22.507188
21	2.91E+08	3.88E+08	14.5	4.85E+07	17717	442924	4.17E+00	1.49E+04	29.668566
	1.94E+08	2.91E+08	14.5	4.85E+07	17717	442924	4.17E+00	1.49E+04	29.668566
	1.45E+08	1.94E+08	8	2.45E+07	9775	244372	5.36E+00	2.29E+05	1.065899
	9.69E+07	1.45E+08	3.5	2.41E+07	4277	106913	5.39E+00	2.47E+05	0.433002
	4.85E+07	9.69E+07	1.5	2.42E+07	1833	45820	5.38E+00	2.41E+05	0.190245
	2.42E+07	4.85E+07	0	1.22E+07	0	0	6.58E+00	3.79E+06	0.000000
	0	2.42E+07	8	1.21E+07	9775	244372	6.59E+00	3.85E+06	0.063415
				0.00E+00					136.738707

Figure C.19: Perforated monopile, Rainflow analysis result and fatigue damage calculation(SZ), SS18-SS21

SS	min amp	max amp	cycle	avg amp	total cycles	design life	log S		Eq. Fatigue da
	5.03E+08	5.59E+08	2	2.80E+07	3599	89973	5.13E+00	1.34E+05	0.669493
	4.47E+08	5.03E+08	1.5	2.80E+07	2699	67480	5.13E+00	1.34E+05	0.502120
	3.91E+08	4.47E+08	1	2.80E+07	1799	44987	5.13E+00	1.34E+05	0.334747
	3.35E+08	3.91E+08	8.5	2.80E+07	15295	382387	5.13E+00	1.34E+05	2.845345
	2.80E+08	3.35E+08	8.5	2.75E+07	15295	382387	5.16E+00	1.44E+05	2.647486
	2.24E+08	2.80E+08	11.5	2.80E+07	20694	517347	5.13E+00	1.34E+05	3.849585
22	1.68E+08	2.24E+08	11.5	2.80E+07	20694	517347	5.13E+00	1.34E+05	3.849585
	1.12E+08	1.68E+08	19.5	2.80E+07	35090	877240	5.13E+00	1.34E+05	6.527557
	8.39E+07	1.12E+08	9	1.41E+07	16195	404880	6.33E+00	2.12E+06	0.190999
	5.59E+07	8.39E+07	3	1.40E+07	5398	134960	6.33E+00	2.15E+06	0.062765
	2.80E+07	5.59E+07	1.5	1.40E+07	2699	67480	6.34E+00	2.18E+06	0.030937
	1.40E+07	2.80E+07	0	7.00E+06	0	0	7.54E+00	3.44E+07	0.000000
	0	1.40E+07	17	7.00E+06	30591	764774	7.54E+00	3.44E+07	0.022229
				0.00E+00					21.532847
	4.35E+08	4.83E+08	0.5	2.40E+07	900	22493	5.40E+00	2.49E+05	0.090344
	3.86E+08	4.35E+08	0.5	2.45E+07	900	22493	5.36E+00	2.29E+05	0.098111
	3.38E+08	3.86E+08	1	2.40E+07	1799	44987	5.40E+00	2.49E+05	0.180688
	2.90E+08	3.38E+08	2.5	2.40E+07	4499	112467	5.40E+00	2.49E+05	0.451720
	2.42E+08	2.90E+08	2.5	2.40E+07	4499	112467	5.40E+00	2.49E+05	0.451720
	1.93E+08	2.42E+08	9.5	2.45E+07	17095	427373	5.36E+00	2.29E+05	1.864111
	1.45E+08	1.93E+08	8.5	2.40E+07	15295	382387	5.40E+00	2.49E+05	1.535847
29	9.66E+07	1.45E+08	12	2.42E+07	21594	539840	5.38E+00	2.41E+05	2.241438
	7.25E+07	9.66E+07	11.5	1.21E+07	20694	517347	6.59E+00	3.92E+06	0.132047
	4.83E+07	7.25E+07	11.5	1.21E+07	20694	517347	6.59E+00	3.85E+06	0.134253
	2.42E+07	4.83E+07	6	1.21E+07	10797	269920	6.59E+00	3.92E+06	0.068894
	1.21E+07	2.42E+07	5.5	6.05E+06	9897	247427	7.79E+00	6.17E+07	0.004013
	0	1.21E+07	34	6.05E+06	61182	1529547	7.79E+00	6.17E+07	0.024808
				0.00E+00					7.277993
	2.17E+08	2.41E+08	1	1.20E+07	1577	39420	6.60E+00	3.98E+06	0.009896
	1.93E+08	2.17E+08	0.5	1.20E+07	788	19710	6.60E+00	3.98E+06	0.004948
	1.69E+08	1.93E+08	1	1.20E+07	1577	39420	6.60E+00	3.98E+06	0.009896
	1.45E+08	1.69E+08	5	1.20E+07	7884	197100	6.60E+00	3.98E+06	0.049478
	1.21E+08	1.45E+08	7	1.20E+07	11038	275940	6.60E+00	3.98E+06	0.069269
	9.64E+07	1.21E+08	7	1.23E+07	11038	275940	6.56E+00	3.61E+06	0.076460
23	7.23E+07	9.64E+07	9	1.21E+07	14191	354780	6.59E+00	3.92E+06	0.090554
	4.82E+07	7.23E+07	16.5	1.21E+07	26017	650430	6.59E+00	3.92E+06	0.166016
	3.62E+07	4.82E+07	4.5	6.00E+06	7096	177390	7.80E+00	6.37E+07	0.002783
	2.41E+07	3.62E+07	8	6.05E+06	12614	315360	7.79E+00	6.17E+07	0.005115
	1.21E+07	2.41E+07	3	6.00E+06	4730	118260	7.80E+00	6.37E+07	0.001855
	6.03E+06	1.21E+07	4	3.04E+06	6307	157680	8.99E+00	9.74E+08	0.000162
	0	6.03E+06	64.5	3.02E+06	101704	2542590	9.00E+00	1.00E+09	0.002543
				0.00E+00					0.488974
	1.89E+08	2.10E+08	0.5	1.05E+07	788	19710	6.83E+00	6.80E+06	0.002900
	1.68E+08	1.89E+08	0.5	1.05E+07	788	19710	6.83E+00	6.80E+06	0.002900
	1.47E+08	1.68E+08	0.5	1.05E+07	788	19710	6.83E+00	6.80E+06	0.002900
	1.26E+08	1.47E+08	3	1.05E+07	4730	118260	6.83E+00	6.80E+06	0.017402
	1.05E+08	1.26E+08	2	1.05E+07	3154	78840	6.83E+00	6.80E+06	0.011601
	8.40E+07	1.05E+08	3.5	1.05E+07	5519	137970	6.83E+00	6.80E+06	0.020302
23 (5%	6.30E+07	8.40E+07	3.5	1.05E+07	5519	137970	6.83E+00	6.80E+06	0.020302
damping)	4.20E+07	6.30E+07	10.5	1.05E+07	16556	413910	6.83E+00	6.80E+06	0.060906
	3.15E+07	4.20E+07	13	5.25E+06	20498	512460	8.04E+00	1.09E+08	0.004713
	2.10E+07	3.15E+07	4	5.25E+06	6307	157680	8.04E+00	1.09E+08	0.001450
	1.05E+07	2.10E+07	9.5	5.25E+06	14980	374490	8.04E+00	1.09E+08	0.003444
	5.25E+06	1.05E+07	8	2.63E+06	12614	315360	9.24E+00	1.74E+09	0.000181
	0	5.25E+06	106	2.63E+06	167141	4178520	9.24E+00	1.74E+09	0.002402
				0.00E+00					0.151405
	2.29E+08	2.54E+08	1	1.25E+07	631	15768	6.53E+00	3.38E+06	0.004660
	2.03E+08	2.29E+08	1.5	1.30E+07	946	23652	6.46E+00	2.89E+06	0.008178
	1.78E+08	2.03E+08	3	1.25E+07	1892	47304	6.53E+00	3.38E+06	0.013981
	1.52E+08	1.78E+08	3	1.30E+07	1892	47304	6.46E+00	2.89E+06	0.016356
	1.27E+08	1.52E+08	7.5	1.25E+07	4730	118260	6.53E+00	3.38E+06	0.034952
	1.02E+08	1.27E+08	9	1.25E+07	5676	141912	6.53E+00	3.38E+06	0.041943
24	7.62E+07	1.02E+08	10.5	1.29E+07	6623	165564	6.47E+00	2.98E+06	0.055504
	5.08E+07	7.62E+07	15	1.27E+07	9461	236520	6.50E+00	3.18E+06	0.074487
	3.81E+07	5.08E+07	4.5	6.35E+06	2838	70956	7.71E+00	5.08E+07	0.001397
	2.54E+07	3.81E+07	3	6.35E+06	1892	47304	7.71E+00	5.08E+07	0.000931
	1.27E+07	2.54E+07	4.5	6.35E+06	2838	70956	7.71E+00	5.08E+07	0.001397
	6.35E+06	1.27E+07	3	3.18E+06	1892	47304	8.91E+00	8.13E+08	0.000058
	0	6.35E+06	65.5	3.18E+06	41312	1032804	8.91E+00	8.13E+08	0.001271
				0.00E+00					0.255115

Figure C.20: Perforated monopile, Rainflow analysis result and fatigue damage calculation(SZ), SS22-SS24

SS	min amp	max amp	cycle	avg amp	total cycles	design life	log S		Eq. Fatigue da
	4.92E+08	5.47E+08	1	2.75E+07	883	22075	5.16E+00	1.44E+05	0.152839
	4.38E+08	4.92E+08	1	2.70E+07	883	22075	5.19E+00	1.55E+05	0.142023
	3.83E+08	4.38E+08	3.5	2.75E+07	3091	77263	5.16E+00	1.44E+05	0.534938
	3.28E+08	3.83E+08	5.5	2.75E+07	4857	121414	5.16E+00	1.44E+05	0.840617
	2.74E+08	3.28E+08	10.5	2.70E+07	9272	231790	5.19E+00	1.55E+05	1.491245
	2.19E+08	2.74E+08	9	2.75E+07	7947	198677	5.16E+00	1.44E+05	1.375555
25	1.64E+08	2.19E+08	16.5	2.75E+07	14570	364241	5.16E+00	1.44E+05	2.521851
	1.09E+08	1.64E+08	15.5	2.75E+07	13687	342166	5.16E+00	1.44E+05	2.369011
	8.21E+07	1.09E+08	7.5	1.35E+07	6623	165564	6.40E+00	2.52E+06	0.065593
	5.47E+07	8.21E+07	5	1.37E+07	4415	110376	6.37E+00	2.34E+06	0.047071
	2.74E+07	5.47E+07	1.5	1.37E+07	1325	33113	6.38E+00	2.38E+06	0.013916
	1.37E+07	2.74E+07	1	6.85E+06	883	22075	7.57E+00	3.75E+07	0.000588
	0	1.37E+07	23.5	6.85E+06	20751	518767	7.57E+00	3.75E+07	0.013827
				0.00E+00					9.569076
	4.37E+08	4.85E+08	0.5	2.40E+07	442	11038	5.40E+00	2.49E+05	0.044332
	3.88E+08	4.37E+08	1	2.45E+07	883	22075	5.36E+00	2.29E+05	0.096287
	3.40E+08	3.88E+08	1	2.40E+07	883	22075	5.40E+00	2.49E+05	0.088664
	2.91E+08	3.40E+08	5.5	2.45E+07	4857	121414	5.36E+00	2.29E+05	0.529580
	2.43E+08	2.91E+08	3.5	2.40E+07	3091	77263	5.40E+00	2.49E+05	0.310326
	1.94E+08	2.43E+08	9.5	2.45E+07	8389	209714	5.36E+00	2.29E+05	0.914729
25 5% damping	1.46E+08	1.94E+08	16	2.40E+07	14128	353203	5.40E+00	2.49E+05	1.418631
	9.70E+07	1.46E+08	10.5	2.45E+07	9272	231790	5.36E+00	2.29E+05	1.011017
	7.28E+07	9.70E+07	10.5	1.21E+07	9272	231790	6.59E+00	3.85E+06	0.060150
	4.85E+07	7.28E+07	8	1.22E+07	7064	176602	6.58E+00	3.79E+06	0.046591
	2.43E+07	4.85E+07	5	1.21E+07	4415	110376	6.59E+00	3.85E+06	0.028643
	1.21E+07	2.43E+07	5	6.10E+06	4415	110376	7.78E+00	5.97E+07	0.001850
	0	1.21E+07	28.5	6.05E+06	25166	629143	7.79E+00	6.17E+07	0.010204
				0.00E+00					4.561005
	6.23E+08	6.92E+08	0.5	3.45E+07	536	13403	4.77E+00	5.83E+04	0.229865
	5.54E+08	6.23E+08	2	3.45E+07	2144	53611	4.77E+00	5.83E+04	0.919458
	4.84E+08	5.54E+08	4	3.50E+07	4289	107222	4.74E+00	5.50E+04	1.947860
	4.15E+08	4.84E+08	6	3.45E+07	6433	160834	4.77E+00	5.83E+04	2.758374
	3.46E+08	4.15E+08	7	3.45E+07	7506	187639	4.77E+00	5.83E+04	3.218103
	2.77E+08	3.46E+08	12	3.45E+07	12867	321667	4.77E+00	5.83E+04	5.516748
26	2.08E+08	2.77E+08	16.5	3.45E+07	17692	442292	4.77E+00	5.83E+04	7.585529
	1.38E+08	2.08E+08	16.5	3.50E+07	17692	442292	4.74E+00	5.50E+04	8.034922
	1.04E+08	1.38E+08	6.5	1.70E+07	6969	174236	6.00E+00	9.89E+05	0.176171
	6.92E+07	1.04E+08	5	1.74E+07	5361	134028	5.95E+00	9.01E+05	0.148728
	3.46E+07	6.92E+07	2	1.73E+07	2144	53611	5.96E+00	9.22E+05	0.058135
	1.73E+07	3.46E+07	2	8.65E+06	2144	53611	7.17E+00	1.48E+07	0.003633
	0	1.73E+07	13.5	8.65E+06	14475	361876	7.17E+00	1.48E+07	0.024526
				0.00E+00					30.622052
	8.52E+08	9.47E+08	1.5	4.75E+07	1987	49669	4.21E+00	1.62E+04	3.060988
	7.58E+08	8.52E+08	5	4.70E+07	6623	165564	4.23E+00	1.69E+04	9.780416
	6.63E+08	7.58E+08	1.5	4.75E+07	1987	49669	4.21E+00	1.62E+04	3.060988
	5.68E+08	6.63E+08	8	4.75E+07	10596	264902	4.21E+00	1.62E+04	16.325268
	4.74E+08	5.68E+08	12.5	4.70E+07	16556	413910	4.23E+00	1.69E+04	24.451041
	3.79E+08	4.74E+08	11	4.75E+07	14570	364241	4.21E+00	1.62E+04	22.447244
27	2.84E+08	3.79E+08	15	4.75E+07	19868	496692	4.21E+00	1.62E+04	30.609878
	1.89E+08	2.84E+08	14.5	4.75E+07	19205	480136	4.21E+00	1.62E+04	29.589549
	1.42E+08	1.89E+08	3.5	2.35E+07	4636	115895	5.43E+00	2.71E+05	0.427893
	9.47E+07	1.42E+08	2	2.37E+07	2649	66226	5.42E+00	2.64E+05	0.250813
	4.74E+07	9.47E+07	2.5	2.37E+07	3311	82782	5.42E+00	2.64E+05	0.313517
	2.37E+07	4.74E+07	2.5	1.19E+07	3311	82782	6.62E+00	4.19E+06	0.019761
	0	2.37E+07	11	1.19E+07	14570	364241	6.62E+00	4.19E+06	0.086948
				0					140.424305
	1.68E+09	1.87E+09	0.5	9.50E+07	1072	26806	3.01E+00	1.01E+03	26.431387
	1.49E+09	1.68E+09	0	9.50E+07	0	0	3.01E+00	1.01E+03	0.000000
	1.31E+09	1.49E+09	3.5	9.00E+07	7506	187639	3.10E+00	1.26E+03	149.036832
	1.12E+09	1.31E+09	5	9.50E+07	10722	268056	3.01E+00	1.01E+03	264.313870
	9.33E+08	1.12E+09	8	9.35E+07	17156	428890	3.03E+00	1.08E+03	396.818544
	7.47E+08	9.33E+08	9.5	9.30E+07	20372	509306	3.04E+00	1.10E+03	461.222970
28	5.60E+08	7.47E+08	14	9.35E+07	30022	750557	3.03E+00	1.08E+03	694.432451
	3.73E+08	5.60E+08	14	9.35E+07	30022	750557	3.03E+00	1.08E+03	694.432451
	2.80E+08	3.73E+08	8	4.65E+07	17156	428890	4.25E+00	1.77E+04	24.274893
	1.87E+08	2.80E+08	3.5	4.65E+07	7506	187639	4.25E+00	1.77E+04	10.620266
	9.33E+07	1.87E+08	6	4.69E+07	12867	321667	4.23E+00	1.71E+04	18.760532
	4.67E+07	9.33E+07	5	2.33E+07	10722	268056	5.45E+00	2.80E+05	0.956421
	0	4.67E+07	39	2.34E+07	83633	2090837	5.44E+00	2.78E+05	7.524327
				0					2748.824945

Figure C.21: Perforated monopile, Rainflow analysis result and fatigue damage calculation(SZ), SS25-SS28

SS	min amp	max amp	cycle	avg amp	total cycles	design life	log S		Eq. Fatigue da
	4.59E+08	5.10E+08	0.5	2.55E+07	536	13403	5.29E+00	1.95E+05	0.068605
	4.08E+08	4.59E+08	1	2.55E+07	1072	26806	5.29E+00	1.95E+05	0.137210
	3.57E+08	4.08E+08	5	2.55E+07	5361	134028	5.29E+00	1.95E+05	0.686051
	3.06E+08	3.57E+08	5	2.55E+07	5361	134028	5.29E+00	1.95E+05	0.686051
	2.55E+08	3.06E+08	3	2.55E+07	3217	80417	5.29E+00	1.95E+05	0.411630
	2.04E+08	2.55E+08	6.5	2.55E+07	6969	174236	5.29E+00	1.95E+05	0.891866
29 5%	1.53E+08	2.04E+08	4	2.55E+07	4289	107222	5.29E+00	1.95E+05	0.548841
damping	1.02E+08	1.53E+08	8.5	2.55E+07	9114	227848	5.29E+00	1.95E+05	1.166286
	7.65E+07	1.02E+08	5	1.28E+07	5361	134028	6.49E+00	3.13E+06	0.042878
	5.10E+07	7.65E+07	8.5	1.28E+07	9114	227848	6.49E+00	3.13E+06	0.072893
	2.55E+07	5.10E+07	19	1.28E+07	20372	509306	6.49E+00	3.13E+06	0.162937
	1.28E+07	2.55E+07	36.5	6.35E+06	39136	978404	7.71E+00	5.08E+07	0.019258
	0	1.28E+07	193.5	6.40E+06	207475	5186884	7.69E+00	4.92E+07	0.105348
				0					4.999854
	4.62E+08	5.13E+08	0.5	2.55E+07	536	13403	5.29E+00	1.95E+05	0.068605
	4.10E+08	4.62E+08	0.5	2.60E+07	536	13403	5.26E+00	1.81E+05	0.074146
	3.59E+08	4.10E+08	0	2.55E+07	0	0	5.29E+00	1.95E+05	0.000000
	3.08E+08	3.59E+08	3	2.55E+07	3217	80417	5.29E+00	1.95E+05	0.411630
	2.57E+08	3.08E+08	4.5	2.55E+07	4825	120625	5.29E+00	1.95E+05	0.617446
	2.05E+08	2.57E+08	4.5	2.60E+07	4825	120625	5.26E+00	1.81E+05	0.667316
29	1.54E+08	2.05E+08	3.5	2.55E+07	3753	93820	5.29E+00	1.95E+05	0.480236
	1.03E+08	1.54E+08	8.5	2.55E+07	9114	227848	5.29E+00	1.95E+05	1.166286
	7.70E+07	1.03E+08	6.5	1.30E+07	6969	174236	6.46E+00	2.89E+06	0.060244
	5.13E+07	7.70E+07	6.5	1.29E+07	6969	174236	6.48E+00	3.03E+06	0.057511
	2.57E+07	5.13E+07	26.5	1.28E+07	28414	710348	6.49E+00	3.08E+06	0.230840
	1.28E+07	2.57E+07	37	6.45E+06	39672	991807	7.68E+00	4.77E+07	0.020781
	0	1.28E+07	297	6.40E+06	318451	7961263	7.69E+00	4.92E+07	0.161697
				0					4.016738
	8.75E+08	9.72E+08	2	4.85E+07	2452	61295	4.17E+00	1.49E+04	4.105767
	7.78E+08	8.75E+08	2.5	4.85E+07	3065	76619	4.17E+00	1.49E+04	5.132209
	6.81E+08	7.78E+08	3	4.85E+07	3678	91943	4.17E+00	1.49E+04	6.158650
	5.83E+08	6.81E+08	7.5	4.90E+07	9194	229857	4.16E+00	1.43E+04	16.041425
	4.86E+08	5.83E+08	10	4.85E+07	12259	306477	4.17E+00	1.49E+04	20.528835
	3.89E+08	4.86E+08	7.5	4.85E+07	9194	229857	4.17E+00	1.49E+04	15.396626
	2.92E+08	3.89E+08	20.5	4.85E+07	25131	628277	4.17E+00	1.49E+04	42.084112
30	1.94E+08	2.92E+08	12.5	4.90E+07	15324	383096	4.16E+00	1.43E+04	26.735708
	1.46E+08	1.94E+08	5.5	2.40E+07	6742	168562	5.40E+00	2.49E+05	0.677025
	9.72E+07	1.46E+08	3	2.44E+07	3678	91943	5.37E+00	2.33E+05	0.394528
	4.86E+07	9.72E+07	2	2.43E+07	2452	61295	5.37E+00	2.37E+05	0.258733
	2.43E+07	4.86E+07	3	1.22E+07	3678	91943	6.58E+00	3.79E+06	0.024256
	0	2.43E+07	16.5	1.22E+07	20227	505686	6.58E+00	3.79E+06	0.133409
				0					137.671284
	1.69E+09	1.88E+09	2.5	9.50E+07	2605	65126	3.01E+00	1.01E+03	64.217102
	1.50E+09	1.69E+09	0	9.50E+07	0	0	3.01E+00	1.01E+03	0.000000
	1.32E+09	1.50E+09	4	9.00E+07	4168	104202	3.10E+00	1.26E+03	82.764921
	1.13E+09	1.32E+09	3	9.50E+07	3126	78152	3.01E+00	1.01E+03	77.060523
	9.40E+08	1.13E+09	5.5	9.50E+07	5731	143278	3.01E+00	1.01E+03	141.277625
	7.52E+08	9.40E+08	13	9.40E+07	13546	338657	3.02E+00	1.06E+03	320.089215
	5.64E+08	7.52E+08	13.5	9.40E+07	14067	351682	3.02E+00	1.06E+03	332.400339
31	3.76E+08	5.64E+08	10.5	9.40E+07	10941	273530	3.02E+00	1.06E+03	258.533597
	2.82E+08	3.76E+08	7.5	4.70E+07	7815	195379	4.23E+00	1.69E+04	11.541678
	1.88E+08	2.82E+08	4.5	4.70E+07	4689	117227	4.23E+00	1.69E+04	6.925007
	9.40E+07	1.88E+08	11.5	4.70E+07	11983	299581	4.23E+00	1.69E+04	17.697240
	4.70E+07	9.40E+07	2	2.35E+07	2084	52101	5.43E+00	2.71E+05	0.192361
	0	4.70E+07	36	2.35E+07	37513	937818	5.43E+00	2.71E+05	3.462504
				0					1316.162112
	4.28E+08	4.75E+08	0.5	2.35E+07	797	19921	5.43E+00	2.71E+05	0.073550
	3.80E+08	4.28E+08	3	2.40E+07	4781	119526	5.40E+00	2.49E+05	0.480073
	3.33E+08	3.80E+08	3	2.35E+07	4781	119526	5.43E+00	2.71E+05	0.441299
	2.85E+08	3.33E+08	2	2.40E+07	3187	79684	5.40E+00	2.49E+05	0.320048
	2.38E+08	2.85E+08	1.5	2.35E+07	2391	59763	5.43E+00	2.71E+05	0.220650
	1.90E+08	2.38E+08	4	2.40E+07	6375	159368	5.40E+00	2.49E+05	0.640097
	1.43E+08	1.90E+08	12.5	2.35E+07	19921	498025	5.43E+00	2.71E+05	1.838748
32	9.50E+07	1.43E+08	14.5	2.40E+07	23108	577708	5.40E+00	2.49E+05	2.320351
	7.13E+07	9.50E+07	7	1.19E+07	11156	278894	6.62E+00	4.19E+06	0.066575
	4.75E+07	7.13E+07	10	1.19E+07	15937	398420	6.61E+00	4.12E+06	0.096723
	2.38E+07	4.75E+07	10	1.19E+07	15937	398420	6.62E+00	4.19E+06	0.095107
	1.19E+07	2.38E+07	15	5.95E+06	23905	597629	7.82E+00	6.59E+07	0.009068
	0	1.19E+07	128	5.95E+06	203991	5099771	7.82E+00	6.59E+07	0.077378
				0					6.679667
	4.35E+08	4.83E+08	0.5	2.40E+07	797	19921	5.40E+00	2.49E+05	0.080012
	3.86E+08	4.35E+08	0.5	2.45E+07	797	19921	5.36E+00	2.29E+05	0.086891
	3.38E+08	3.86E+08	0.5	2.40E+07	797	19921	5.40E+00	2.49E+05	0.080012
	2.90E+08	3.38E+08	2	2.40E+07	3187	79684	5.40E+00	2.49E+05	0.320048
	2.42E+08	2.90E+08	4	2.40E+07	6375	159368	5.40E+00	2.49E+05	0.640097
	1.93E+08	2.42E+08	3.5	2.45E+07	5578	139447	5.36E+00	2.29E+05	0.608237
32 5%	1.45E+08	1.93E+08	8.5	2.40E+07	13546	338657	5.40E+00	2.49E+05	1.360206
damping	9.66E+07	1.45E+08	6	2.42E+07	9562	239052	5.38E+00	2.41E+05	0.992552
	7.25E+07	9.66E+07	8.5	1.21E+07	13546	338657	6.59E+00	3.92E+06	0.086439
	4.83E+07	7.25E+07	8	1.21E+07	12749	318736	6.59E+00	3.85E+06	0.082713
	2.42E+07	4.83E+07	27	1.21E+07	43029	1075733	6.59E+00	3.92E+06	0.274570
	1.21E+07	2.42E+07	29	6.05E+06	46217	1155417	7.79E+00	6.17E+07	0.018740
	0	1.21E+07	299	6.05E+06	476510	11912746	7.79E+00	6.17E+07	0.193212
				0					4.823728

Figure C.22: Perforated monopile, Rainflow analysis result and fatigue damage calculation(SZ), SS29-SS32

SS	min amp	max amp	cycle	avg amp	total cycles	design life	log S		Eq. Fatigue da
33	3.20E+08	3.55E+08	1	1.75E+07	1072	26806	5.94E+00	8.81E+05	0.030435
	2.84E+08	3.20E+08	1	1.80E+07	1072	26806	5.90E+00	7.87E+05	0.034066
	2.49E+08	2.84E+08	1	1.75E+07	1072	26806	5.94E+00	8.81E+05	0.030435
	2.13E+08	2.49E+08	6.5	1.80E+07	6969	174236	5.90E+00	7.87E+05	0.221426
	1.78E+08	2.13E+08	6.5	1.75E+07	6969	174236	5.94E+00	8.81E+05	0.197830
	1.42E+08	1.78E+08	10.5	1.80E+07	11258	281459	5.90E+00	7.87E+05	0.357688
	1.07E+08	1.42E+08	11.5	1.75E+07	12331	308264	5.94E+00	8.81E+05	0.350006
	7.10E+07	1.07E+08	17	1.80E+07	18228	455695	5.90E+00	7.87E+05	0.579115
	5.33E+07	7.10E+07	2.5	8.85E+06	2681	67014	7.13E+00	1.35E+07	0.004977
	3.55E+07	5.33E+07	7.5	8.90E+06	8042	201042	7.12E+00	1.32E+07	0.015270
	1.78E+07	3.55E+07	3.5	8.85E+06	3753	93820	7.13E+00	1.35E+07	0.006967
	8.88E+06	1.78E+07	3	4.46E+06	3217	80417	8.32E+00	2.09E+08	0.000385
	0	8.88E+06	42	4.44E+06	45033	1125835	8.33E+00	2.13E+08	0.005297
				0					1.833897
34	1.40E+08	1.55E+08	2	7.50E+06	1225	30625	7.42E+00	2.61E+07	0.001173
	1.24E+08	1.40E+08	1	8.00E+06	612	15312	7.30E+00	2.02E+07	0.000759
	1.09E+08	1.24E+08	1	7.50E+06	612	15312	7.42E+00	2.61E+07	0.000587
	9.33E+07	1.09E+08	4	7.85E+06	2450	61250	7.34E+00	2.18E+07	0.002816
	7.77E+07	9.33E+07	9	7.80E+06	5512	137812	7.35E+00	2.23E+07	0.006175
	6.22E+07	7.77E+07	12.5	7.75E+06	7656	191406	7.36E+00	2.29E+07	0.008359
	4.66E+07	6.22E+07	12	7.80E+06	7350	183750	7.35E+00	2.23E+07	0.008234
	3.11E+07	4.66E+07	21.5	7.75E+06	13169	329218	7.36E+00	2.29E+07	0.014378
	2.33E+07	3.11E+07	9	3.90E+06	5512	137812	8.55E+00	3.57E+08	0.000386
	1.55E+07	2.33E+07	8	3.90E+06	4900	122500	8.55E+00	3.57E+08	0.000343
	7.77E+06	1.55E+07	13	3.87E+06	7962	199062	8.57E+00	3.70E+08	0.000538
	3.89E+06	7.77E+06	4	1.94E+06	2450	61250	9.77E+00	5.83E+09	0.000011
	0	3.89E+06	13.5	1.95E+06	8269	206718	9.76E+00	5.77E+09	0.000036
				0					0.043794
35	1.18E+08	1.32E+08	4.5	7.00E+06	2636	65910	7.54E+00	3.44E+07	0.001916
	1.05E+08	1.18E+08	2	6.50E+06	1172	29293	7.67E+00	4.63E+07	0.000633
	9.21E+07	1.05E+08	5	6.45E+06	2929	73234	7.68E+00	4.77E+07	0.001534
	7.90E+07	9.21E+07	7.5	6.55E+06	4394	109850	7.65E+00	4.49E+07	0.002448
	6.58E+07	7.90E+07	18.5	6.60E+06	10839	270964	7.64E+00	4.35E+07	0.006224
	5.26E+07	6.58E+07	9.5	6.60E+06	5566	139144	7.64E+00	4.35E+07	0.003196
	3.95E+07	5.26E+07	13	6.55E+06	7616	190407	7.65E+00	4.49E+07	0.004243
	2.63E+07	3.95E+07	18	6.60E+06	10546	263641	7.64E+00	4.35E+07	0.006056
	1.97E+07	2.63E+07	6.5	3.30E+06	3808	95204	8.84E+00	6.97E+08	0.000137
	1.32E+07	1.97E+07	6	3.25E+06	3515	87880	8.87E+00	7.40E+08	0.000119
	6.58E+06	1.32E+07	7	3.31E+06	4101	102527	8.84E+00	6.88E+08	0.000149
	3.29E+06	6.58E+06	4	1.65E+06	2343	58587	1.01E+01	1.13E+10	0.000005
	0	3.29E+06	16	1.65E+06	9374	234348	1.01E+01	1.13E+10	0.000021
									0.026681

Figure C.23: Perforated monopile, Rainflow analysis result and fatigue damage calculation(SZ), SS33-SS35

Table C.1: Equivalent Fatigue Damage per sea state

SS	Reference Cone	Reference ML	Perforated ML	Perforated Perf
1	3.48E-08	4.24E-08	6.01E-12	5.11E-08
2	1.65E-02	8.10E-03	3.48E-04	5.08E-02
3	6.92E-04	2.78E-04	8.36E-05	2.78E-02
4	3.11E-06	2.35E-06	4.16E-08	2.09E-05
5	4.51E-01	2.33E-01	1.57E-01	8.48E+01
6	7.64E-07	5.15E-07	2.85E-09	1.07E-06
7	1.90E-01	1.08E-01	5.94E-02	4.92E+01
8	1.19E-01	4.32E-02	2.73E-02	1.59E+01
9	3.43E-06	1.54E-06	5.74E-07	4.63E+01
10	2.22E-06	1.66E-06	6.61E-08	3.14E-05
11	2.51E-07	1.69E-07	1.26E-04	3.09E-02
12	7.46E-03	3.93E-03	3.05E-03	3.99E-01
13	3.09E-03	3.08E-03	1.17E-03	3.94E-01
14	9.01E-02	5.07E-02	1.76E-02	8.11E+00
15	3.20E-01	1.33E-01	2.86E-02	6.67E+01
16	1.41E+00	6.56E-01	5.65E-01	7.99E+01
17	1.63E+01	6.75E+00	3.28E+00	1.09E+03
18	1.22E-03	1.48E-03	7.35E-04	2.22E-01
19	2.21E-03	1.25E-03	1.39E-02	5.80E+00
20	1.62E-01	7.40E-02	2.26E-01	2.94E+01
21	1.70E+00	9.83E-01	3.98E-01	1.37E+02
22	1.25E-02	5.74E-03	3.94E-02	2.15E+01
23	1.94E-04	1.13E-04	1.34E-03	4.89E-01
24	7.95E-04	1.04E-03	7.09E-04	2.55E-01
25	4.25E-03	1.24E-03	1.48E-02	9.57E+00
26	2.31E-01	1.24E-01	6.17E-02	3.06E+01
27	1.75E+00	1.03E+00	3.26E-01	1.40E+02
28	3.50E+01	1.50E+01	5.38E+00	2.75E+03
29	1.84E-03	1.94E-03	1.65E-02	5.00E+00
30	1.69E+00	1.07E+00	4.02E-01	1.38E+02
31	1.01E+00	4.59E-01	3.73E+00	1.32E+03
32	1.88E-03	2.55E-03	1.44E-02	6.68E+00
33	1.38E-03	1.67E-03	5.93E-04	1.83E+00
34	3.56E-05	3.46E-05	1.05E-04	4.38E-02
35	2.32E-05	3.03E-05	5.31E-05	2.67E-02

D

Appendix D: 3D Scatter diagram

					DLC 1.1, 1.2, 7.2																								
				DLC 6.4																	DLC 6.4								
	Preliminary lumping of load cases			Parked	Power production																Extreme load case					total		
						Cut-in				Vr-2		Vr		Vr+2					Cut-out										
					0	1	2	3	4	5	6	7	8	9	10	11	12	14	16	18	20	22	24	26	30			
	Hs	Tz(avg)	Tp		0	1	3	4	6	7	9	10	12	13	15	16	18	20	23	26	29	32	35	38	44	Vw	Tz	
					1	3	4	6	7	9	10	12	13	15	16	18	20	23	26	29	32	35	38	44	50			
					1	2	3	4	5	6	7	8	9	10	11	12	14	16	18	20	22	24	26	30	34			
					0.3	1.4	2	2.5	2.9	2.6	2	1	0.4													15.1	15.2	
DLC 1.1, 1.2, 6.4, 7.2	0<Hs<1	3.5	3.0	0.06	0.29	0.42	0.53	0.61	0.55	0.42	0.21	0.08															3.2	
		4.5	5.5	0.16	0.74	1.05	1.32	1.53	1.37	1.05	0.53	0.21															8	
		5.5	8.8	0.06	0.26	0.37	0.46	0.53	0.48	0.37	0.18	0.07															2.8	15.2
		6.5	12.2	0.01	0.06	0.09	0.12	0.13	0.12	0.09	0.05	0.02															0.7	
		7.5	13.0	0	0.02	0.03	0.03	0.04	0.03	0.03	0.01	0.01															0.2	
		8.5	16.3	0	0.01	0.01	0.02	0.02	0.02	0.01	0.01	0															0.1	
					0.9	1.8	2.7	3.8	4.6	5.2	5	4.1	2.6	1.4	0.7											32.8	33.3	
	1<Hs<2	3.5	4.0		0.01	0.01	0.02	0.02	0.03	0.03	0.03	0.02	0.02	0.01	0												0.2	
		4.5	6.2		0.33	0.66	1	1.4	1.7	1.92	1.85	1.51	0.96	0.52	0.26												12.3	
		5.5	8.4		0.39	0.78	1.17	1.64	1.99	2.25	2.16	1.77	1.12	0.61	0.3												14.4	33.3
		6.5	10.6		0.13	0.26	0.39	0.55	0.66	0.75	0.72	0.59	0.37	0.2	0.1												4.8	
		7.5	12.8		0.03	0.06	0.1	0.14	0.17	0.19	0.18	0.15	0.09	0.05	0.03												1.2	
		8.5	15.0		0.01	0.02	0.02	0.03	0.04	0.05	0.05	0.04	0.02	0.01	0.01												0.3	
						0.6	0.8	1.2	1.7	2	2.7	3.2	3.5	3.1	2.5	2.4	0.6									24.3	24.7	
	2<Hs<3	4.5	5.0			0	0.01	0.01	0.01	0.02	0.02	0.03	0.03	0.03	0.02	0.02	0										0.2	
		5.5	7.5			0.31	0.42	0.63	0.89	1.04	1.41	1.67	1.83	1.62	1.31	1.25	0.31										12.9	
		6.5	10.0			0.21	0.28	0.42	0.6	0.7	0.95	1.13	1.23	1.09	0.88	0.85	0.21										8.7	24.7
		7.5	12.5			0.06	0.08	0.12	0.17	0.19	0.26	0.31	0.34	0.3	0.24	0.23	0.06										2.4	
		8.5	15.0			0.01	0.02	0.02	0.03	0.04	0.05	0.06	0.07	0.06	0.05	0.05	0.01										0.5	
							0.3	0.3	0.5	0.6	0.8	1	1.4	1.7	2.1	3.4	1.7									13.8	14.6	
	3<Hs<4	5.5	6.0				0.01	0.01	0.02	0.02	0.03	0.04	0.06	0.07	0.09	0.14	0.07										0.6	
		6.5	9.0				0.22	0.22	0.36	0.44	0.58	0.73	1.02	1.23	1.52	2.47	1.23										10.6	14.6
		7.5	12.0				0.06	0.06	0.1	0.12	0.15	0.19	0.27	0.33	0.4	0.65	0.33										2.8	
		8.5	15.0				0.01	0.01	0.02	0.02	0.03	0.04	0.06	0.07	0.09	0.14	0.07										0.6	
												0.3	0.3	0.6	0.8	1.7	1.7	0.9							6.3	7.1	
	4<Hs<5	6.5	8.0									0.08	0.08	0.16	0.21	0.45	0.45	0.24								1.9	
		7.5	11.5									0.19	0.19	0.39	0.52	1.1	1.1	0.58								4.6	7.1
		8.5	15.0									0.02	0.02	0.03	0.05	0.1	0.1	0.05								0.4	
															0.2	0.7	0.8	1.2	0.7						3.6	4.5	
	5<Hs<7	7.5	8.0												0.1	0.36	0.41	0.61	0.36							2.3	
		8.5	11.0												0.08	0.3	0.34	0.51	0.3							1.9	4.5
		9.5	14.0												0.01	0.05	0.05	0.08	0.05							0.3	
	7																									0.4	0.4
		8.5	9.5																							0.3	
	total				2.5	4.6	6.4	8.2	9.4	9.9	9.8	9.1	8.1	7.1	6.2	4.8	3.8	3	2.2	1.5	1.1	0.7	0.4	0.3		100	

Figure D.1: 3D scatter diagram with corresponding load cases following DNV-GL, 2016.

E

Appendix E: Analysis of stress response signals

Th

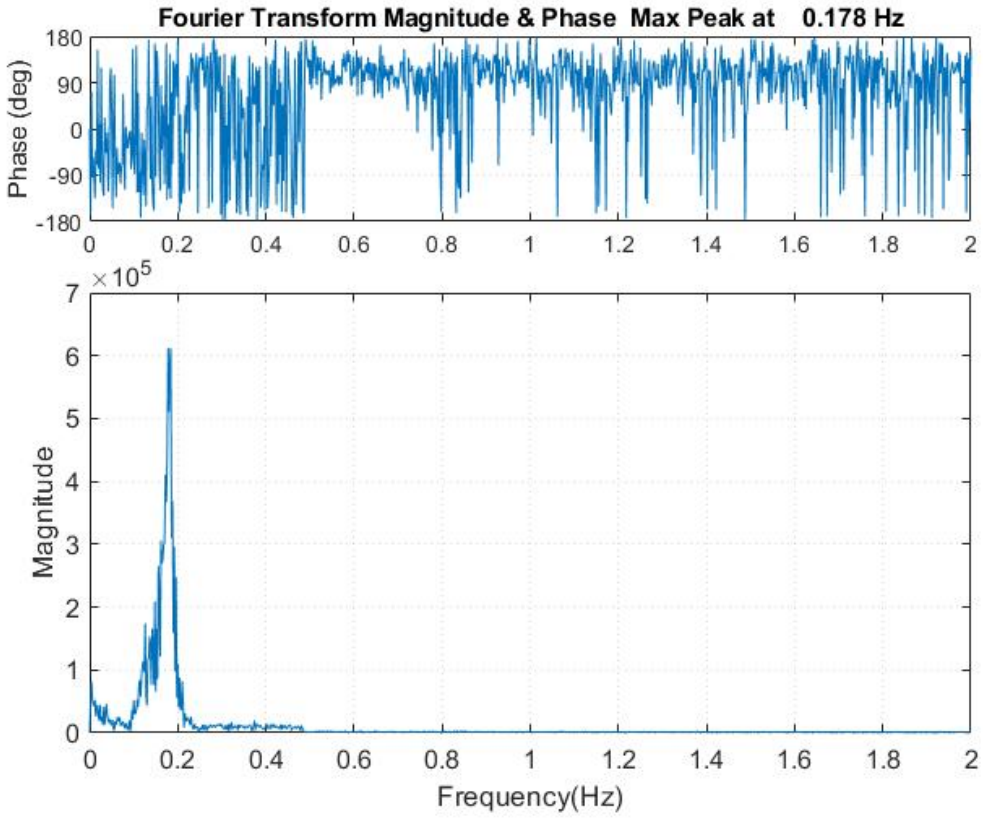

Figure E.1: Reference MP, SS6, Stress response FT and phase(ML).

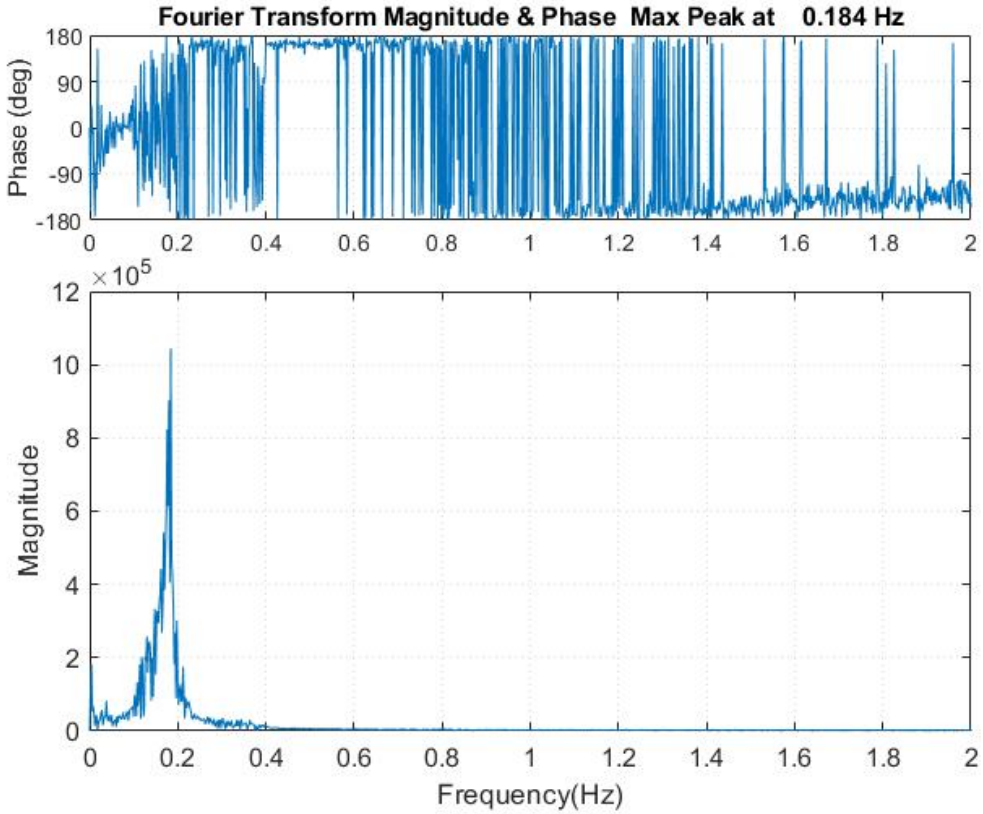

Figure E.2: Reference MP, SS10, Stress response FT and phase(ML).

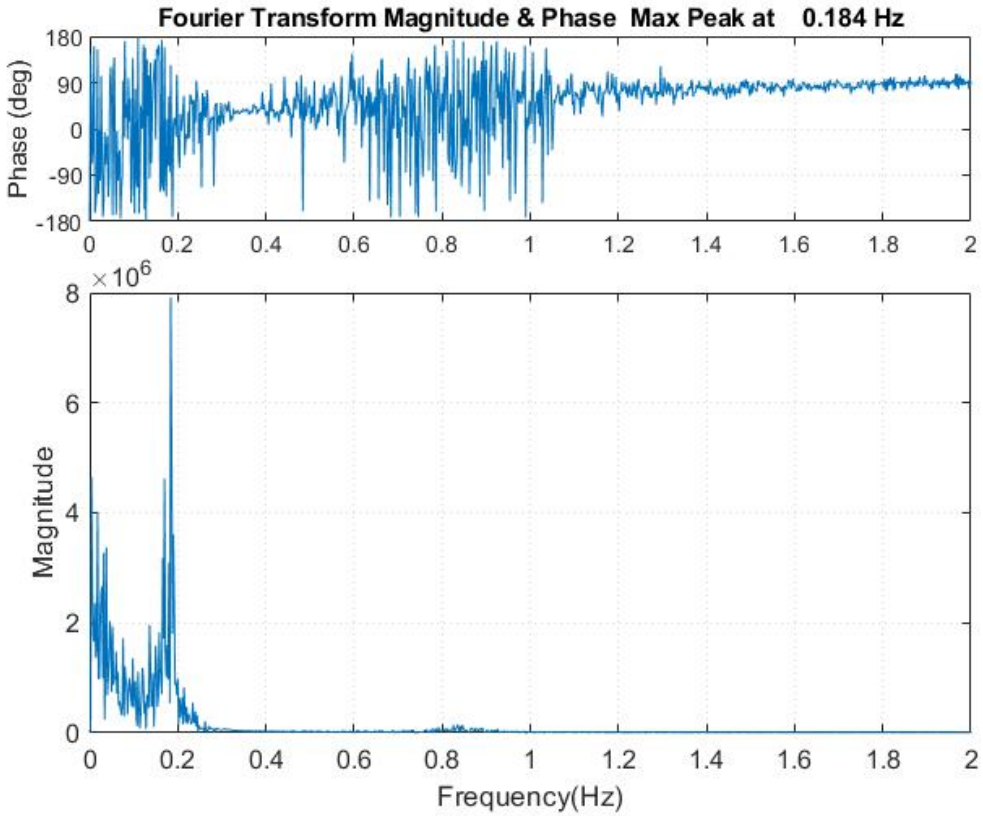

Figure E.3: Reference MP, SS19, Stress response FT and phase(ML).

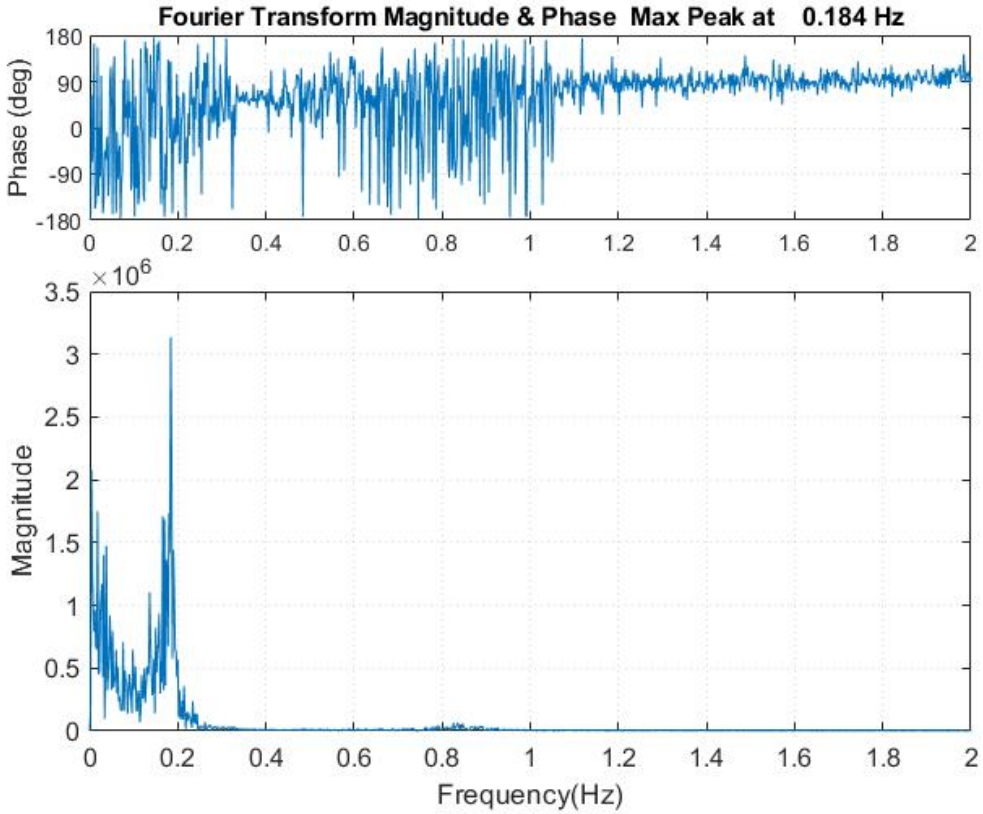

Figure E.4: Reference MP, SS23, Stress response FT and phase(ML).

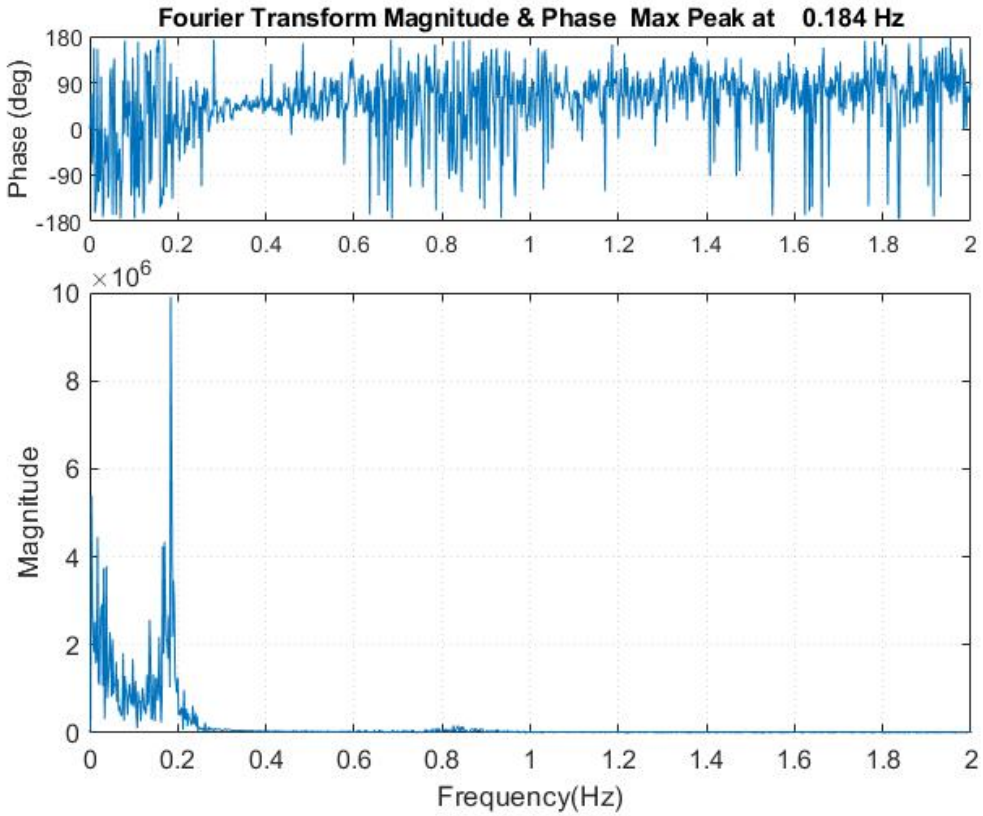

Figure E.5: Reference MP, SS32, Stress response FT and phase(ML).

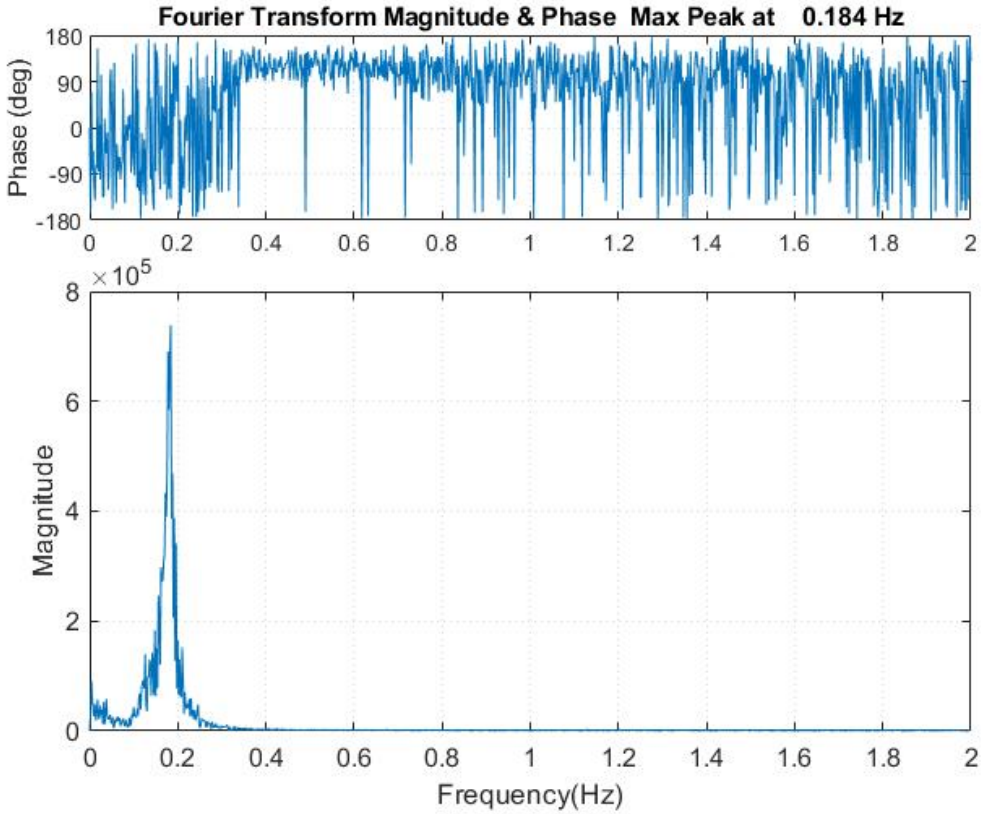

Figure E.6: Reference MP, SS6, Stress response FT and phase(SZ).

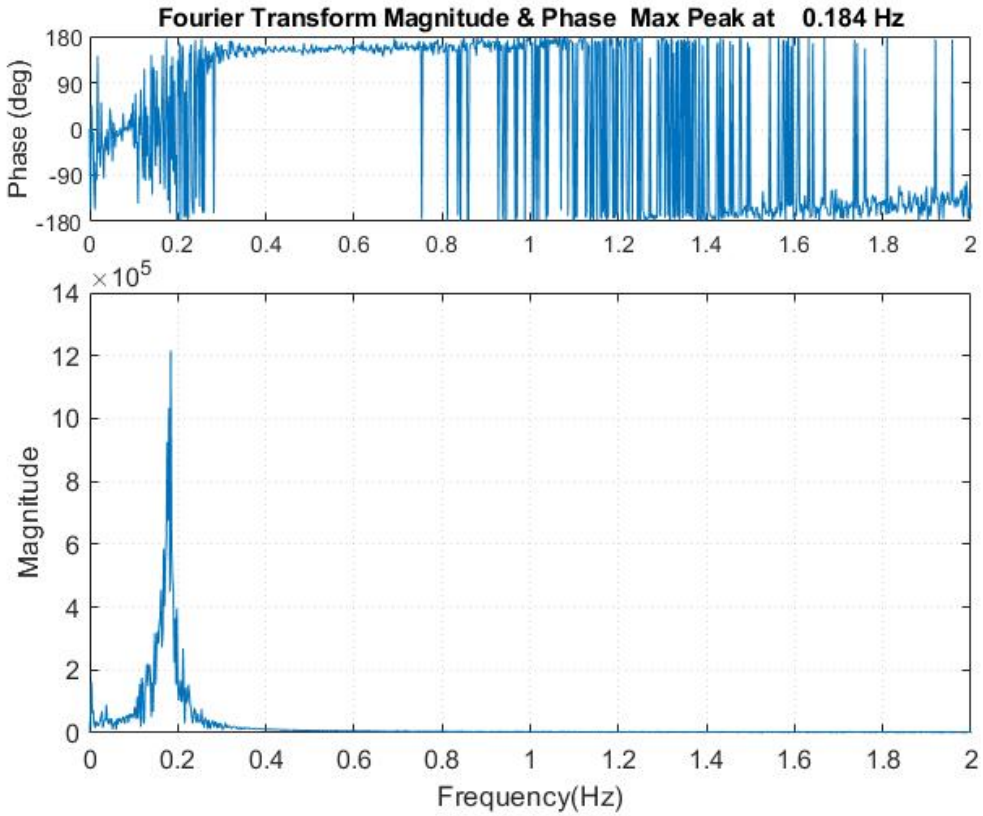

Figure E.7: Reference MP, SS10, Stress response FT and phase(SZ).

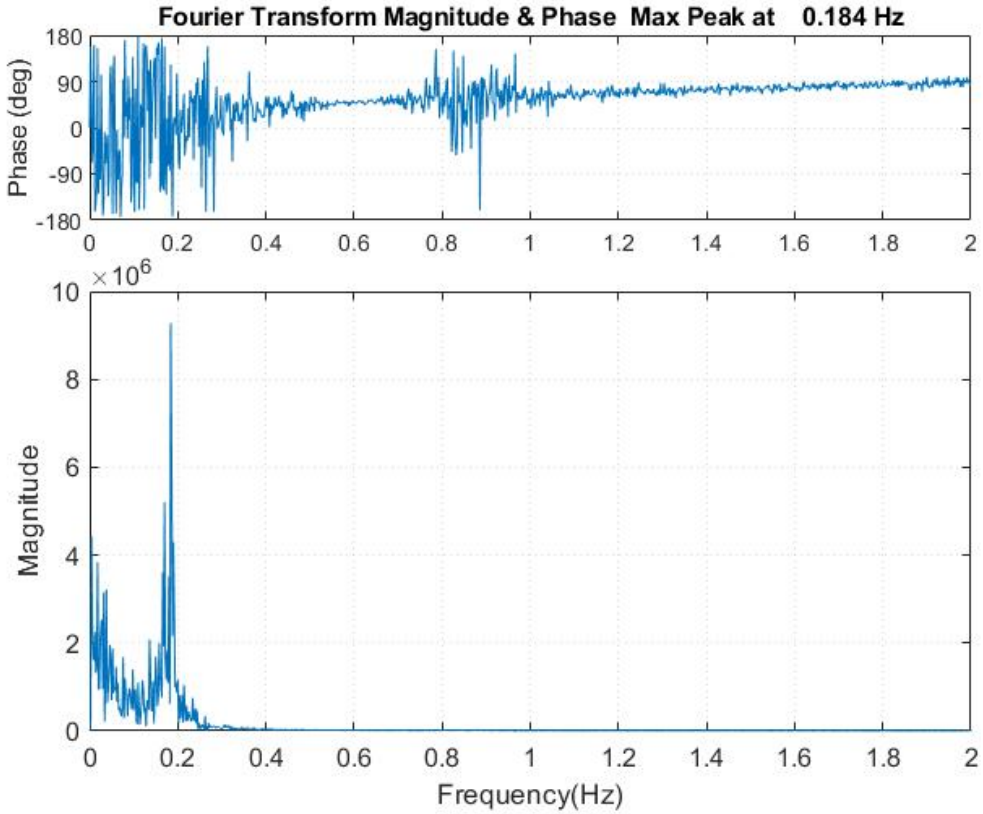

Figure E.8: Reference MP, SS19, Stress response FT and phase(SZ).

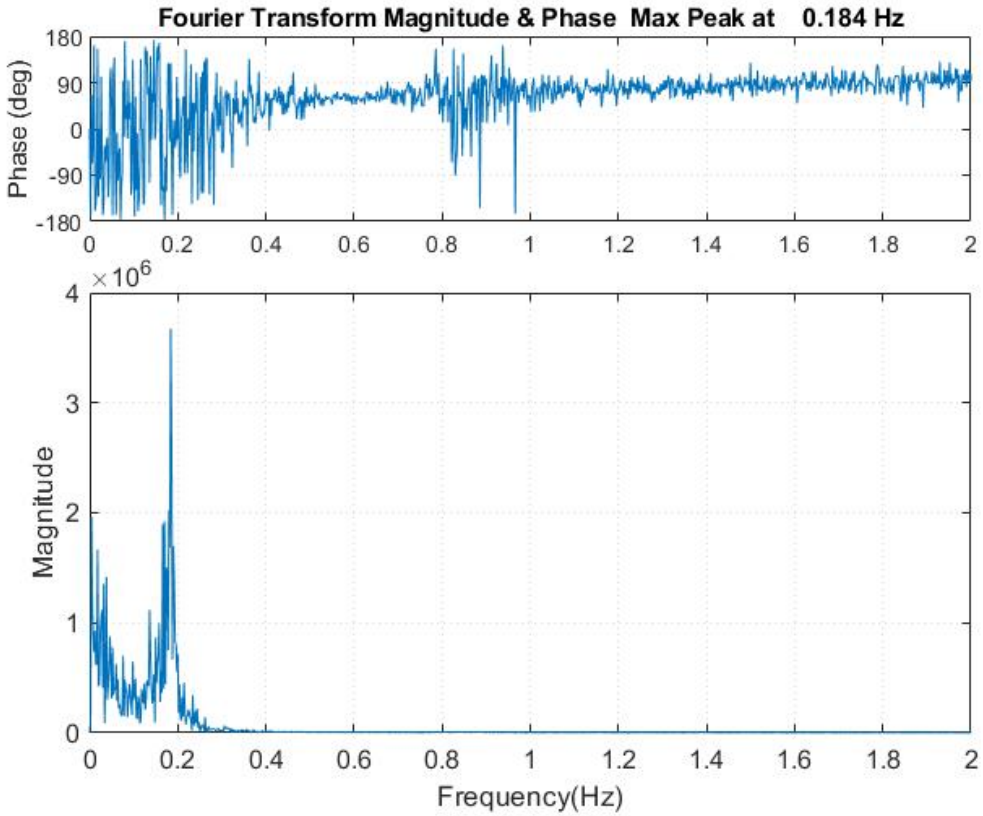

Figure E.9: Reference MP, SS23, Stress response FT and phase(SZ).

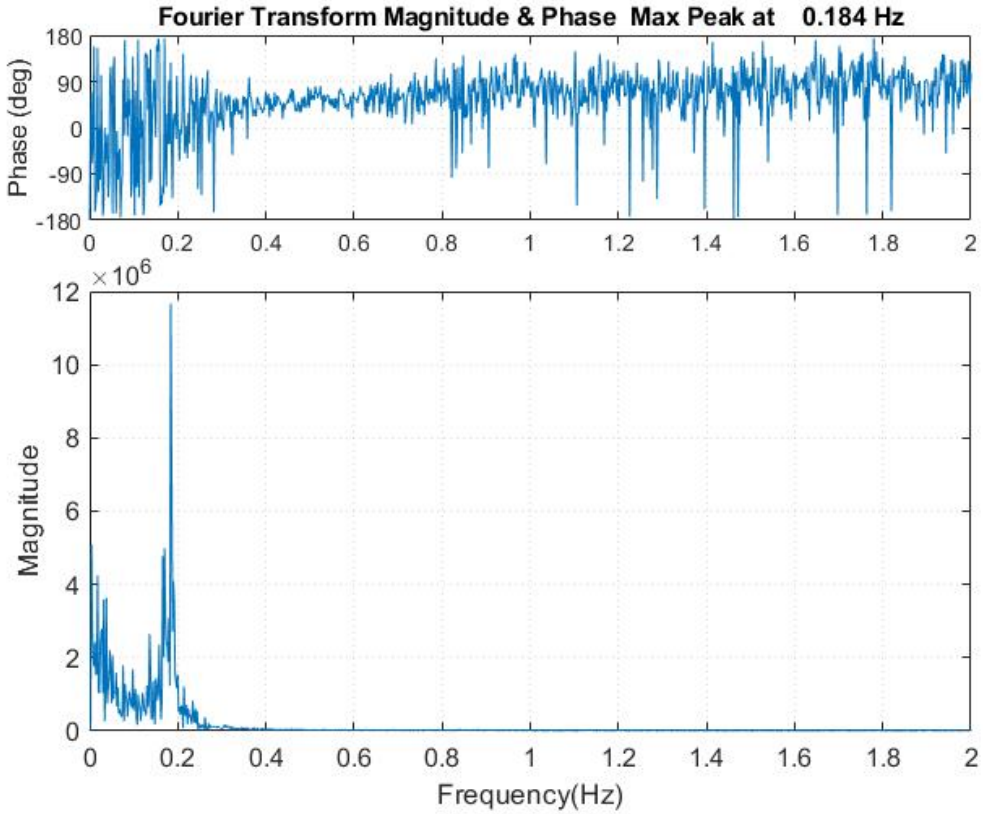

Figure E.10: Reference MP, SS32, Stress response FT and phase(SZ).

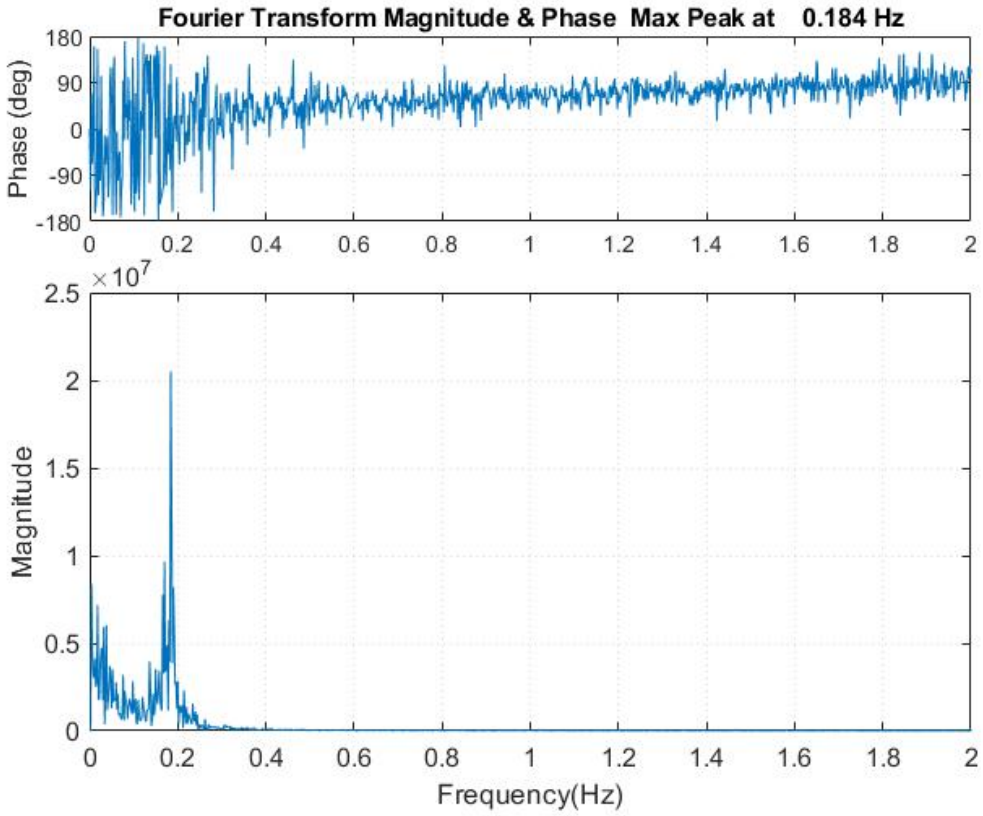

Figure E.11: Reference MP, SS5, Stress response FT and phase(SZ).

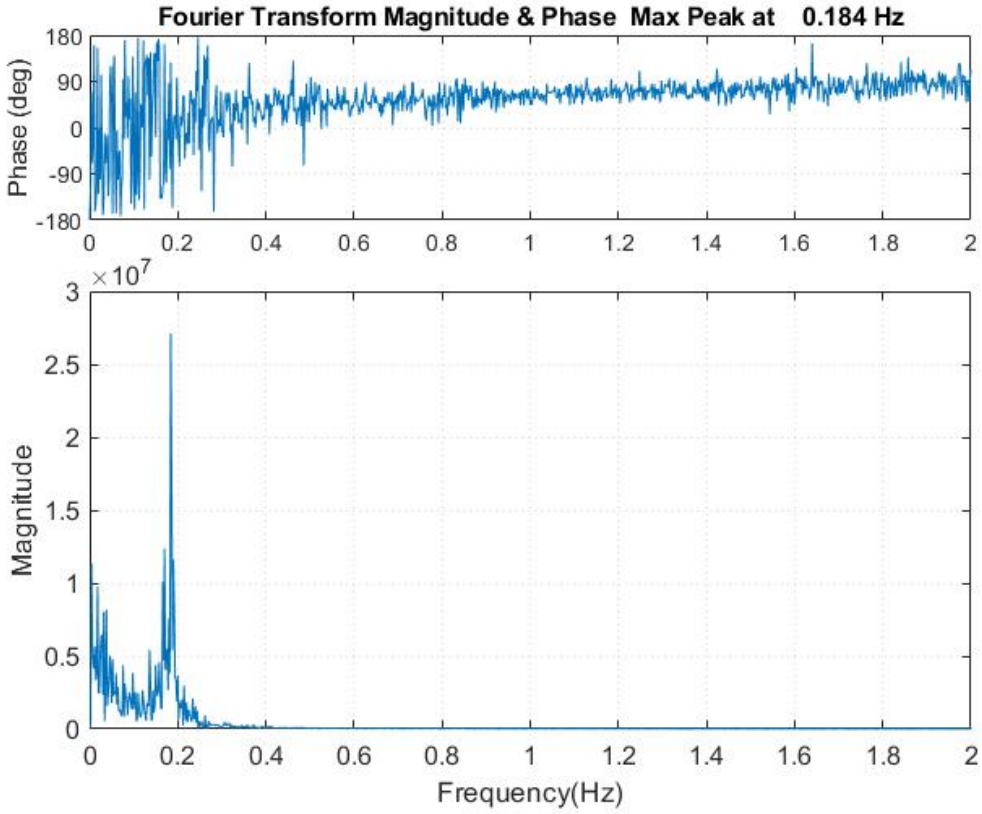

Figure E.12: Reference MP, SS8, Stress response FT and phase(SZ).

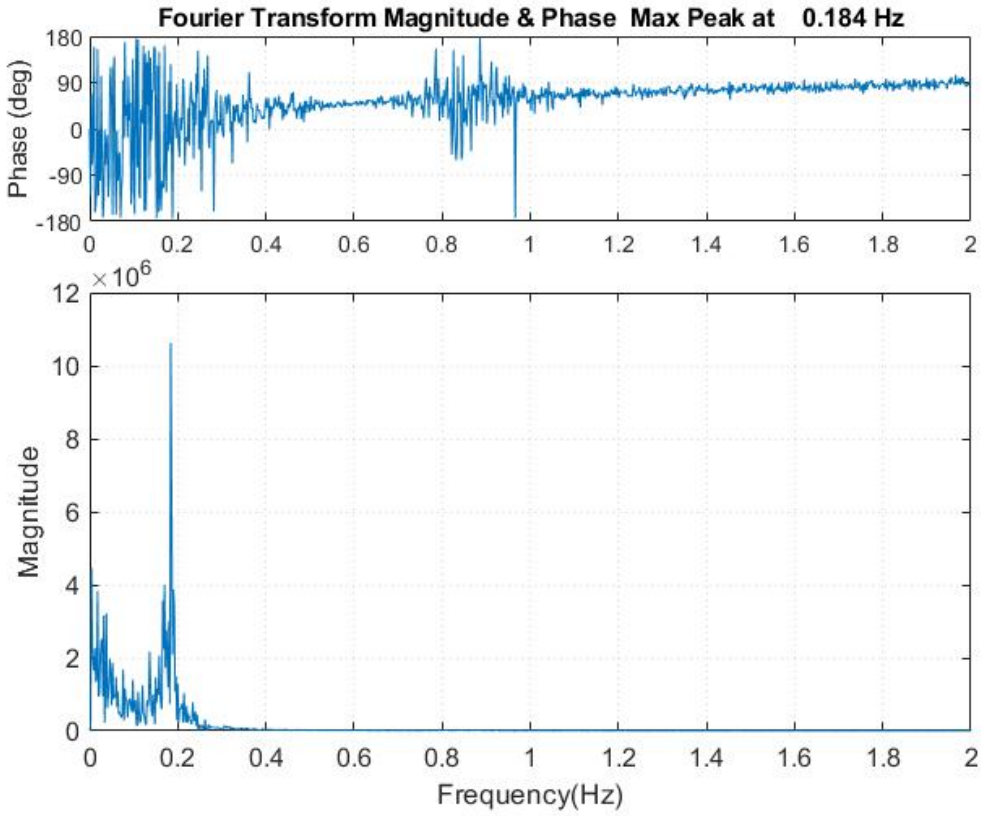

Figure E.13: Reference MP, SS17, Stress response FT and phase(SZ).

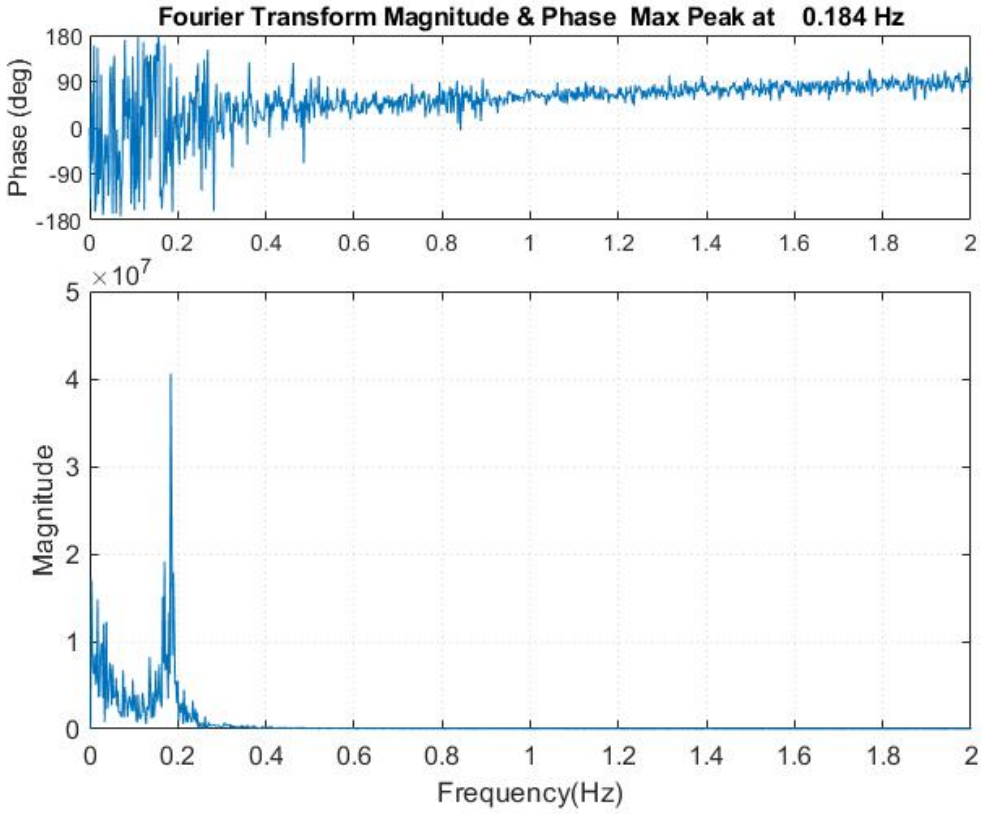

Figure E.14: Reference MP, SS21, Stress response FT and phase(SZ).

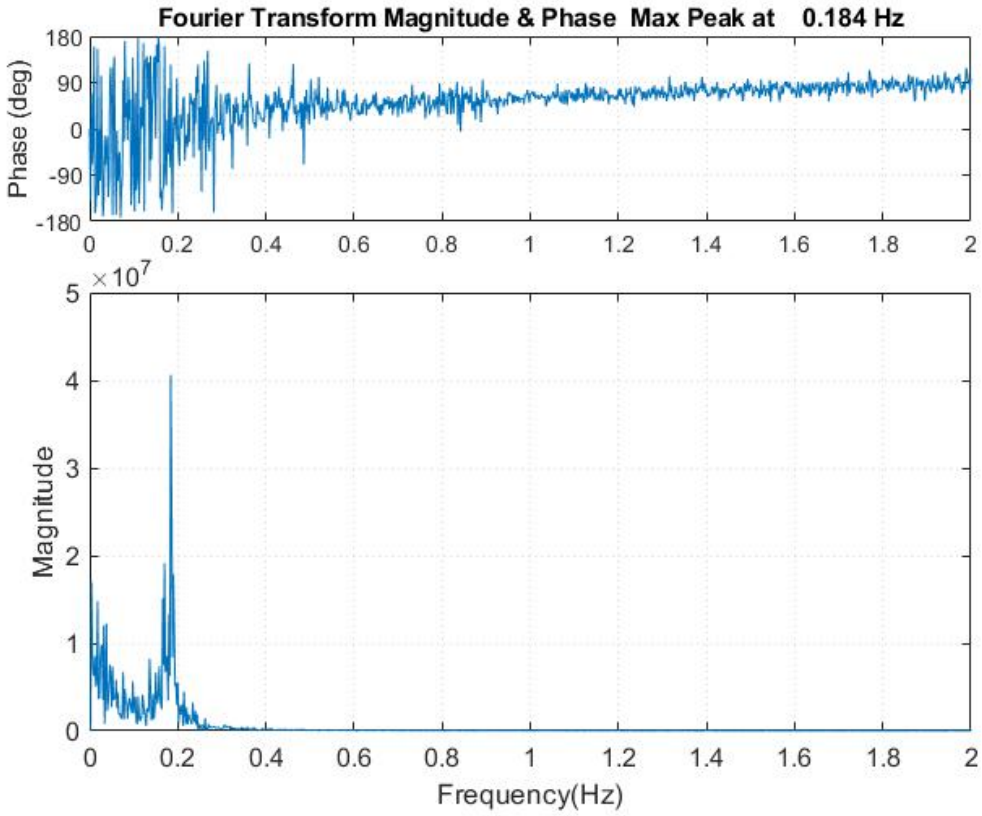

Figure E.15: Reference MP, SS28, Stress response FT and phase(SZ).

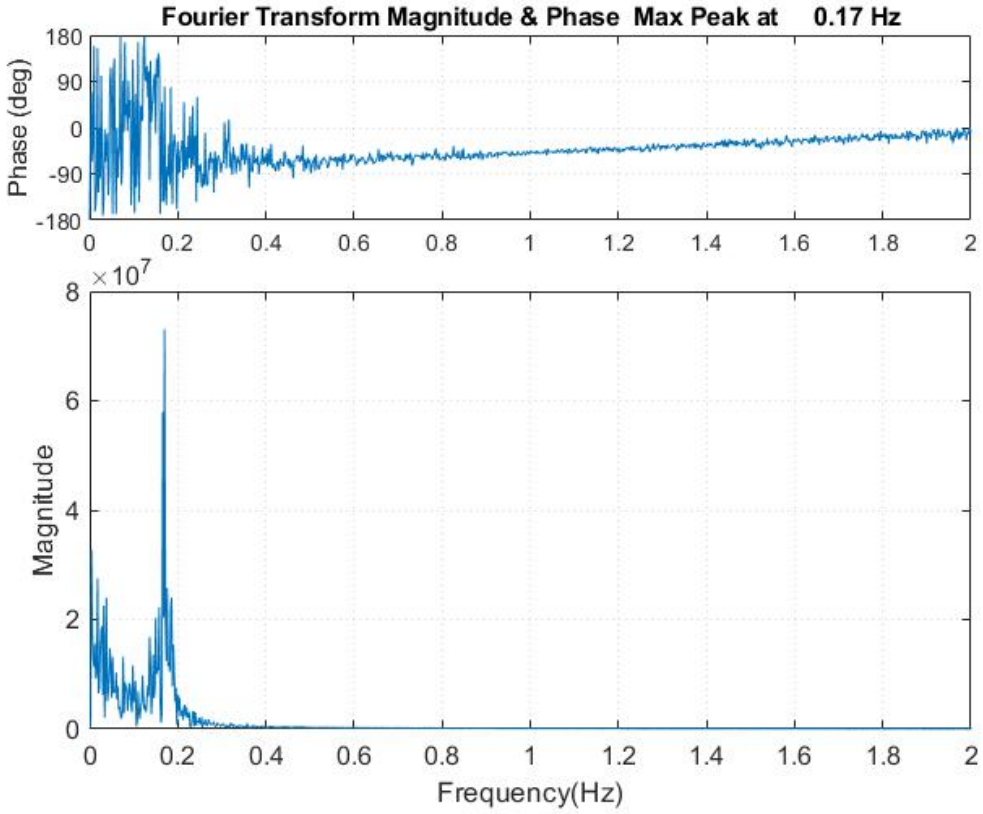

Figure E.16: Perforated MP, SS5, Stress response FT and phase(SZ).

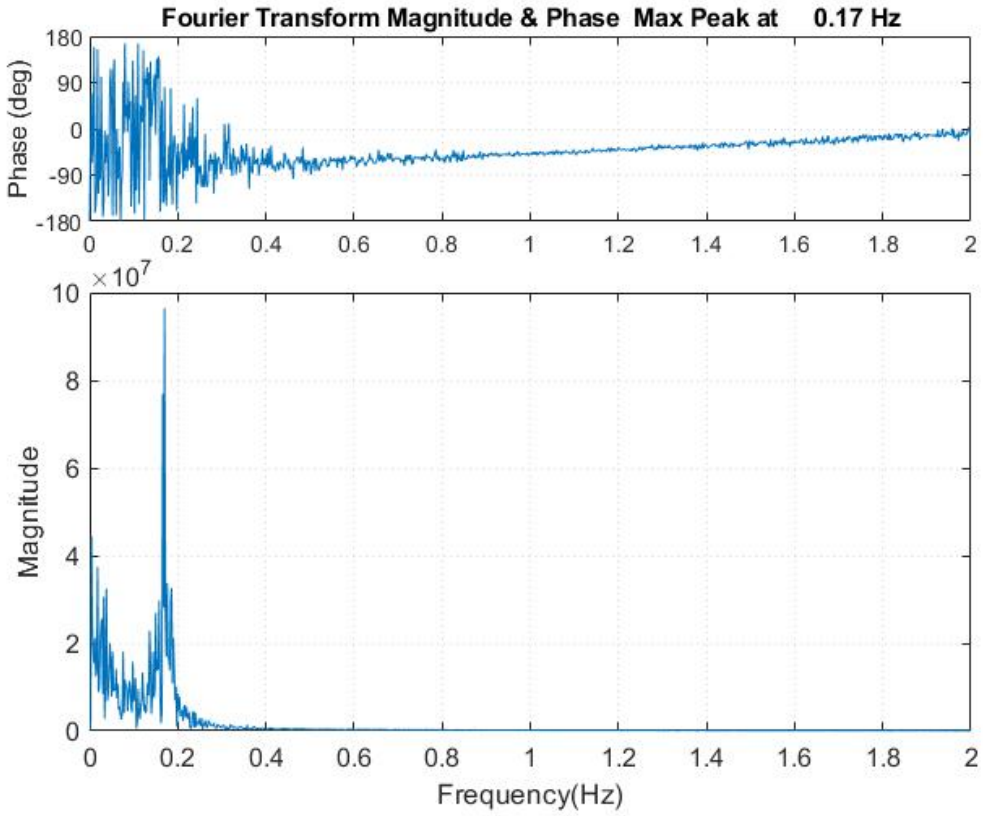

Figure E.17: Perforated MP, SS8, Stress response FT and phase(SZ).

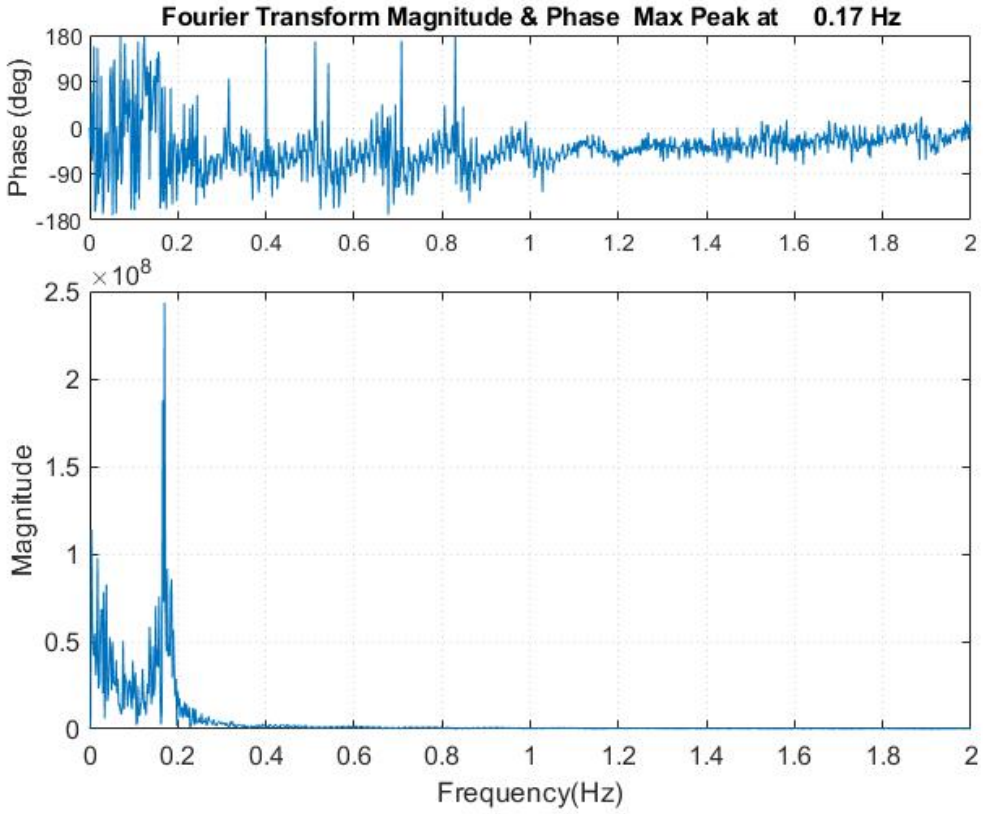

Figure E.18: Perforated MP, SS17, Stress response FT and phase(SZ).

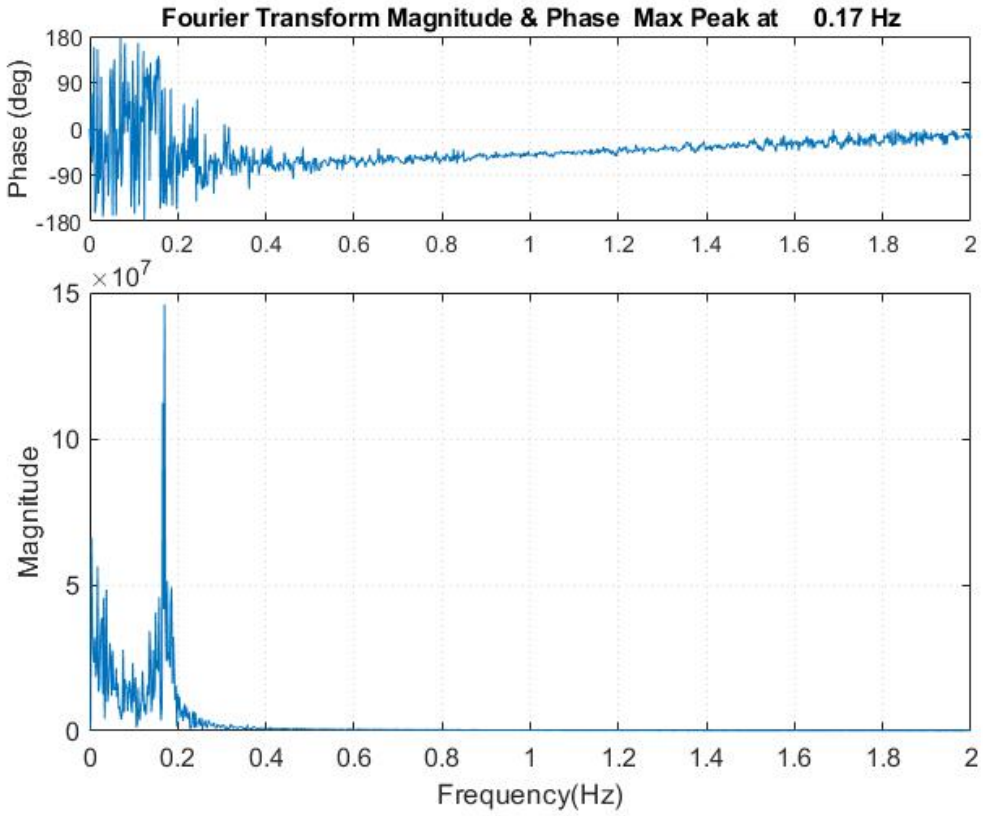

Figure E.19: Perforated MP, SS21, Stress response FT and phase(SZ).

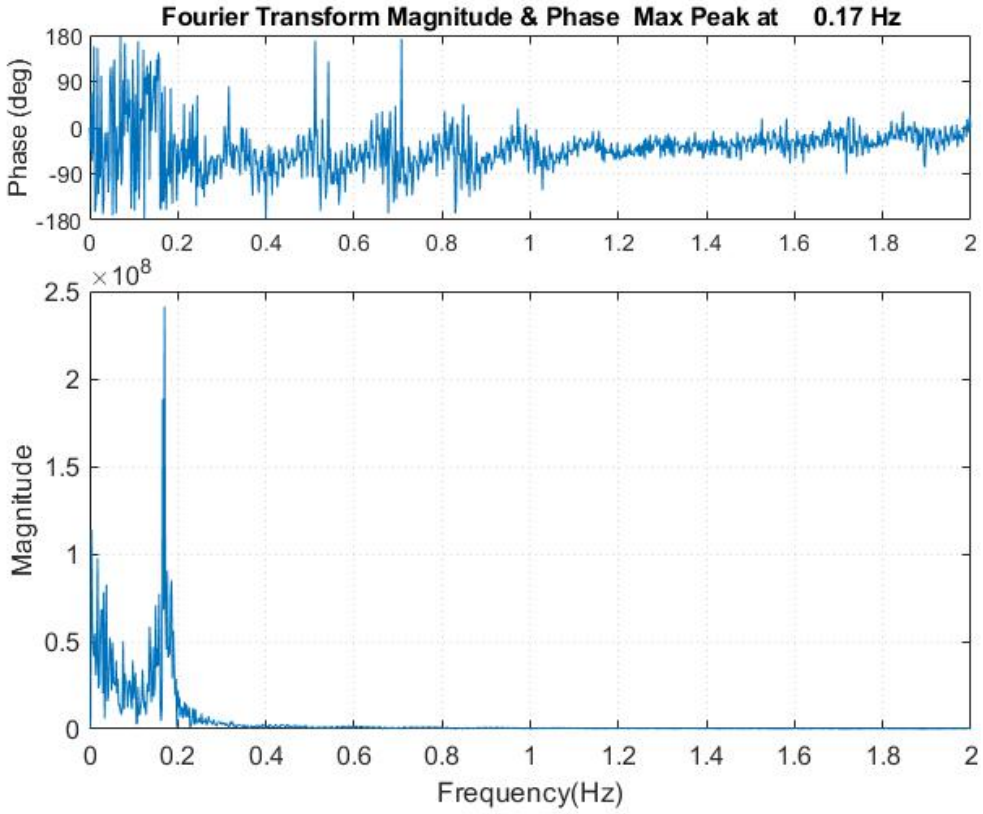

Figure E.20: Perforated MP, SS28, Stress response FT and phase(SZ).

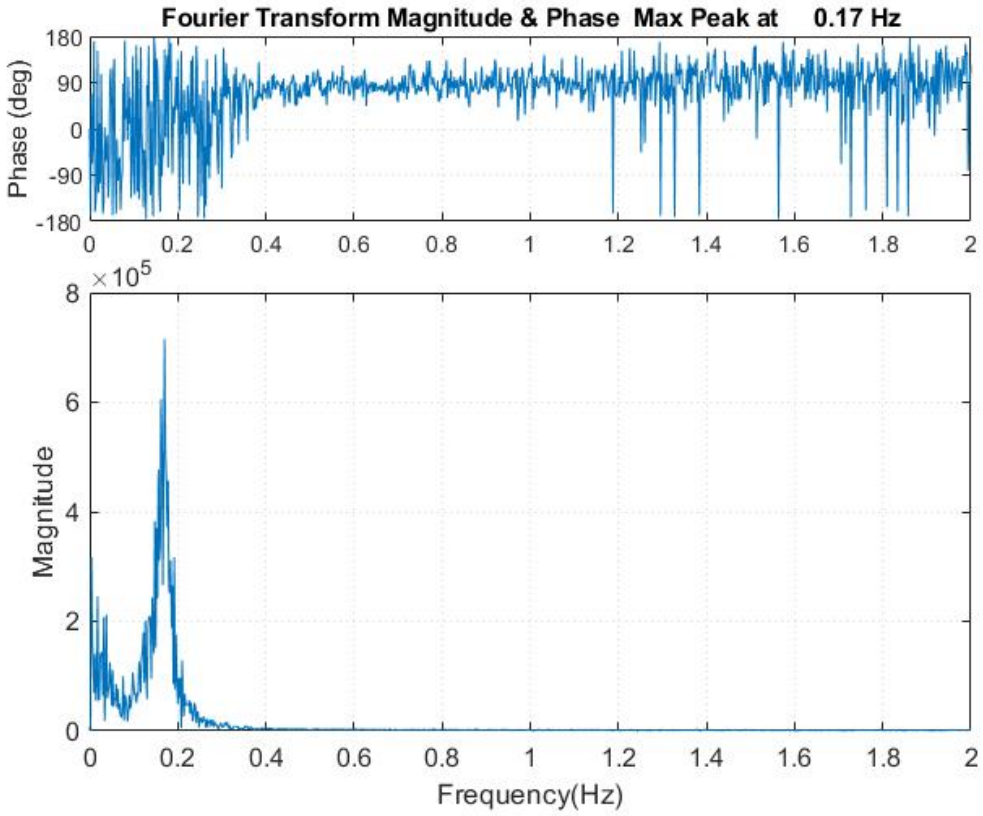

Figure E.21: Perforated MP, SS6, 5% damping Stress response FT and phase(SZ).

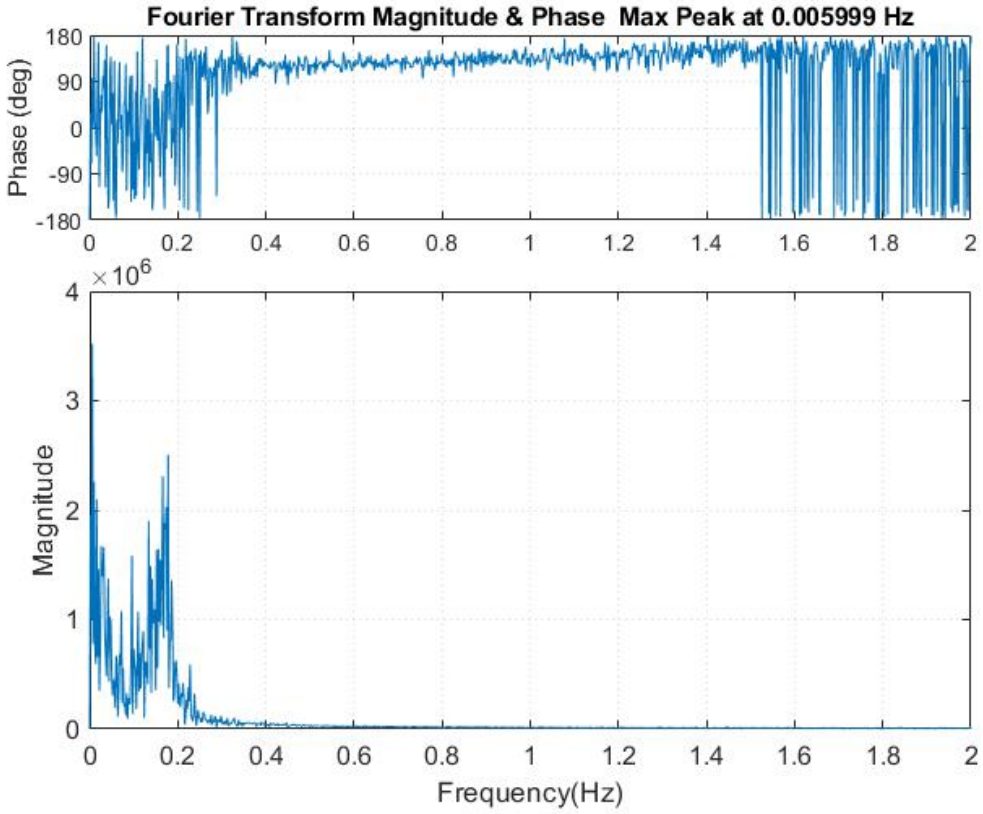

Figure E.22: Perforated MP, SS9, 5% damping Stress response FT and phase(SZ).

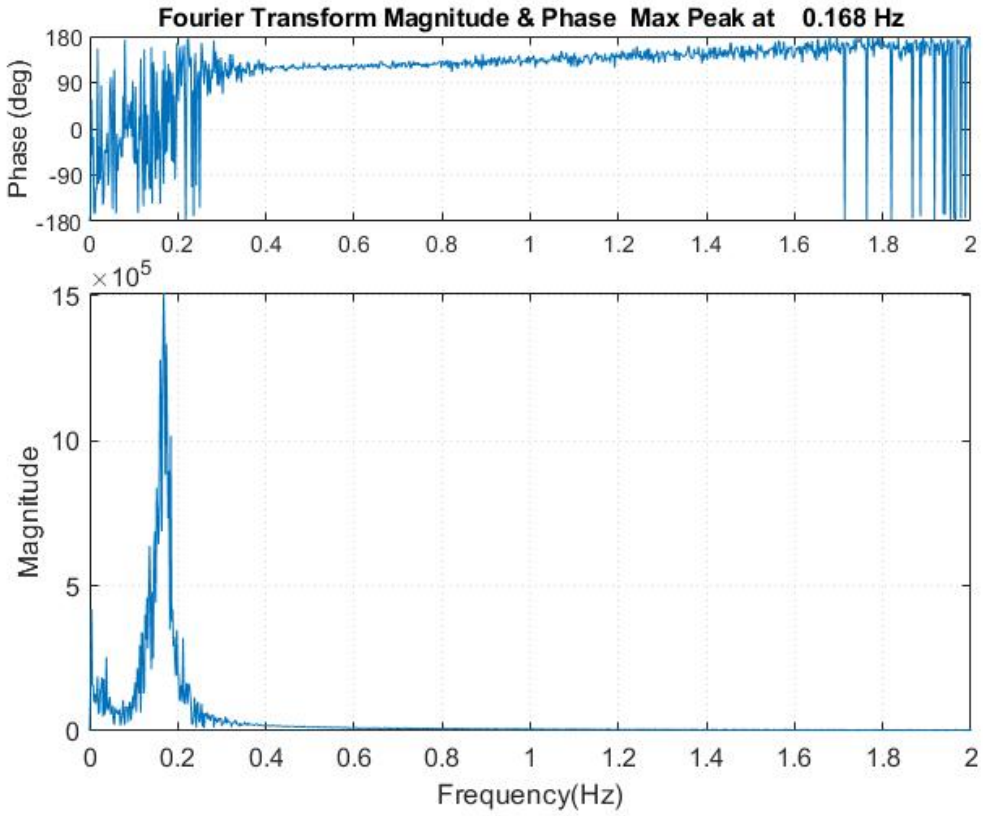

Figure E.23: Perforated MP, SS10, 5% damping Stress response FT and phase(SZ).

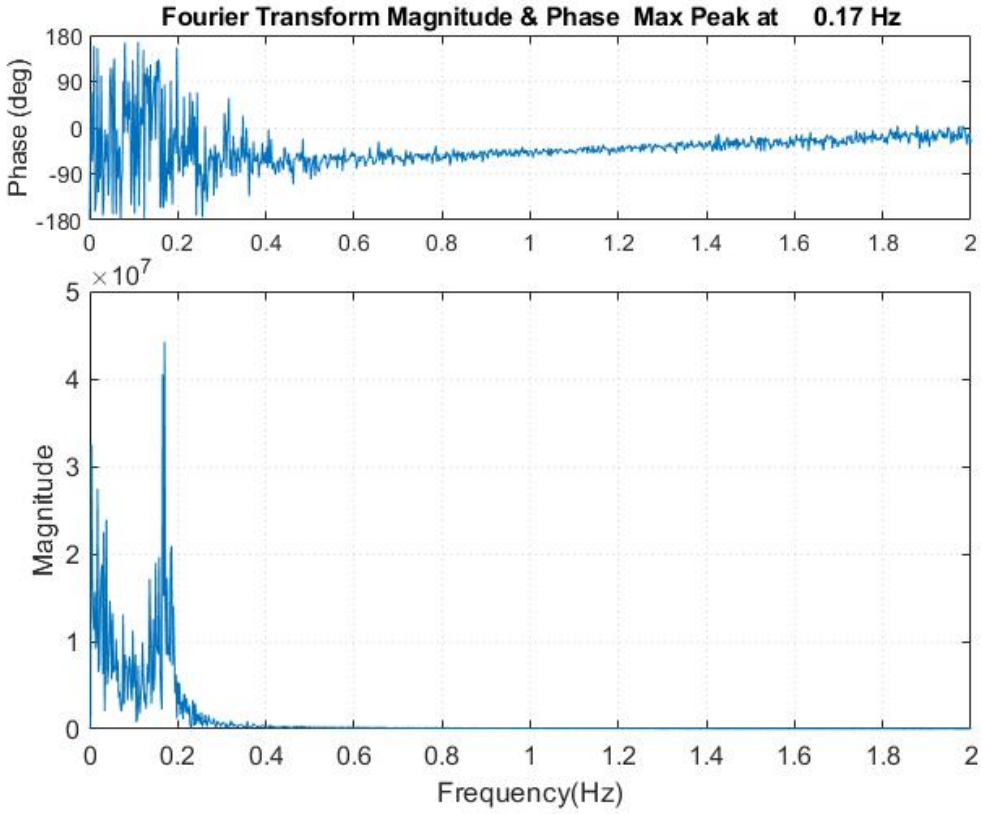

Figure E.24: Perforated MP, SS19, 5% damping Stress response FT and phase(SZ).

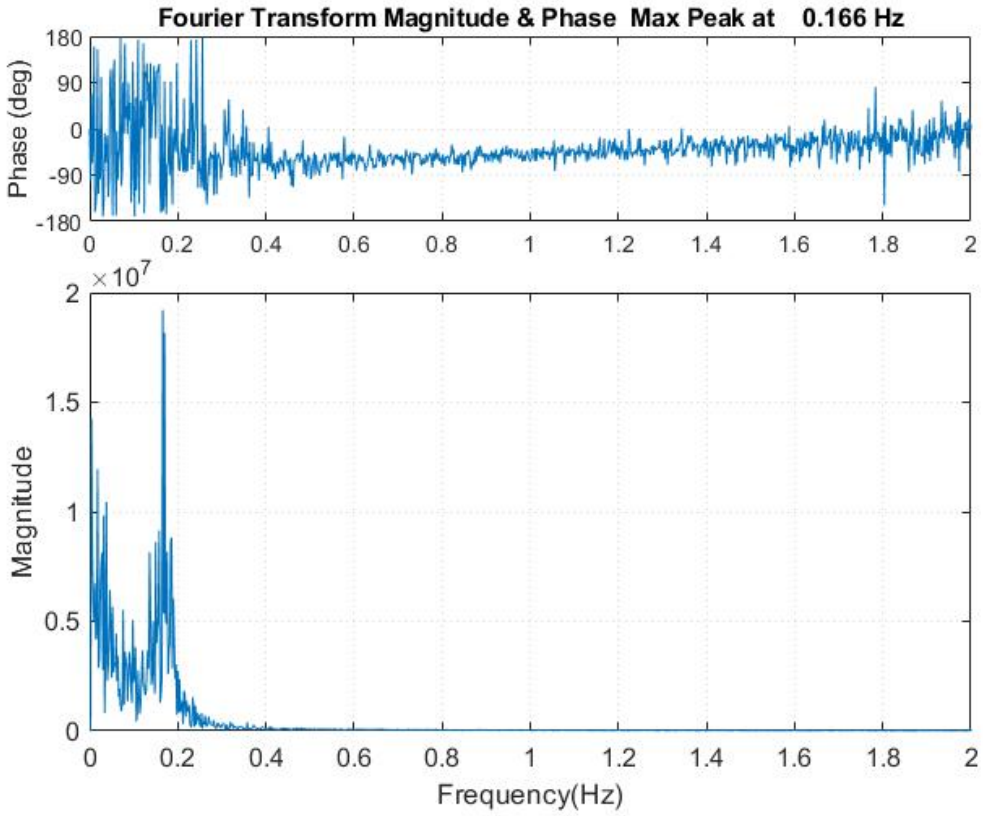

Figure E.25: Perforated MP, SS23, 5% damping Stress response FT and phase(SZ).

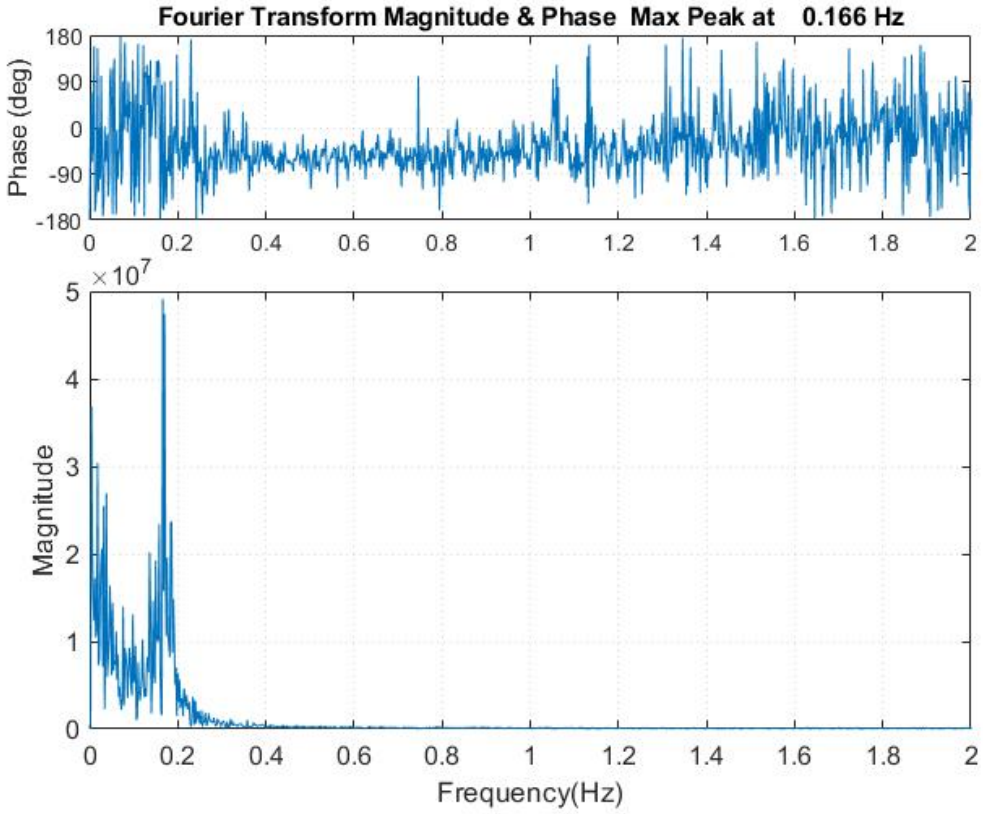

Figure E.26: Perforated MP, SS32, 5% damping Stress response FT and phase(SZ).